A STUDY OF AN ADAPTIVE CONTROL CONSTRAINT SYSTEM FOR MILLING

by

© MOHAMED A. A. ELBESTAWI, B.Sc. (Eng.), M. Eng.

A Thesis

Submitted to the School of Graduate Studies

in Partial Fulfilment of the requirements

for the Degree

Doctor of Philosophy

McMaster University

February, 1980

A STUDY OF AN ADAPTIVE CONTROL CONSTRAINT SYSTEM FOR MILLING

TO THE MEMORY OF MY FATHER

DOCTOR OF PHILOSOPHY (1980) McMaster University
(Mechanical Engineering) Hamilton, Ontario, Canada

TITLE: A Study of an Adaptive Control Constraint System for Milling

AUTHOR: MOHAMED ABDEL AZIZ ELBESTAWI
B.Sc. (Production Eng.)
(Alexandria University, Alexandria, Egypt)
M.Eng. (Mechanical Eng.)
(McMaster University, Hamilton, Ontario, Canada)

SUPERVISOR: Professor J. Tlusty

NUMBER OF PAGES: xviii, 264

ABSTRACT:

This thesis deals with an adaptive control constraint system for end milling with constant force. The control criterion is to hold the force acting on the cutter at a value safely below the force which would break the cutter. This criterion is applicable to finish milling of complex shapes, typically of die cavities. The controlled variable is the command feed rate.

Two other constraints were considered for the adaptive control system, namely: chatter and overload of the cutting edge.

The work presented in this thesis was based on a home-made Computer Numerical Control (CNC) and Adaptive Control (A/C) System consisting of an NC retrofitted No. 4 vertical milling machine and an HP 2100A minicomputer.

The operating characteristics of this system were examined both experimentally and by digital computer simulation. The analytical analysis of the A/C system concen-

trated on its behaviour as a servomechanism, i.e. mainly with respect to the speed of its response to step inputs and to its stability. In this analysis both the Laplace transform approach as well as a numerical simulation (State-Space approach) were used.

In order to improve the system response to collision or step changes in cutting loads caused by abrupt changes in work surface contact area, special action strategies are presented. These strategies are allowed to operate for a limited time during impact before the system switches back to a slower acting (lower gain) strategy. This leads to improved reaction time whilst maintaining system stability.

The A/C experiments were conducted using two different types of dynamometers for the on-line measurement of cutting force. Two different workpiece materials were used: Al. Alloy (95 BHN) and steel AISI 1020 (155 BHN). High Speed Steel end mills were used in all experiments.

An experimental investigation of the chatter constraint was also carried out as well as a review of the basic features of the phenomenon of cutting edge overload.

It is shown that the flexibility of the end milling cutters is beneficial in attenuating the overload in a sudden transient situation and it is also beneficial in attenuating chatter. These benefits are obtained for a certain range of diameters and lengths of cutters. Within this range constraints on feed rate for edge overload must be considered and outside of this range the chatter constraint has to be included.

ACKNOWLEDGEMENTS

I would like to thank Dr. J. Tlusty for his advice and guidance throughout the duration of the present investigation, as well as Dr. A. Cowley for his assistance.

I would like also to thank the members of my Ph.D Supervisory Committee:- Professor J. N. Siddall, Dr. N. K. Sinha, and Dr. I. Yellowley.

The author also expresses his appreciation to Mr. F. Drieman and Mr. D. Schick for their assistance during the experimental work.

I would also like to thank Mrs. M. Ayers for her expert typing of the manuscript.

The financial assistance from McMaster University in the form of a Teaching and Research Scholarship is gratefully acknowledged.

TABLE OF CONTENTS

LIST OF FIGURES

LIST OF TABLES

NOMENCLATURE

SYMBOLS	DESCRIPTION
a	Acceleration
B	A/C Derivative Gain Constant
b	Axial Depth of Cut
C	Cutting Force Coefficient
e_f	Relative Force Error
F_x	Horizontal Component of Radial Cutting Force
F_y	Vertical Component of Radial Cutting Force
F_r	Radial Cutting Force
F_{act}	Actual Force
F_{nom}	Nominal Cutting Force
F	Tooth Force
f_t	Feed Per Tooth
$(G)_{min}$	Minimum of the Real Part of the Transfer Function
h_c	Chip Thickness
K_{ac}	A/C Gain Constant
K_S	Spindle Stiffness
K_C	Cutting Stiffness
l	Cutter Lengths
N	Spindle Speed
r	Cutter Radius
s	Laplace Operator
t	Time

SYMBOLS	DESCRIPTION
τ	Time Period Between the Cutter Teeth
μ	Stiffness Ratio K_C / K_S
v	Milling Machine Table Velocity
V	Peripheral Speed
x_4	Initial Distance Input to the NC Loop
x_5	Speed Command Signal
x_{11}	Resolver Output
x_6	Input to the Correcting Network
x_{10}	Output of the Servo motor
x_7	Intermediate State-Space Variable
x_8	Output of the Correcting Network
x_9	Armature Current
$(Y-Yo)$	Variation in the Undeformed Chip Thickness
z	Number of Cutter Teeth

CHAPTER 1

INTRODUCTION

The use of a digital computer for on-line control of a machine tool shows promise of leading to a new era in manufacturing techniques. The largest single benefit of a digital computer is its ability to do, simultaneously, a number of unrelated tasks.

Beyond Numerical Control (NC), there are two areas of possible improvement in machining. The first involves decreasing the non-machining time by improving loading, unloading, scheduling and shop routing. The second involves decreasing the actual machining time. It is in this second area that Adaptive Control (A/C) lies.

Adaptive Control is a logical extension from NC in the further automation of metalworking machinery. Under adaptive control, the cutting process is continuously monitored by observing certain important process variables. The A/C controller, using these process variables as input, alters selected control variables to improve the cutting process. In metal cutting, the term "improvement of the cutting process" means either increasing the metal removal rate (MRR), or decreasing the unit cost.

The interconnection of an adaptive control system with a numerically controlled milling machine, used as an illustrative example, is shown in figure 1.1. Two feedback loops

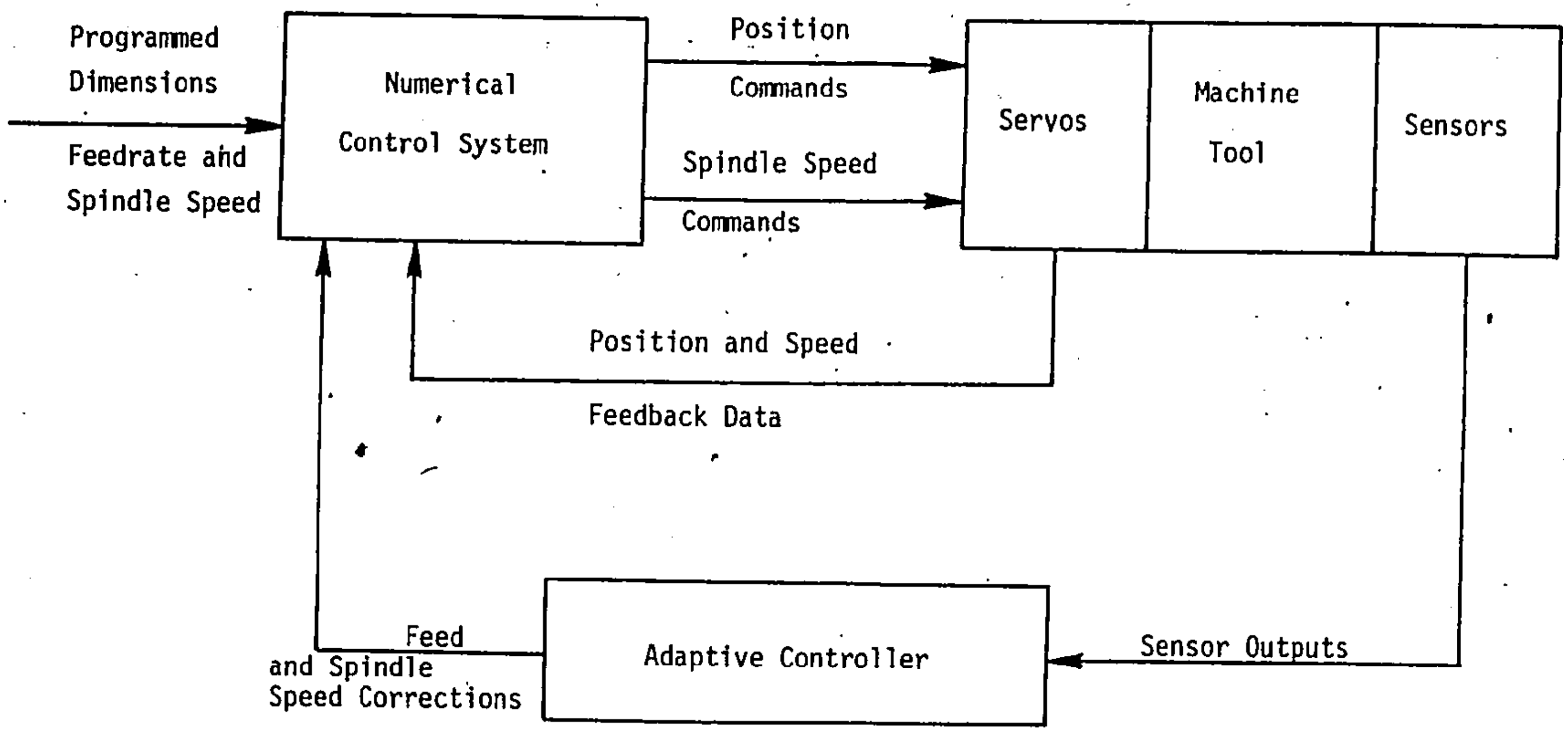

FIGURE 1.1

Interconnection of an Adaptive Control with a Numerically Controlled Milling Machine are closed around the machining process, the primary feedback from the machine tool to the numerical control system, the secondary or the adaptive loop is closed around the entire process.

Since the field of adaptive control has witnessed many very complex and cumbersome systems, there remains a need for simple yet efficient A/C systems.

This thesis deals with an adaptive control constraint system for end milling where the control criterion is to hold the force acting on the cutter at a value safely below the force which would break the cutter. The controlled variable is the command feed rate.

It is assumed that this criterion is applicable to finish milling of complex shapes, typically of die cavities where small diameter mills are used to remove irregular "chunks" of material left behind by the larger roughing cutter in those parts of the cavity where this larger cutter could not enter. The purpose of the Adaptive Control is then to let the small cutter move with a rather rapid feed in those parts of the job where the load is small and to slow down when the load increases.

Other constraints considered were chatter and overload of the cutting edge.

In the present work an attempt is made to analyze the A/C system from the point of view of its behaviour as a servomechanism, i.e. mainly with respect to the speed of its response to step inputs and to its stability. Special attention is devoted to the behaviour of the system during tool-work impact under rapid traverse conditions. In this analysis both the Laplace transform approach as well as a numerical simulation (state-space approach) are used.

In an attempt to improve the system response to collision or step changes in cutting loads caused by abrupt changes in work surface contact area, special action strategies are presented. These strategies are allowed to operate for a limited time during impact before the system switches back to a slower acting (lower gain) strategy. This leads to improved reaction time whilst maintaining system stability.

The operating characteristics of the A/C system were examined experimentally. The A/C experiments were conducted using two different dynamometers for the on-line measurement of cutting force. Two different workpiece materials were used in these experiments, Al. Alloy (95 BHN) and steel AISI 1020 (155 BHN). High speed steel end mills were used in all experiments.

A study of the phenomenon of chatter in end milling was carried out with the aim of including chatter as a constraint in the A/C system. This study included the investigation of the dynamics of the machine tool as well as the necessary cutting tests. A review of the basic features of the phenomenon of cutting edge overload is also presented in this thesis.

It is shown that the flexibility of the end milling cutters is beneficial in attenuating the overload in a sudden transient situation and it is also beneficial in attenuating chatter. These benefits are obtained for a certain range of diameters and lengths of cutters. Within this range constraints on feed rate for edge overload must be considered and outside of this range the chatter constraint has to be included.

The work presented in this thesis was based on a homemade CNC, A/C system consisting of an NC retrofitted No.4 vertical milling machine and an HP 2100A minicomputer.

CHAPTER 2

LITERATURE SURVEY

The American Standards Association [1] defines an adaptive control system as "a control system within which automatic means are used to change the system parameters in a way intended to improve the performance of the control system" and a parameter as "a controllable or variable characteristic of a system, temporarily regarded as a constant, the respective values of which serve to distinguish the various specific states of a system".

It has been stated [2] that the main factors pushing for the development of adaptive control (A/C) systems in chip-removing machine tools are:

1. A definite need for employing higher metal cutting rates for better utilization of new NC machine tools.
2. A keen awareness of the tool and scrap costs due to excessive tool wear.
3. An increasing use of hard-to-machine aerospace alloys requiring more control on tool wear rates.
4. The continuous introduction of new tool grades as well as work materials leading to the absolute necessity of using the automatic approach in order to optimize machining conditions.
5. The necessity of automatic tool changing before production parts are lost, due to excessive tool wear

or catastrophic tool failure.

Adaptive Control systems are classified according to their objective, structure and operating modes into Adaptive Control Optimization (ACO) and Adaptive Control Constraint (ACC) as shown in figure 2.1 {3,4}. A further subdivision exists into technological and geometrical A/C.

ACO systems for the machining process usually vary one or more of the cutting parameters - speed, feed or depth of cut - in order to satisfy a predetermined performance criterion. This criterion will usually be either minimum machining cost, maximum productivity, or acceptable quality of the workpiece. The acceptable quality to which a machine adapts itself could be assessed by either surface finish or dimensional tolerances.

In ACC systems on the other hand, the performance index is not directly evaluated, but one or more of the cutting conditions (e.g. feed rate) are maximized within the prescribed limits of the constraints such as maximum force, torque, or horsepower.

Both in adaptive control optimization and adaptive control constraint, in order to control the cutting conditions at each instant of time (simultaneously sensing), it is necessary to solve sensing problems measuring on-line one or more of the process variables. This signal is the input to the AC system which is set according to a criterion using constraints

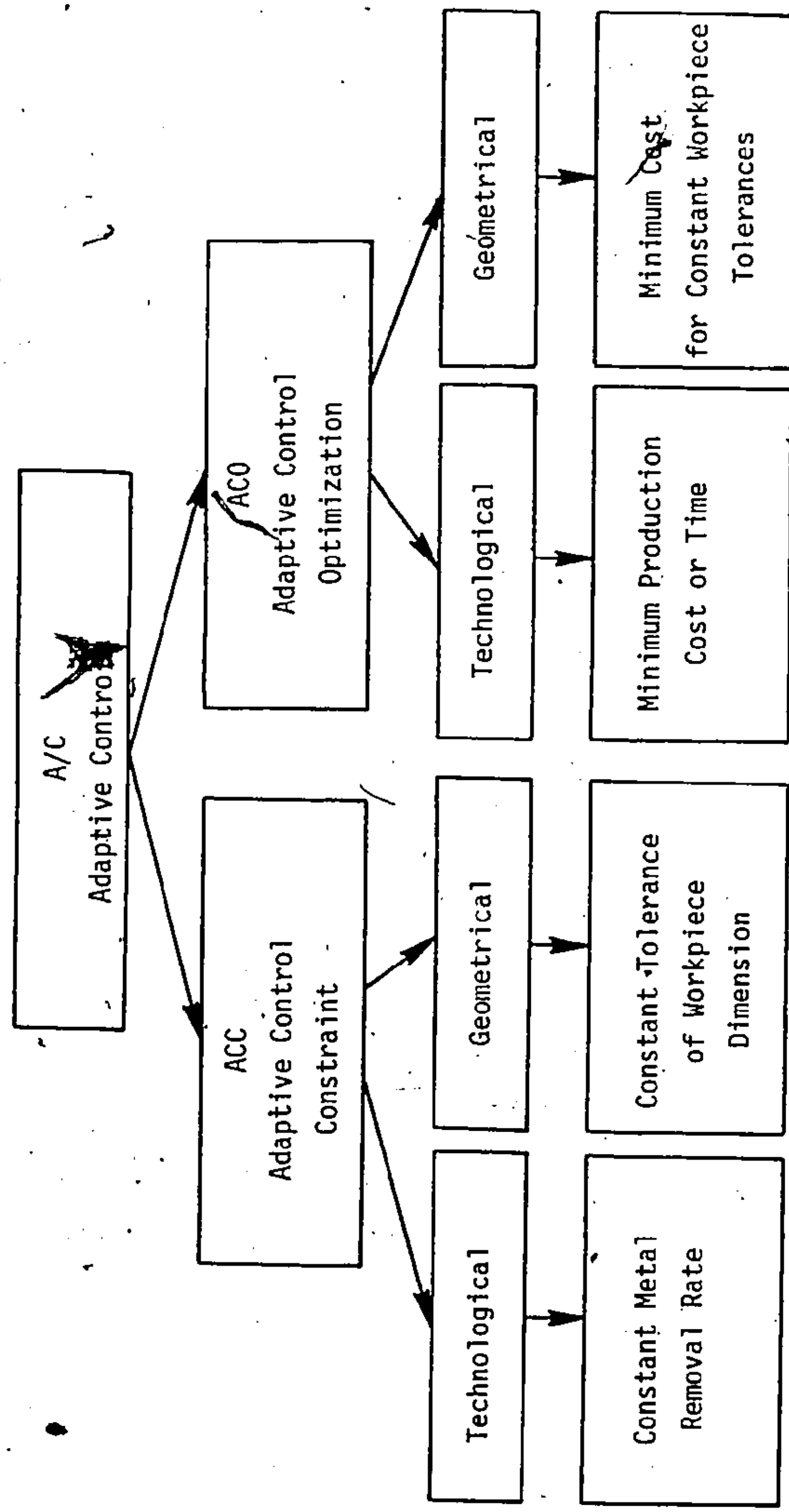

Subdivision of the Term "Adaptive Control" [2]

FIGURE 2.1

or optimization.

Process variables investigated by many researchers include tool wear, cutting forces, spindle torque, spindle horsepower consumption, spindle deflection, temperature at the tool-work piece interface, table vibrations, spindle vibrations, motor current, and motor temperature. If cost is taken to represent the process as it is the case in most ACO systems, then the problem becomes one of measuring the tool wear on line. A simple analysis of the machining cost will reveal that it is composed of two elements. One is dependent on the time it takes to machine a part and hence, the metal removal rate, MRR. The other represents the part of the tool's cost consumed during the operation, which in turn will depend on the tool wear rate, TWR. Since the MRR is directly evaluated from the known cutting conditions, (from the N/C controller), the problem becomes one of sensing the tool wear on-line.

Figure 2.2 shows the principal classification of tool wear sensors [5]. Since tool wear affects the behaviour of the machine tool-workpiece system, the tool wear sensor can detect the signal from different parts of the system; directly from the tool or from the workpiece or finally from the process (machine), continuously or intermittently. The tool wear sensing setup is based on direct or indirect measurement methods. In the first case the sensor evaluates the volumetric loss from the tool due to wear, while in the second case equations are established describing the correlations between tool wear and

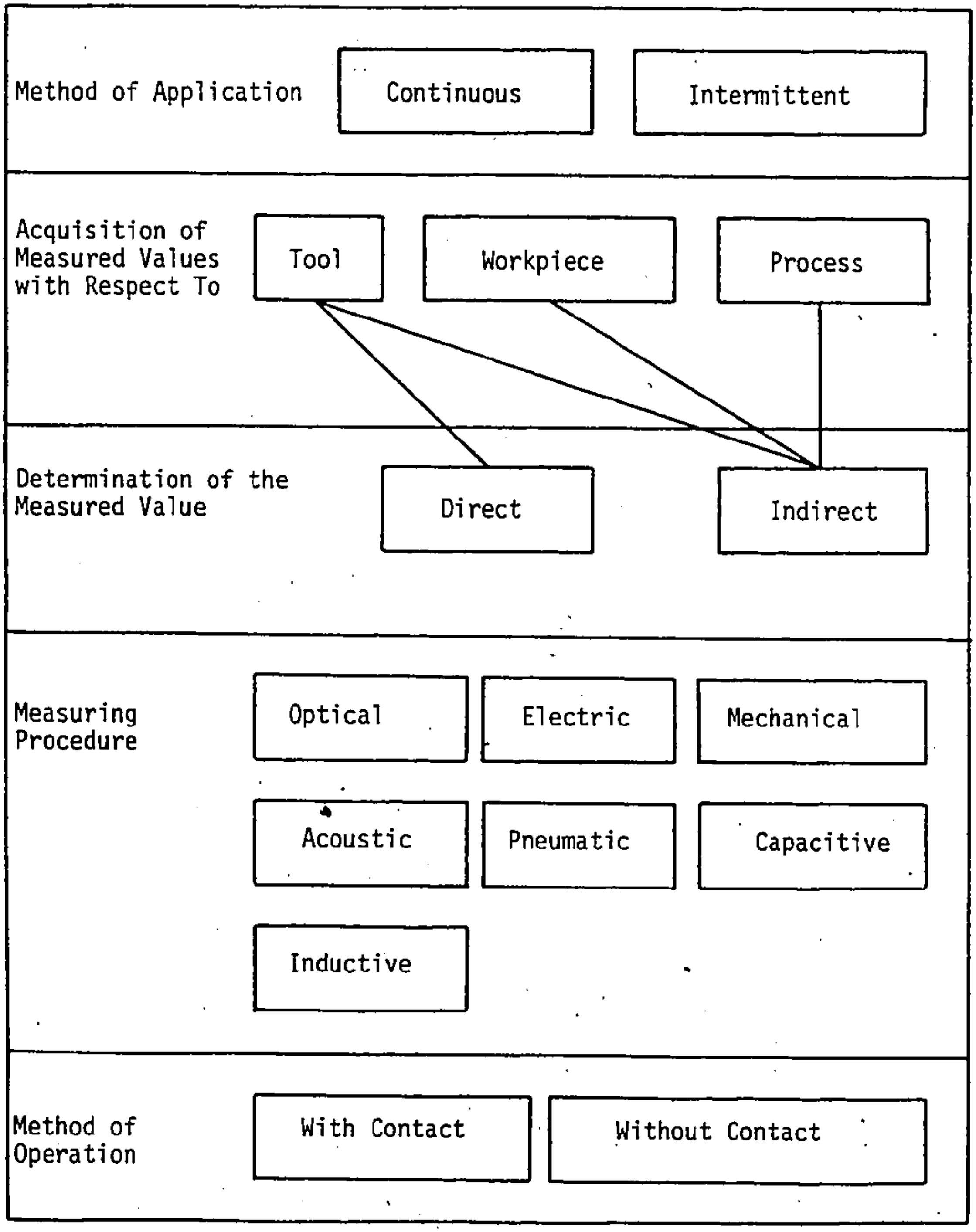

Principal Classification of Tool Wear Sensors {5}

FIGURE 2.2

other parameters easier to measure. The measuring procedure can be optical, electric, mechanical, acoustic, pneumatic, inductive or capacitive. The method of operation can be with or without contact. In the following a survey of the different methods of sensing tool wear, reported in the literature will be presented:

I) Direct Measurement Methods:

As stated previously, in these methods the sensor measures the tool geometry detecting the volumetric loss of the tool (land wear, crater wear or both together). These methods are generally very difficult (in some cases impossible) to use on-line especially when there is a continuous contact between the tool and the workpiece, e.g. turning. The sensing setup using the direct method includes the following types: Optical sensors (e.g. light reflection, T.V. camera), electrical resistance sensors, radioactive sensors, and pneumatic sensors. Optical and Electro-Optical methods analyse the image of the illuminated wear zone when the cutting tool is not continuously in contact with the workpiece (e.g. milling). As an example of these methods, the optical-electronic sensor {[6]} basically focuses a magnified image of the wear land on an optical slit preceeding the cathode of a photo-multiplier. Therefore, when the land is present, a signal is obtained from the photo-multiplier and, as the cutter rotates, the signal has a duration dependent on the amount of wear present and on the cutting speed of the tool tip. This signal is measured by using it to gate a train of high frequency pulses to a digital counter. A schematic of the Optical-electronic sensor is shown in figure 2.3. Electrical resistance sensors are generally based on the constriction electrical resistance principle which can detect flank wear of turning tools. In reference {7}, the system described depends upon measuring the reduction in electrical resistance through the tool work junction which occurs as the tool wear and its contact are with the work increases. Radioactive Sensors {8,9,10} are used to measure the volumetric overall loss of the tool. The cutting tool is activated with neutrons or charged particles, which during cutting leave on the chip a small quantity of activated material. The abraded radioactive wear particles are transported by a continuous flow of oil to the measuring head where the activity is detected and then recorded with the appropriate set up. The intensity of the radioactivity in the chips is correlated to the volume of tool material that adheres to the chips and hence to total wear. Pneumatic sensors have been used for on-line measurement of wheel wear in grinding {11}. It is generally accepted however, that the use of direct measurement methods is at best impractical, especially on the workshop floor. Accordingly, many studies have been made, exploring possibilities of measuring other parameters, closely correlated with tool wear.

II) Indirect Measurement Methods:

The proposed parameters reported in the literature are:

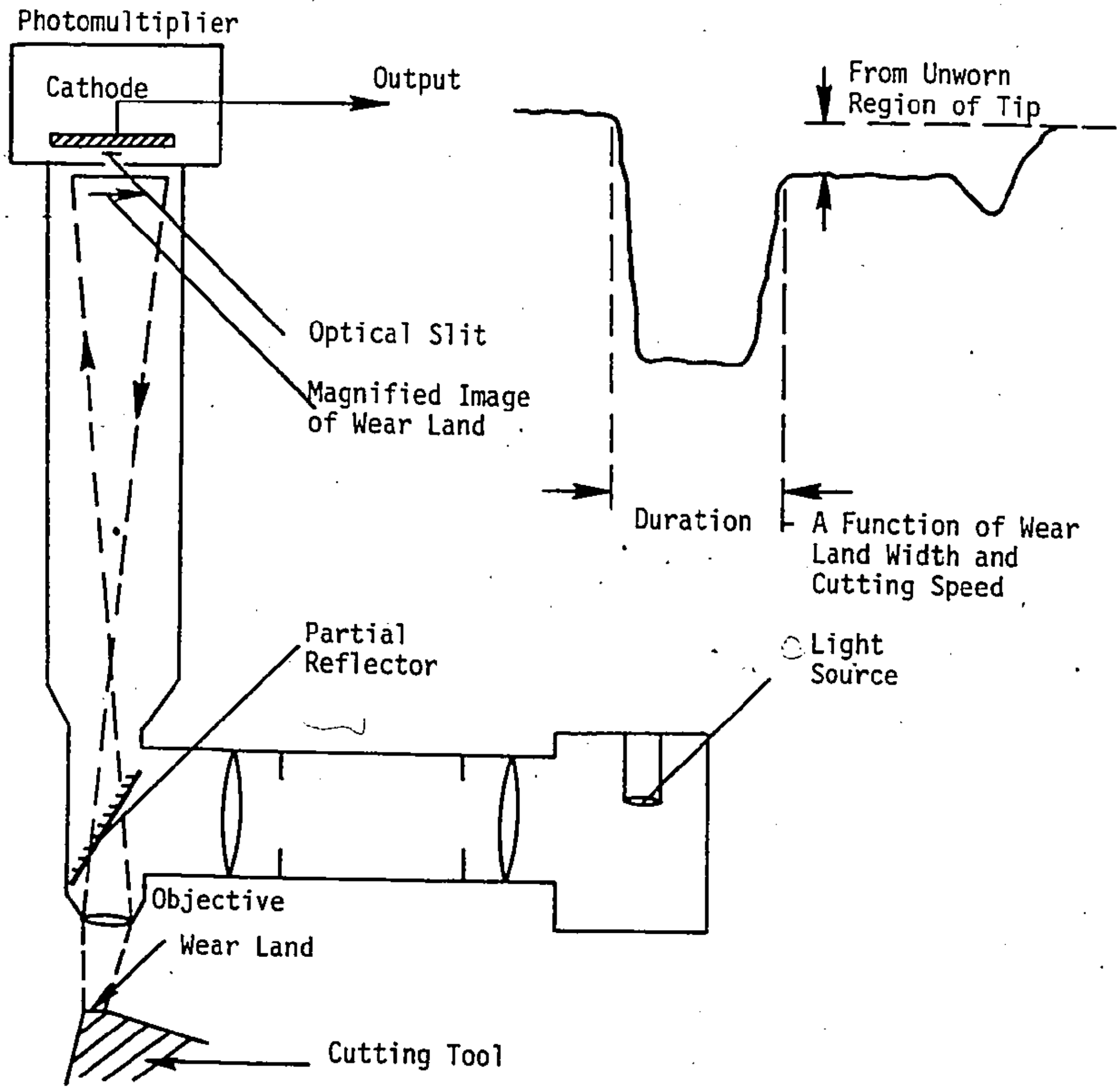

Optical - Electronic Sensor [6]

FIGURE 2.3

1. Cutting forces and/or torque
2. Vibrations and sonic analysis (noise)
3. Roughness of machined surfaces
4. Workpiece dimensions change
5. Distance between tool post and the workpiece
6. Temperature and thermoelectric effects

The research work for determining the correlation between cutting forces and tool wear started some years ago {12,13} by considering that cutting forces are rather easy to measure on-line. Since machinability of workpiece material affects to a large extent the wear rate of the tool, measuring the wear rate continuously through the measurement of cutting forces can give a proper input signal for adaptive control. Particularly, it is possible to define a correlation between one of the components of the resultant cutting force F and the width of the flank wear land VB{14}. Figure 2.4 shows an example of the relation between cutting force and tool wear. Dynamometers are used for measuring the cutting forces (or torque). They can measure different components of the cutting force and can be fixed to the tool holder (e.g. in the case of a lathe) or rotated with the spindle {15}. Some systems measure the deflection of the cutter {16}. The deflection calibration is made by applying known forces at different points on the tool mounted on the spindle of the machine and the deflection at the tool plus the deflection at the spindle are recorded. The transducers for detecting spindle displacement can be induction, non-contacting types {17}. Also,

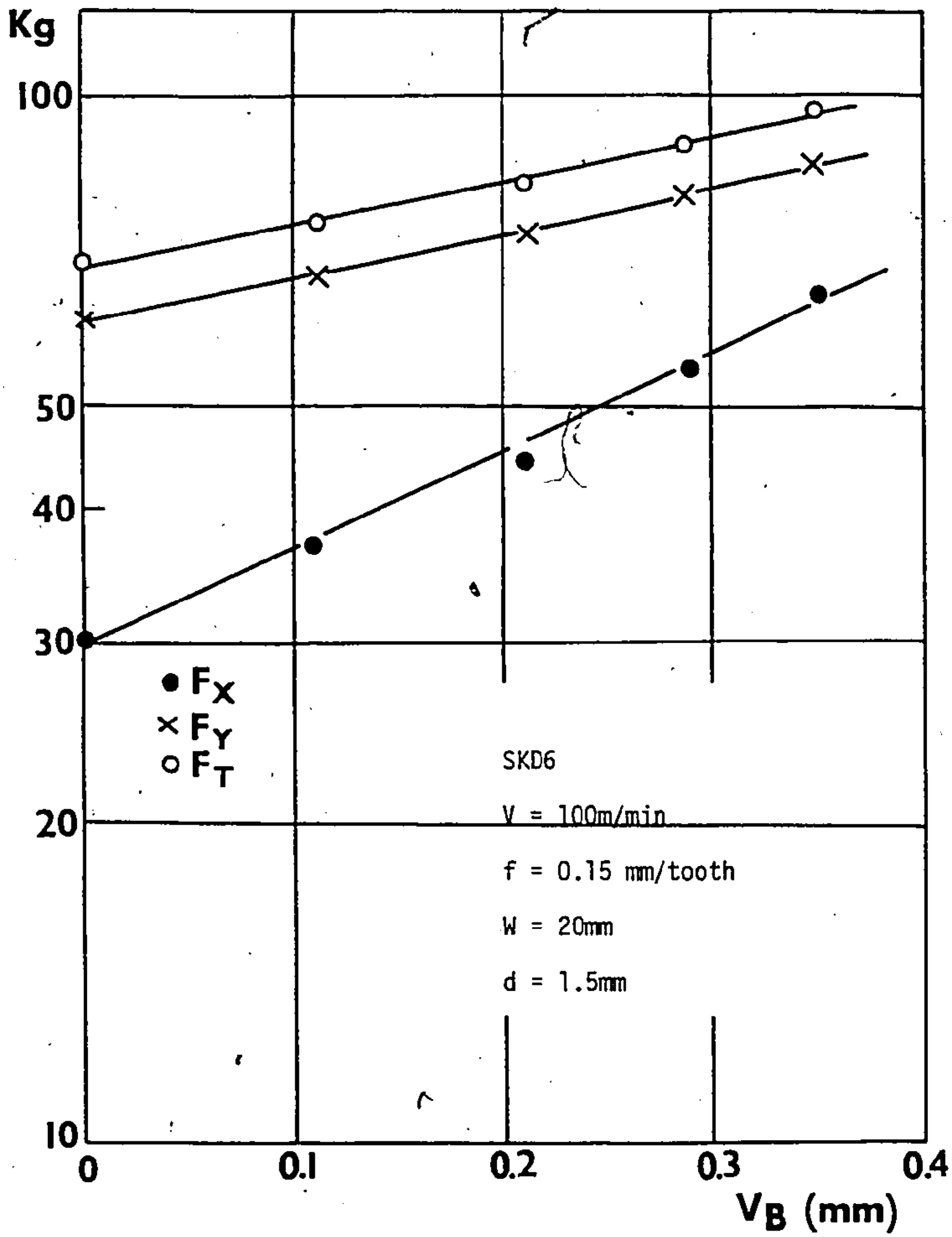

Example of Relation Between Cutting Force and Tool Wear {15}

FIGURE 2.4

magnetic transducers have been proposed for measurement of forces and torques [18].

A correlation between the vibrations of a machine tool (particularly lathes) and tool wear has been reported by several researchers [19,20]. It has been stated in reference [19] that the vibration of a tool in turning and in stable conditions is produced by the friction of the flank face of the tool on the workpiece. Martin, et al. [21] measured the vibrations in the direction of the main cutting force of a lathe tool during conventional cutting as a function of the cutting and wear parameters. The variables considered were:-cutting speed V, feed rate S, land wear of the tool VB. In the range of the tests performed, the power of the acceleration signal determined by spectral analysis was found to be a linear function of the cutting speed and of the tool wear. The signal increased in the ratio 1:10 between the new tool and the worn tool. Figure 2.5 shows that the power spectral density P, proportional to the real power versus SV (volume of material removed in the unit of time), varies with different values of wear land. The power P versus tool wear for different cutting conditions is shown in figure 2.6.

Grinding wheel wear was also measured using vibration signals [22]. The measurement of tool wear by sonic vibration has also been studied [19,23]. By dividing the vibration signal in two components, high and low frequency, it has been reported that the ratio between these two components can pro-

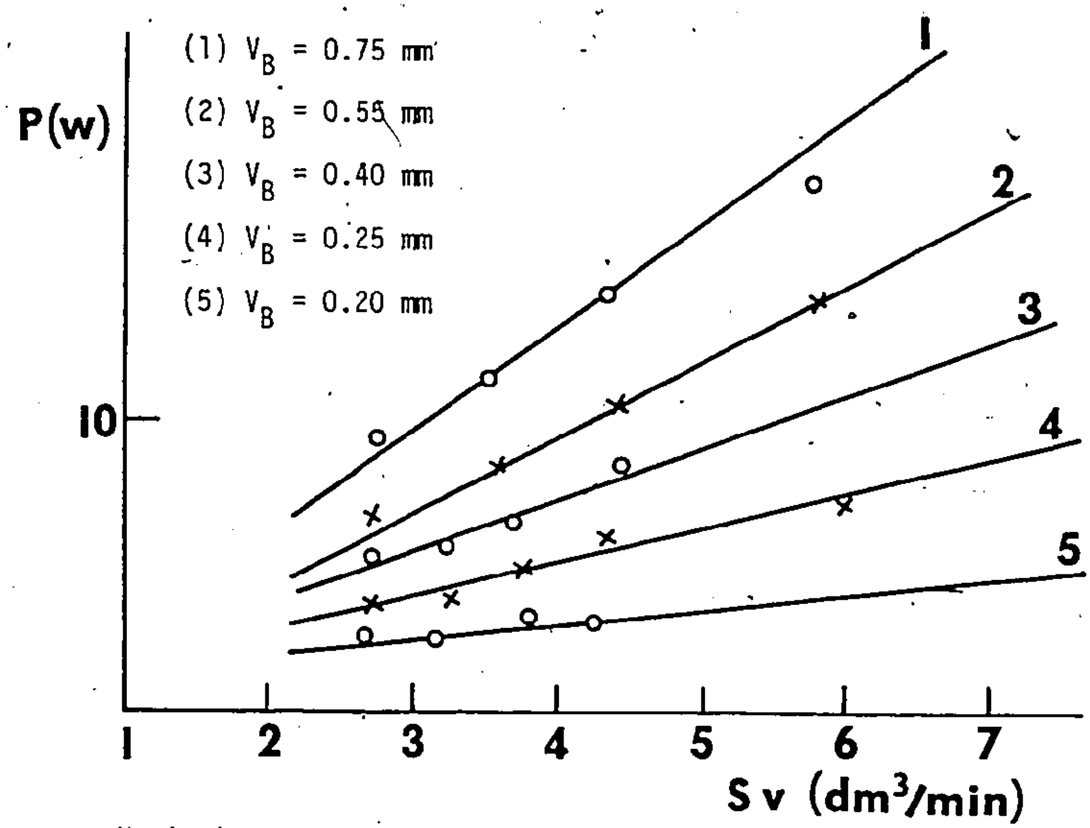

Variation of the Experimental Acceleration Signal Power P with S v[21]

FIGURE 2.5

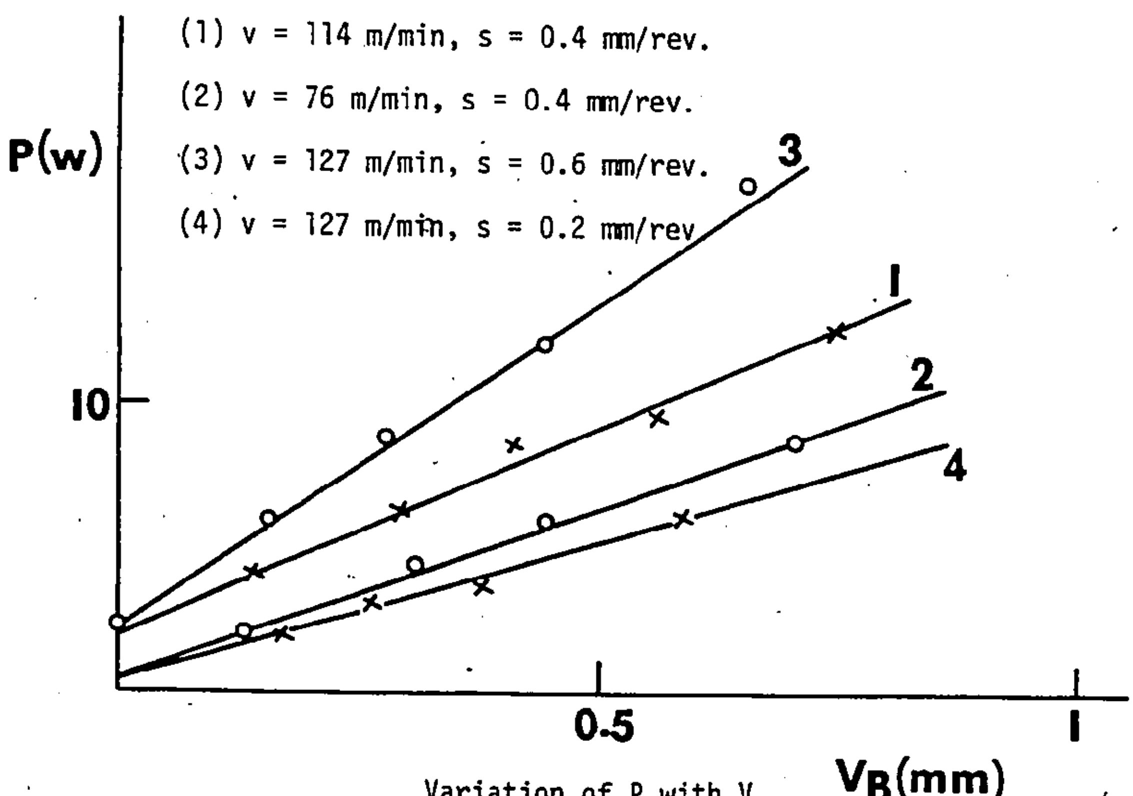

Variation of P with V_B

FIGURE 2.6

vide a measure of tool wear. The high frequency component, due to the rubbing of the flank against the workpiece increases in amplitude as tool wear develops.

Olsen {24} has studied the problem of detecting surface roughness as a parameter to keep constantly under control in AC machine tools. Spurgeon and Slater {25} have shown the influence of a worn tool on surface roughness. Murray {26} measured on-line the surface roughness in grinding, using a laser beam.

Some researchers {27,28} have attempted to detect changes in the workpiece dimensions (depth of cut) as the cutting tool wears during the cutting operation. The diameter of the rotating workpiece (e.g. turning) can be measured in process with contacting or non-contacting devices (electrical, pneumatic, etc.), and especially in grinding, this technique is simple to apply. Tool wear is then directly related to the dimensional change in the workpiece - the depth of cut variation corresponding to the land wear of the tool in turning.

Electric feeler micrometers, ultrasonic methods, and pneumatic gauges have been suggested to determine on-line the distance between the tool post and the workpiece {29,30}. The idea is that during the cutting operation, as the tool wears, the distance between the tool post and the workpiece decreases.

For several years, attempts have been made to measure temperature of the tool tip {31,32,33,34} and to use the signal as an adaptive control parameter. The methods used to measure cutting temperature are based:- a) on the tool workpiece thermocouple, b) on remote or imbedded thermocouple, c) on infrared system. There are some difficulties in the application of these methods at the shop floor, mostly because of calibration and sensitivity to the composition of the tool and workpiece materials.

Pioneer work in the field of ACO was done by Centner and Idelsohn [35]. In their paper, an adaptive milling machine controller to maximize operating profits is described. An index of performance (P) was proposed in reference [35] for milling machine applications:

$$P = \frac{M\,R\,R}{K_1 + \frac{(K_1\tau + K_2B)\ TWR}{Wo}} \qquad (2.1)$$

where MRR = Metal - removal rate in.^{3}/min.

TWR = Tool-Wear rate, in./min.

Wo = Maximum allowable tool wear, in.

K_1 = Direct labour plus overhead rate, dollars/min.

K_2 = Cost per grind + $\frac{\text{initial tool cost, dollars}}{\text{maximum number of regrinds}}$

τ = Tool change down time, min.

B = Constant: $0 \leq B \leq 1$

The chosen value of B determines the relative emphasis upon production rate and total cost. When B = 1, cost is emphasized, where as B = 0 emphasizes production rate. Intermediate values provide a compromise between the two extremes. A development of P as given by equation (2.1) is provided in reference [35], as well as an argument justifying its maximization at each instant of time by controlling milling rate (MRR) as a desirable outcome of adaptive action. In the study program reported, the method of steepest ascent and the incremental adjustment method were compared and it was found that steepest ascent provides superior performance in this particular application.

A further realization of ACO systems was the Cincinnati Acramizer System [37,38] in which an analog computer optimizes feed rate and spindle speed conditions for the maximum chip per tooth compatible with the constraints and simultaneously tries to maintain a constant rate of tool wear in order to accomplish the economic tool life required. Porter and Summers [39] investigated the problems related to the selection of an appropriate control strategy as far as convergence and stability were concerned. The performance of some eleven strategies, working each on three metal cutting models, were simulated on a digital computer. Takeyama, et al. [40], based on an extensive set of experiments, suggested a performance index suited to the on-line optimizing control of a machine tool. The optimization is achieved by measuring the derivative of cutting force, which is proportional to the tool wear rate, and by computing the performance index taking important constraints into consideration. The constraints suggested by the authors are cutting force, power and surface roughness. Frost-Smith [41] argues that to get maximum benefit from optimizing the cutting process it is necessary to study the overall workshop process from machine scheduling to cutter wear control and thus to consider the possibility of on-line control in the widest sense. Bedini, et al. [42,43,44] described a test installation for a research on adaptive control of metal cutting process for milling operations. A time-shared IBM-1800 computer operates as adaptive controller on a numerically controlled machining center. Simulation studies were reported in this paper in order to examine the performance of the chosen optimization algorithm and to test the convergence and stability of the control loop. The authors explained that for the common optimization criteria (e.g. minimum cost, maximum production), neglecting tool cost, the optimum working conditions correspond to the maximum feed rate compatible with the maximum available power. The authors also realized that gap elimination is of importance in gaining added productivity. Whenever the controller senses a bending signal lower than a prefixed value, it sets the maximum feed rate for the air gaps and a spindle speed which allows the lowest feed per tooth. As the cutter again encounters metal, the controller immediately reduces the feed rate to a safe value imposing at the same time a spindle speed corresponding to the minimum feed per tooth.

Yamazaki, et al. [15] carried out an optimizing control test in end milling. They have suggested three methods of in-process measurement of tool wear:

1. Indirect measurement by using cutting forces
2. Indirect measurement through cutting sound
3. Direct measurement by light reflection.

On the other hand, in order to identify the relationship between tool wear and net cutting time, an expanded tool life equation model involving cutting conditions, tool wear and net cutting time has been suggested, it is for constant width of cut:

$$V_B = e^{-4.90} V^{0.56} d^{0.25} f^{0.06} T^{0.46} \text{ ------- } (2.2)$$

for $V_B \leq 0.3$ mm

where V_B = width of flank wear (mm)

V = cutting speed (m/min.)

f = feed/tooth (mm/tooth)

d = depth of cut (mm)

T = net cutting time (min.)

Furthermore, because of intermittence in the milling process, the authors indicate that the tool wear may be more adversely affected by the impact on the tool bit than by continuous cutting such as turning. Accordingly chipping of the cutting edge caused by impact becomes a problem.

Prior to this occuring, it is necessary to identify the safety zone for cutting speed and feed, where catastrophic failure such as chipping rarely happens. An adaptive control algorithm was also suggested and simulated in order to verify the feasibility of this approach.

Selim and Moisan {45} proposed a method for verifying the validity of the selected performance index in ACO with a view to meeting certain requirements.

Fujita et al. [46] described an ACO system for an NC Lathe using a minicomputer. In this system a highly sensitive micrometer is used as collision detector and the control is carried out by signals from it.

A more general approach to the problem of adaptive control of metal cutting machine tools would require considering the geometrical and technological problem together. Very little has been done in this direction. Peklenik [47] gave a systematic survey of the basic concepts of the geometrical adaptive control (GAC), which must be integrated into the automated manufacturing systems for maintaining the stability of the output quality at the required level. Peklenik's concept of a manufacturing system is illustrated in figure 2.7. The manufacturing process represents the process to be controlled by means of variation of various parameters affecting its transfer functions. The inputs are defined as follows:- geometry of the component to be manufactured; the physical properties of the material and the shape of the tool, as well as the physical properties of the cutting tool material. The output parameters are:- the material removed; the surface generated considering the shape, dimensions and surface, as well as the accuracy of these parameters, various disturbances such as displacements, force temperatures, etc.

The machine tool represents the feed-back of the manufacturing system and basically consists of three different

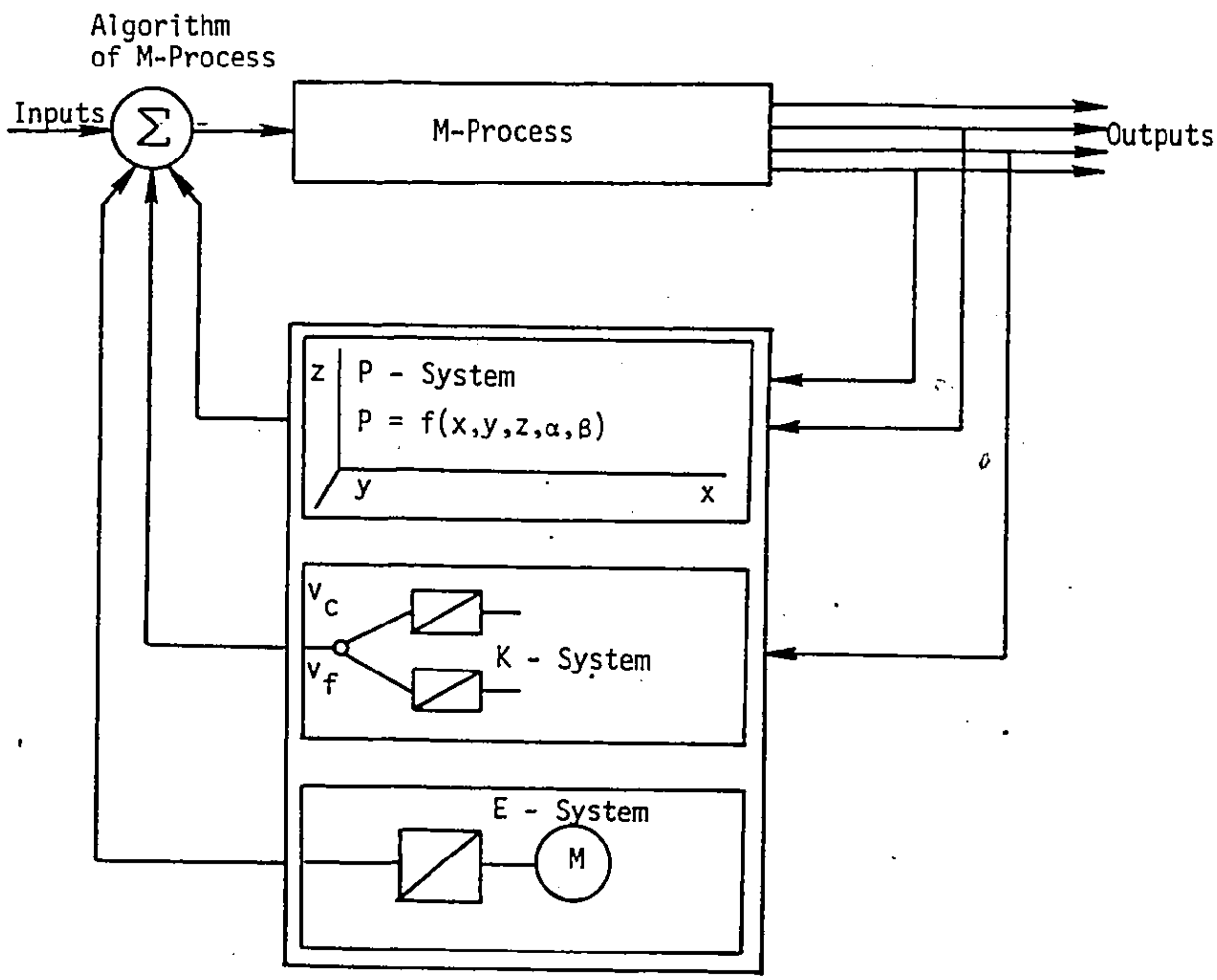

Concept of a Manufacturing System [47]

FIGURE 2.7

systems:- the positioning, kinematics and power system. Through the kinematic system the component enters repeatedly into the process. The summation point Σ embraced all the input parameters provided by the machine tool, the part and the tool characteristics. The geometrical adaptive control system is primarily designed for maintaining the stability of the dimensional accuracy, for improving the shape accuracy and surface roughness, as well as for adaption of the geometrical position of the tool relative to the generated surface in order to improve the efficiency of a manufacturing system and prevent a catastrophic event of tool damage. The assessment of the input geometry takes place "on-line" by various measuring systems representing one of the basic units of adaptive controls. The second unit is the compensation system for controlling the tool position according to geometrical requirements of the output.

Jona [48] indicated that in order to make geometrical adaptive control feasible an adequate reference system and an adequate transducer must be found. He suggested that there is no general solution to this problem and that each type of machine tool must be analysed separately. For the case of a late, the author concluded in his paper that a transducer attached to the tool-post could indicate any periodic deviation from the correct form due to relative motion between tool-post and workpiece, and measure deviations due to other causes (tool wear, irregularities of the cutting process, etc.).

Surface roughness should always be measured along the direction which gives the maximum roughness value. When the surface texture shows a definite lay, the maximum reading is obtained with measurements along a direction perpendicular to the surface lay. Experimental results are given for low-speed tracing of reference turned surface using the "Fotonic Sensor", which is defined as an optical proximity detector that utilizes fiber optics to guage the distance between probe and any reflecting surface through the intensity of reflected light. The author suggested that the same transducer could be used for monitoring roughness (high-frequency component), waviness (low-frequency component) and overall dimension variations, such as would, for instance be caused by tool nose wear (very slow variation, d.c. component). Band-pass filters could be used for this purpose. These signals could naturally be used to control the machine tool's settings.

For a lathe also, Spur and Pritschow [49] described a geometrical adaptive controller which adjusts the depth of cut and therefore, modifies the tool path. It would appear however, that many difficulties could arise in extending this approach to a three-dimensional milling process.

An alternative approach to ACO systems is often reported as "AC operating per constraints" because the performance index is not directly evaluated but the controller acts on the inputs in order that some process variables attain prefixed constraints. These preset constraints could be:-

1. Maximum spindle speed
2. Minimum spindle speed

3. Maximum force
4. Maximum chip load
5. Maximum torque
6. Maximum feed-rate
7. Maximum vibration
8. Minimum chip load
9. Maximum power

Early realizations of such AC constraints systems could be found in references 37, 50, 51 and 52. Ledergerber [53] described an ACC system for turning operations. The sensend variables were the torque and the cutting force. The controlled variables were the cutting speed and feed. Based on a set of experiments of machining forged blanks, the author reported 30% savings in programming time.

Lankford [54] used an IBM-1800 minicomputer to control a milling machine in adaptive mode. In this system, adaptive control of the cutting process is based on control of the feed rate of the cutting tool. The feed rate is repeatedly changed in real time in response to varying conditions at the point where the tool cuts metal. Feed rate modification was based primarily on measurement of force of deflection on the tool. The tool is moved at high feed rates in air gaps. Air gaps were sensed either by the absence of electrical contact between the tool and part or by the change in deflection force, depending on the algorithm in use. When contact between the tool and part is sensed, the feed rate is reduced drastically to prevent tool breakage and marring of the part. In his paper, the author reported that based on experimental results, the machining time was cut by one-third.

A similar system is reported in references 55 and 56. The author in these papers pointed out the importance of obtaining experimentally the practical constraints for adaptive control of feed rate, and most important obtaining the relationship of cutter deflection with respect to the changes of depth of cut, width of cut, feed rate, spindle speed, physical properties of the material being cut, tool wear and other related environment parameters.

Beadle and Bollinger {34} described a test installation, designed and constructed in order to investigate various techniques for adaptively controlling the cutting process, and pointed out the future prospectiveness offered by the modern systems of direct and computerized numerical control.

Tlusty, et al. {57} used an HP 2100A minicomputer as an adaptive controller for a retrofitted vertical milling machine. The purpose of the adaptive control in this system is to keep the force acting on end milling cutters in die sinking operations constant, and at a value safely below the one which would break the cutter. The controlled variable is the feed rate.

Stute and Goetz {58} explained that one of the problems encountered in the use of adaptive control constraint systems for milling machines, is the possible large variation of the gain of the controlled process which depends on the machining conditions. For example, according to the variations in width or depth of cut, the ratio of cutting force to feed rate widely changes, and so does the gain of the open loop transfer function of the system. If there is a controlled process in which the gain changes, then the behaviour of the control may become worse because the parameters of the controller are constant. If the gain of the controlled process becomes too large, the stability and therefore, the safety of machining will be in danger. The authors therefore, suggested that with the aid of a dynamic model parrallel to the controlled process, the variable gain can be determined and compensated by changing the control signal.

A second problem is reported in ACC systems for milling which uses the cutting force as the sensed variable and the feed rate as the controlled variable. This problem is the time lag of the feed rate response to an actual cutting force variation {59}. This time lag is due to the interval between the action of individual cutter teeth and may cause instability in the adaptive control loop.

Gieseke {60} described an adaptive control constraint and automatic cut distribution system for turning operations. The system regulates cutting power according to a pre-determined value and permits automatic distribution of the cutting volume in individual cuts, using a special cutting distribution plan. The NC program only contains technological data and the description of the finished part contour, so that the shape and size of the rough part need not be known. These can therefore, vary as they occur, without unnecessary idle travel. The control system consists of an analogue part for power control and a digital part for the automatic cut distribution. The functions of the digital part are handled to a large extent by the minicomputer, which is already available in the computer numerical control (CNC) system. The author explained that cutting power control can be carried out either directly, that is with a power sensor and a power controller, or indirectly with a cutting speed and cutting force controller and the appropriate sensors. The advantage with the indirect method is that in addition to the performance regulation or supervision over the whole turning radius range, a defined cutting speed can be pre-determined and a defined cutting force can be adhered to, so that apart from machine supervision a tool supervision is also possible. A Proportional Integral (P-I) controller was suggested in planning the cutting force controller. It was explained in the reference also that the control amplification must be made proportional to the workpiece revolutions per minute and the integration constant proportional to the square of the workpiece revolution per minute. Finally a program saving of 75% was reported using this technique.

The application of digital adaptive control can provide, at relatively low expense, a control circuit behaviour which is suited to the particular requirements of turning operations [61]. By switching over the controller parameters with relation to work sequence, serious control deviations, especially overshoot, can be corrected quickly. The optimum circuit behaviour can be obtained in the whole spindle speed range, by quasi-continuous adjustment of the controller parameters to the changed path parameters (changes in spindle speed).

The flexibility of digital adaptive control permits a simplified adaptation to different paths and reduces the outlay in integrating the controller into the system of control and machine.

Adaptive Control for milling with strategies for avoiding chatter vibrations and for automatic distributions was reported in references [3,4]. The measured spindle torque serves as an input quantity for the adaptive control unit, which maintains the machine load at a constant value. The setting parameter is the feed rate. The torque signal is also used to recognize the entry into and the exit from the workpiece by the milling cutter, as well as to recognize superimposed self-excited and forced vibrations. When such instabilities arise, the spindle revolution rate or the depth of cut act as setting values in a control strategy for automatic cut distribution.

It was shown in these two references that the frequencies of self-excited vibrations vary according to the dynamic characteristics of the machine in the approximate range of

15 Hz. to 500 Hz. The frequencies of forced vibrations, however, seldom reach values higher than 100 Hz. for milling machines. The differentiation between forced and self-excited vibrations is therefore possible by selection of the frequency components. From the whole signal spectrum obtained from the pickup, the frequency range of forced vibrations is selected. This may be performed by a narrow band-pass filter. In doing so, it is assumed that the frequencies of forced vibrations, i.e. frequencies of tooth impacts of the cutter in the case of milling are known. The frequency of the self-excited (chatter) vibrations can only appear in the residual band-rejection spectrum (see figure 2.8).

Brecker and Shum [62] pointed out that the successful application of in-process adaptive control depends on the characteristics of the machine tool to which the control is applied as well as the characteristics of the control itself. The response time of the control has to match the response characteristics of the machine tool. The high-gain control required to react to tool work collision and to control small cuts can lead to operational instabilities. Tool-work collision detection systems based on power, force, and vibration are discussed in this reference as is variable gain control. Experimental data are presented to show the importance of reducing tool impact; a significant reduction in flank wear in climb milling occurs when the tool is eased into the work.

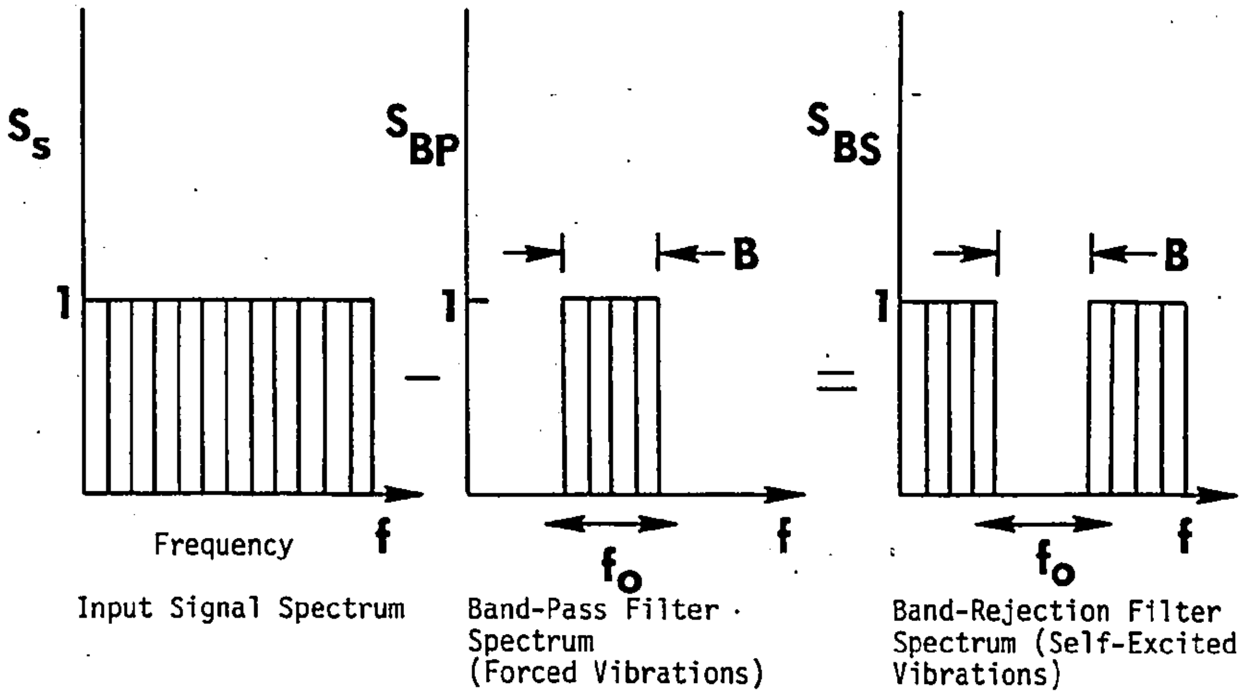

Frequency Selection of the Input Signal Spectrum Obtained from the Pick-Up {4}

FIGURE 2.8

An air gap sensing system is described which permits controlled tool-work impact. This sensing system is particularly of interest since most adaptive control constraint systems used in practice switch off AC for penetration of walls and for approach of corners and program slow feed rate {63,64,65}. The air-gap sensor described in reference {62} detects changes in magnetic flux as the tool approaches the work. As shown in figure 2.9, an excitation coil, 1, is mounted on the machine spindle housing and a search coil, 2, is mounted below it close to the tool. The magnetic flux changes as the distance between tool and workpiece varies. A mutual inductance bridge is used to sense the change. When the air gap is smaller than a preset value, say 1/8 inch (3 mm.), the feed is changed to an allowable impact feed rate. As a result, pre-positioning can be done at rapid traverse feed rate with a consequent reduction in air cutting time.

One of the necessary requirements for successful operation of the adaptive control is the availability of reliable and accurate relationships between the machining conditions and machining response as well as constraints. Very little data has been published about practical values for the constraints in AC systems. Tipnis, et al. {66} used the results of a set of statistically planned experiments to develop mathematical models of the machining response in terms of end mill cutter wear, tool life, cutting forces, surface finish, etc. Figure 2.10 shows the cutter breakage forces vs. axial depth of cut for 1 inch (25.4 mm.) dia., 2 inch (50.8 mm.)

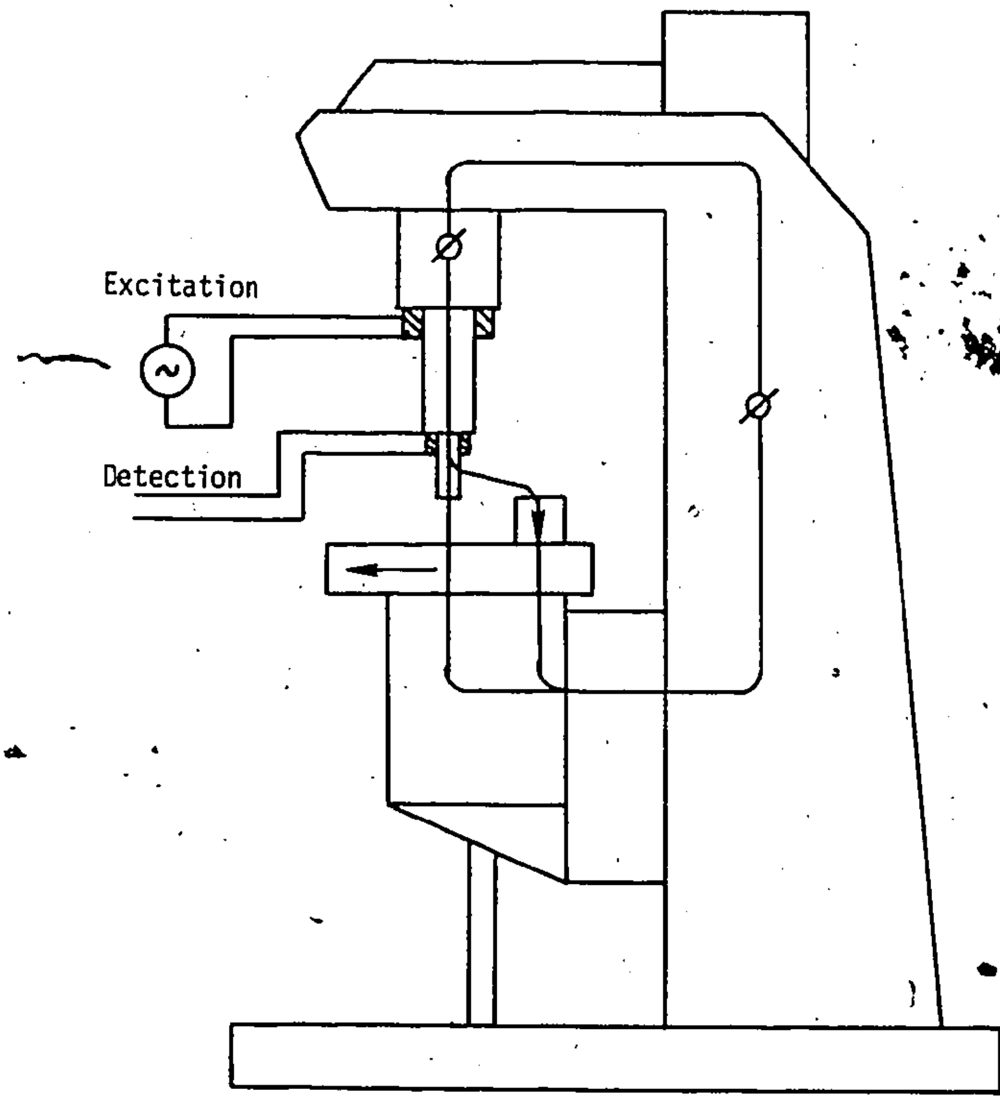

Air Gap Sensing System for Tool-Work Impact Control [62]

FIGURE 2.9

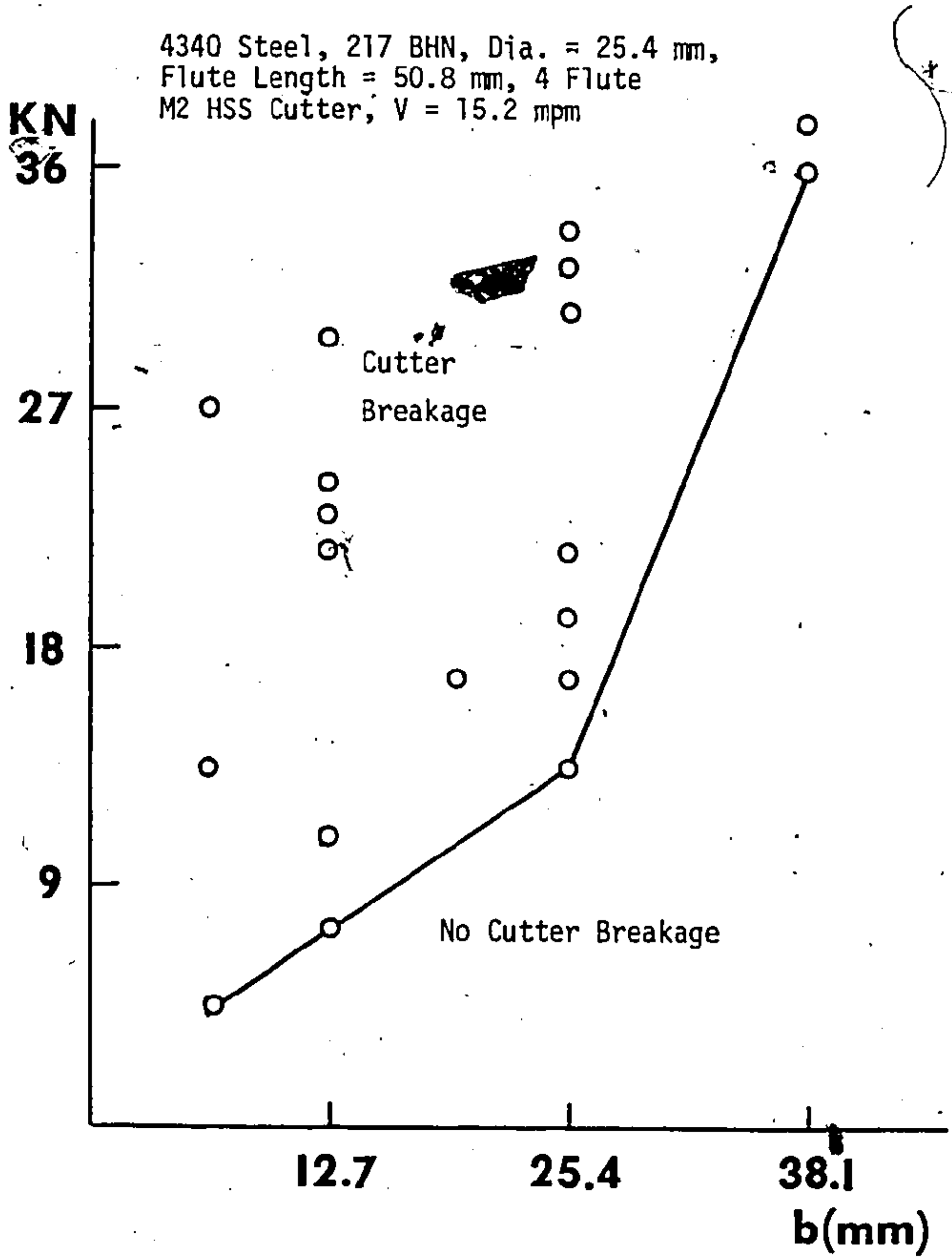

Cutter Breakage Forces vs. Axial Depth of Cut {66}

FIGURE 2.10

flute length end milling cutter. This graph, however, does not distinguish between tool and shank breakages. It might be more practical to separate tooth breakage and relate it to a maximum feed per tooth.

CHAPTER 3

GENERAL DESCRIPTION OF THE CNC/AC SYSTEM

3.1 General

The CNC concept means to have a mini-computer for on-line control of a machine tool. The block diagram of the system is shown in figure 3.1. It includes five major components:

1. The milling machine itself which is a 2½ axis NC retrofit of a conventional vertical knee type milling machine (No.4) model ZBROJOVKA - FA4V.
2. A Hewlett Packard mini-computer model 2100A with 16 bit word and 32K of core memory which otherwise is a part of a Fourier Analyzer System.
3. A data conversion system.
4. A time Base Generator (TBG).
5. A controller which contains 3 control circuits for the 3 axes of motion of the milling machine.

The milling machine is equipped with DC servomotors as feed drives, resolvers as positional feedback elements and DC tacho-generators as velocity feedback devices. The spindle is driven by a three phase motor and its speed is not controlled by the CNC system.

A special sensor for on-line measurements of the radial cutting force is used. In order to determine the force "F_R", two perpendicular components "F_X" and "F_Y" are sensed. The

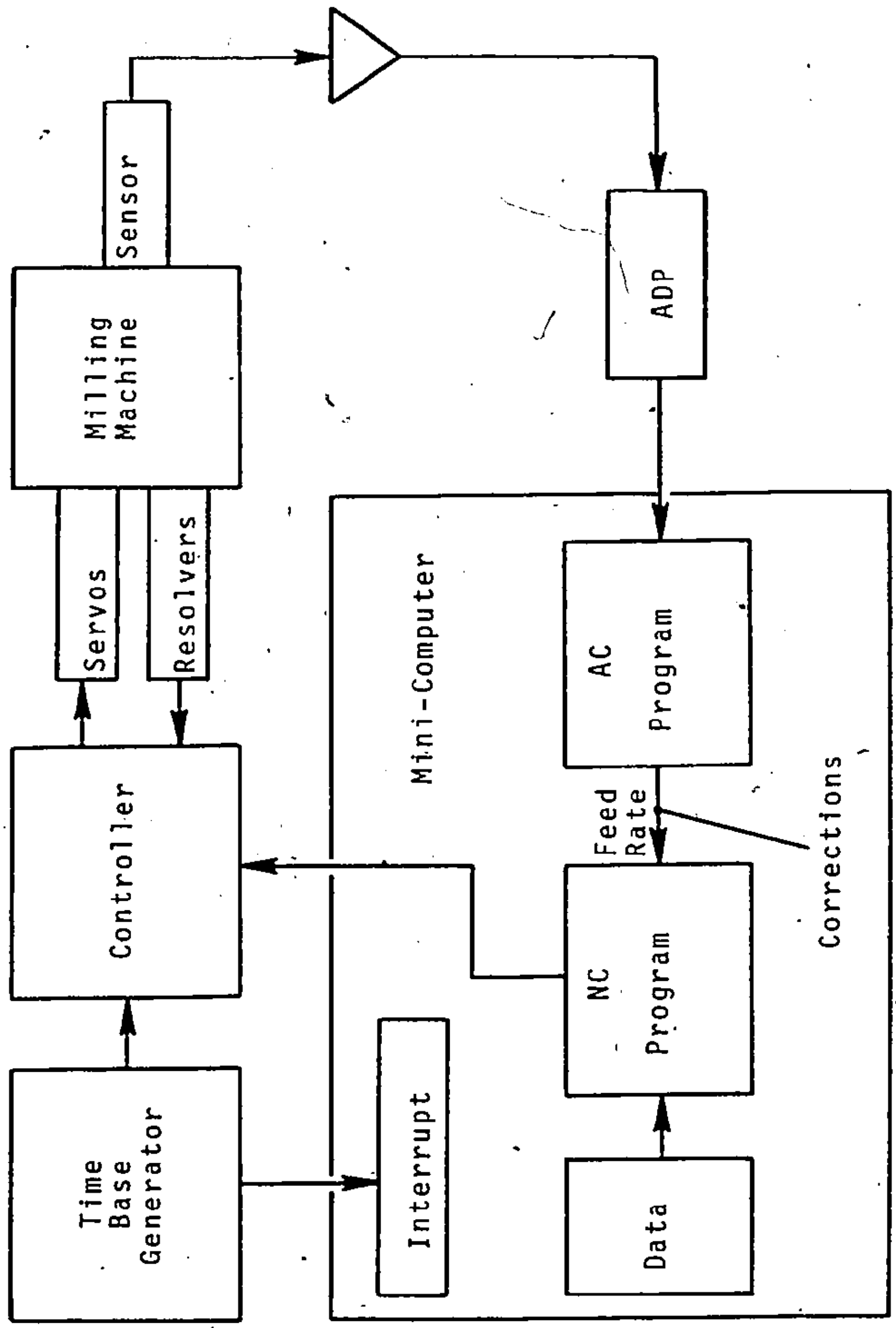

Block Diagram of the CNC/AC System

FIGURE 3.1

sensor outputs are fed through an Analog-To-Digital Processor (ADP) to the computer. The computer handles two programs: NC and adaptive control (A/C) programs. The interrupt system of the computer takes care of the simultaneous running of both programs. The A/C program accepts the sensor outputs and uses them to calculate a feed-rate correction which is supplied to the NC program. The corrections are provided continuously throughout the cutting process in order to maintain maximum feed-rate compatible with the limitations imposed by the constraints. Normally the computer carries out the A/C program, and whenever an interrupt occurs, the JSB instruction (JSB = Jump to Subroutine) causes the computer to transfer its control to the NC program. This instruction also automatically saves the return address for a later return to the A/C program, thus when the NC program is terminated the computer continues to perform the A/C program from the point at which it was interrupted.

The computer is equipped with three types of lines: Interrupt input line, Digital output line, Digital input line. The digital output lines are used for transferring data from the computer through the controller to the machine drives. For each machine axis two lines are required: one for the sign and the other for command pulses. Each pulse will cause a motion of 0.0001 inch/(0.0025 mm). This unit is the system resolution and will be denoted henceforth as the basic length unit (BLU).

The data for the A/C program has to be updated by continuous information about the cutting process. The measured variables "F_X" and "F_Y" are converted to a binary form by Analog-To-Digital Converters (ADC) and transferred to the computer via the digital input lines. The two ADC's are included in the ADP.

The TBG controls the timing of the system. It provides the following functions:

1. Supplying clock pulses of 2.5 MHZ frequency to the control loops.

2. Providing interrupt pulses to the computer. Each interrupt pulse starts the NC program running. the frequency of the interrupt pulses establishes the maximum feed-rate which can be achieved . This is calculated by using the following formula:

$$FRM = IPF \times BLU \times 60 \quad \text{------------------}(3.1)$$

where FRM is maximum feed-rate (in contouring) in ipm.

IPF - Interrupt pulses frequencies in pps.

The IPF is limited by the number of instructions in the NC program, and by the instruction execution time. In our own system IPF = 5000 pps and therefore, FRM = 30 ipm (750 mm/min.).

3. Producing two sine-waves, 90 degrees phase-shifted, which are fed as reference signals to the stators of the resolvers. The frequency of these signals is 2.5 KHZ. In order to synchronize the system, a 2.5 MHZ pulse-generator is used as the source for all these signals.

The controller contains a control circuit for each axis-of-motion. The circuit transforms the train of pulses from the computer command line into a phase-modulated command signal and compares it with the phase-modulated feedback signal. The result is the velocity command, which is fed via an amplification unit to the feed motor.

The positional control is performed by the position loop and software counters, which are contained in the NC program. The counters are loaded with the require incremental distance at the beginning of a segment. Each axis-of-motion is provided with a counter. Each time a command pulse is sent out by the computer, the contents of the appropriate counter are reduced by the one unit. The phase-comparators in the control circuits are never in saturation, thus accomplishing the positional control.

3.2 The CNC/AC Hardware System

3.2.1 Position Control

Position control in the system is carried out in a closed-loop mode with synchro resolvers as feedback devices. A block diagram of the position control loop in which the resolver is used as sensing device is shown in figure 3.2. This block diagram is identical for all three axes of the milling machine.

In the software interpolator in the mini-computer the simulated Digital Differential Analyzers send command pulses to each controlled axis of the table. Each pulse causes an advance of one BLU along the appropriate axis-of-motion.

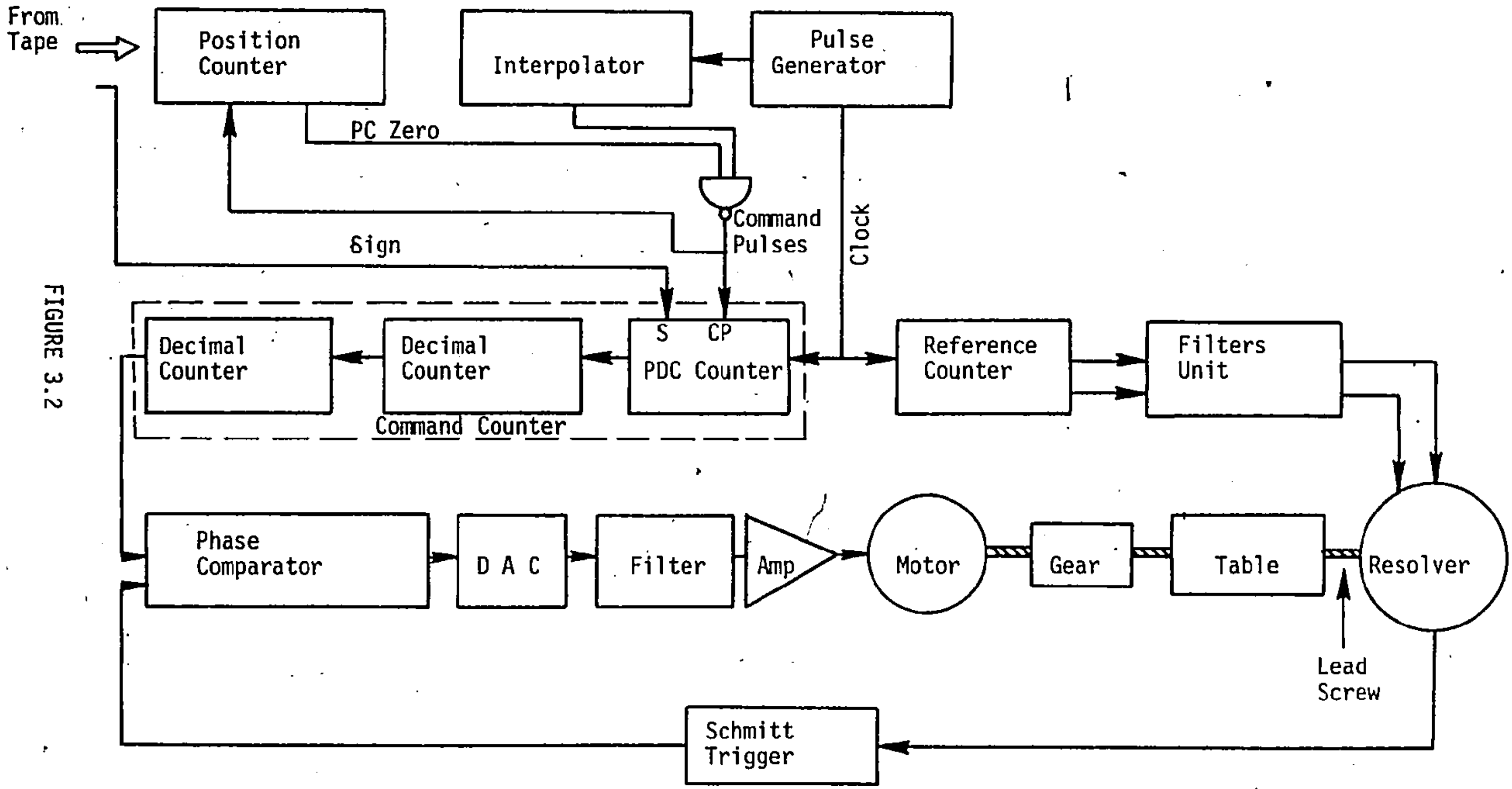

Block Diagram of the Position Control System

FIGURE 3.2

This means that the frequency of the command pulses is proportional to the velocity of the table in the corresponding direction.

Positional control is effected by position counters. Each axis-of-motion is provided with a counter to which the required incremental distance is fed from the perforated tape.

The reference counter divides the clock frequency, emitted by the pulse generator (2.5 MHZ), by a factor of 1000 and provides (by digital techniques) two square-wave signals in exact quadrature, characterized as the reference signals. The latter are converted by low-pass filters into sine-wave signals, which are used as excitation voltages V_1 and V_2 for the resolver stator windings. It is:-

$$V_1(t) = V_a \sin W_o t \qquad (3.2a)$$

$$V_2(t) = V_a \cos W_o t \qquad (3.2b)$$

The output of the resolver is the rotor signal, which is a function of the rotating angle and is obtained by inductive coupling between stator and rotor. The rotor output voltage, V_o, consists of two components:

$$V_o(t) = n\{V_1(t) \cos \phi + V_2(t) \sin \phi\} \qquad (3.3)$$

where n is a constant dependent on the rotor/stator turns ratio. Substituting $V_1(t)$ and $V_2(t)$ as above, we have:

$$V_o(t) = n\, V_a\, (\sin W_o t \cos \phi + \cos W_o t \sin \phi) \qquad (3.4)$$

or, denoting $n\, V_a = V$

$$V_o(t) = V \sin (W_o t + \phi) \qquad (3.5)$$

where $W_o = 2\pi f_o$ and f_o is the reference voltage frequency.

The phase angle ϕ depends on the angular position of the rotor axis. The rotor output voltage is fed through a wave shaping circuit (Schmitt Trigger) to a phase comparator or discriminator, where it is compared with a command signal. The phase difference between the command and feedback signals is converted into a DC voltage, passed through a single pole low pass filter, amplified and used to drive the motor.

The command signal is produced by a command counter which consists of two fixed decimal counters and a programmable -division-factor counter (PDC). The PDC is fed by the command pulses (the CP input), a clock (typical frequency 2.5 MHZ), and a logic signal called the "sign" which indicates the required direction of motion. The PDC converts the command pulses into a phase-modulated signal. Each command pulse causes a phase shift of 0.001 cycle (0.36 degree) with respect to the reference signal. The phase shift is forward or backward (i.e., leading or laggging) depending on the sign logic level. The division factor, N, of the PDC also varies in accordance with the logic level at its CP and S (sign) inputs, as shown in table 3.1.

CP	S	N
0	0	5
0	1	∞^*

1	0	10
1	1	10

* ∞ denotes a no-count condition

Table 3.1: PDC Division Factor

So long as the CP input is at the "1" level, the PDC acts as a decimal counter and its input clock frequency (2.5 MHZ) is divided by 10. Therefore, so long as the resolver is at rest, the feedback and command signals have the same frequency (2.5 KHZ) and are exactly in phase; as a result, the velocity command signal (V_c) is zero and the motor also remains at standstill.

In the case CP = 1, a single cycle of the command signal is emitted by the command counter for every 1000 clock pulses. Assume now that S = 1 and CP = 0 for an interval covering a single clock pulse (400 nsec when a 2.5 MHZ clock is used). According to Table 3.1 for S = 1, the clock pulse sent in this interval is not counted ($N = \infty$), so that 1001 clock pulses are required to effect one cycle of the command signal. This means that the falling edge of the command signal lags by 1/1000 of a cycle compared with its previous state.

To illustrate a lead case, assume that CP = 0 for an interval of 10 clock pulses (i.e., 4000 nsec), and that S =0). In this interval the PDC sends only 2 pulses (since N = 5); for the following 980 pulses the PDC emits 98 pulses (since CP is reset to 1). Altogether the PDC sends 100 pulses for 990 clock pulses. In other words, 990 clock pulses are required to effect one cycle of the command signal, which means that the command signal leads by 10/1000 of a cycle. The CP input is fed by negative pulses of 400 nanoseconds width, each of which caused advance along the appropriate axis-of-motion by one BLU, i.e., 0.0001 inch. At S = 0 these pulses make the command signal lead the reference signal in phase and the motor rotates in a certain direction, similarly, at S = 1 the motor rotates in the opposite direction. When standstill is required, the CP input is at the "1" level and the PDC divides by 10.

When the command pulses are sent through the CP input, the average division factor of the PDC varies according to their frequency. The duration of each negative pulse is $T = 1/f$, f being the clock frequency (i.e., 2.5 MHZ). The highest possible frequency of the command pulses is $f/2$. If n pulses are sent in the interval to the CP input, the average frequency of the command pulses is n/t pps. We denote the ratio of the two frequencies by p:

$$p = \frac{n/t}{f} = n\frac{T}{t} \quad \text{------------------------}(3.6)$$

Since the n pulses are negative, the CP input is at the "0" level in the interval:

$$nT = pt \text{ ------------------------------- } (3.7)$$

during which the PDC count depends on the S input level. The interval in which the CP input is at the "1" level is :

$$t - nT = t(1-p) \text{ ---------------------- } (3.8)$$

during which the PDC operates as a decimal counter. The average output frequency from the PDC (while the motor rotates) is obtained from table 3.1 and equations (3.7) and (3.8). For S=1, the frequency is:

$$\frac{1}{t}\left\{\frac{f}{10} \times (1 - p)\, t + 0 \times pt\right\} = \frac{f}{10}\,(1-p) \text{ -- } (3.9)$$

For S = 0) the frequency is:

$$\frac{1}{t}\left\{\frac{f}{10} \times (1-p)t + \frac{f}{5} \times pt\right\} = \frac{f}{10}\,(1 + p) \text{ ---- } (3.10)$$

The command counter comprises two additional decimal counters which divide the PDC output by a factor of 100. Therefore, the range of the command signal frequency f_c, which is the output of the command counter, may be:

$$\frac{f}{1000}(1-p) \leq f_c \leq \frac{f}{1000}(1 + p) \text{ ---------- } (3.11)$$

Introducing the definitions:

$$f_r = \frac{f}{1000}\ ; \quad f_o = pf_r$$

f_r being the reference frequency and f_o is 1/1000 of the frequency of the command pulses entering the PDC, equation (3.11) becomes:

$$f_r - f_o \leq f_r + f_o \text{ ---------------------- } (3.12)$$

where the range of the factor p is $o \leq p \leq 1/2$.

3.2.2 Velocity Control

In order to improve the performance of the control an additional feedback loop, which uses a DC tacho generator as the feedback device, is added. The velocity command signal V_c and the tacho output are summed to generate an error signal. The error signal is fed to a stabilizing network which is shown in figure 3.3.

The output of this network is amplified and applied to the armature of the DC motor. The Servo Drive Unit contains an amplifier and a stabilizing network for each axis of motion. The stabilizing network consists of an operational amplifier and R-C network.

The Servo Drive Unit is basically a velocity controller which controls the DC motors by a switching technique known as Pulse Width Modulation (PWM). To do this the Servo Controls the width of pulses applied to the motor circuit, at a rate of 2000 pulse per second (pps). The armature current produced is related to the average pulse width. Thus, varying the pulse width effectively varies the applied motor voltage over a continuous range.

3.2.3 A/C Hardware

The block diagram of the A/C hardware system is shown in figure 3.4. Two perpendicular components "Fx" and "Fy" of the radial cutting force "F_R" were measured using two different dynamometers. The details of the design, static, and dynamic characteristics of the dynamometers used in the A/C system are

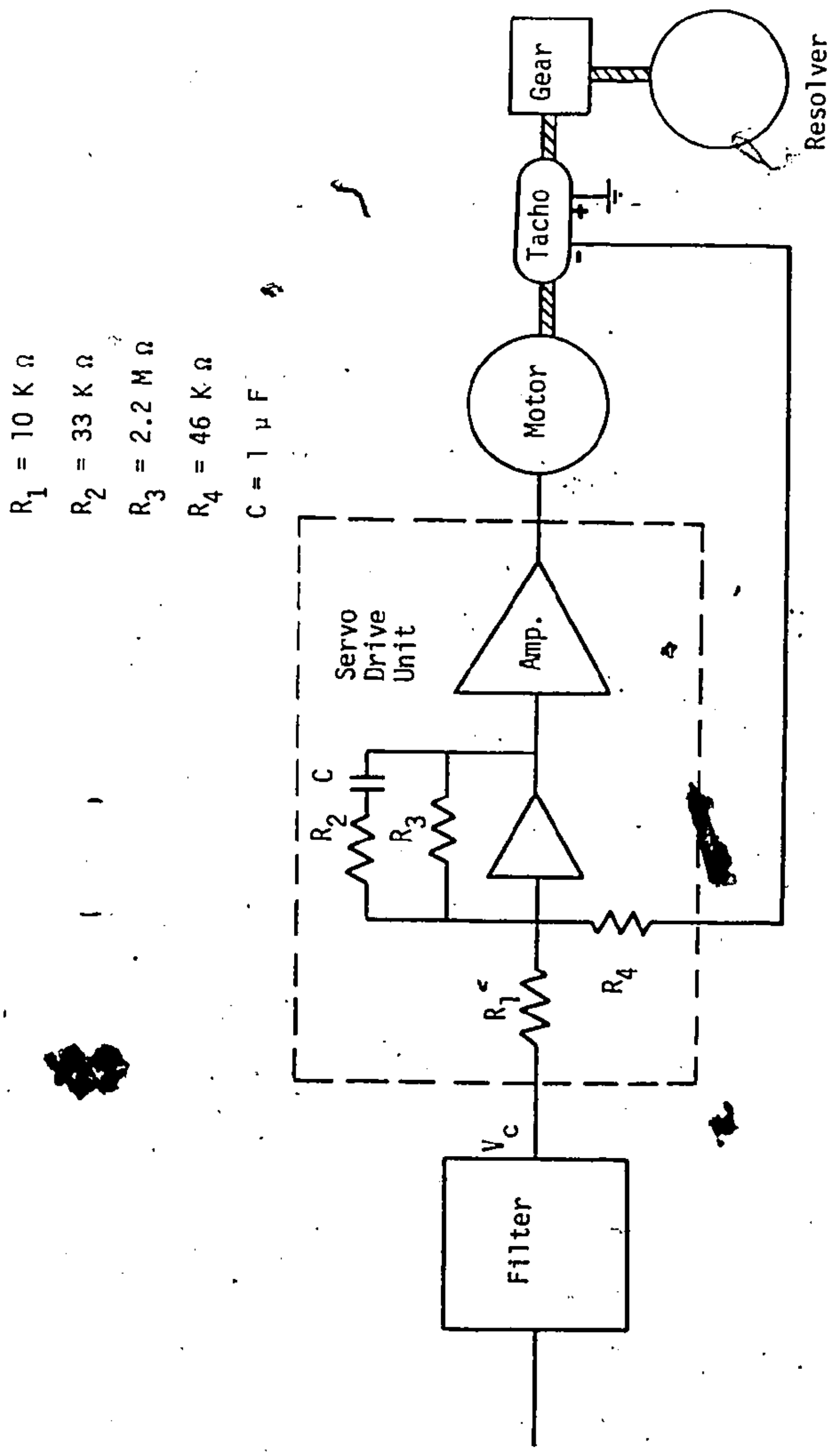

The Velocity Loop

FIGURE 3.3

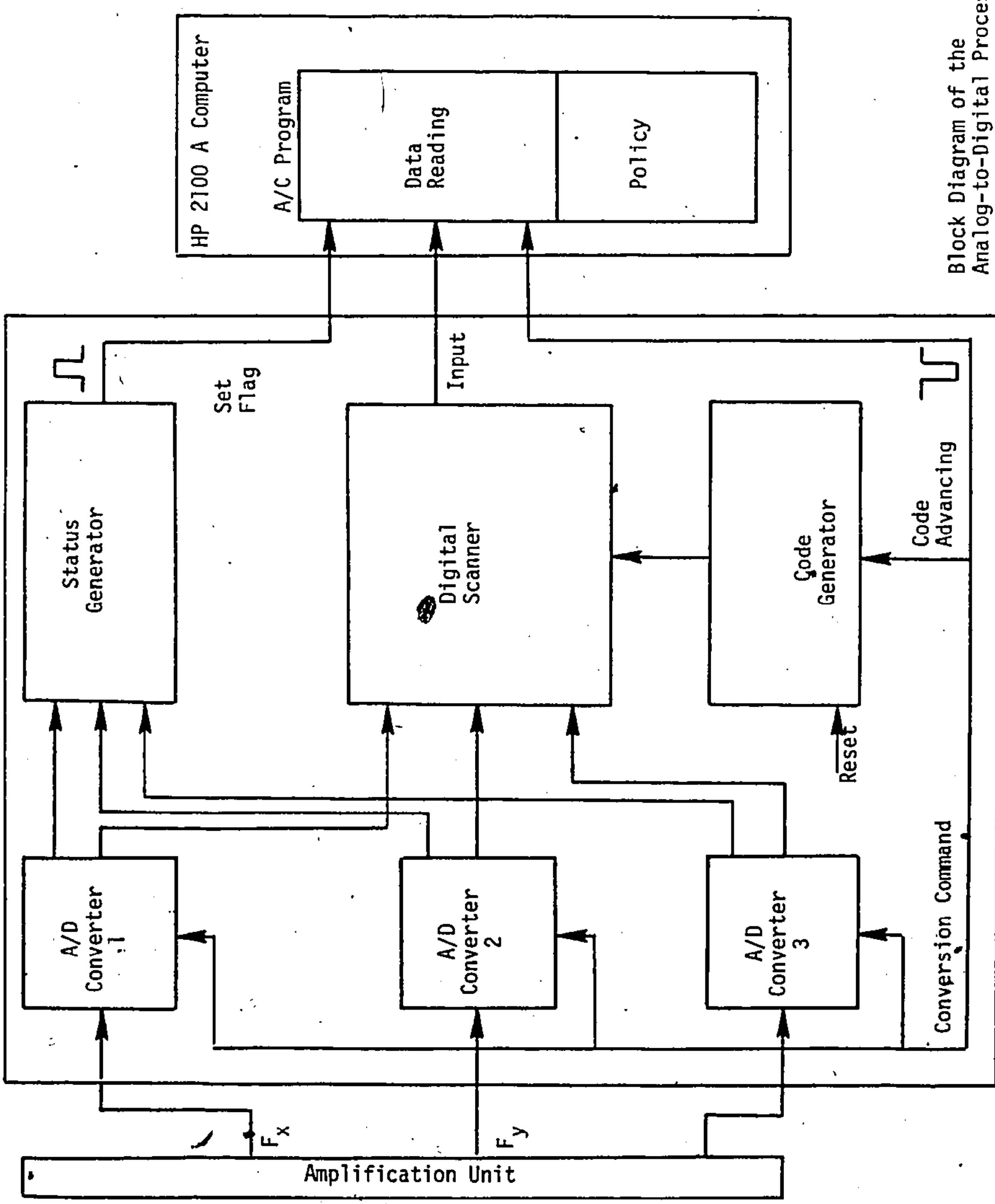

FIGURE 3.4

Block Diagram of the Analog-to-Digital Processor given in appendices I and II.

The sensor outputs are fed to an amplification unit with adjustable gain. The amplification unit consists of two operational amplifiers (Fig. 3.5) and has an output range of 0 to +10 volts. This is the voltage range acceptable by the A/D converters (ADC) used in the system.

The outputs of the amplifiers are connected to an Analog-to-Digital Processor (ADP). The ADP contains the following circuits:
two identical 10-bit ADC's, a digital scanner, a code generator and a status generator.

The data conversion begins, simultaneously in the two ADC's, on the trailing edge of a conversion command pulse. The latter pulse is generated by the Data Reading Routine (DRR) of the A/C program. The data conversion time is 20 microseconds. At a completion of a conversion, the "status" output of the appropriate ADC sends a signal to the status generator. Theoretically the two signals are received simultaneously, but in practice a time difference might exist. Therefore, when the second status signal is received, the status generator produces a pulse which is sent to set the flag of the DRR I/O Channel (located on the interface board of the computer). The set of the flag informs the DRR that the entire conversion has been accomplished and that the input data is available.

The input to the A/C program is a 13-bit word consisting of 10-bits of data plus a 3-bit code which is generated by the code generator and identifies the ADC channel. In each cycle of

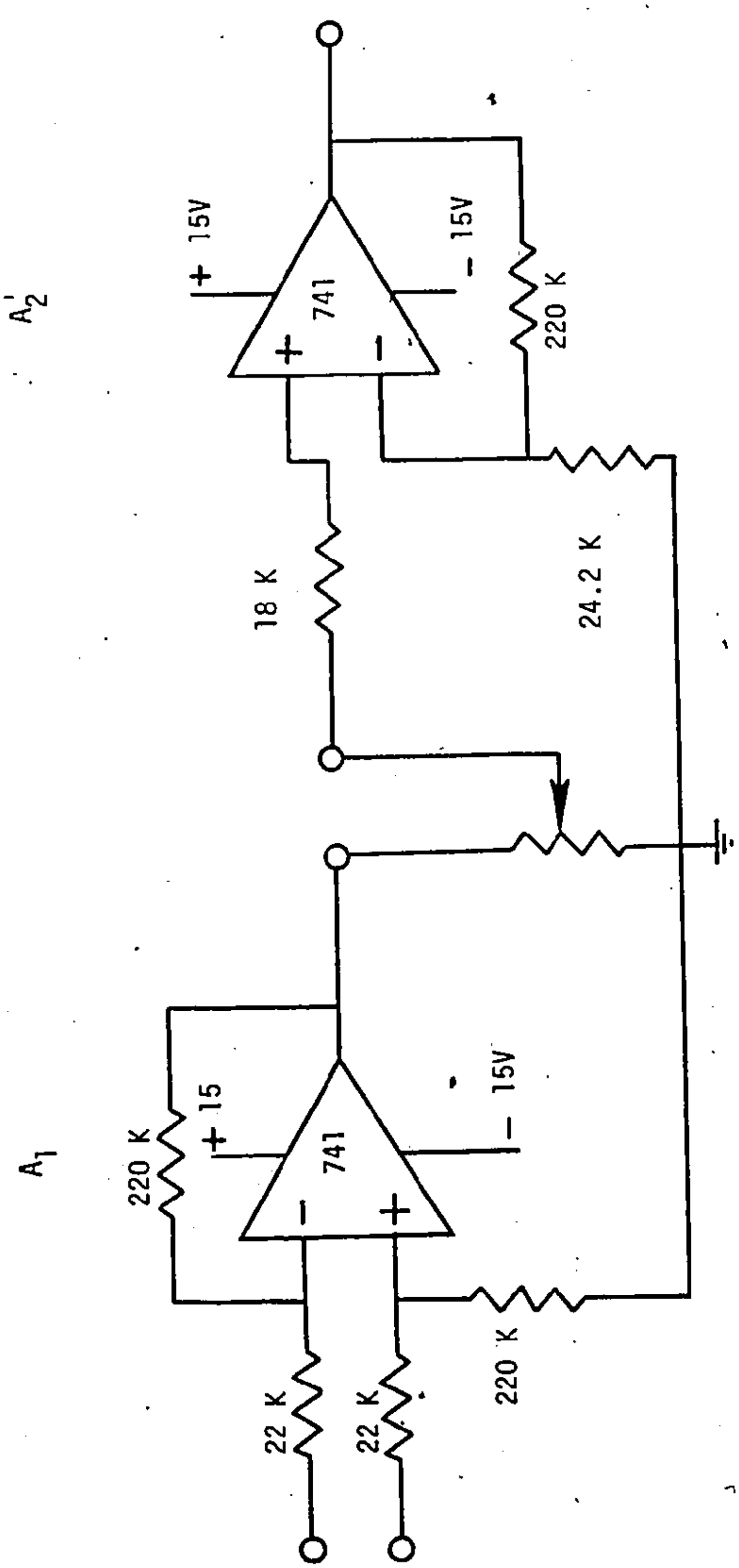

Circuit Diagram of the Amplification Unit

FIGURE 3.5

the DRR only one of the ADC outputs is fed into the computer. Each of the two ADC has its own code. The conversion command pulse is also fed into the code generator and is used for changing the code. The digital scanner picks up only one of the ADC outputs, combines it with the appropriate code and sends the 13-bit word to the computer. Thus, the ADC outputs are selected successively by the digital scanner.

In the DRR the data of each ADC is identified by means of its code. The DRR runs in a closed loop during a period of approximately 2.0 milliseconds, and then the program is switched into the A/C policy routine. This means that the latter will use the last data read from the converters.

3.3 The CNC/AC Software System

The software was developed in a modular form, so as to enable the operation of some programs independently of the rest of the software system, or without the use of all the perepheral devices. These software routines may be divided into three separate groups:

a) Control routines;

b) N/C data service routines;

c) A/C auxiliary routines.

Supervising all of these routines is a command routine which allows the user to access any of these routines easily from the teletype.

3.3.1 Control Routines

Control of the milling machine is done in a foreground-background mode; the computer continuously loops in the A/C program until an interrupt occurs causing a transfer of control to the CNC routine which executes the N/C data program. Interrupts occur at regular intervals, caused by an external clock. The routines in this group, therefore, are:-

1) CNC routine - its purpose is to duplicate the operation of a conventional N/C controller. A preliminary version of this routine was discussed in detail in References {57} and {67}.

2) A/C routine - this program is used to control the feed rate in the adaptive control application.

3.3.1.1 The NC Program

The general structure of the NC program is shown in figure 3.6. In this program one can distinguish between the "frame" which enables the cooperation between the NC and the A/C programs, and the major part which contains six subroutines: Point-to-Point (PTP), Feed, Interpolator, Transient, Output and Position. The NC program includes an additional routine denoted as the Initiator Routine. The main function of the Initiator Routine is the loading of a new data block to the memory locations which the NC program is using. The "frame" includes the following:

1. When the interrupt occurs, the contents of the arithmetic-unit registers are stored in the computer memory. This stored

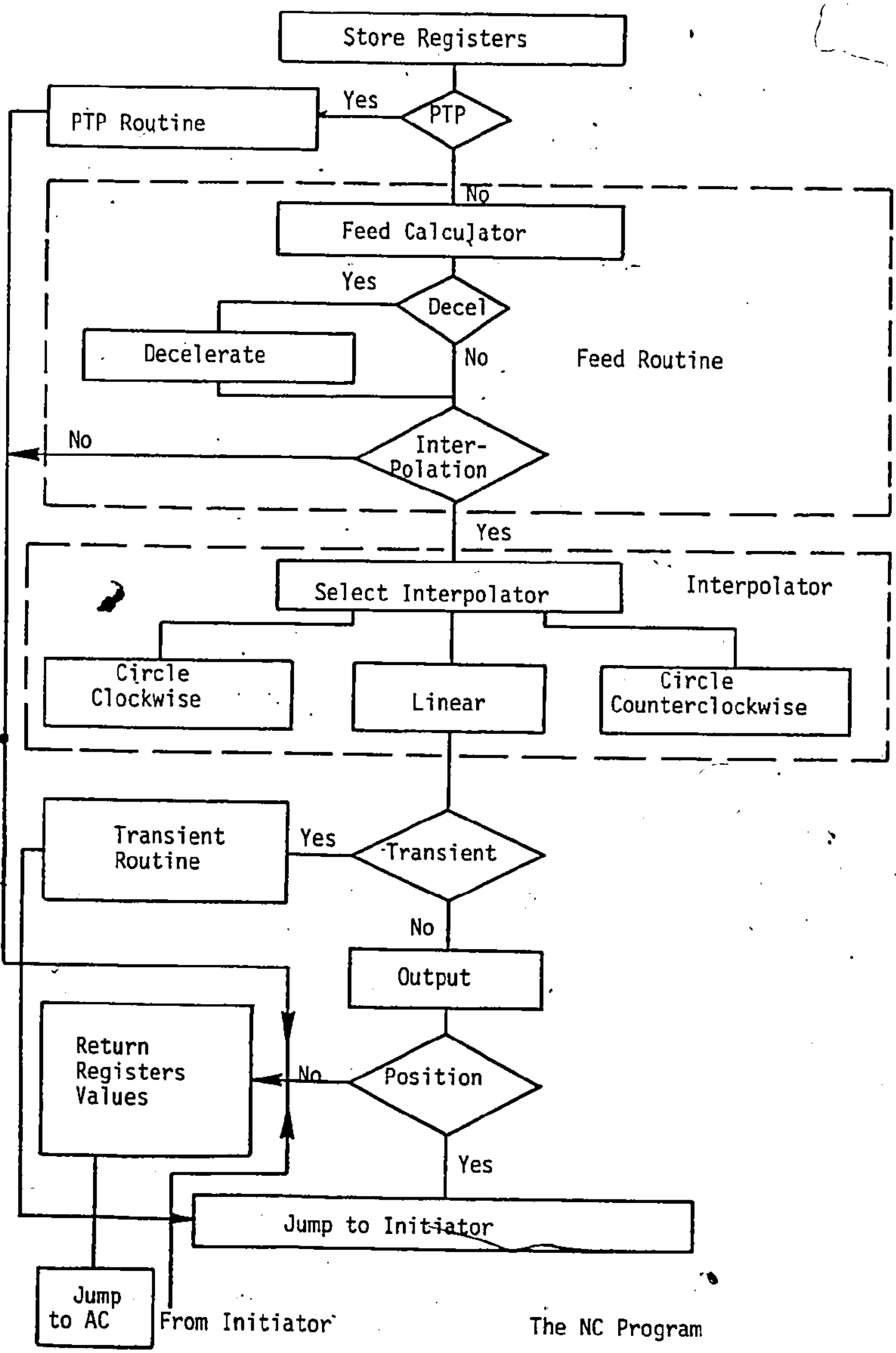
Store Registers
PTP
Yes
PTP Routine
No
Feed Calculator
Yes
Decel
Decelerate
No
Feed Routine
No
Inter-
Polation
Yes
Select Interpolator
Interpolator
Circle
Clockwise
Linear
Circle
Counterclockwise
Transient
Routine
Yes
Transient
No
Output
Return
Registers
Values
No
Position
Yes
Jump to Initiator
Jump
to AC
From Initiator
The NC Program

FIGURE 3.6

data is required for the continuation of the A/C program.

2. After executing the major part of the program, the stored values are returned and then,

3. The flag of the interrupt pulses channel is cleared and

4. Control is returned to the point of interruption in the A/C program.

The principles of the six subroutines in the Continuator routine are as follows:-

PTP

In a point-to-point operation the axes move in the highest feedrate. An interrupt pulse activates the PTP routine, and then henceforth, it starts to run in a closed loop supplying command pulses, the frequency of which depends on the cycle time of this loop. The rapid traverse is 158 inch/min. per axis. A subtraction of the appropriate counter by one unit is carried out for each command pulse.

FEED

The Feed routine generates interpolation command in a rate dependent on the feed-word in the data block. The maximum rate of interpolation commands is equal to the frequency of the interrupt pulses, i.e., 5000 per second. This is compatible with a feed rate of 30 ipm according to equation 3.1.

INTERPOLATOR

Three types of interpolation are available: linear and two circular interpolations (clockwise and counter-clockwise). The principle of each interpolator is a simulation of two

Digital Differential Analyzers (DDA) integrators. The simulated registers of the DDA's are loaded by the Initiator Routine. For every interpolation command which is produced by the Feed routine, a single cycle of the DDA is simulated.

TRANSIENT

This routine is activated upon detection of a transient condition by the A/C program. A full explanation of the function of this routine is given in Chapter 5.

OUTPUT

If as the result of a DDA cycle, an overflow pulse is generated either in one or two axes, this routine sends a command pulse to the controller.

POSITION

For every command pulse the position counter of the appropriate axis is decremented by one unit. A zero position check of both counters is performed. When the machining of the current segment has terminated (i.e. when both counters are zero), the program jumps to the Initiator Routine, in order to load a new block and process its data.

A detailed discussion of the operation of the DDA's is given in Reference {68}, and therefore will not be repeated here. A complete listing of the NC program is given in Appendix III.

3.3.1.2 The A/C Program

The flow chart of the A/C program is shown in figure 3.7. This program consists of three routines: Data Reading Routine (DRR), Error Calculator Routine (ECR) and Feed-rate

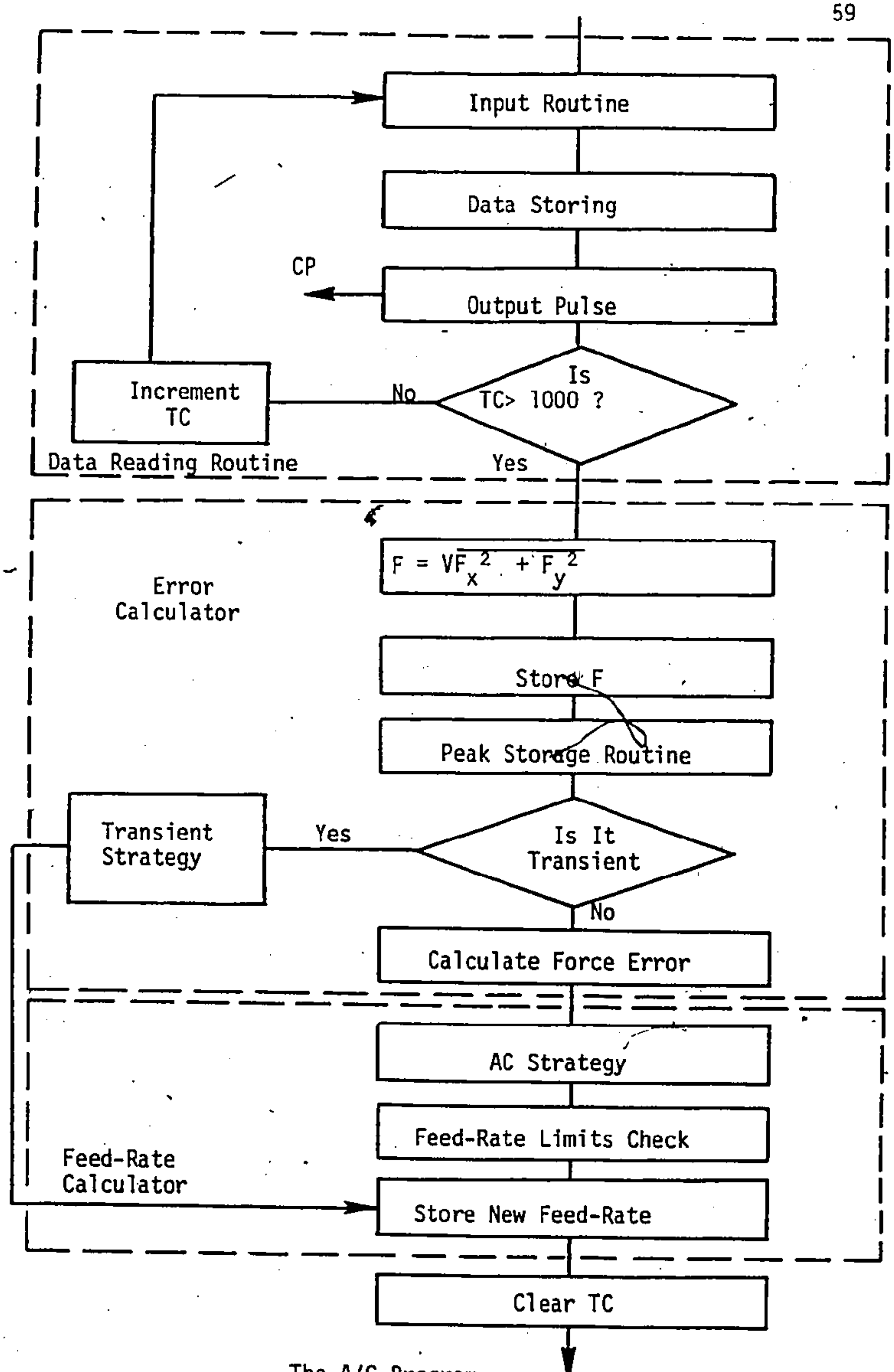

The A/C Program

FIGURE 3.7

Calculator (FRC). The DRR receives the input from the Analog-To-Digital Processor and stores it in the appropriate memory locations. With the completion of this stage an output pulse CP is sent and simultaneously the flag in the I/O channel is cleared. The conversion time is 20 μ sec, and therefore a new data will be available, approximately 11 computer instructions after the output pulse. At that time the Analog-To-Digital Processor will send a pulse to set the flag of the I/O channel and a new cycle of the DRR will start.

Approximately every 2 m sec the program is switched from the DRR to the ECR. The time measurement is done indirectly by counting the computer instructions which are executed and bearing in mind that execution time of each instruction is 2 μ sec. Each time a group of instructions, either in the NC or in the A/C program, is performed, a software counter (TC) is incremented by the appropriate number. Whenever the counter exceeds the value of 1000, which is equivalent to 2 m sec, a new feed-rate calculation takes place.

The ECR starts with the calculation of the radial cutting force F_R from the two force signals, F_X and F_Y, which are 90 degrees phase-shifted. The cutting force F is then stored and the control is switched to the peak holding routine. This routine operates by recognizing only increases in sampled force values over a period corresponding to the tooth period. The The advantage of using the peak holding routine will be shown in Chapter 4., The error calculator routine then tests for transient condition. This condition is identified by the absence of force signal for a period corresponding to one cutter revolution or the sudden increase (by a factor of 2) in the sampled force values.

Accordingly, in cases of tool-work impact under rapid traverse conditions or sudden increases in the cutting force due to, for example, a step increase in the axial depth of cut, control is switched to a transient routine. The strategies used in this routine will be explained in details in Chapter 5. Otherwise, the ECR calculates a force error "e_f" by comparing the actual sampled cutting force with a predetermined "nominal" value "Fnom". The value of "Fnom" is calculated before the start of the work and set as constant to the computer.

Based on the A/C strategy described in Chapter 4, the FRC routine calculates the new feed-rate. The obtained feed-rate is checked to see whether it exceeds the extreme limits. If it does, the limit which was exceeded will be used as the new feed-rate. The new feed-rate is stored and the computer control is transferred to the Data Reading Routine to receive a new input.

3.3.2 NC Data Service Routines

These routines manipulate the NC data program so as to exploit the inherent capabilities of the CNC system.

1) READ Routine: This routine enables the computer to read an NC data tape via the high speed tape reader.

2) PRINT AND PUNCH Routine: This routine enables the user

to obtain a listing of the N/C data program on the teletype or a paper tape of the NC data program from the high speed punch.

3) DATA EDITOR Routine: This routine is used to correct and edit the NC data stored in the computer.

4) DATA DIAGNOSTIC Routine: This routine is helpful in debugging NC data programs.

5) CUTTER COMPENSATION Routine: This routine performs a cutter radius compensation algorithm on a stored NC data program according to input parameters entered via the teletype. The use and description of the NC data service routines was discussed in detail in reference {69}.

3.3.3 A/C Auxiliary Routines

These routines service only the adaptive control function.

1) INITIALIZATION Routine: This routine calculates a nominal force (for use in the A/C routine)according to requested inputs.

2) TRANSDUCER CALIBRATION Routine: This routine prints out values of the two channels of the adaptive controller. It is useful in transducer calibration.

3) DATA COLLECTION Routine: This routine stores and prints the value of the radial cutting force "F_R" as calculated by the A/C routine at each sampling interval.

CHAPTER 4

ANALYSIS OF TRANSIENTS IN THE ADAPTIVE CONTROL SERVOMECHANISM

4.1 Introduction

This chapter deals with the A/C system from the point of view of its behaviour as a servomechanism, i.e., mainly with respect to the speed of its response to step inputs and from the point of view of stability.

Of all the possible applications of Adaptive Control in machining the one concerning the die sinking is perhaps the most obvious and straight forward. It is a natural extension of the long established practice in copy milling machines where feed-rate used to be controlled from a sensor of the load on the cutter.

The reasons for this application of Adaptive Control are, on one side, the practically unpredictable and usually large variation of the load on the cutter, and on the other side, the vulnerability of the usually long and slender end milling cutters used in die work.

Let us consider an elementary example in fig. 4.1 of a rectangular cavity with a sloping bottom. Its rough machining starts with drilling a flat bottomed hole in position 1. A cutter with a comparatively large diameter is used first starting from this hole, moving to point 2, point 3, point 4, etc. The cut Aa represents high load by milling width d and depth R_A. The reset move b from point 2 to point 3 goes in

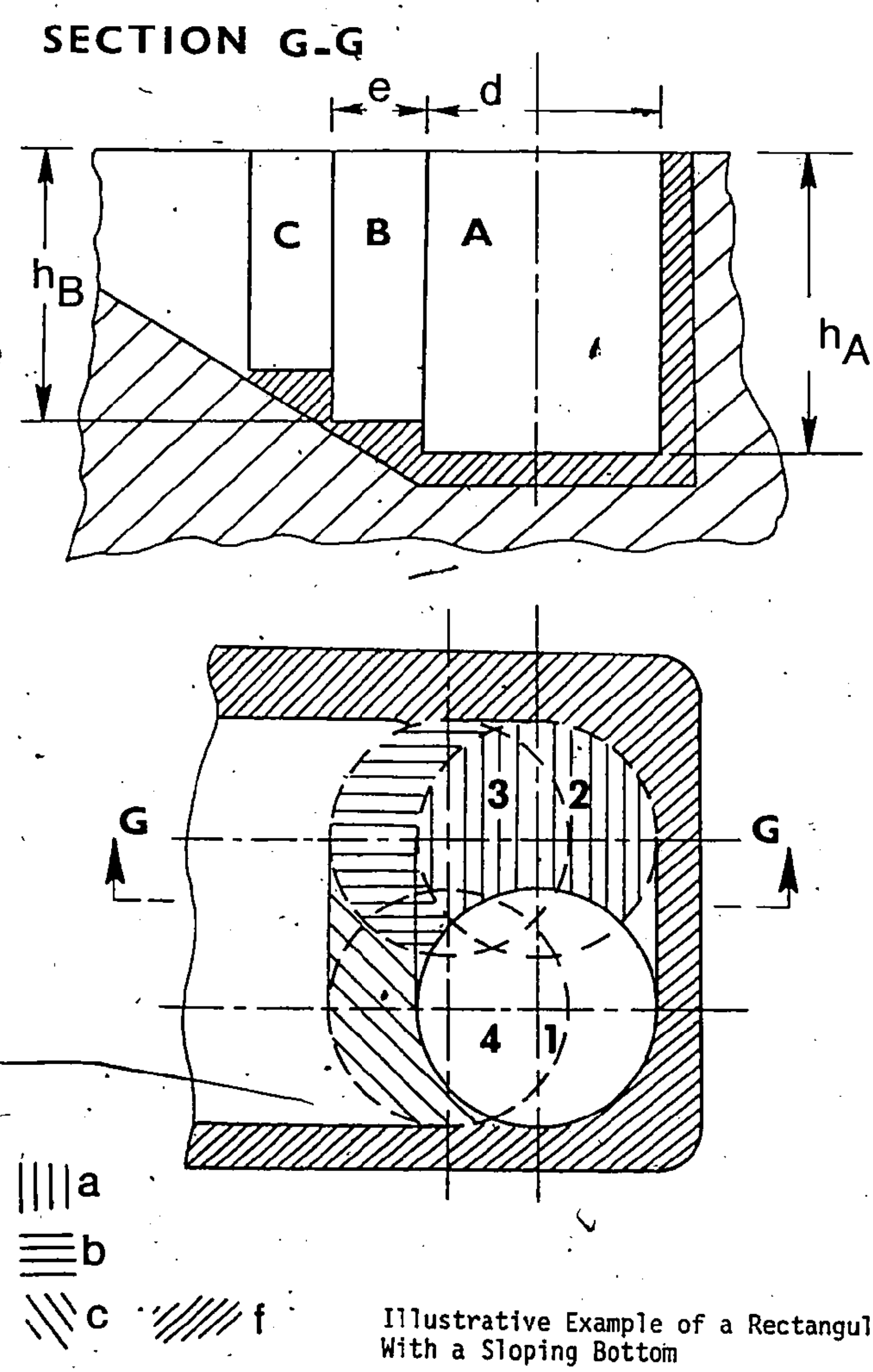

Illustrative Example of a Rectangular Cavity With a Sloping Bottom

FIGURE 4.1

lesser depth h_B and still full diameter width. The section c from point 3 to point 4 represents milling width e which is less than d/2. Cuts B, C, D, E follow with width e and decreasing depth of cut. After this operation stock f is left to be removed by a smaller diameter cutter in the corners and by a ball ended cutter on the steps of the sloped bottom. It is obvious that loads on these cutters will vary again considerably. In actual practical cases of dies the situation is usually much more complicated than in this simple example which, however, illustrates well the point concerned.

Without Adaptive Control a safe, very low feed-rate has to be set. With Adaptive Control varying the feed-rate so as to keep the load on the cutter at its full capacity large savings of finishing time are achievable.

Thus, consideration is limited to the rather simple, constraint type A/C system with feed variation for constant cutting force. Such a system is, however, so far the only type of an A/C system used successfully in practice and seriously considered for wider use in milling [63,64].

In such a system the maximum challenge is -- could we program rapid traverse and let the cutter hit the part and expect the system to slow down fast enough so as not to exceed the set maximum force. The systems presently used in practice switch off A/C for penetration of walls and for approach of corners and program slow feed-rate. Another interesting question is -- if the systems response is made very fast, how will it deal with periodic variation of the cutting force. This chapter is an attempt to give some answers to these questions and systematically investigate the dynamics of the A/C system with its three feed-back loops - velocity, position, force.

The work was based on a homemade CNC, A/C system consisting of an NC retrofitted No. 4 vertical milling machine and an HP 2100A mini-computer, which otherwise is a part of a Fourier Analyzer System. The equipment is shown in the photograph Fig. 4.2 and it was described inclusive the software of CNC and A/C in Chapter 3.

In the present analysis the NC servomechanism is briefly summarized. Its parameters and behaviour have been experimentally established in all necessary detail {70}. The analysis of the A/C system was carried out by simulation on a CDC 6400 computer using a model for the velocity and positional loops matched to the experimental reality and, of course, the NC control and A/C algorithm being in software anyway, were simulated truly. The crucial part is the transfer function between the motion of the table and the cutting force which is very complicated and depends on many parameters. This transfer function was studied in reference {59}, and some of the results obtained are used in this chapter.

4.2 The Numerical Control Servomechanism

The Numerical Control (NC) servomechanism, per one axis, is illustrated in the block diagram in fig. 4.3. The output from the mini-computer which represents the commanded

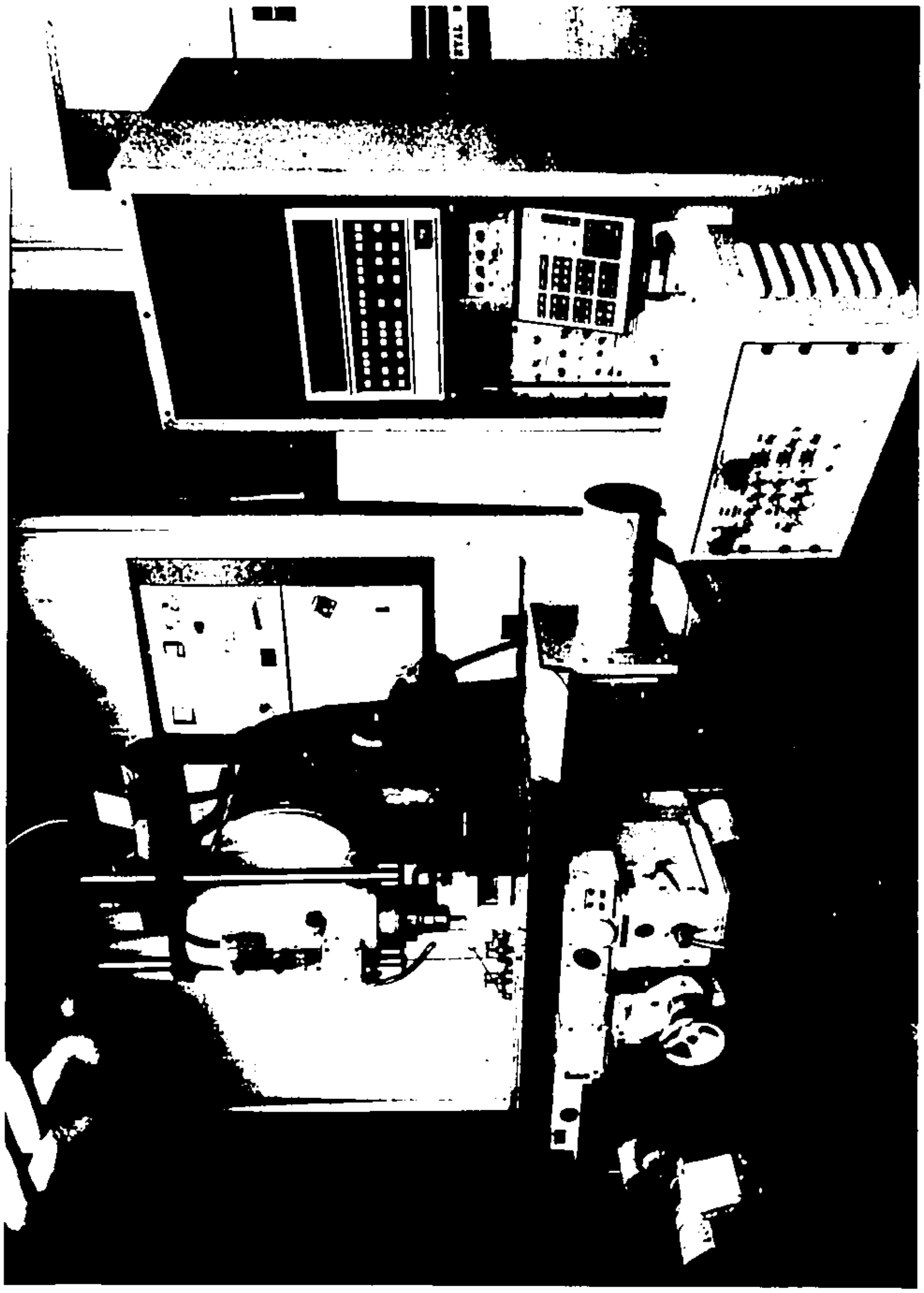

The CNC System

FIGURE 4.2

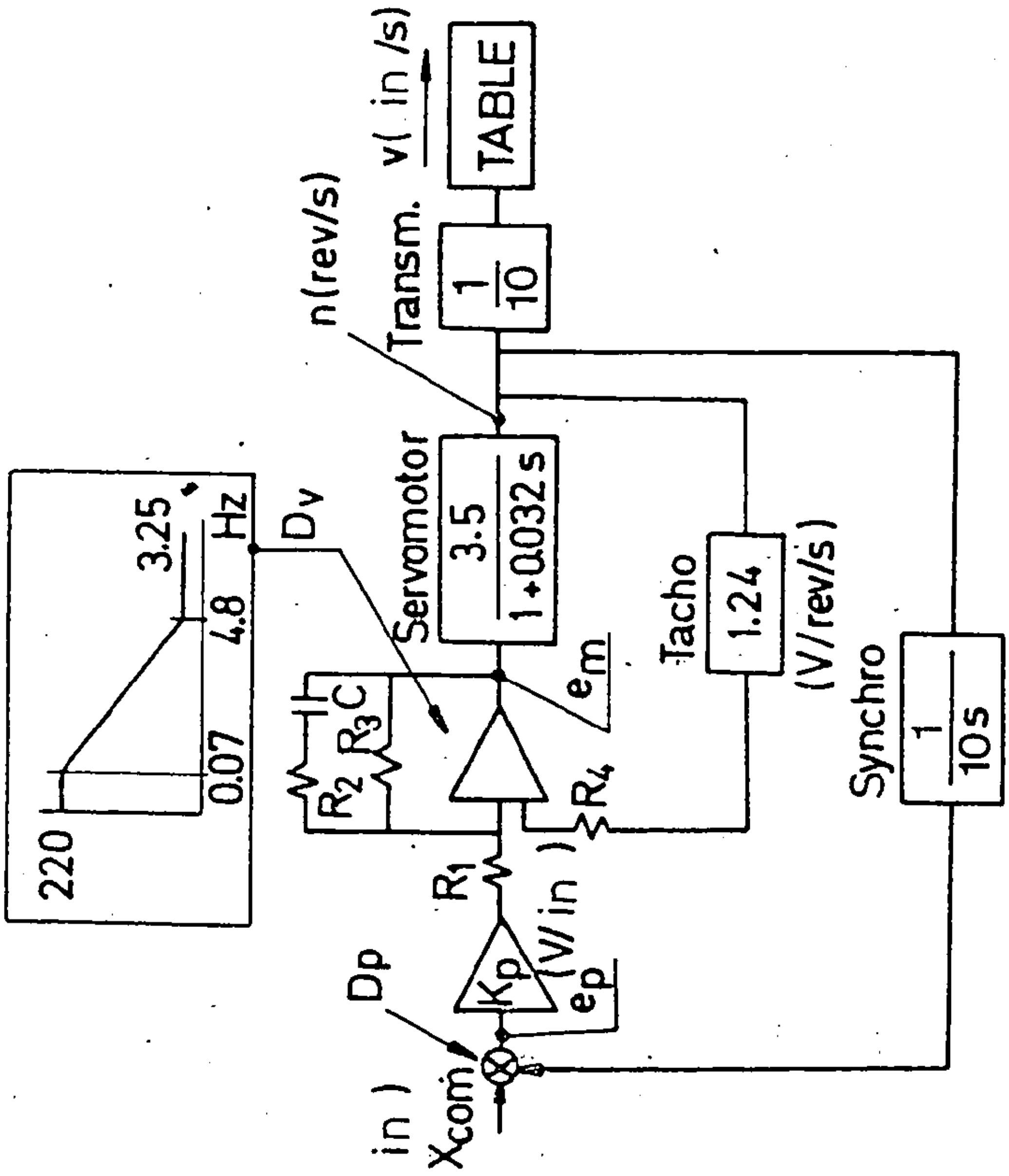

Block Diagram of the NC Servomechanism

FIGURE 4.3

position X com is converted from the series of pulses into phase-modulated 2500 Hz in the hardwired positional discriminator Dp, where also the positional feed-back signal from the synchro-resolver is subtracted and the positional error e_p established. After amplification Kp it becomes the speed command which enters into the velocity discriminator D_v represented by an operational amplifier which acts simultaneously as a correcting network. Its low frequency gain is 220 and its high frequency gain is 3.25. In this amplifier the velocity feed-back signal coming from the Tachogenerator is subtracted after multiplication by a factor R1/R4. Varying the ratio of R2/R4 is the most practical means of changing the high frequency gain in the velocity loop.

The servomotor is represented as a first order system with a time constant $\tau m = 0.032$ sec. This representation was found adequate as the time constant due to the inductance of the armature is much smaller than the above mentioned one which results from the inertia mass of the rotor. The motor drives the table through transmissions including recirculating ball screw and nut. The transmission ratios to the table as well as to the tacho and the synchro, which are driven from the lead screw are indicated in the block diagram.

The dead zone in the system which is due to the flexibility of the mounting of the lead screw and of the nut and to friction in table guideways is negligible. The only explicit non linearity in the system is the current limitation in the servomotor. With the given characteristics of the servomotor and the dynamics of the system, this limitation does not activate for velocity step inputs below 480 mm/min. [71]. Thus, it does not apply practically through the range of working feeds at all and becomes active only for step inputs of rapid traverse.

This servomechanism has been investigated both theoretically and experimentally and both these approaches have then been matched and a rather accurate mathematical model of the servo was obtained. Its parameters were adjusted so that the presently used gains are -- the open position loop gain = table velocity/positional error = 0.95 mm/min/um; the open velocity loop gain = 950 V/V. Maximum acceleration obtainable on the table is 478 mm/sec^2 = 28.6 m/min/sec.

These parameters are well comparable to typical NC servomechanisms of contemporary machine tools.

In order to be better able to appreciate the performance of the Adaptive Control system which is built around this NC servo, some of the basic characteristics of the NC servo alone will be presented here. A detailed discussion of these characteristics has been given by the author in a previous thesis [70].

Fig. 4.4 shows a record of the step input response of the closed velocity loop alone (positional feed-back disconnected). Line <u>a</u> is the voltage input to the velocity discriminator, Line <u>b</u> is the current analog showing current

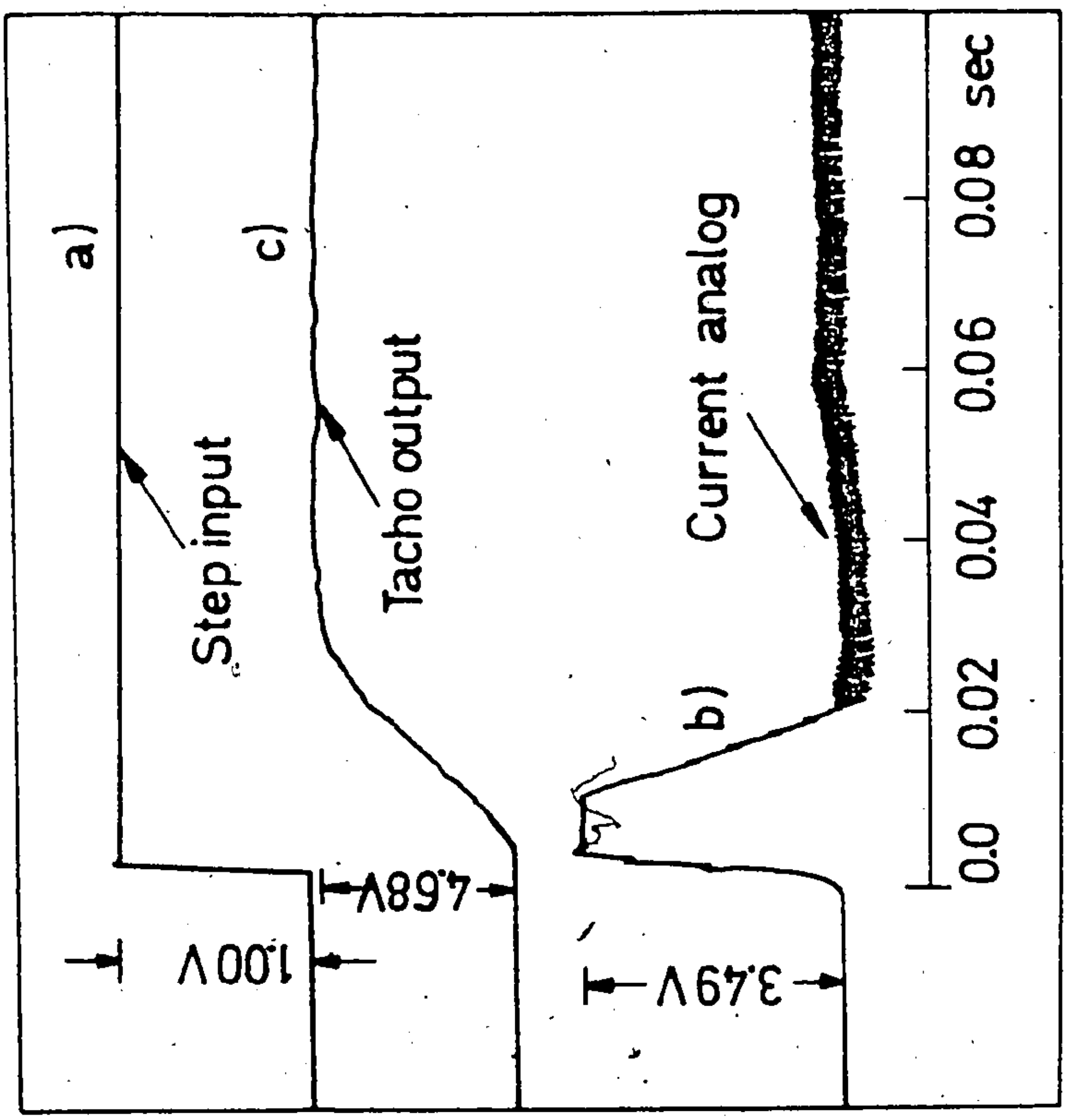

Step Input Response of the Closed Velocity Loop

FIGURE 4.4

limitation and Line c is the tacho output showing the actual velocity. The time constant of the response is about 20 ms., this is a case of a rather large velocity command -- 580 mm/min. For smaller step inputs where the current limit does not apply and with a subsequent increase of high frequency velocity gain a time constant of about 12 ms. was obtained. However, in any case, the speed of the response is mainly limited by the correcting network. In fig. 4.5 the calculated (solid line) and experimentally established (broken line) transfer function of the open position loop is shown. The measurement was carried out using a digital Fourier Analyzer. The graph shows that the system is safely stable. The response of the closed position loop to a step input measured as the tacho voltage responding to a positional ramp (velocity step of 100 mm/min.) command generated by the NC Control system is shown in fig. 4.6. The response time is about 25 ms. Cases a) and b) differ in the velocity feed-back gain and show consequently different degree of damping.

4.3 The Adaptive Control Loop

As mentioned in the introduction this is a rather simple Adaptive Control (A/C) approach in which the purpose is to vary the table velocity so as to keep the cutting force constant. The A/C loop is added around the existing NC servo. The corresponding block diagram is shown in figure 4.7. In the software interpolator in the mini-computer the simulated digital differential analyzers generate the X and Y positional

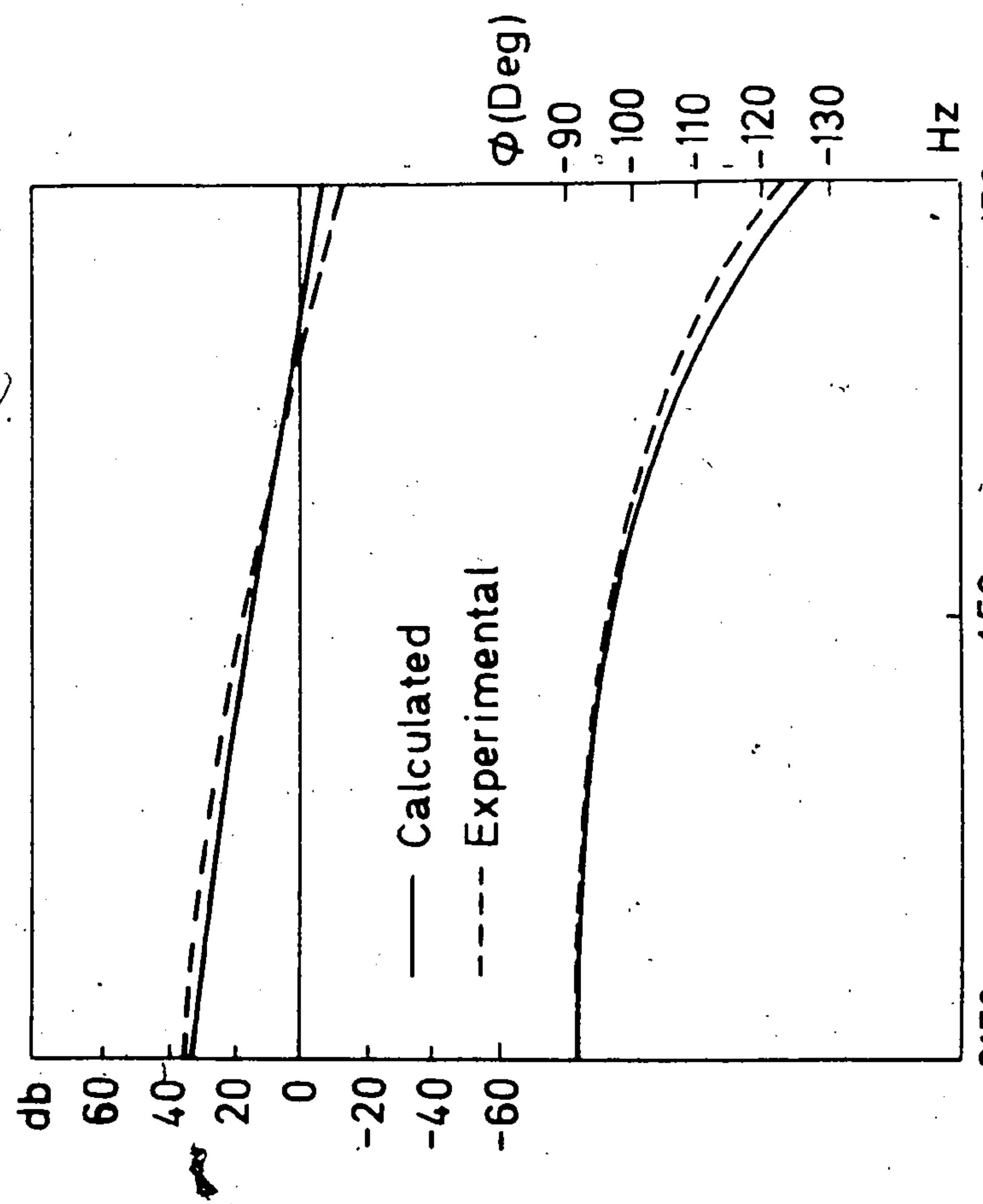

Bode Plot of Open Position Loop

FIGURE 4.5

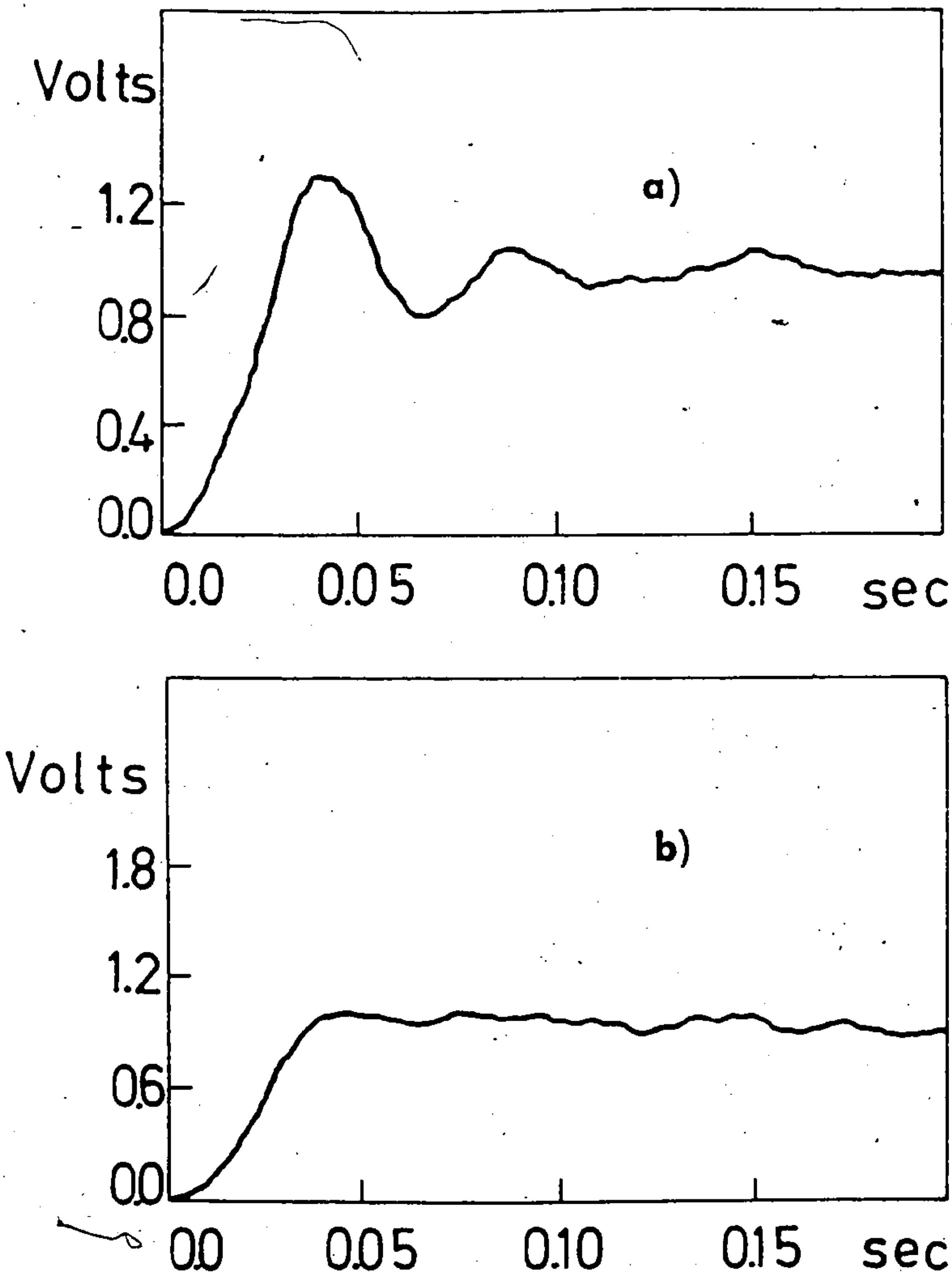

Step Input Response of Closed Position Loop

FIGURE 4.6

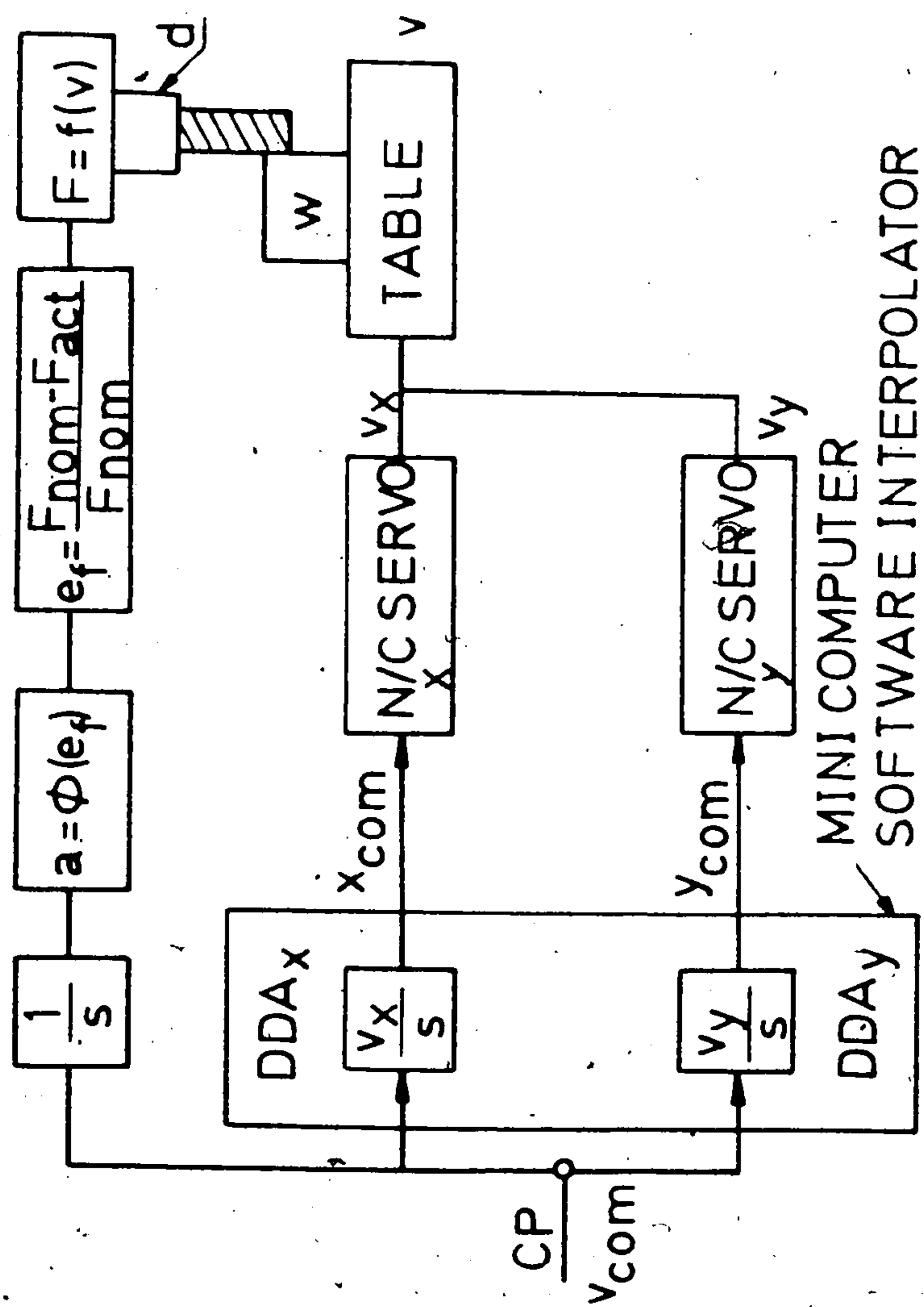

Block Diagram of Adaptive Control Loop

FIGURE 4.7

commands from the data of the commanded resulting velocity V_{com} as well as the ratio v_x/v_y of the component velocities. The table is driven in the two coordinates by two servomechanisms such as described in figure 4.3 and it moves the workpiece W with resulting velocity v. The cutting force F_R is a function of velocity v and is measured by the dynamometer d attached to the spindle. The design of the rotary dynamometer is described as well as its interface with the mini-computer in appendix I. The force signal is compared with the nominal force Fnom which is the desired value at which the servo should maintain the cutting force. The result of the comparison is the relative force error e_f. According to the established value of e_f a desired change of velocity is expressed as acceleration $a = \phi(e_f)$. By integrating this acceleration the value of commanded velocity Vcom is obtained as frequency of the control pulses CP for the Digital Differential Analyzers in the software interpolator which act as integrators and produce positional commands Xcom, Ycom.

In order to investigate the characteristics of the A/C system, it is fully satisfactory to consider motion in each coordinate separately as if, e.g., a motion along x-axis only were commanded. It is as well to consider the positional command just as a final limit of the motion and realize that now the actual input to the servo is the desired cutting force Fnom. Consequently, the block diagram of figure 4.7 may be reconfigured as shown in figure 4.8 where the upper part shows the A/C loop

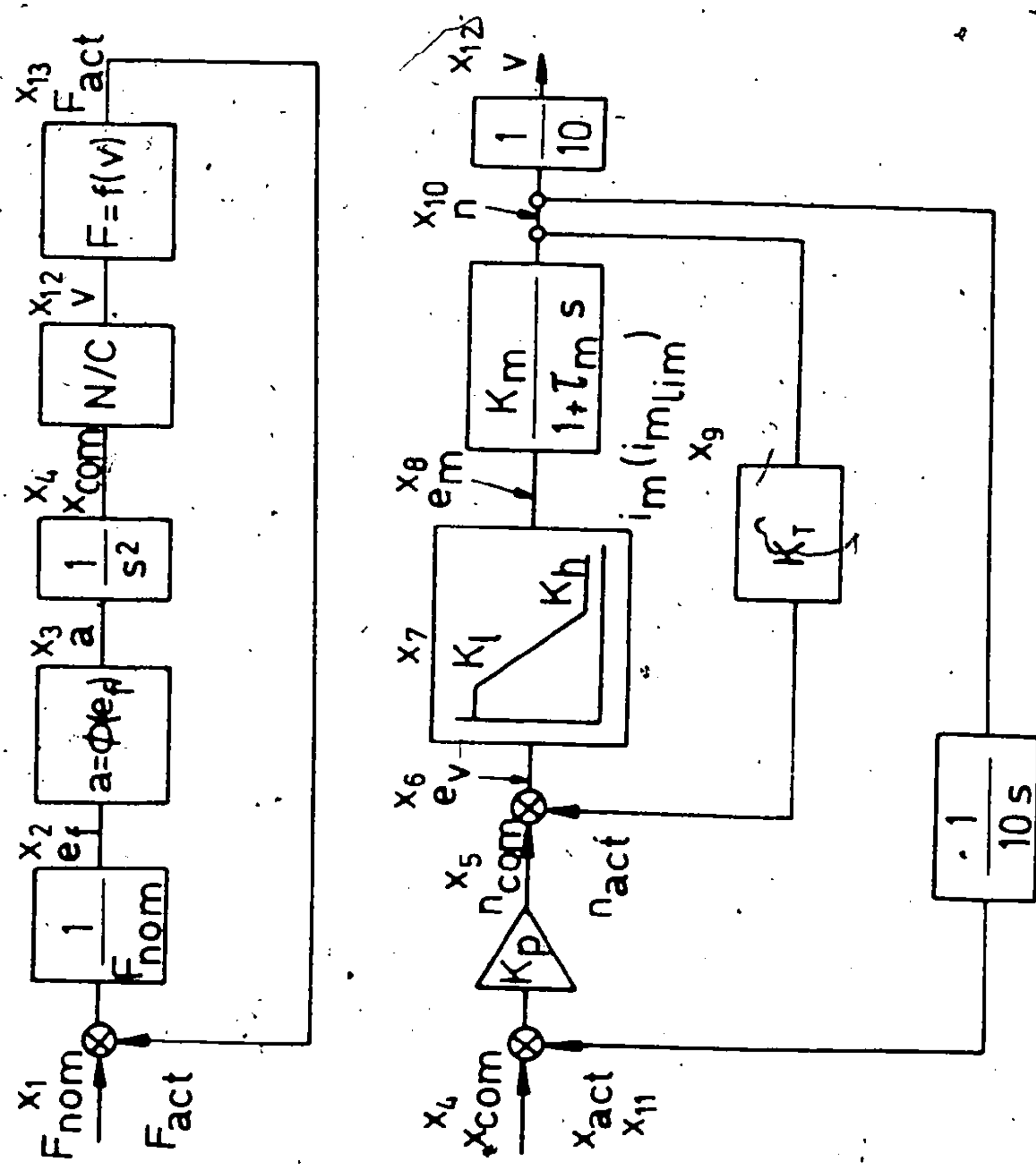

Reconfigured A/C Loop and Details of NC Block

FIGURE 4.8

and the lower part shows the details of the NC block.

At the input of the system there is now the force discriminator which gives the relative force error

$$e_f = \frac{F_{nom} - F_{act}}{F_{nom}}.$$

The NC block is shown in detail in the lower part of the diagram. The notations are as in figure 4.3. The positional error after amplification k_p becomes the speed command signal n_{com} which after comparison with n_{act} gives the velocity error e_v. The output of the correcting network is the command voltage e_m of the servomotor. The current in the armature of the motor is i_m.

4.4 Classical Analysis of Simplified A/C System

Full analysis of the A/C system will be presented further on and it will be carried out numerically in the time domain using state-space approach. However, in a preliminary way a linearized version of the system will briefly be discussed first using the Laplace transform approach.

In this simplified way no current limitation in the servomotor is considered and the acceleration function is simply

$$a = K_{ac}.\ e_f = K_{ac}\frac{F_{nom} - F_{act}}{F_{nom}} \text{ -----------------(4.1)}$$

As regards to the relationship between cutting force and velocity it is important to refer to [59] where it was explained that there is an inherent time delay between velocity change and force change. To illustrate this point, assume e.g.

that the table velocity increases suddently while a tooth of the cutter is cutting. The cutter will not sense this velocity change fully until the reset tooth arrives in the cut, and the chip thickness being the travel executed in the meantime. Including this delay in the transfer function F/v while neglecting the periodic character of the cutting force, it may be written:

$$F(t) = Cv(t-\tau) \quad \text{------------------------------------(4.2)}$$

or

$$F(s) = Cv(s)\, e^{-\tau s} \quad \text{------------------------------(4.3)}$$

where s is the Laplace operator and τ is the time period between the cutter teeth and the proportionality constant depends on the material of the workpiece and is itself, proportional to the axial depth of cut <u>b</u> and approximately proportional to the radial depth of cut <u>a</u>.

$$C = Kba \ (N/mm/sec) \quad \text{---------------------------------(4.4)}$$

Assuming first $\tau = 0$, and $K_p = 1150$ (V/mm), the correcting network gains K_l (low freq.) = 220, K_h (high freq.) = 2.2, servomotor gain $K_m = 3.5$ (rev/sec/V), tachogenerator gain $K_T = 1.24$ (V/rev/sec), the transfer function of the A/C loop open at the force feedback is: -

$$G(s) = \frac{F_{act}(s)}{F_{nom}(s)} = 1070\, \frac{C\, K_{ac}}{F_{nom}} \cdot \frac{(s + 45)}{s(s + 23)(s^2 + 72s + 2560)} \quad \text{--(4.5)}$$

It is important to notice that the gain in the A/C loop is variable and, according to equations (4.4) and (4.5) it increases in proportion to the radial and axial depths of cut and it decreases in proportion to the increase of F_{nom}, i.e., practically it decreases with the strength (diameter) of the cutter.

For illustration of stability margins and of the effects on them of the delay τ in the cutting force, let us assume a case; cutter diameter d = 20 mm, 4 teeth, cutting speed v_c = 32 m/min, corresponding spindle speed N = 500 rev/min, time period per tooth τ = 0.030 sec; for feed per tooth f_t = 0.1 mm, radial depth of cut a = d = 20mm (slotting), axial depth of cut b = 10mm, we may estimate the cutting force F = 4200N. At these conditions the feed rate is $v = f_t/\tau$ = 3.33 mm/sec (200 mm/min) which gives the constant K in equation (4.4): K = 6.3(N/mm^2/mm/sec), and C = 1260 (N/mm/sec). For safety of the teeth of the cutter we shall have to assume that the cutter might be running at as low an axial depth of cut as b = 2 mm, which would then for the same force lead to a feed per tooth f_t = 0.5 mm and we shall take on top of this a factor 1.25 and assume a target force F_{nom} = 5250 N. Assuming further the gain in the acceleration transfer function equation (4.1) as K_{ac} = 1, the corresponding Bode plot of equation 4.5 is obtained as shown in figure 4.9, where the phase curve 1) applies to the case with no delay between velocity change and cutting force change. In this case on the magnitude curve a gain margin K_{ac} = 372 is found. For values of the acceleration constant higher than this the system becomes unstable. Practically, because the maximum possible value of the force error is e_f = 1, this is also the maximum acceleration beyond which the system becomes unstable. Introducing time delays $\tau = 30$ ms and $\tau = 60$ ms phase curves 2) and 3) are obtained. It is obvious that the term $e^{-J\tau\omega}$ in transfer function equation 4.3 has magnitude 1, therefore the magnitude curve in figure 4.9 is not affected by the introduction of these delays. It may be seen that the delay τ has strong influence on stability. The gain margins for limit of stability are summarized in table 4.1.

Table 4.1

τ(msec)	$K_{ac_{lim}}$ (mm/sec^2)	f_{lim}(Hz)
0	372	4.2
30	180	1.8
60	98	1.5

4.5 Attempts at Optimizing the A/C System

The actual system differs in several respects from the one analyzed in the preceding section. Because of that and also because we are interested in the response of the system in the time domain all the following analysis was carried out by the state-space method, i.e., by simulating the system on a computer by using simple relationships including first order differential equations between the state variables of the system and computing their variations in small time increments T. The state variables are indicated in the block diagram figure 4.8 using a sequence of subscripts on the letter x.

Let the initial distance input to the NC loop be

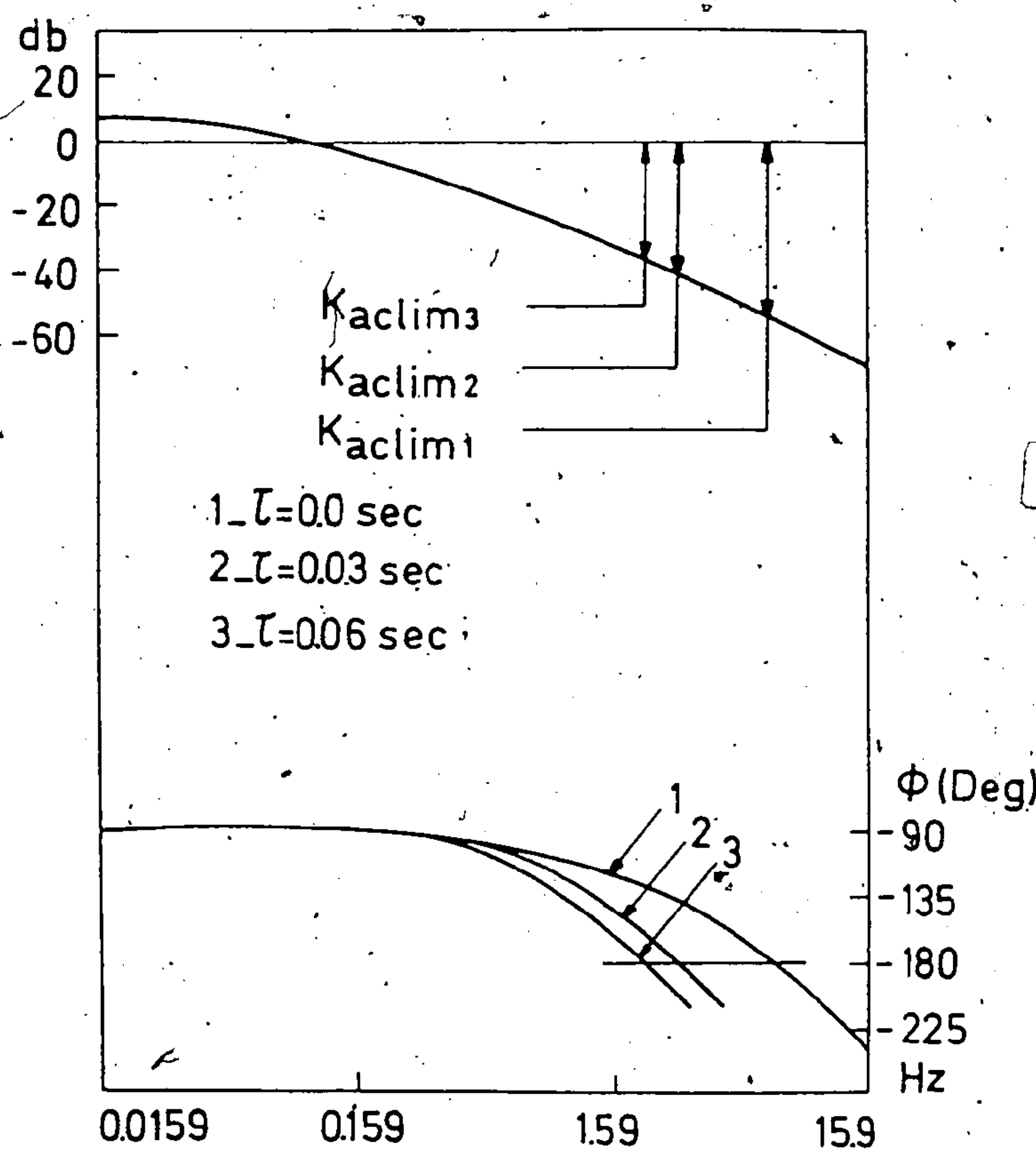

Effect of the Time Lag "T_L" On The Bode Plot of The Open A/C Loop

FIGURE 4.9

labelled as x_4. The positional error after amplification K_p becomes the speed command signal n_{com}, it is:

$$n_{com} = x_5 = K_p(x_4 - x_{11}) \quad \text{------------------------------(4.6).}$$

Where x_{11} is the resolver output, the gain in the D/A converter is usually set at 7.0 V/mm. The input to the correcting network x_6 is defined as:

$$x_6 = x_5 - x_{10}.K_T.R1/R4 \quad \text{------------------------------(4.7).}$$

Where K_T is the gain of the tacho stated by the manufacturer as 1.24 volt/rev/sec, and x_{10} is the output of the servo motor in rev/sec, R1 and R4 are defined in figure 3.3. The operation of the correcting network is next represented by the following equations: -

$$\dot{x}_7 R2 + \frac{x_7}{C\Phi} = \dot{x}_8 \quad \text{------------------------------(4.8)}$$

and

$$\frac{x_6}{R1} = x_7 + \frac{x_8}{R3} \quad \text{------------------------------(4.9)}$$

where x_7 is an intermediate state space variable used in the state space description of the network and x_8 is the output of the correcting network (see figure 3.3). For the servomotor, there is the basic equation expressed by the transfer function in figure 4.3:

$$K_m x_8 = \tau m \dot{x}_{10} + x_{10} \quad \text{------------------------------(4.10)}$$

and the armature current x_9 is expressed by the equation:

$$x_8 = R_m x_9 + K_e x_{10} \quad \text{------------------------------(4.11)}$$

where R_m is the armature resistance and K_e is the co-efficient for induced voltage. In the computation x_9 is never permitted to exceed the permissible limit value.

Taking into account the transmission ratio in the mechanical drive, the resolver output x_{11} is obtained from the expression:

$$\dot{x}_{11} = \frac{x_{10}}{10} \qquad (4.12)$$

Further it is:

$$x_2 = \frac{x_1 - x_{13}}{F_{nom}} \qquad (4.13)$$

and

$$\ddot{x}_4 = x_3 \qquad (4.14)$$

where $x_2 = e_f$, $x_1 = F_{nom}$, $x_{13} = F_{act}$, $x_3 = a$.

Using Euler's method, the integration of the above equations were evaluated as follows:

$$\dot{x}(t) = \lim_{\Delta t \to 0} \frac{x(t + \Delta t) - x(t)}{\Delta t} = \frac{x(t + T) - x(t)}{T} \qquad (4.15)$$

for a small increment of time $\Delta t = T$.

The most important relationship for the simulation of the whole process is the transfer function between the motion of the table as input and the cutting force as output which in the preceding section was expressed by equation 4.2.

Here it is necessary to refer to {59} where a detailed analysis was presented of cutting forces in end milling. For the analysis of the A/C system, three cases based on this reference are selected. It is necessary to point out that the force variation, taking the usual case of a cutter with helical teeth, depends strongly on the ratio of the radial to axial depth of cut a/b and of course on the number of teeth of the cutter. The three cases to be considered will all represent slotting, i.e., the radial depth of cut is equal to the diameter of the cutter which we take again d = 20 mm; thus it is a = 20 mm.

In figure 4.10, the cutting force variation in slotting is shown. The axial depth of cut is b = d = 20 mm. Graph a) represents the case of a cutter with 2 teeth, graph b) of a cutter with 4 teeth. In the latter case the force is practically constant and it is 1.11 times higher than the peak force in the former case in which the force could be approximated by

$$F = A(1 + \sin w\, t) \qquad (4.16)$$

where $w = 2\pi N z$, where N is the spindle speed in rev/sec and z is the number of teeth.

Although we shall be considering variation of the depth of cut we shall for simplicity keep the forms of force variation as indicated.

An important feature is the transient occurring when the cutter starts penetrating a wall. Figure 4.11 shows that the peaks of the periodic force increase rather fast and reach the final maximum mostly at penetrations p much smaller than the radius r of the cutter. How fast this increase is, depends on the ratio of the axial depth of cut to the radial

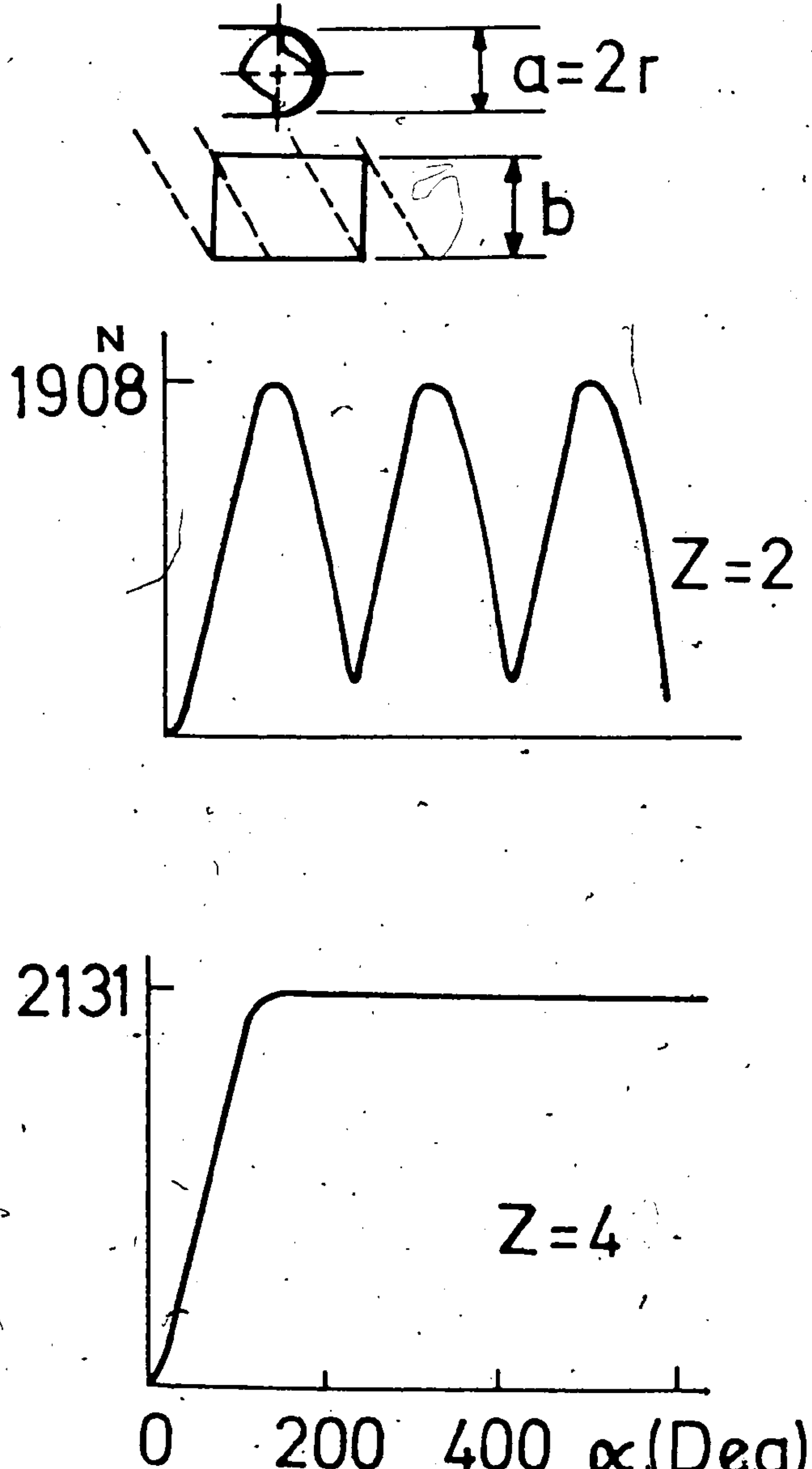

Cutting Force Variation in Slotting, Cutter with Two and with Four Teeth

FIGURE 4.10

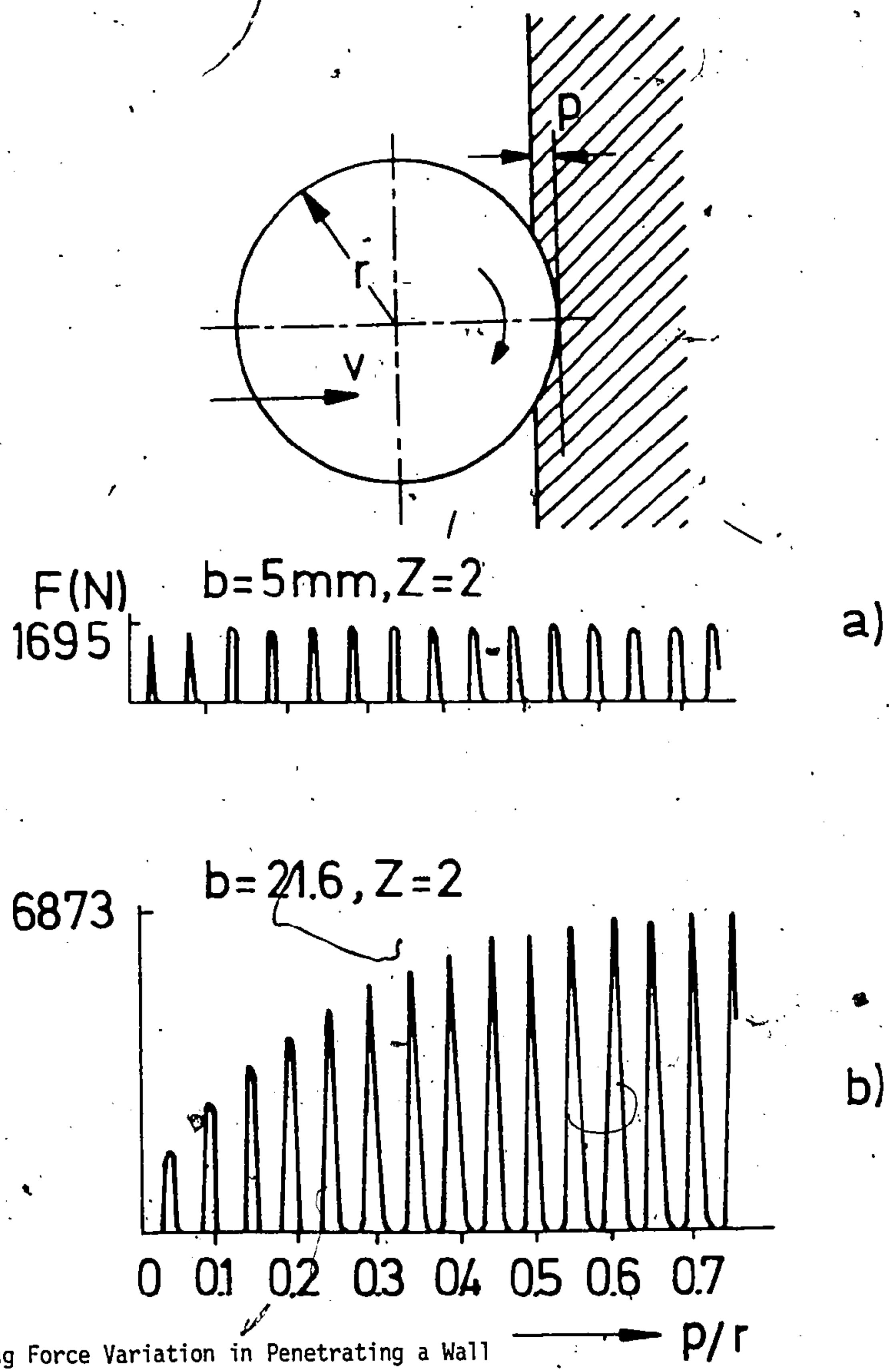

Cutting Force Variation in Penetrating a Wall

FIGURE 4.11

depth of cut b/a; in this case this is identical with b/d. In case a) this ratio is b = o.8 d while in case b) this ratio is b = 3.4 d. In the case a) the peaks of the force reach their final maximum value almost immediately after the first contact of the cutter with the wall; in the case b) the maximum is not reached until penetration p = o.7 r.

Combining these various features we choose the following three cases for investigations:-

A) Periodic component of the force is zero (as in figure 4.10 b). With sudden changes in depth of cut b, the cutting force increases immediately (as in figure 4.11 a) except for the delay caused by the intermittent action of cutter teeth, as it was explained in relation to equation 4.2.

For this case our investigation will concentrate on the maximum possible speed of the response of the system to a step change in the depth of cut b and on the question of stability.

B) Force is periodic as in figure 4.10 a) and in equation 4.16 it increases as steeply with a step change in depth of cut as in the previous case.

The problem of the response of the system to the periodic variation of the force will be discussed.

C) Force is periodic as in case B, however, it increases gradually with penetration of a wall as in gigure 4.11 b).

The transient behaviour of the system when penetrating a wall (meeting a side of the workpiece) will be discussed.

It is further necessary to point out that the system reads the actual force in finite intervals which are assumed Δt_s = 10 ms. Thus we deal with a sampled data system and variables x_{13} (actual force), x_2 (force error), x_3 (commanded acceleration), x_4 (positional command) change in steps every Δt_s = 10 ms. However, during every Δt_s they all remain constant.

Case A

Similarly as in section 4.4, cutter diameter 20 mm is assumed with N = 500 rev/min, 4 teeth, tooth period τ = 0.030 sec, radial depth of cut a = 20 mm. Norminal force is set at F_{nom} = 4100 N, which e.g. for an axial depth of cut b = 10 mm corresponds to feed per tooth f_t = 0.1 mm, i.e. v = 3.33 mm/sec.

Cutting force formula 4.2 is not used here because it represented a simplification of reality especially as regards the delay between velocity V and force F. Now it will be accepted:

$$F = 205\ ab\ \{x_{11}(t) - x_{11}(t - \tau)\} \text{ ------------------(4.17)}$$

The magnitude of the force is assumed proportional to axial and radial depth of cut (the latter being constant in the present case) and to the actual feed per tooth as expressed by table travel $x_{act} = x_{11}$ during the last tooth period. In this way the delay between table motion and cutting force is included because the force depends both on the present position of the table and on that part by a tooth period. A case is simulated where the table starts from zero velocity and goes through a cut with a depth b = 2.5 mm for an actual travel length x_{11} = 10 mm (first phase). There the depth of cut suddenly increases to be = 10 mm (second phase). According to equation (4.17) the steady state in the first part with b = 2.5 mm should be:

F_{nom} = 4100N = 205 N/mm^3 * 20 mm * 20 mm * 2.5 mm * f_t,
f_t = 0.4 mm, v = 13.333 mm/sec.

This value of v exceeds the rapid traverse velocity which is set at 12.7 mm/sec. Thus, in the first phase the system will settle at this velocity and at a corresponding force of 3900N. In the second phase, at b = 10 mm the system should stabilize at v = 3.333 mm/sec and F = F_{nom} = 4100N.

First, for the acceleration in the A/C loop the formula is accepted:

$a = K_{ac} \cdot e_f$, with K_{ac} = 200 mm/sec^2

The resulting velocity of motion and force are shown in figure 4.12 a) and b) respectively. In the first phase the velocity stabilizes correctly at v = 12.7 mm/sec and the force at F = 3900N. At the moment of meeting the step in the depth of cut the force increases suddenly to 15,600N. The system starts to react rather fast and the force drops in 0.11 sec to F_{nom}. However, in this phase, the system is unstable. The difference in stability of the two phases is understood when we remember that according to equation (4.17) the gain in the A/C loop is proportional to depth of cut b and thus, it is four times higher in the second phase than in the first phase. With these results, it was decided to introduce a rate term in the acceleration

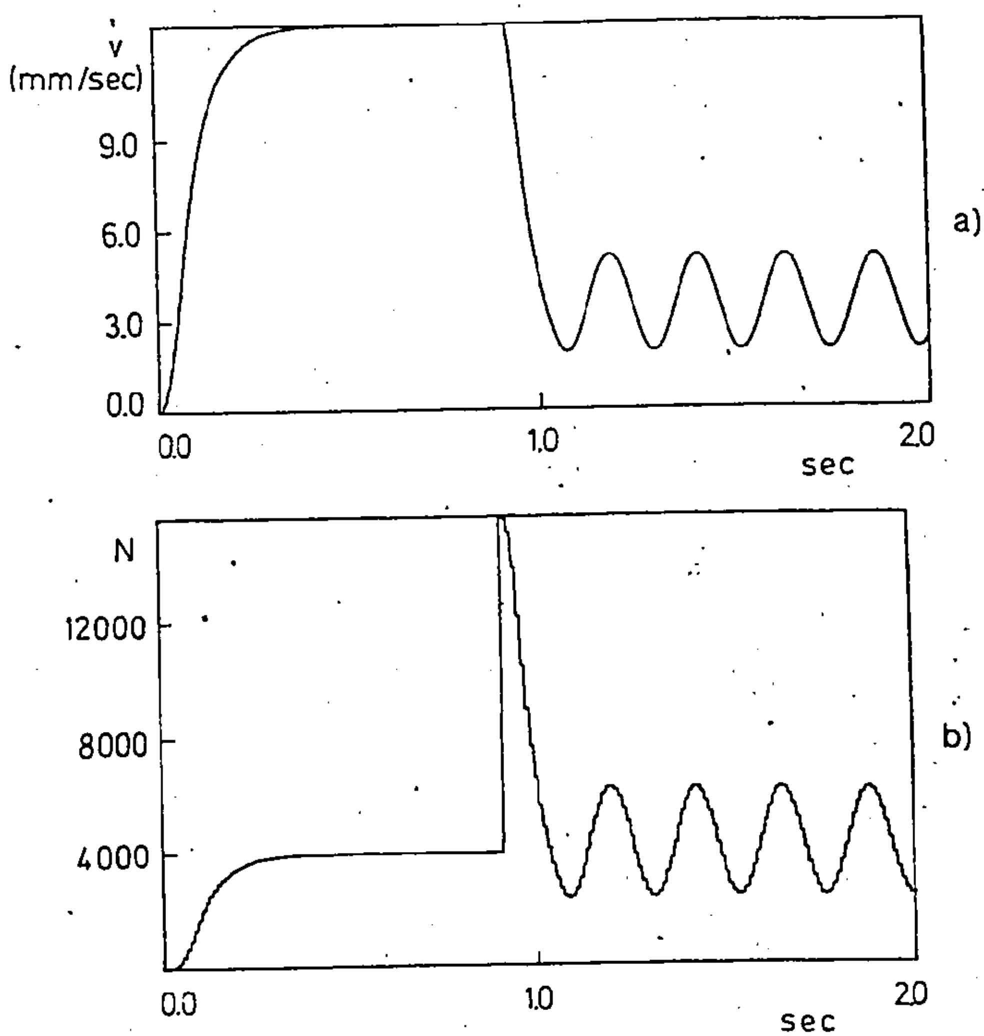

(a) Velocity and (b) Force Transients Moving Across a Step in Depth of Cut. Four Teeth, K_{ac} = 200, B = 0

FIGURE 4.12

formula:

$$a = K_{ac}\, e_f + B\, de_f/dt \text{ ------------------------------- } (4.18)$$

Various values of the constant B were tried and for $B = 7.6 \text{ mm/sec}^2$ the best result was obtained as it is shown in figure 4.13 which shows the variation of F_{act} for otherwise the same case as in figure 4.12 b). At the point where depth of cut suddenly increases from b = 2.5 mm to b = 10 mm, there is the same sudden increase of force to $F_{act} = 4\, F_{nom}$ which is subsequqntly regulated down to F_{nom} = 4100N in about 110 msec. However, after that the process remains stable.

Next, a longer time interval is assumed between individual cutter teeth τ = 0.060 s, as e.g. it would be produced by slowing down spindle speed to N = 250 rev/min. This results in half the steady state velocity in both phases than in the preceding cases and, therefore, the rapid traverse limitation does not set in the first phase in which the force settles on F_{nom} = 4100N and velocity on v = 6.66 mm/sec. Consequently, at the point of the sudden increase of depth of cut the force shoots out to 16,400N as shown in figure 4.14. However, the longer delay τ in the transfer function equation (4.17) makes the system more susceptible to instability. Therefore, the acceleration gain constants had to be decreased to $K_{ac} = 50 \text{ mm/sec}^2$ and $B = 1.5 \text{ mm/sec}^2$. Still, some overshoot remains at the beginning of phase two.

Case B

All the conditions are the same as in the case A,

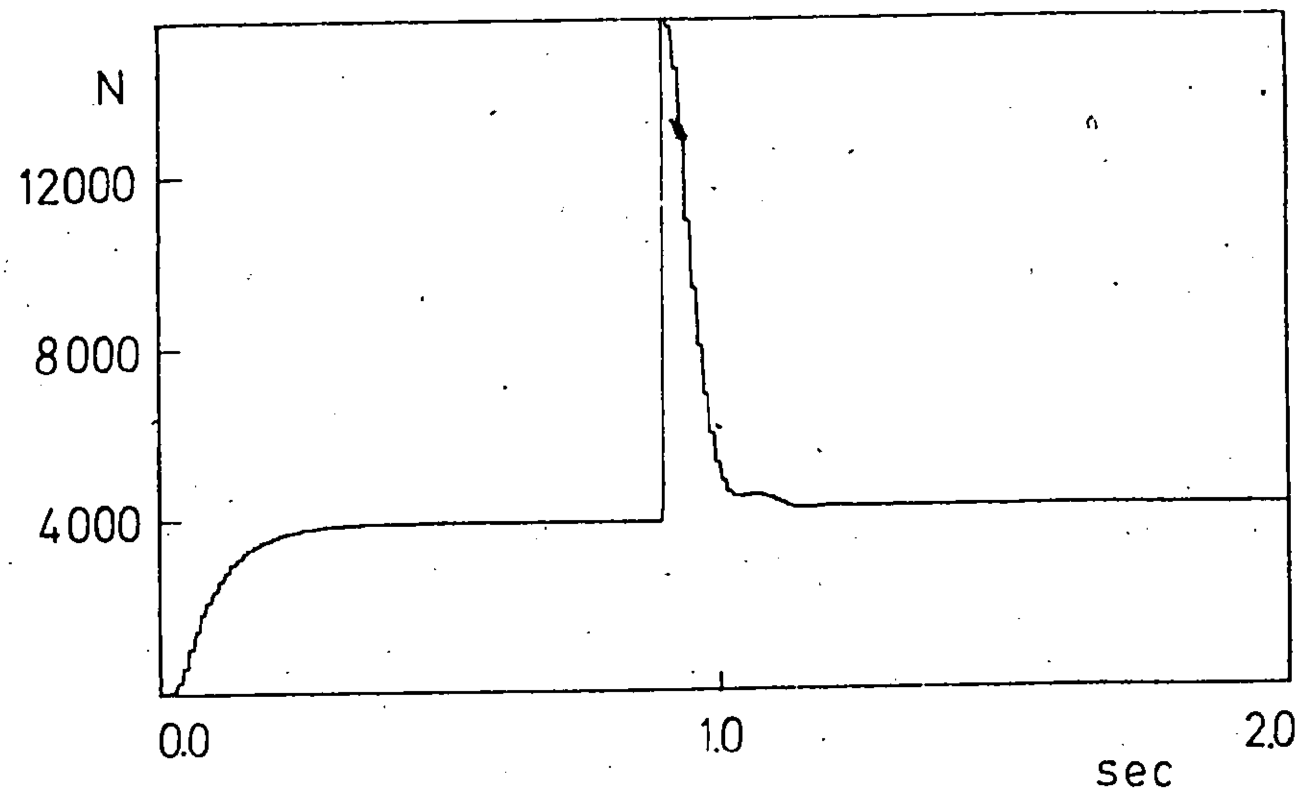

Force Transients Moving Across a Step in Depth of Cut. Four Teeth, K_{ac} = 200, B = 7.6

FIGURE 4.13

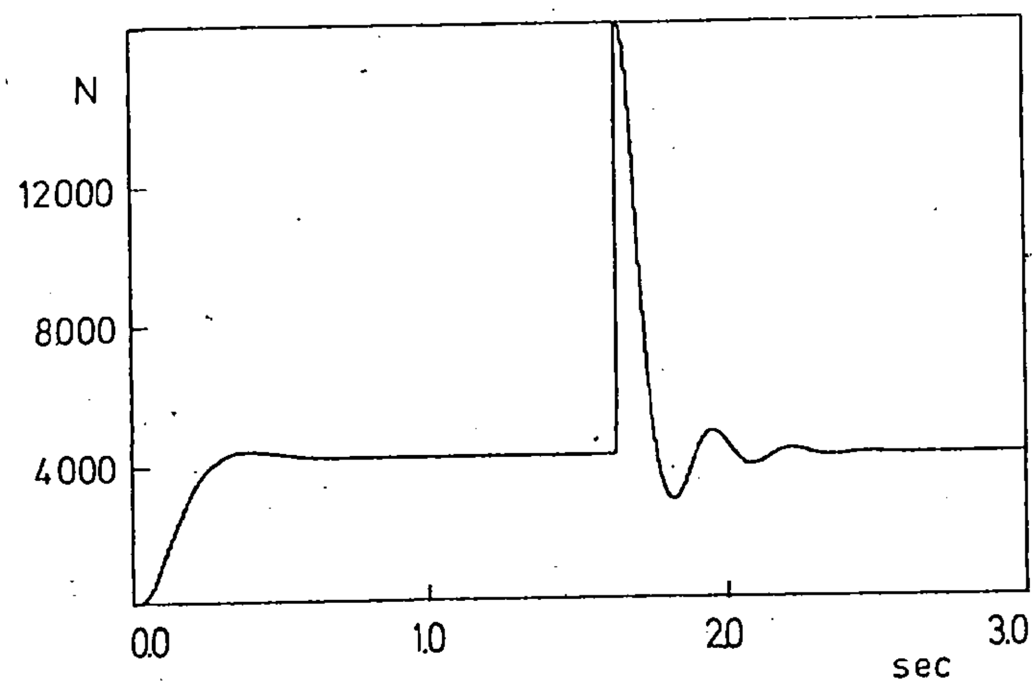

Force Transients Moving Across a Step in Depth of Cut. K_{ac} = 50, B = 1.5

FIGURE 4.14

except that cutter with 2 teeth only is assumed and thus with spindle speed N = 500 rev/min the time interval between cutter teeth is τ=0.060s and correspondingly also table velocities are half of those in case A for the same feed per tooth f_t. The force is periodically variable as in gigure 4.10 a) and as in formula(4.16) which in an analogous way to equation (4.17) becomes:

$$F = 93\ ab\ (1 + \text{Sin}\ 105\ t)\ \{x_{11}(t) - x_{11}(t - \tau)\} \quad ---(4.19)$$

Because of the value of τ = 0.060s, the same values of acceleration gain co-efficients are now used as in figure 4.14.

The result is shown in figure 4.15. The system perceives mainly the average of the periodically variable force. Therefore, in the first phase force is established with peaks of 6550N as shown in graph a), while the velocity reaches correspondingly high value of 11.77 mm/sec as shown in graph b). In the second phase the peaks of the force reach in average 8200N which is the double of F_{nom}. The velocity of the system reproduces the periodic variation of the force to still a rather small extent.

In order to emphasize the influence of the peaks of the force on the A/C loop and de-emphasize the readings of the low values of the periodic variation of the force the acceleration gain is decreased to K_{ac} = 10 mm/sec^2 while the decelerating gain is left unchanged:

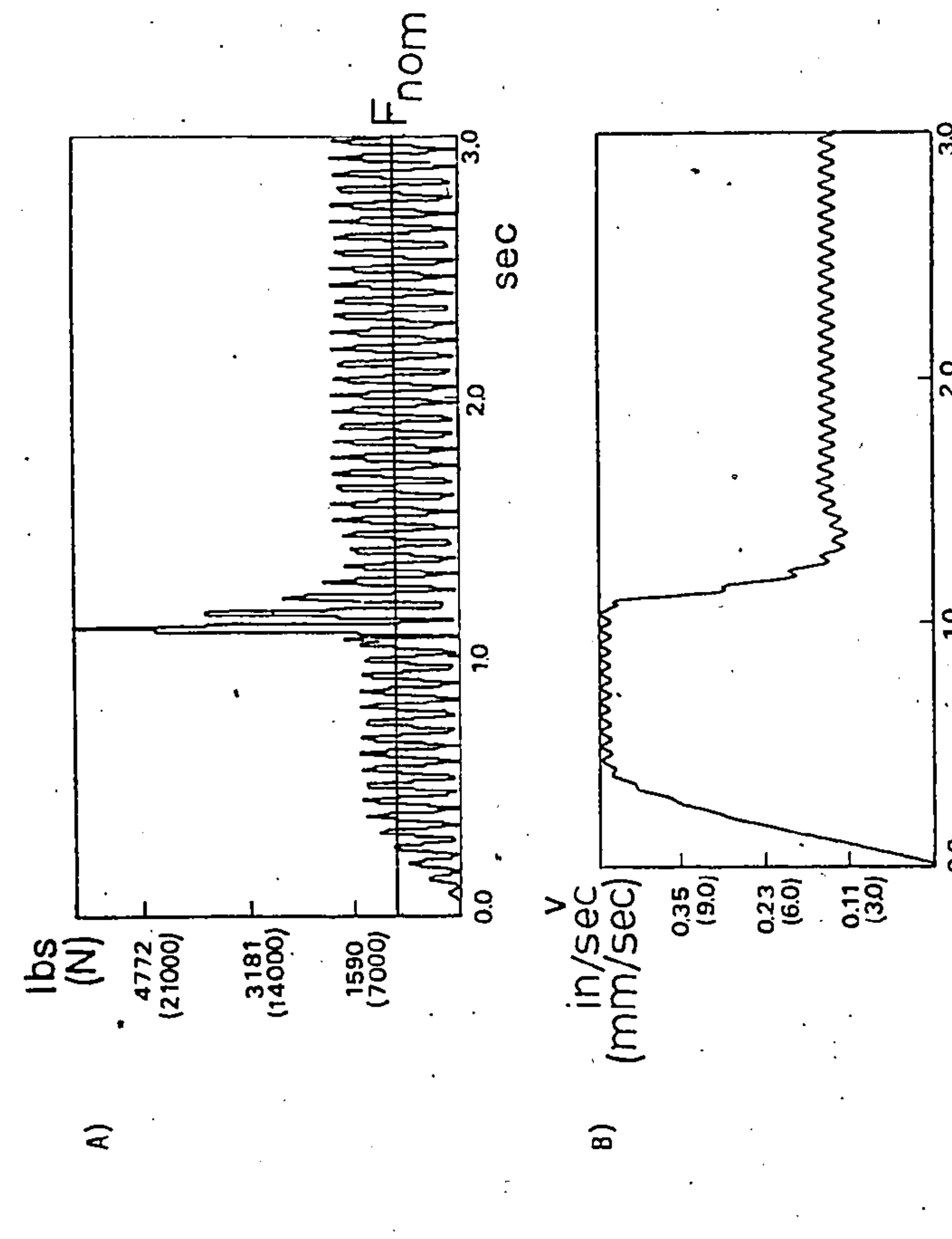

A) Force Transients, B) Velocity, Two Teeth, Periodic Cutting Force

FIGURE 4.15

$F_{act} > F_{nom}$, i.e. $e_f < 0$, $K_{ac} = 50$ mm/sec^2, B = 1.5 mm/sec^2

$F_{act} < F_{nom}$, i.e. $e_v > 0$, $K_{ac} = 10$ mm/sec^2, B = 1.5 mm/sec^2

The result of this change is shown in figure 4.16. The peaks of the force stabilize now at 5108N and the peak at the point of increase of the depth of cut reaches 19975N. This is an improvement to be paid for by the much longer time of increase of velocity and force at the beginning.

Case C

In this case the cutter has again 2 teeth and the time interval between them is $\tau = 0.060$s as in case B. However, this time we assume gradual penetration as in figure 4.11 b). Also, in the first phase there is no cutting at all and the system develops rapid traverse velocity v = 12.7 mm/sec with which it meets the side of the workpiece and enters into depth of cut b = 10 mm. Acceleration constants are used the same as in the last preceding case of figure 4.16.

The definition of the cutting force is now

$$F = 0.372\ r\ q\ b\ a\ \{x_{11}(t) - x_{11}(t - \tau)\} \text{ ------------(4.20)}$$

where parameters r and q are defined in figure 4.17. The values of r for penetration p> 7.5 mm represent the same variation of the force as figure 4.10 a) with a sampling interval Δ_t = 10 msec and a period τ = 60 ms while for penetrations P < 7.5 mm in the various ranges the teeth are out of cut for various periods of time. The parameter q is discretized as function of penetration according to figure 4.11 b). For P > 7.5 formula (4.20) will give the same force variation as

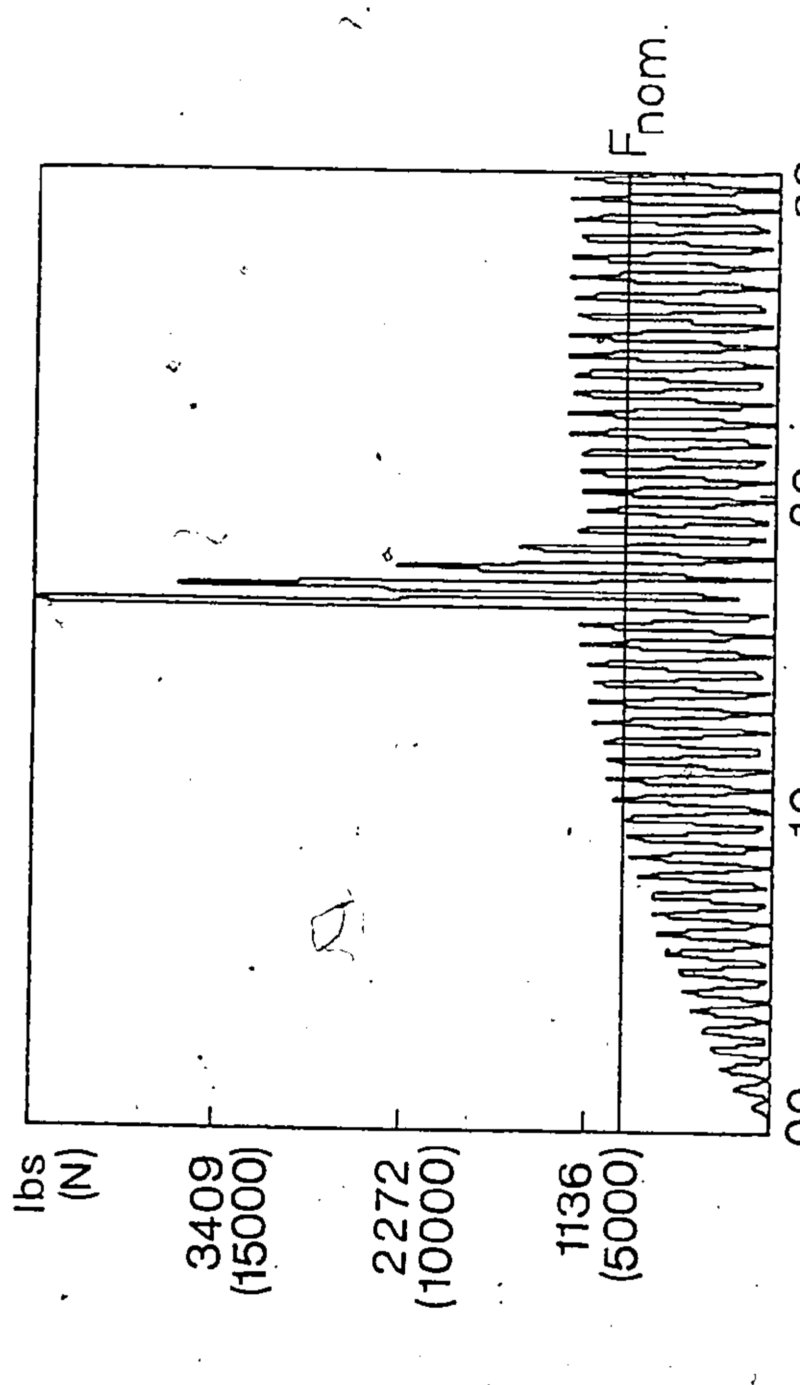

Force Transients Moving Across a Step, But Lower K_{ac} for Positive Force Error

FIGURE 4.16

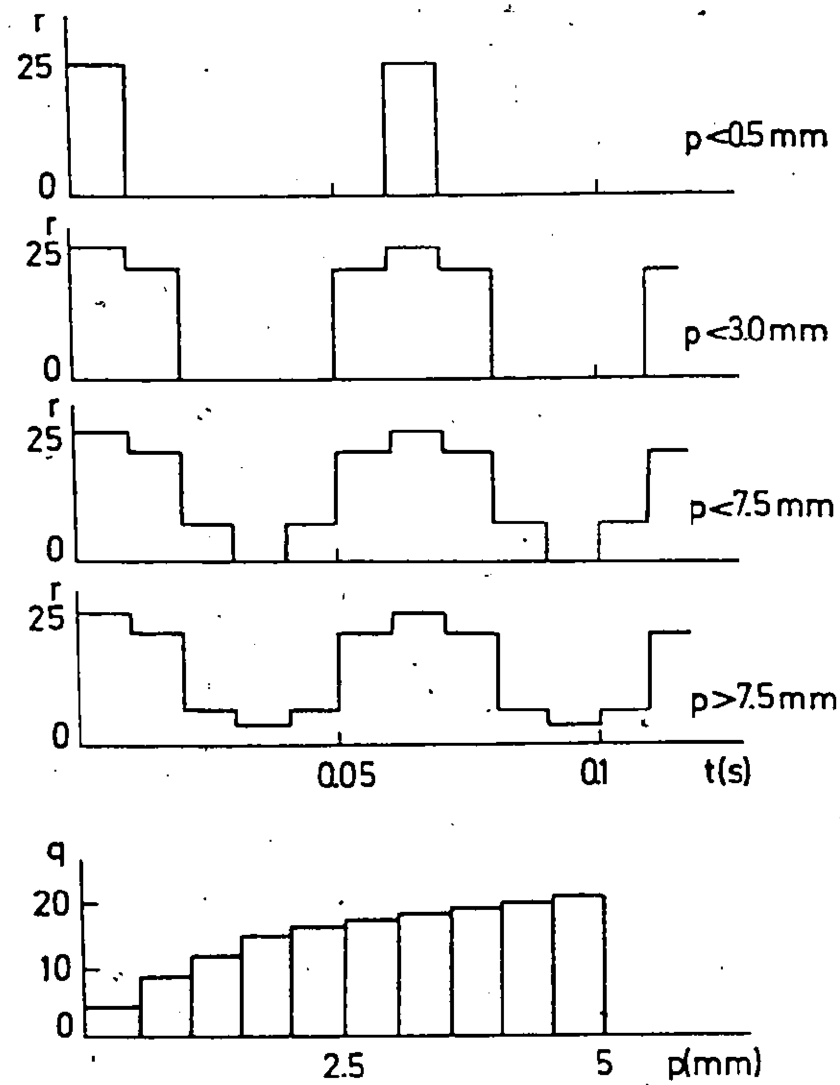

Parameters r and q For Force Formula For Penetrating a Wall

FIGURE 4.17

formula (4.19). The solution of this case of penetrating a wall is shown in figure 4.18. The force reaches a maximum of 15190N and after about 0.280 s it stabilizes with peak values of about 5000N.

Summarizing cases A, B, C:

In case A with non periodic force it was possible to bring down the sudden overload to the desired level in about 100 ms. In steady state the force was kept to F_{nom} = 4100N. In both cases A and B where instant penetration was assumed it was impossible to avoid the force reaching the peak corresponding to the velocity before the contact with the wall and to the depth of the wall (in the discussed cases a peak of four times the steady state force level). In case C with gradual penetration, this ratio of maximum peak to steady state was about 3. For periodic forces the use of acceleration gain 5 times lower than decelerating gain lead to the peaks of force exceeding F_{nom} only by about 25%. A more efficient technique in this respect is achieved by incorporating into the A/C algorithm a peak holding routine. The routine operates by recognizing only increases in sampled force values over a period corresponding to the tooth period. In this way the system attains a steady state with the peak tooth forces corresponding to F_{nom} as shown in figure 4.19.

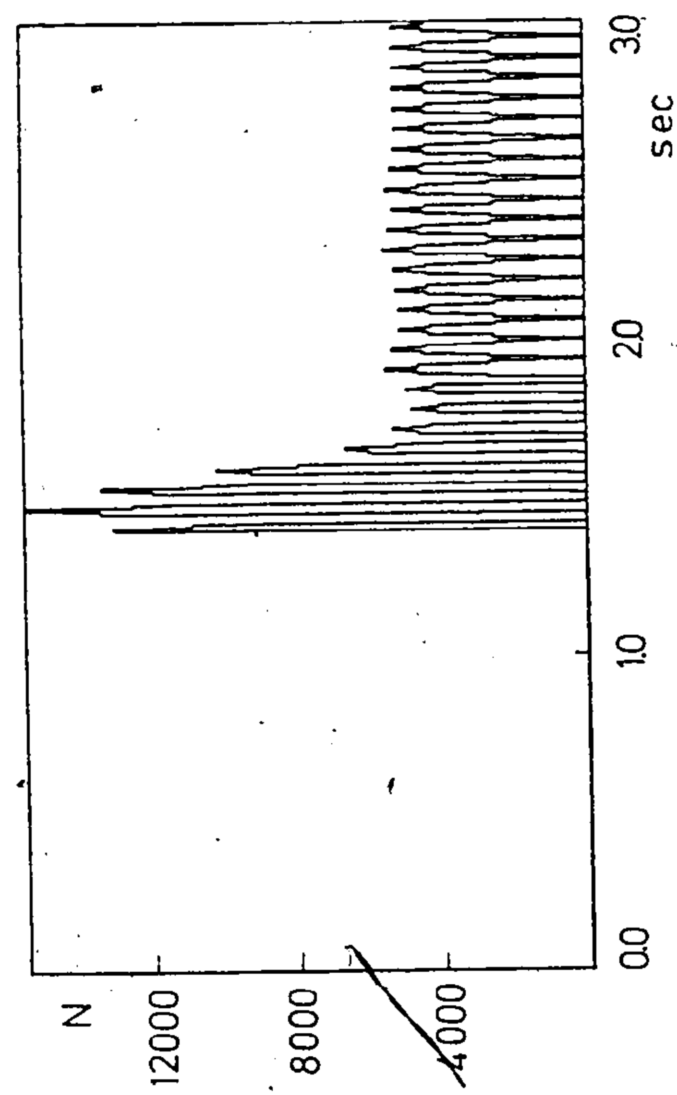

Force Variation in Penetrating a Wall, Two Teeth, τ = 60 ms.

FIGURE 4.18

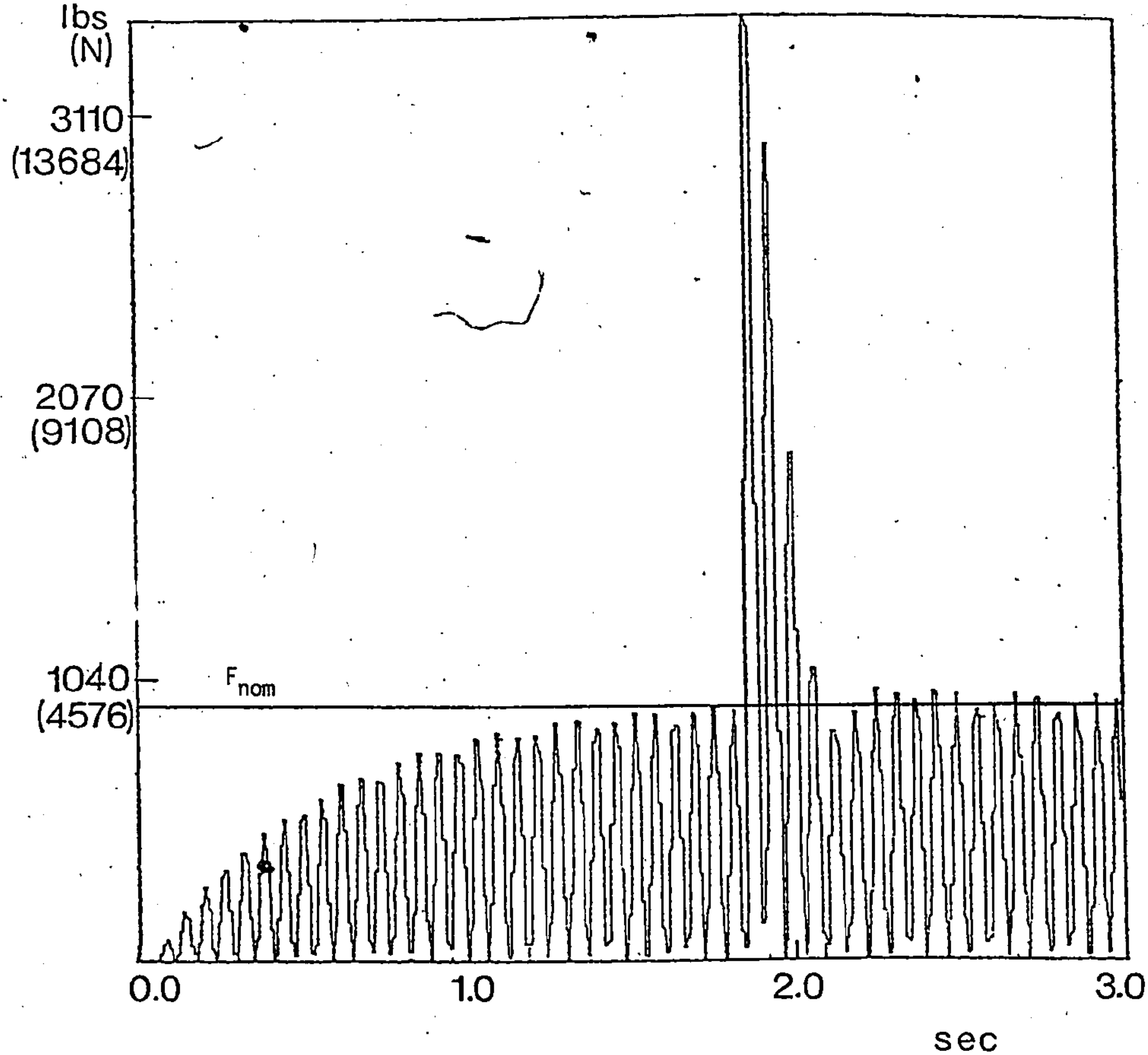

Cutting Force Response to Collision With Peak Holding

FIGURE 4.19

CHAPTER 5

EXPERIMENTAL RESULTS

5.1 Introduction

The use of the cutting force as the control parameter and the contouring velocity as the controlled variable in NC contouring operations leads to a rather simple form of adaptive control system, which, despite its simplicity, offers significant potential savings in machining time. Of special importance is the finishing time in die sinking which with conventional NC is rather long due to the conservative feed rates that have to be programmed to avoid cutter overload when the tool encounters the irregular profile left by the large diameter roughing tools. To predict the roughed contour by computation is possible, but calls for extremely large storage and lengthy computation. The alternative of in-process feed rate selection by adaptive control on the other hand, has found practical application. The most severe test to which the system can be subjected is that of collision with the work surface at rapid traverse. Under these circumstances the cutting force rises very quickly and the feed drive must be capable of decelerating to a safe speed before the force attains a dangerous level.

The results of the preliminary simulation studies presented in Chapter 4 demonstrated clearly that an A/C strategy based upon equations (4.1) and (4.18) results in a system response which although adequate to cope with several practical conditions is totally incapable of preventing excessive cutting forces during rapid changes in depth of cut. Simply increasing the A/C feedback gain K_{ac} leads to instability in the A/C loop. On the other hand, it is equally clear from the results of earlier studies of the NC loop (see e.g. figure 4.6) that the potential response of this system is not being fully exploited by the A/C system.

5.2 Transient Cutting Forces in End Milling

To understand the transient behaviour of the A/C system it is necessary to appreciate the transient nature of the cutting process immediately after tool-work impact. For the purpose of simulating the cutting force in transient condition, it is necessary to consider the motion of two subsequent teeth (in case of a two flute end mill) on cycloids composed of the table motion "x(t)" and the tool rotary motion α. In this section, the cutting force is expressed as the sum of partial forces ΔF_i each of them acting on a small part Δb_i of the total axial length b of the helix of the cutting edge. As shown in figure 5.1, starting with the leading point P of the edge, the individual parts Δb_i are lagging behind each other by an angle of rotation of the cutter ϕ where:

$$\phi = \Delta b.\mathrm{Tan}\ \lambda / r \text{ --------------------------------------- } (5.1)$$

and λ is the helix angle.

In order to take into account the motion of two subsequent teeth on cycloids (see figure 5.2), it is at any given

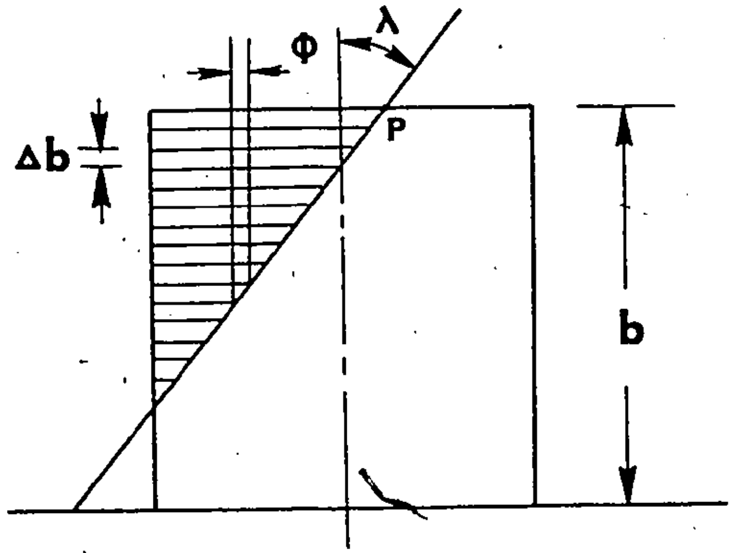

Unrolled View of the Cut Surface

FIGURE 5.1

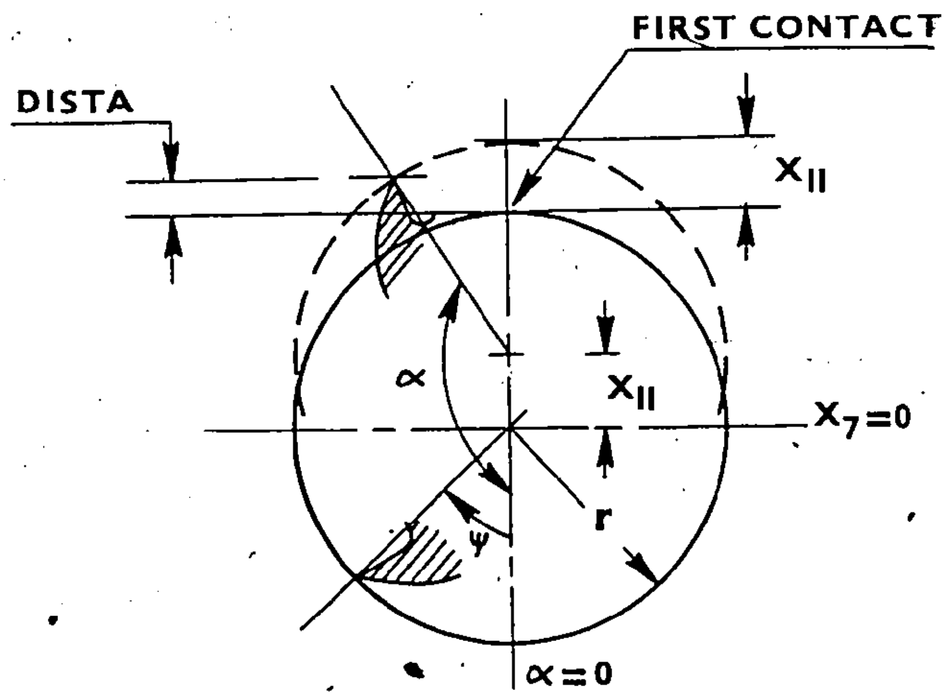

Motion of Two Subsequent Teeth
on Cycloids

FIGURE 5.2

moment:

$$\alpha = wt + \Psi - I.\phi \tag{5.2}$$

where,

$w = \frac{180^\circ}{\tau}$ and τ is the tooth period

t is the time interval from the moment of first contact of the circle diameter of the cutter with the wall.

Ψ is the initial angle of the tooth position as shown in figure 5.2.

I is the subscript of the Section Δb concerned.

The total number of these sections (and of the partial forces ΔF_i) is $IB = b/\Delta b$.

Considering thus, a two flute end mill, the distance "DISTA" by which a tooth has penetrated the workpiece at time t is:

$$DISTA = x_{11}(t) - r + r \cos(\pi - \alpha) \tag{5.3}$$

Let Term = $|\cos(\alpha)|$

Then

$$DISTA = x_{11}(t) - r\{1 - TERM\} \tag{5.4}$$

The penetration of the previous tooth will then be:

$$DISTB = - r\{1 - TERM\} + x_{11}(t - \tau) \tag{5.5}$$

Finally, the chip thickness "CHIP" is defined as:

$$CHIP = (DISTA - DISTB) * TERM \tag{5.6}$$

The force ΔF_i for each part Δb_i of the edge is proportional to chip thickness "CHIP", it is:

$$\Delta F_i = K.\Delta b\ CHIP \tag{5.7}$$

where K is a proportionality constant depending on the workpiece material.

The total radial force, at any instant is the sum of all partial forces acting on all IB parts of the edge, it is:

$$F = \sum_{i=1}^{IB} \Delta F_i \qquad (5.8)$$

Figure 5.3 shows the computed results of radial force for a two flute end mill penetrating a wall at 750 mm/min (30 in/min) with a depth of cut of 5.33 mm (0.210 inch) and a helix angle of 30°. The tooth force is calculated using equations 5.7 and 5.8, where K is assumed 690 N/mm^2 (1×10^5 lb/in^2). Figure 5.4 shows the computed radial force for the same conditions used in the case presented in figure 5.3 except for a different value of the angle Ψ. It is interesting to notice the effect of the angle Ψ on the magnitude of the first force peak. Figure 5.5 illustrates the geometry and resulting radial force for a 4 flute end mill with zero helix angle. Initially, chip thickness and therefore, force rise rapidly upon entry, then harmonically change, followed by a rapid decrease upon tooth exit. For the 4 flute end mill shown in figure 5.5 the first tooth can yield maximum force in 4.1 milliseconds (at zero helix angle) at a feedrate of 750 mm/min. Overlapping of adjacent teeth subsequently leads to a constant cutting force. The finite helix angle will of course, extend the tooth contact times depicted in figure 5.5. For example, the initial tooth contact period will become 14 milliseconds for a 30° helix cutter at a depth of cut of 6.35 mm (0.25 inch).

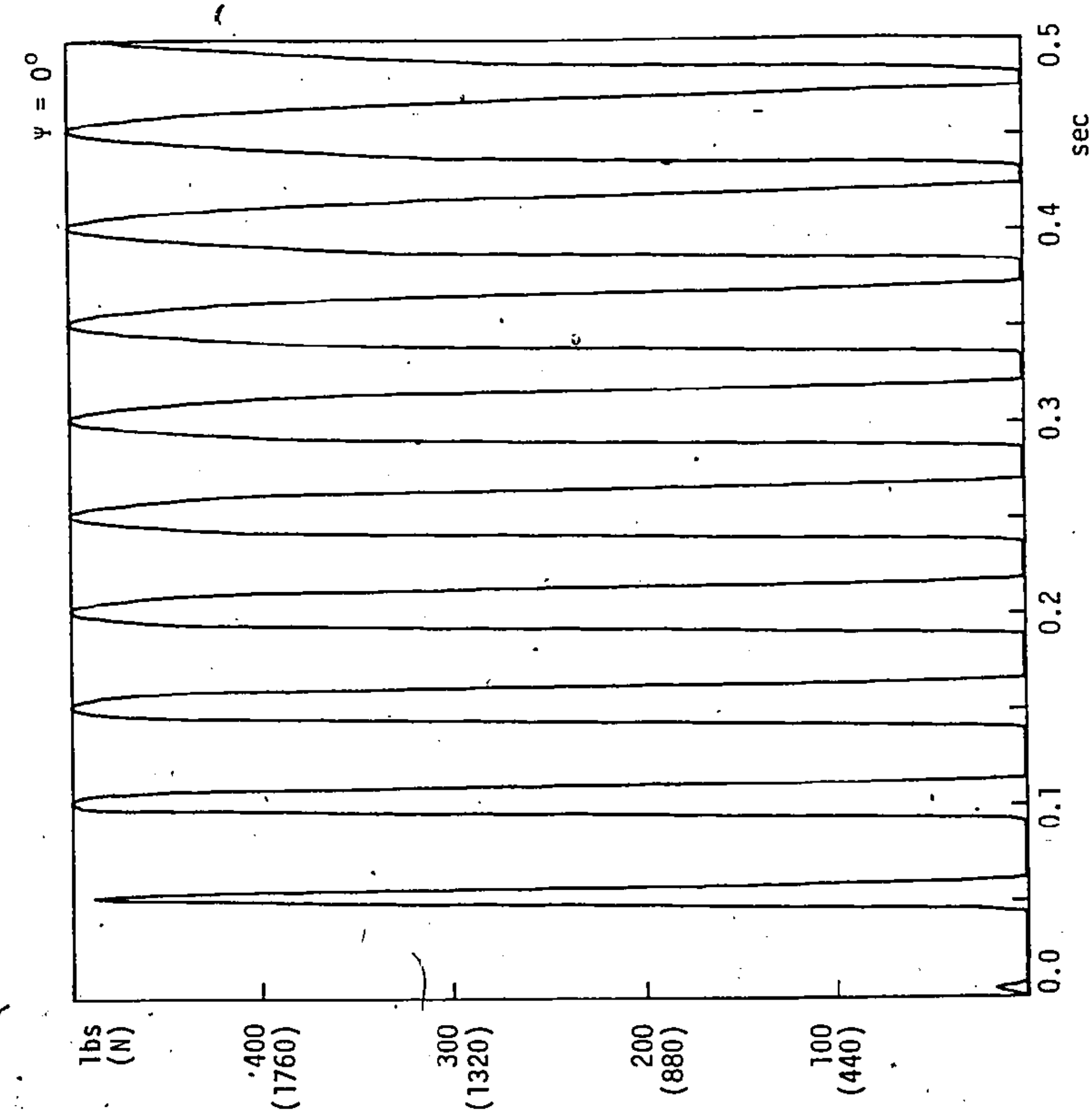

Simulated Force Behaviour - 2 Flute End Mill

FIGURE 5.3

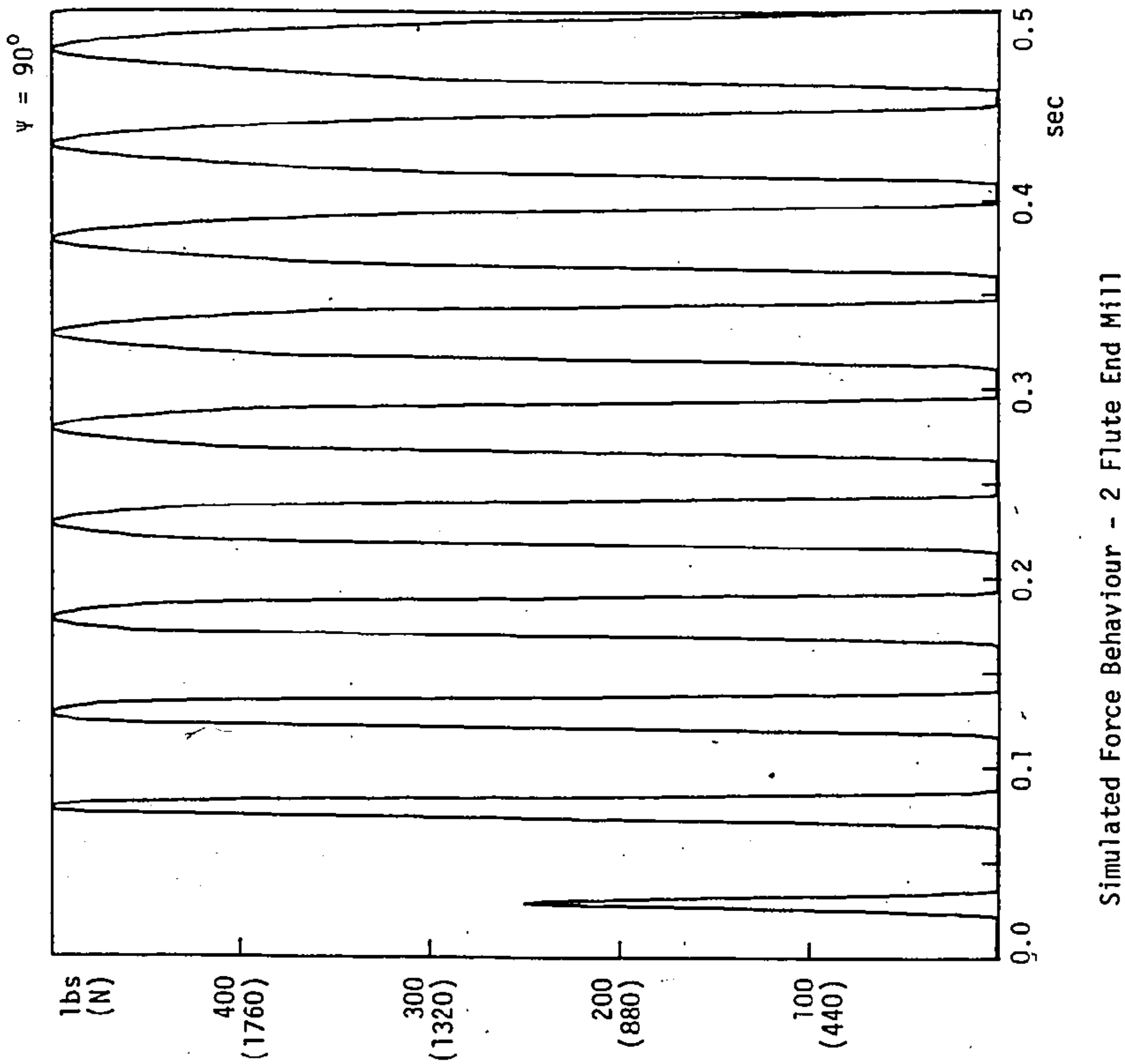

Ψ = 90°
lbs
(N)
400
(1760)
300
(1320)
200
(880)
100
(440)
0.0
0.1
0.2
0.3
0.4
0.5
sec
Simulated Force Behaviour - 2 Flute End Mill

FIGURE 5.4

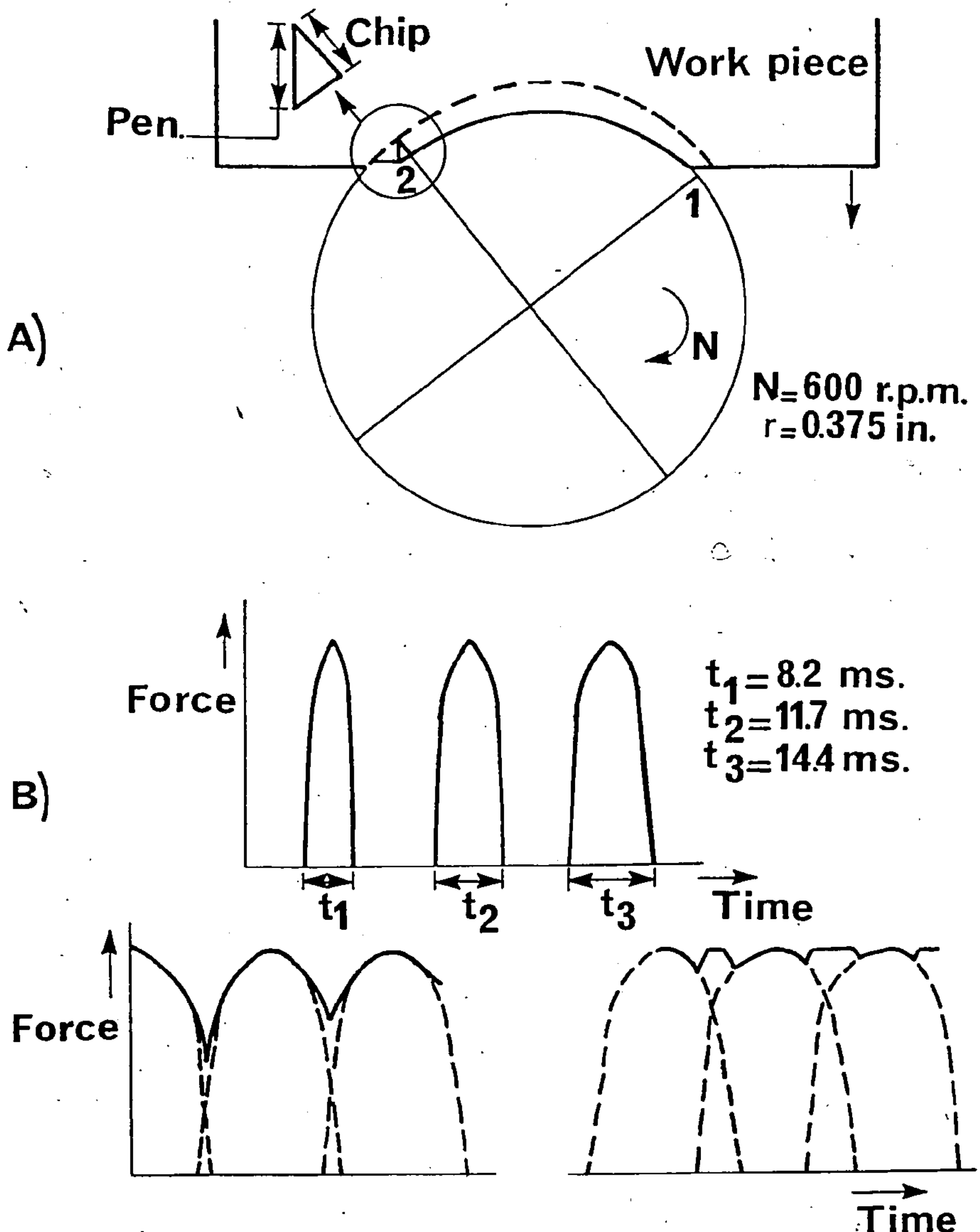

A) Early Stage of Penetration, (B) Transient Tooth Forces

FIGURE 5.5

These values are calculated assuming that a tooth has just missed contact with the work when the cutter envelope meets the work surface and therefore, a complete tooth period corresponding to 90° rotation is required before the first contacting tooth attains its maximum force.

Figure 5.6 shows the computed results of radial force for a four flute end mill penetrating a wall at 750 mm/min with a depth of cut of 6.5 mm(0.26 inch) and a helix angle of 30°. The constant K is assumed $1330 N/mm^2$ (2×10^5 16/in).

It is observed that the first tooth does not attain maximum force due to the effect of the helix angle, but the maximum load is carried by the second tooth 12.5 milliseconds later. Overlapping occurs after one revolution and a rather smooth cutting load is encountered after 3 revolutions.

In view of these analytical findings, it was decided to conduct non-adaptive impact tests to determine the transient forces under these conditions. These tests were conducted using the rotary dynamometer described in appendix I, which is attached to the spindle of the milling machine. Sample results are shown in figures 5.7, 5.8 and 5.9. Referring to figure 5.9, it is seen that after the feedrate has accelerated to rapid traverse rate, impact occurs. The force buildup is rather slow, particularly during the first 100 milliseconds. The result of this experiment is therefore, contrary to the one obtained from simulation studies and presented in figure 5.6 for the case of 4 - flute end mill. This

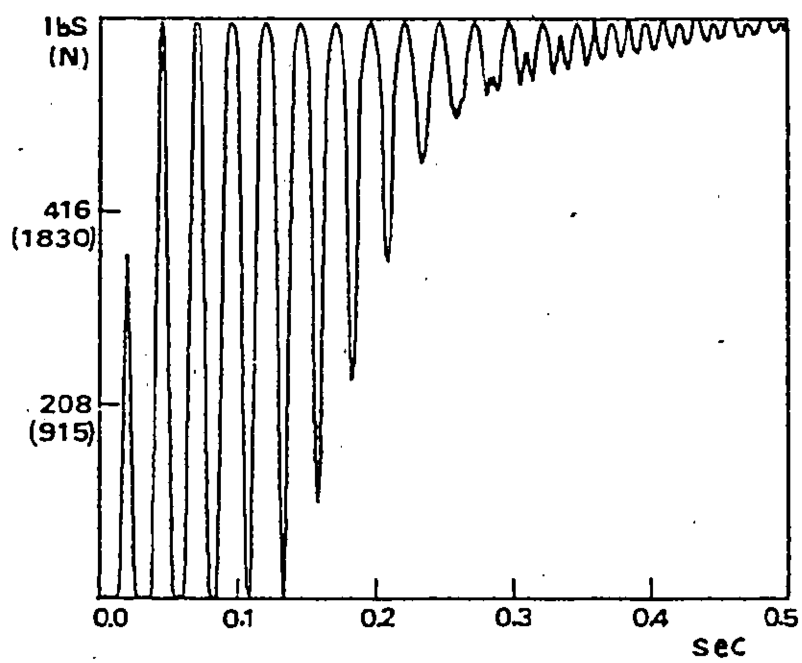

Simulated Force Behaviour -- 4 Flute End Mill
Without A/C

FIGURE 5.6

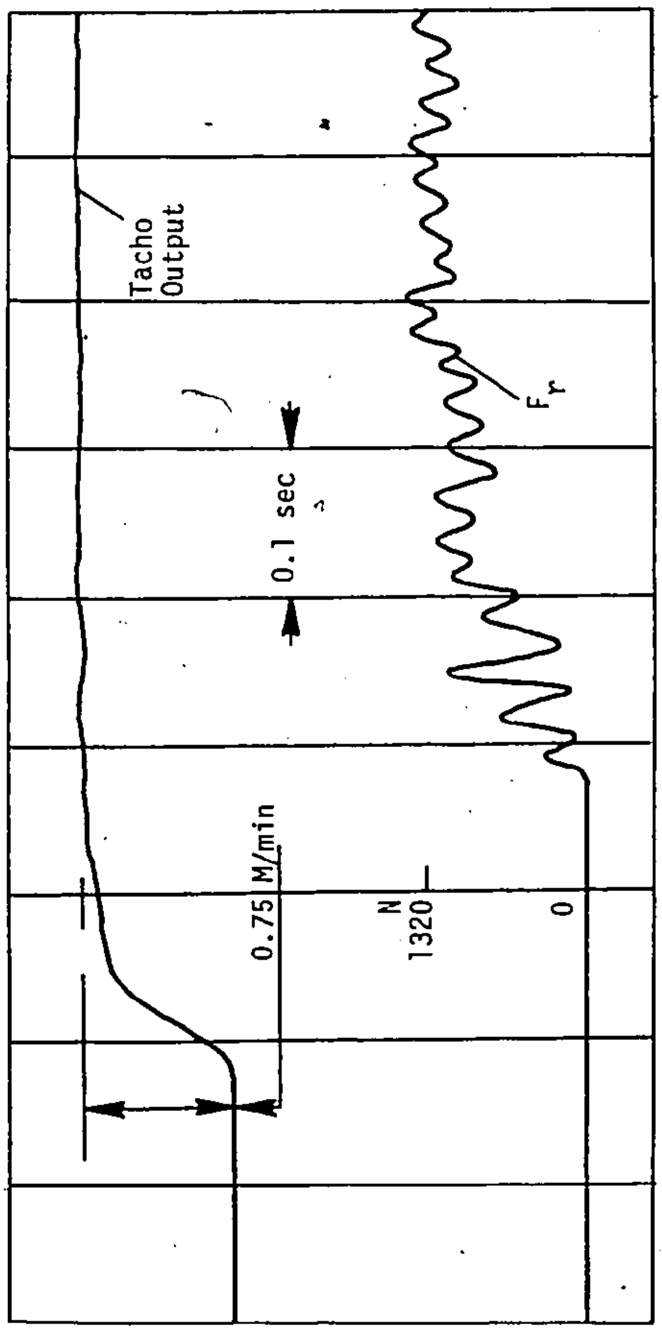

AISI 1020 Work Material, 19.05 mm Dia. - 4 Flute HSS End Mill, V = 35.34 M/min,
b = 1.9 mm

Cutting Force Response Without A/C

FIGURE 5.7

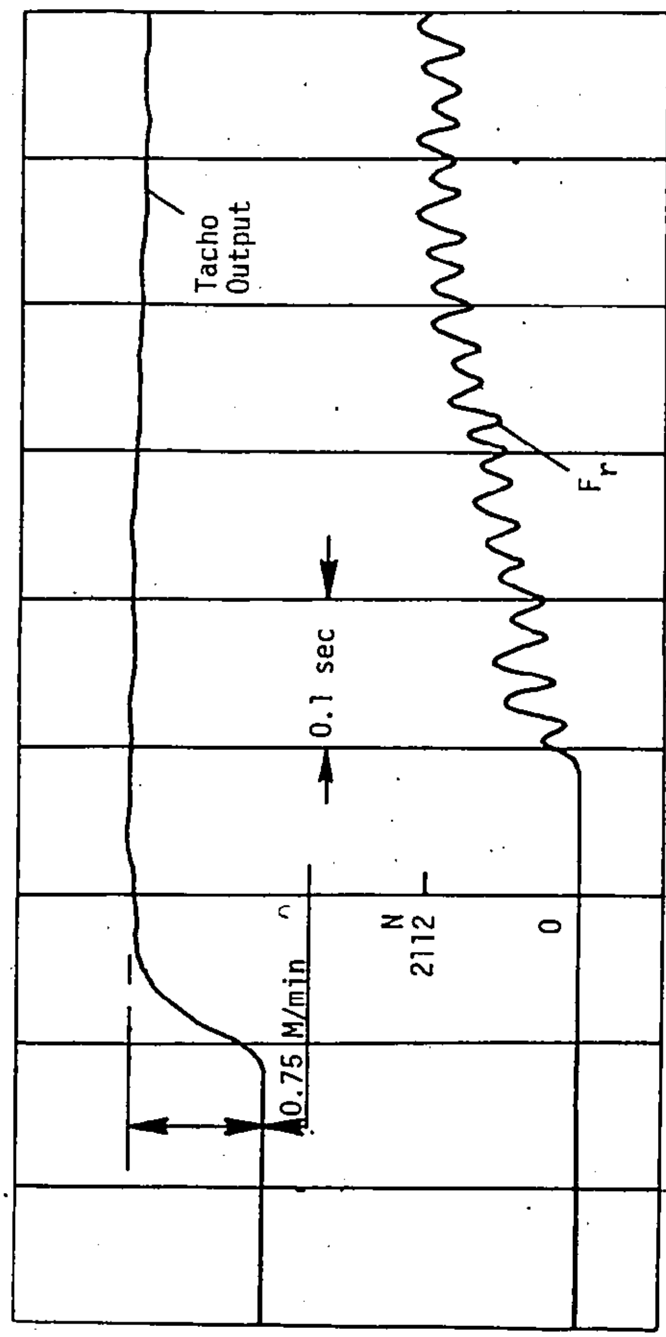

AL. Alloy Work Material, 19.05 mm Dia. - 4 Flute HSS End Mill, V = 35.34 M/min
b = 5.3 mm

Cutting Force Response Without A/C

FIGURE 5.8

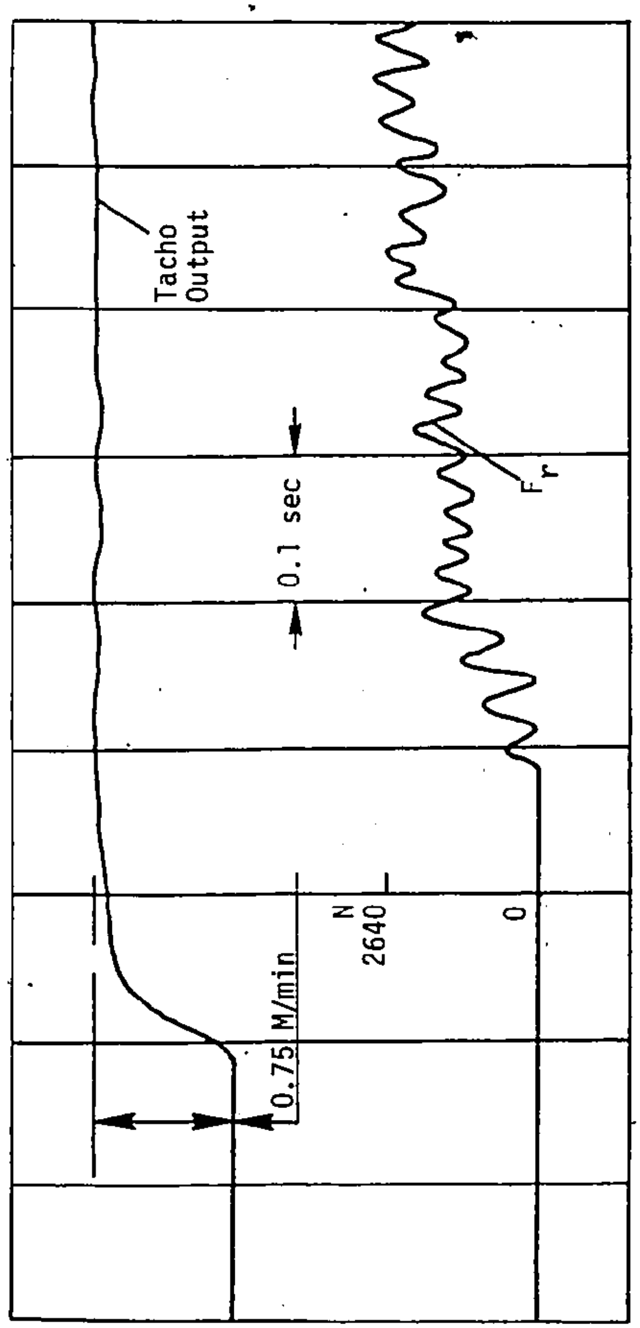

AL. Alloy Work Material, 19.05 mm Dia. - 4 Flute HSS End Mill, V = 35.34 M/min
b = 6.6 mm

Cutting Force Response Without A/C

FIGURE 5.9

result naturally throws doubt upon the dynamometer force measurements and raises the question -- is the dynamometer perceiving the true transient cutting force?

In an attempt to answer this question dynamic tests were conducted on the spindle system both with and without the dynamometer. Figure I.3 in Appendix I shows the resulting real receptance values indicating resonant frequencies of 480 Hz (without dynamometer) and 340 Hz (with dynamometer). Since the fundamental tooth frequency in the experiment was 40 Hz, little attenuation is expected in the dynamometer response. There will be some attenuation of the harmonic content of the force signal, but this is not expected to be significant enough to explain the discrepancies between simulated and experimental force behaviour. Clearly we must look elsewhere for the explanation.

5.3 Effect of Spindle Stiffness on Transient Cutting Force

It is generally accepted that the tool and its clamping to the spindle represent one of the most important sources of flexibility in a vertical knee type milling machine. While the workpiece has usually a small mass compared to that of the table and knee and is rigidly fixed to the table so that it does not influence much the vibratory system of the machine, the change of the tool and its clamping strongly influences the properties of the system.

According to Tlusty [72], in a knee type vertical milling machine, the static analysis would show the following important springs: the spindle and its mounting, the attachment of the cutter to the spindle, the torsion of the upper part of the upright, the knee and its connection with the upright. The dynamic analysis will not find other "weak links". It will, however, place in order the significance of the ones resulting from the static analysis, showing that it is the stiffness of the spindle with its mounting and of the attachment of the cutter to the spindle, which is responsible for the degree of stability, that the twist of the upper part of the upright is of secondary importance and the knee and its connection with the upright has practically no effect.

The direct static stiffness of the spindle was measured at the end of a 19.05 mm (0.75 inch) dia. of a steel bar used to simulate the end mill. The arrangement used for the measurement is shown in figure 5.10. The result of these measurements indicated that the spindle system has a static stiffness of approximately 5800 N/mm(33000 lb/in) when a 38.1 mm (1.5 inch) long steel bar was used.

The spindle flexibility will obviously limit the initial tooth penetration, thereby, reducing the transient chip thickness and therefore the force. The mechanics of chip formation under these conditions has been explained in reference [72] where the transient chip thickness was shown to be dependent upon the ratio of cutting stiffness to machine stiffness. The higher this ratio the slower will be the force buildup.

To explain the phenomenon and to attempt to quantify

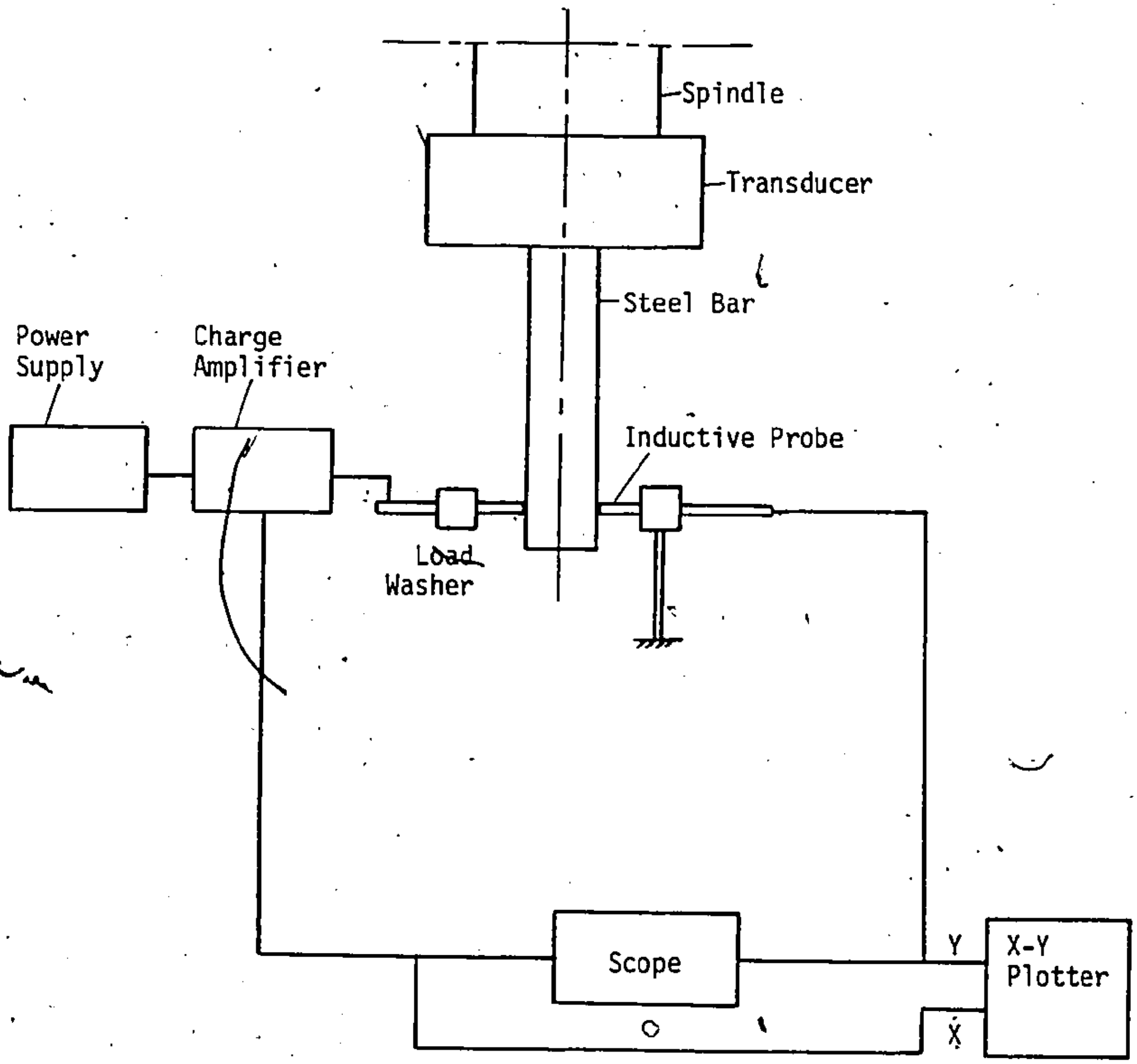

Arrangement Used for Measurement of Direct Stiffness

FIGURE 5.10

its effect, consider a case in which a tooth penetrates the workpiece in a harmonic fashion leading to a force fluctuation given by:

$$F = F|\ \text{Sin}\ wt\ | \text{ -----------------------------------(5.9)}$$

and $w = 2\pi N z$, where N is the spindle speed in rev/sec and z is the number of teeth.

Subsequently, a second tooth cuts over the surface left by the first tooth leading to a further harmonic variation in force. The resulting force would be given by the solid line in figure 5.11 and expressed by equation 5.9 if no tool-work deflection occurred.

In fact, the finite flexibility between tool and workpiece reduces the chip thickness and with it the resulting force. Subsequent teeth are thus attempting to remove a thicker chip than the nominal feedrate demands.

Now let us quantify the effect of tool-work deflection. During the first tooth pass the tool will deflect an amount given by $\frac{F_1|\text{Sin}\ wt|}{K_S}$, where K_S is the stiffness of spindle.

If the original force F is related to the chip thickness by equations 5.7 and 5.8, therefore in general:

$$F = K.b.h_c$$

h_c = Chip Thickness

the cutting stiffness is defined as

$$K_C = \frac{dF}{dh_c} = K.b \text{ -----------------------------------(5.10)}$$

The actual chip thickness removed during pass 1 will therefore be

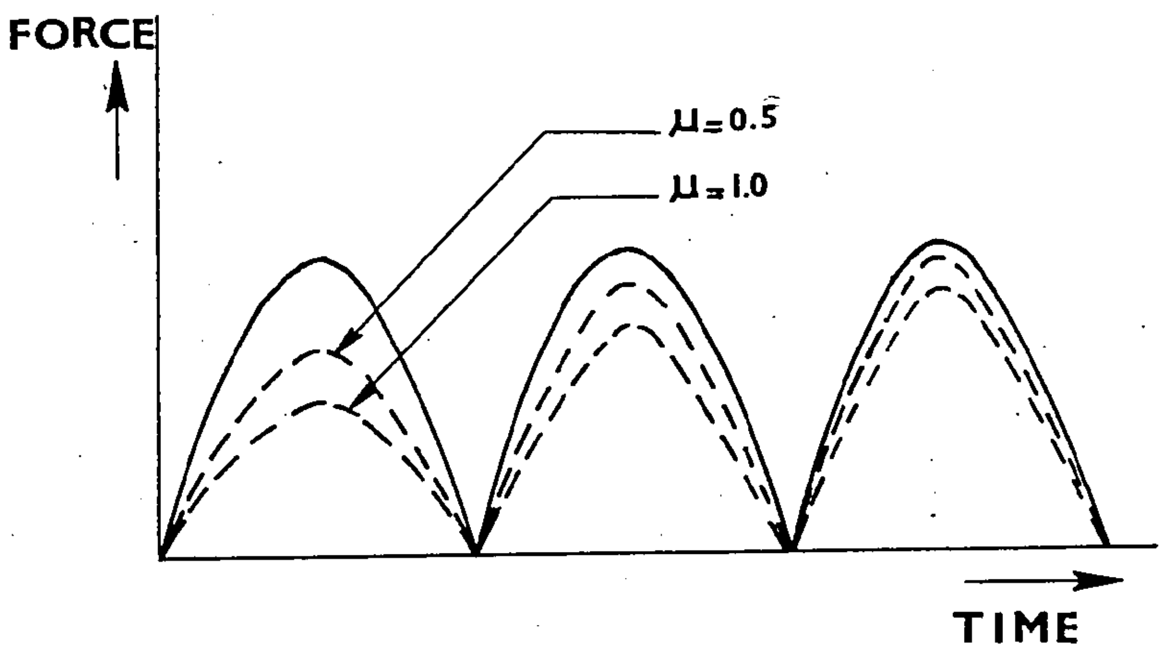

Effect of Spindle Flexibility on Cutting Force

FIGURE 5.11

$$h_{c_1} = h_c - \text{cutter deflection}$$

$$= h_c - \frac{F1}{K_S} \text{ -- (5.11)}$$

but the force F1 corresponding to the chip thickness h_{c_1} is given by:

$$F1 = K_C\, h_{c_1} \text{ -- (5.12)}$$

Therefore:-

$$h_{c_1} = h_c - \frac{K_C\, h_{c_1}}{K_S} \text{ ------------------------------------ (5.13)}$$

or $h_{c_1} = \frac{h_c}{1 + \mu}$ where $\mu = \frac{K_C}{K_S}$

and thus

$$F1 = \frac{F}{1 + \mu} \left| \text{Sin } wt \right| \text{ ---------------------------------- (5.14)}$$

The situation during pass 2 gives

$$h_{c_2} = \frac{h_c}{1 + \mu} + \frac{h_c}{(1 + \mu)^2} \text{ ----------------------------- (5.15)}$$

Generally the force equation becomes

$$F_p = \frac{F\left|\text{ Sin } wt\right|}{1 + \mu} \left\{ \sum_{p=1}^{n} \left(\frac{\mu}{1 + \mu}\right)^{p-1} \right\} \text{ ----------- (5.16)}$$

P = pass number

Figure 5.11 shows the force buildup for values of μ of 1 and 0.5. The force increases gradually from its initial value of $\frac{F\left|\text{Sin } wt\right|}{1 + \mu}$ in a geometric sequence to a final value of $F\left|\text{Sin } wt\right|$.

For the cutting tests with Al. Alloy the cutting stiffness is estimated to be $K_C = 1380.b\ N/mm^2$. Thus, at a depth of cut of

6.6 mm (0.26 inch), the cutting stiffness is 9100 N/mm (52000 lb/in). Using the spindle static stiffness of 5800 N/mm yields:

$\mu = 1.58$

It is obvious from the foregoing that this effect will therefore, be highly significant and cannot be neglected in further simulation studies. The case of penetration without adaptive control is shown in figure 5.12, with $\mu = 1.58$ for the 4 flute end mill. The corresponding case with a rigid spindle was shown in figure 5.6. The rigid system attains maximum force 33 milliseconds after initial tooth contact. The flexible system has only attained 53% of its maximum force in this time and does not develop the maximum until 250 milliseconds. The effect of spindle flexibility is clearly demonstrated and this result compares much more favourably with the experimental result presented in figure 5.9.

5.4 Adaptive Control Algorithm "A"

The results of the simulation studies presented in Chapter 4 demonstrated that an A/C strategy based upon equations 4.1 and 4.18 results in a system response that is incapable of preventing excessive cutting forces during rapid changes in depth of cut. To take advantage of the maximum response of the NC system without causing instability in the A/C loop, calls for a two level A/C strategy. During transient cutting demands such as a step in depth of cut, the A/C feedback will therefore, call for a very rapid deceleration which will be allowed to per-

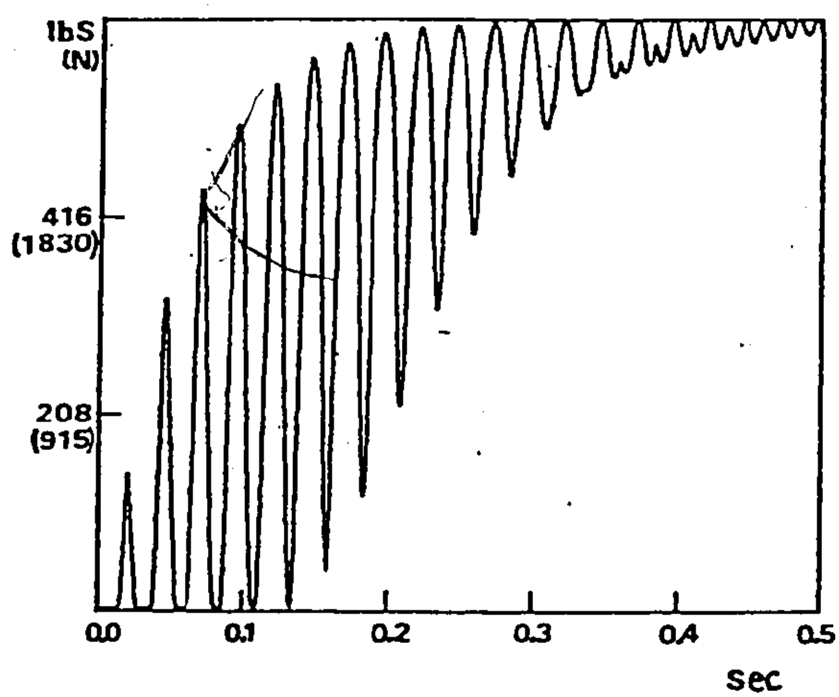

Transient Cutting Force Without A/C - Flexible Spindle - 4 Flute End Mill

FIGURE 5.12

sist only for a limited time before the A/C system automatically switches to the slow acting or limited acceleration condition. Re-entry to the special action strategy will occur only if the sampled peak force exceeds F_{nom} by a given amount.

The A/C strategy is as follows:-

a) For $F_{act} < 10$ lb (45N)

$V_{com} = V_{max} = 30$ in/min (750 mm/min) --------------(5.17)

b) For $F_{act} > 10$ lb

$V_{com} = .03$ in/min (7.5 mm/min) --------------------(5.18)

c) Condition (b) held for 100 milliseconds after which V_{com} is controlled by the equation:

$V_{com} = \int \{K_{ac}\, e_f + B\, de_f/dt\}\, dt$--------------------(5.19)

To demonstrate the behaviour of such a system further simulation results have been obtained for the rather severe condition in which tool-work impact occurs at maximum rapid traverse of 30 in/min (750 mm/min).

5.5 Simulation Results Using Algorithm "A"

Simulated results have been obtained using the special action algorithm expressed by equations (5.17) to (5.19) with the fast action correction held for 100 milliseconds after its onset at a sampled force level of $F_{act} > 10$ lb. The case considered first is the 4 flute end mill under the following conditions:- N = 600 RPM, Cutter Diameter = 19.05 mm (0.75 in), cutting stiffness is 9100N/mm (52000 lb/in), F_{nom} = 1340N (300 lbs.) and cutting force behaviour as given by equations (5.7) and (5.8). The tool-work impact velocity is set to 750mm/min (30 in/min). With the new algorithm, and assuming first a rigid spindle, the force and corresponding feedrate are shown in figures 5.13 and 5.14. After impact the force tries to build up to 2800N (625 lbs.), however the fast acting A/C system immediately reacts reducing the actual feed rate very quickly. Figure 5.14 shows that the feedrate reduces to its steady state value of 365 mm/min (14.1 in/min) in approximately 45 milliseconds. During the same period, it is seen that the actual force increases to 2240N (502 lbs.), albeit only on a single tooth. The force undershoots the value of F_{nom} and then rises slowly under the control of the slow acting algorithm of equation (5.19) to F_{nom}.

The simulation of the four flute end mill was repeated taking into consideration the spindle flexibility and using μ = 1.58. The results are shown in figures (5.15) and (5.16). Comparison of these results with figures (5.13) and (5.14) show quite clearly that although the feedrate response remains substantially unchanged the transient forces now exceed F_{nom} by only 2 - 3%. Figures (5.17) to (5.20) show the simulation of a two flute end mill penetrating a wall at rapid traverse. In this case the wall was assumed to have the same radius of curvature as the cutter envelope. The cutting conditions used are the same as in the case of the four flute end mill presented in figures (5.13) to (5.16).

The feedrate response shown in figure (5.17) shows

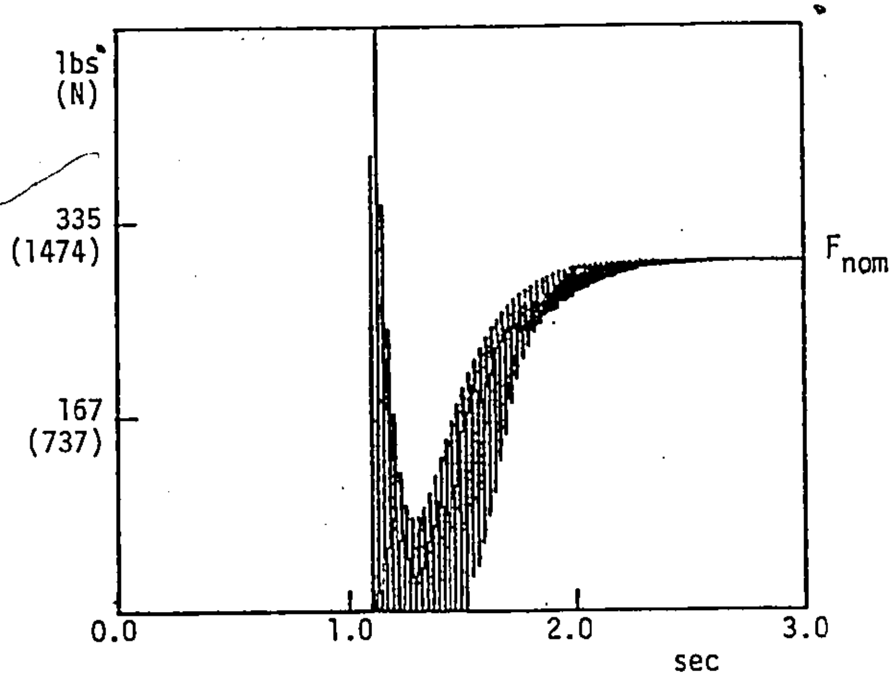

Simulated Collision Using Modified Algorithm "A" -
Cutting Force

FIGURE 5.13

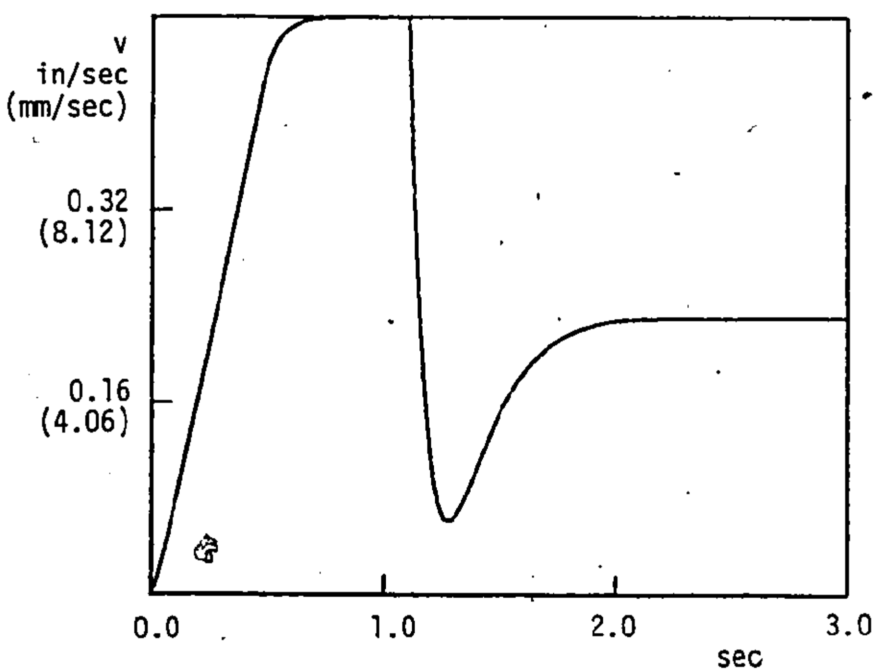

Simulated Collision Using Modified Algorithm "A" -
Feed rate

FIGURE 5.14

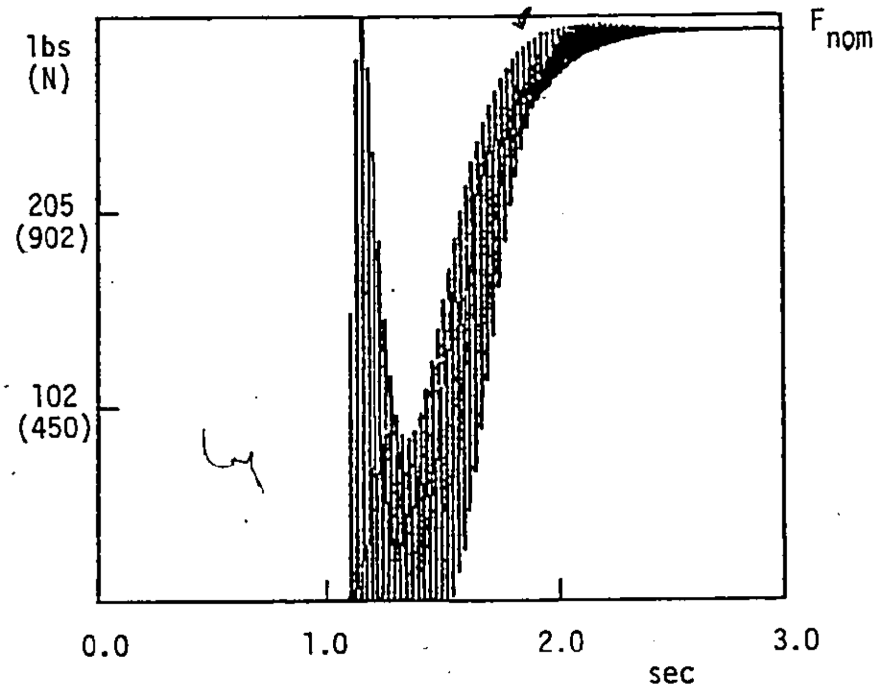

Simulated A/C Response With Flexible Spindle -
4 Flute - Cutting Force

FIGURE 5.15

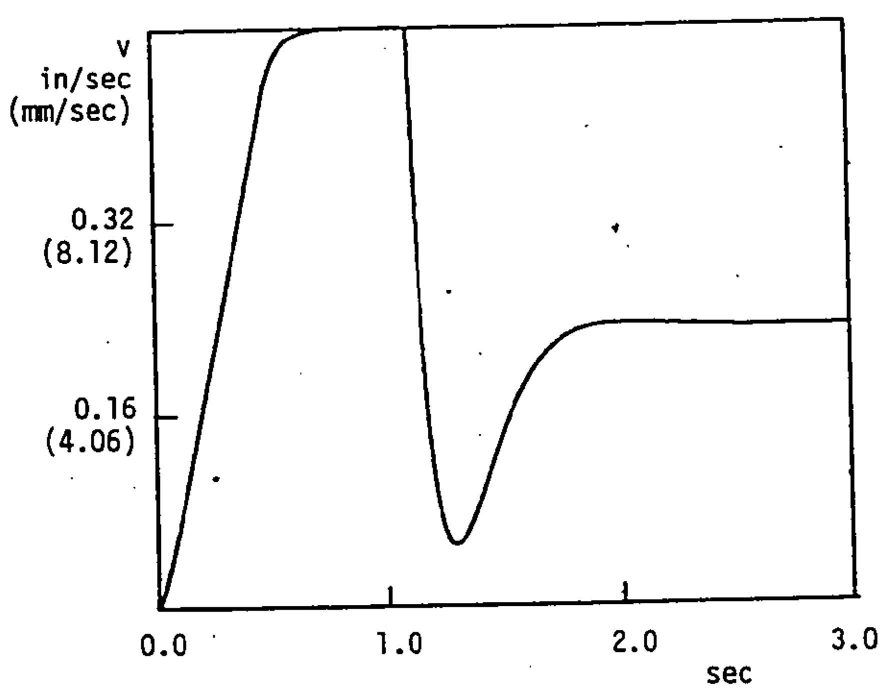

Simulated A/C Response With Flexible Spindle -
4 Flute - Feed rate

FIGURE 5.16

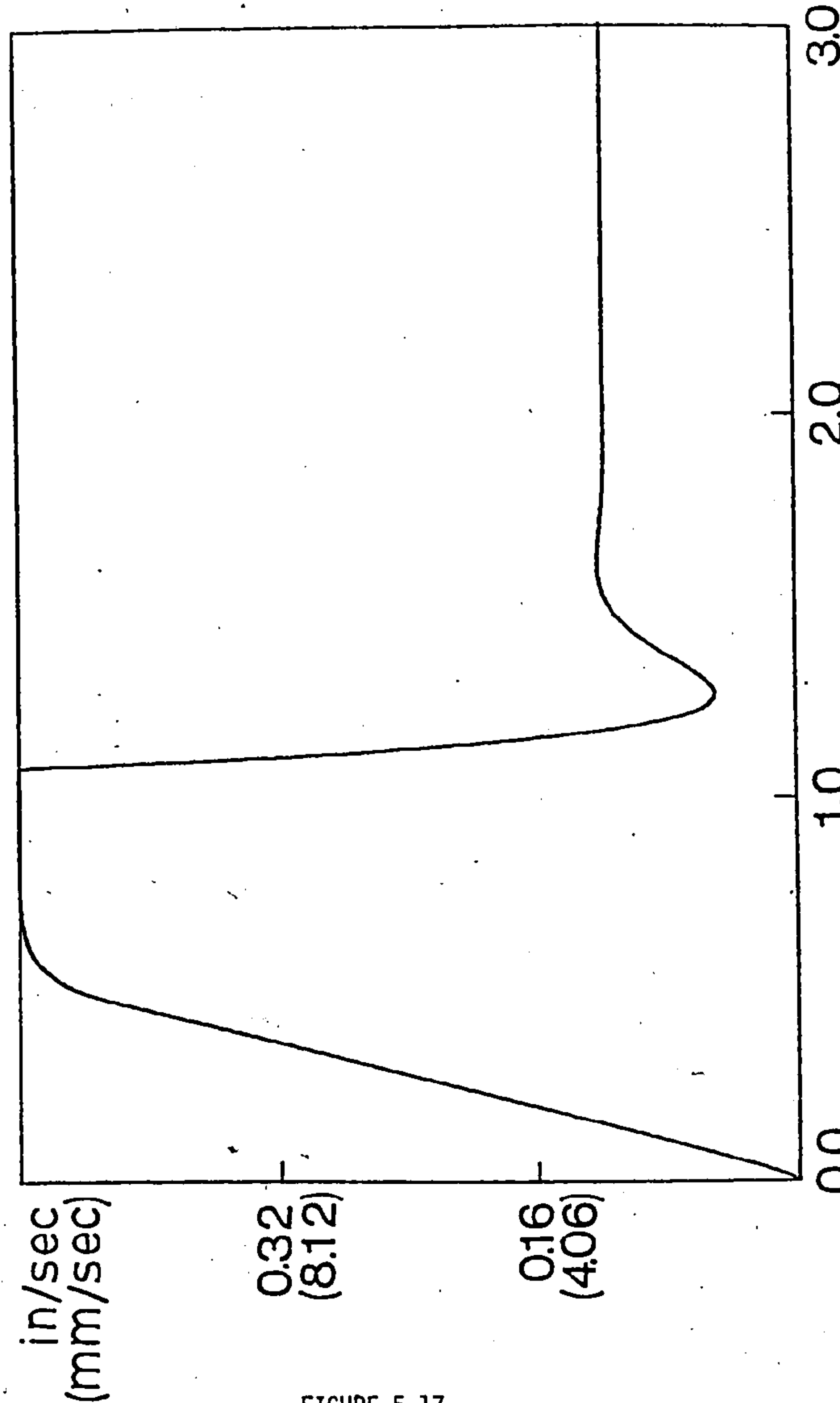

Simulated A/C Response With Rigid Spindle - 2 Flute End Mill - Feed rate

FIGURE 5.17

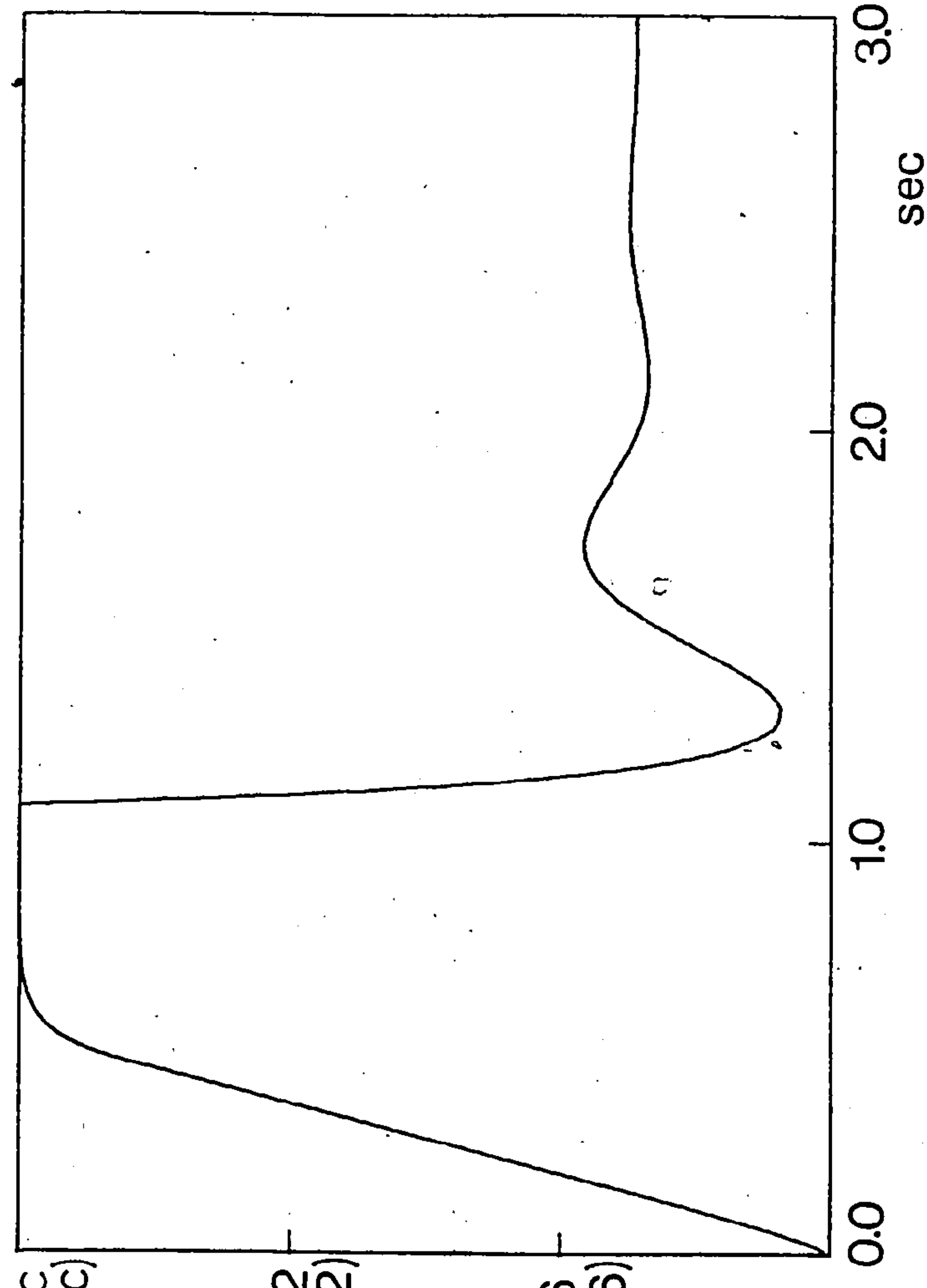

Simulated A/C Response With Flexible Spindle - 2 Flute End Mill - Feed rate

FIGURE 5.18

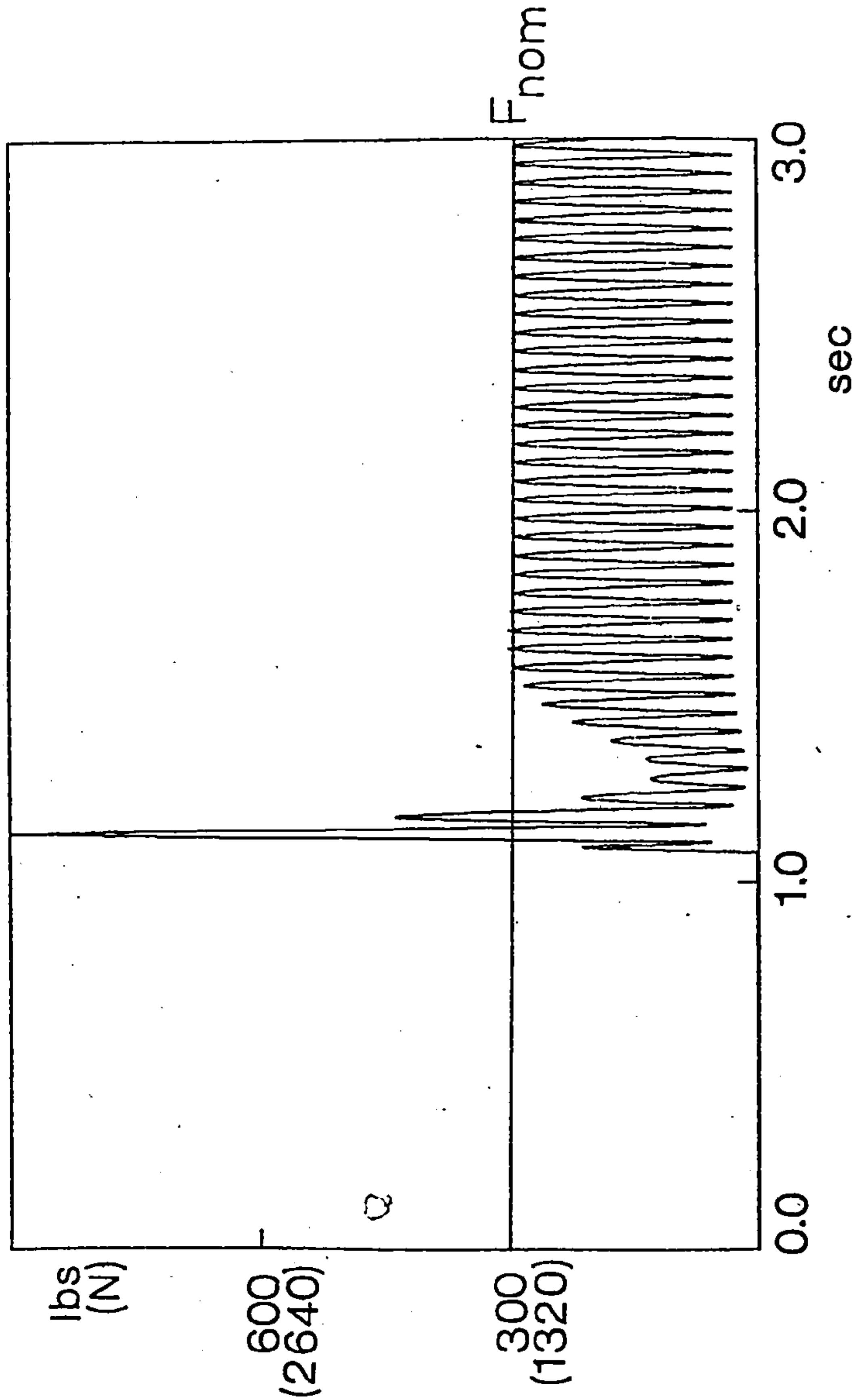

Simulated A/C Response With Rigid Spindle - 2 Flute End Mill - Cutting Force

FIGURE 5.19

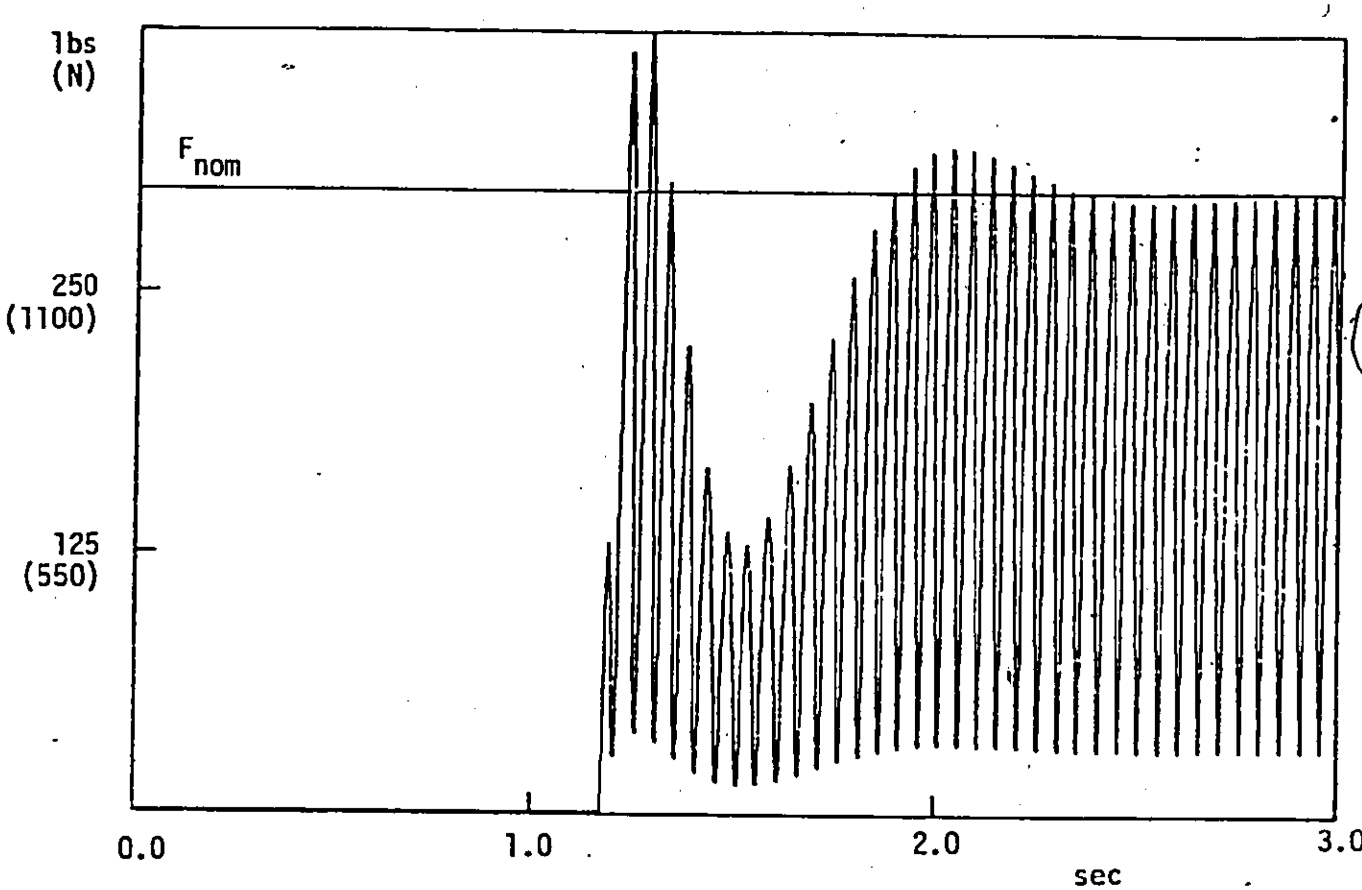

Simulated A/C Response With Flexible Spindle - 2 Flute End Mill - Cutting Force

FIGURE 5.20

the demand for reduced feedrate being obeyed initially rather rapidly under control of the fast algorithm and later more slowly as determined by the slow algorithm. The response for the flexible spindle is shown in figure (5.18). It exhibits slightly reduced damping but otherwise remains substantially the same as for the rigid tool. The force transients for the rigid and flexible spindle simulation are shown in figures (5.19) and (5.20) respectively.

In the former case the peak forces attain a value of 3 times F_{nom} whilst the latter case yields only a 25% increase above F_{nom}. The value of μ used in the above simulation is not unrealistic, it is based upon the measured spindle stiffness of 5800 N/mm (33000 lb/in) which is not particularly low when one considers that the cantilever stiffness of an end mill of diameter 19.05 mm (0.75 inch) and length 76.2 mm (3 inch) would be less than 9100 N/mm (52000 lb/in).

5.6 Experimental Results Using A/C Algorithm "A"

With the aim of experimentally verifying the performance of the A/C strategy (A/C Algorithm "A"), experimental results have been obtained under the impact conditions described in the previous section. Test cuts under different conditions and using the rotary dynamometer described in appendix I were scheduled:

(a) Straight constant depth and width profiling

(b) Variable depth and width profiling to simulate typical variations on cutter load.

(c) Profiling in presence of air gaps.

19.05 mm (0.75 inch) dia. high speed steel end mills were used with two and four teeth. Two different workpiece materials were tested:

i) Al. Alloy (95 BHN)

ii) Steel AISI 1020 (155 BHN)

The first set of tests was carried out with the aim of verifying the ability of the system to reach and maintain the prefixed constraint.

Figure (5.21) shows the experimental response of the A/C system for two different levels of F_{nom} when slotting (full immersion) Al. Alloy (95 BHN). Figure (5.22) shows the experimental response when slotting with a deeper cut (higher value of axial depth of cut). In these figures it is seen that the controlled variable (feedrate) adjusts itself in such a way that the sensor signal is maintained at a constant level. However, F_{nom} corresponds to the mean value of the cutting force. The fluctuations of the force correspond to the individual teeth of the cutter.

In order to control the peaks of the cutting force, a peak holding routine (see section 4.5 - Chapter 4) was added to the A/C algorithm. The effect of controlling the peaks of the cutting force is shown in figures 5.23 and 5.24. Figure 5.23(a) shows the experimental response obtained when slotting Al. Alloy with a two flute end mill, in the case in which the peak holding facility was suppressed. With peak holding

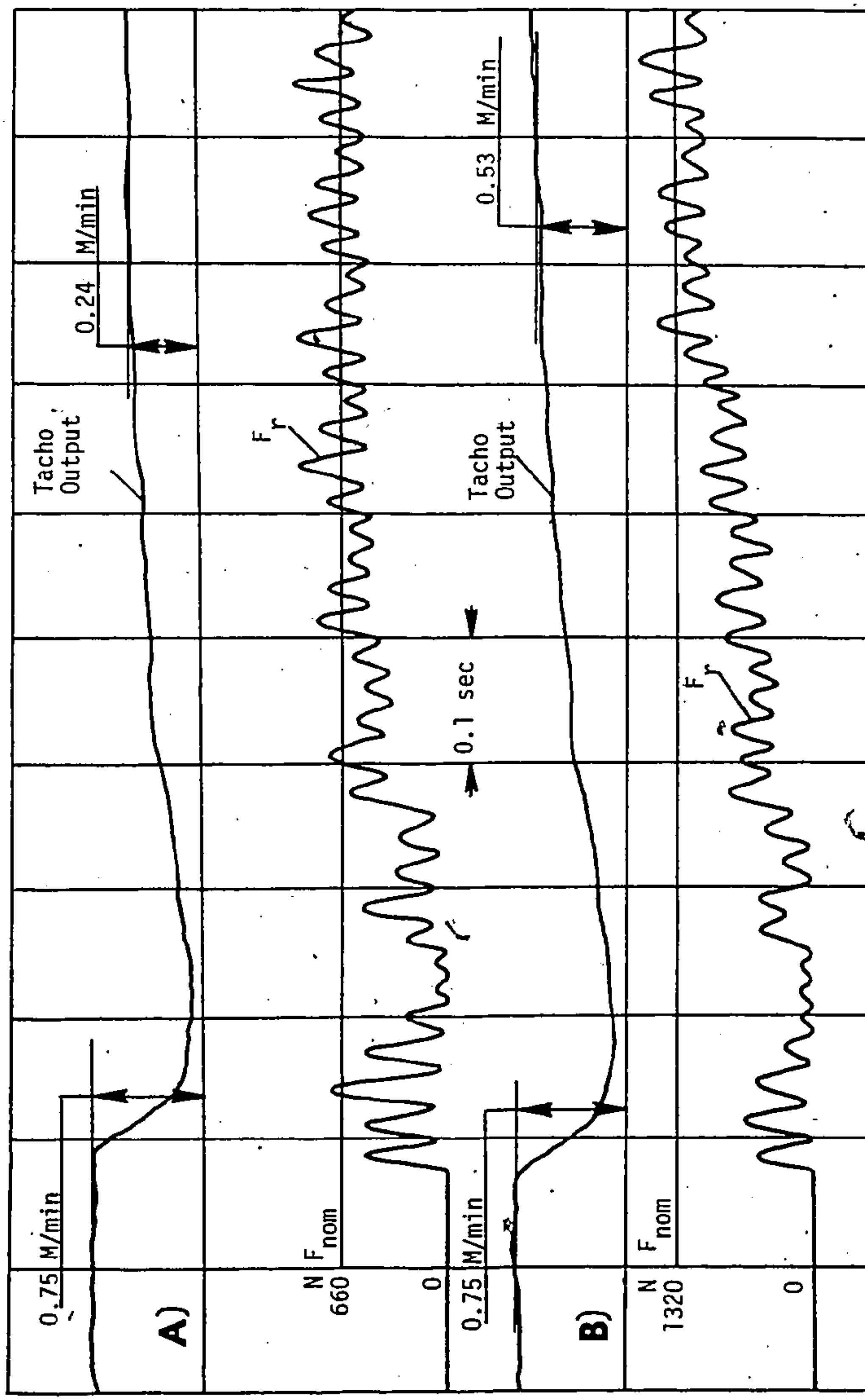

AL. Alloy Work Material, 19.05 mm Dia. - 4 Flute HSS End Mill, V = 35.34 M/min, b = 5.3 mm

Experimental Response of A/C System

FIGURE 5.21

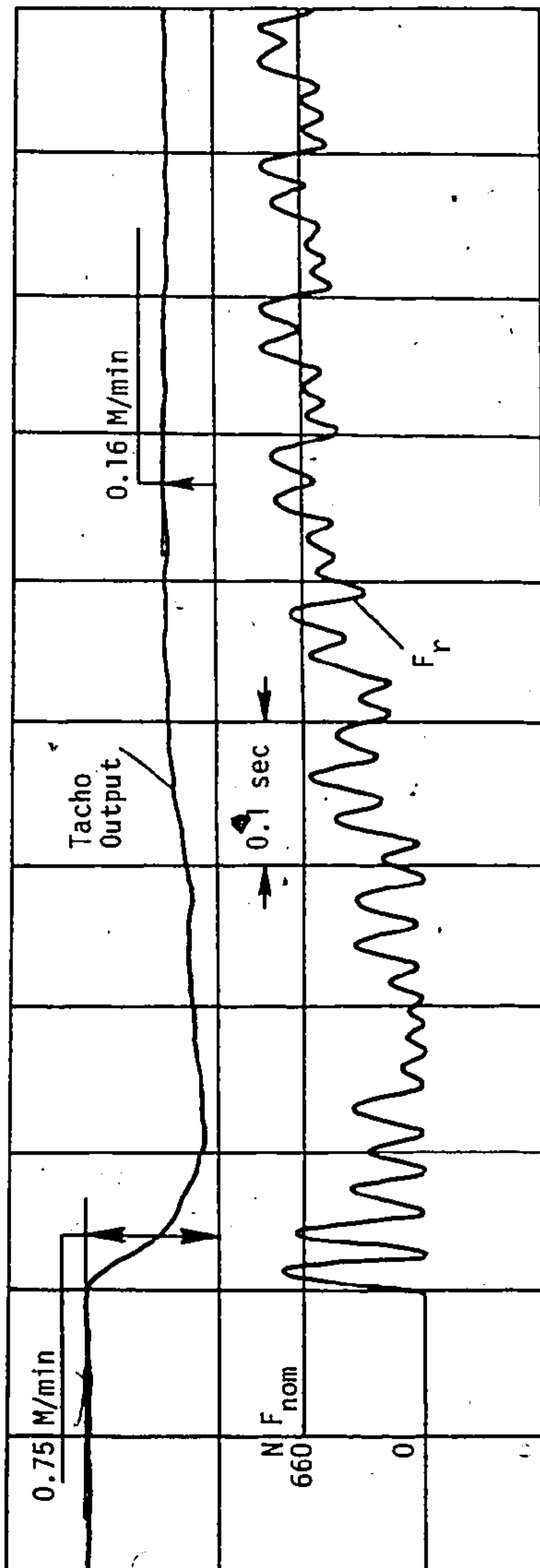

AISI 1020 Work Material, 19.05 mm Dia. - 4 Flute HSS End Mill, V = 35.34 M/min, b = 6.6 mm

Experimental Response of A/C System

FIGURE 5.22

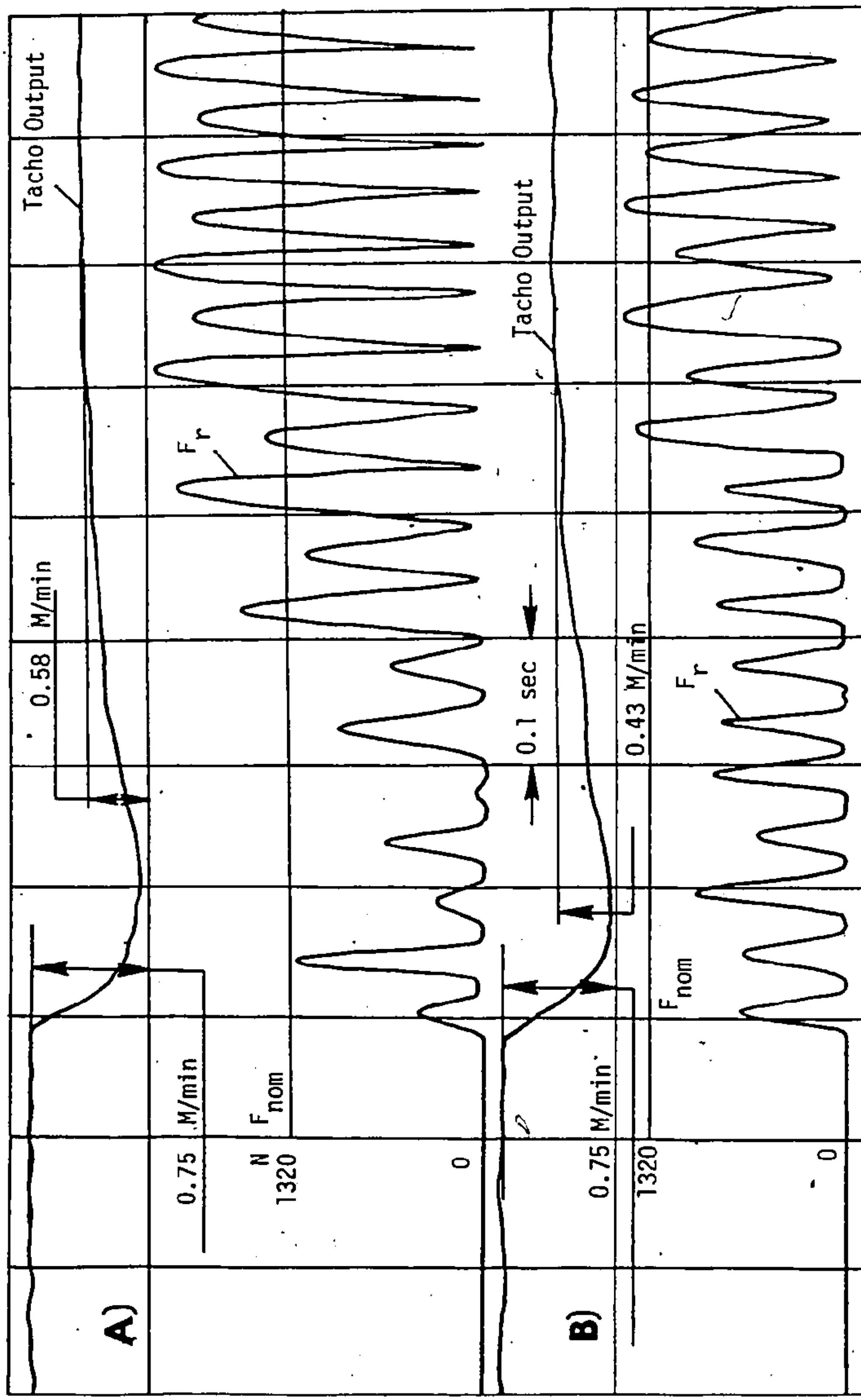

AL. Alloy Work Material, 19.05 mm Dia. - 2 Flute HSS End Mill, V = 35.34 M/min, b = 4.4 mm

Experimental Response of A/C System

FIGURE 5.23

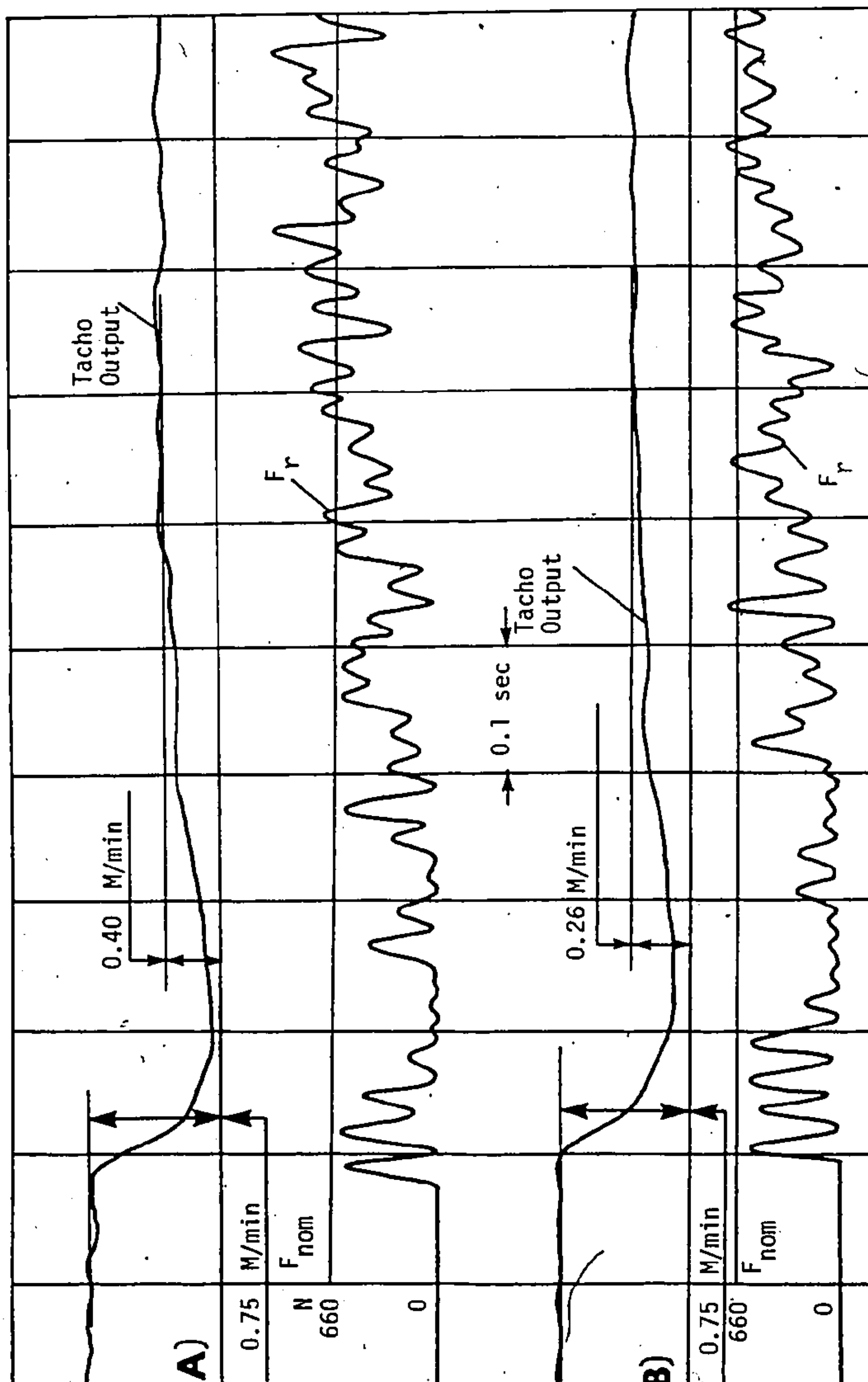

AL. Alloy Work Material, 19.05 mm Dia. - 4 Flute HSS End Mill, V = 35.34 M/min, b = 2.5 mm

Experimental Response of A/C System

FIGURE 5.24

(figure 5.23 b) the feedrate is reduced such that F_{nom} corresponds to the peak forces. Figure 5.24 shows the response in the case of a four flute end mill. Figure 5.24(a) is the case with the peak holding facility suppressed.

Figures 5.25 and 5.26 show the experimental response of the A/C system when slotting AISI 1020 at various values of the axial depth of cut. For all the experimental results presented so far, the feedrate reduces from rapid to its required steady state value in less than 50 milliseconds. The force traces indicate some cutter run out.

Experimental results were also obtained when slotting Al. Alloy with a long series end mill (76.2 mm flute length) at two different levels of axial depth of cut. These results are shown in figure 5.27.

Figures 5.28, 5.29, and 5.30 show the experimental response of the A/C system in cases of typical variations on cutter load encountered in profiling. Figure 5.28 shows the case of variable axial depth of cut, figure 5.29 shows the case of variable radial width of cut and finally figure 5.30 shows the case of slotting in presence of an air gap. In these figures, it can be seen that the feedrate varies in accordance with the changing cutting conditions in such a way that the resulting cutting force is maintained at a constant level.

The experimental results obtained with the rotary dynamometer compare more favourably with the results obtained from the simulation studies when including the effect of the

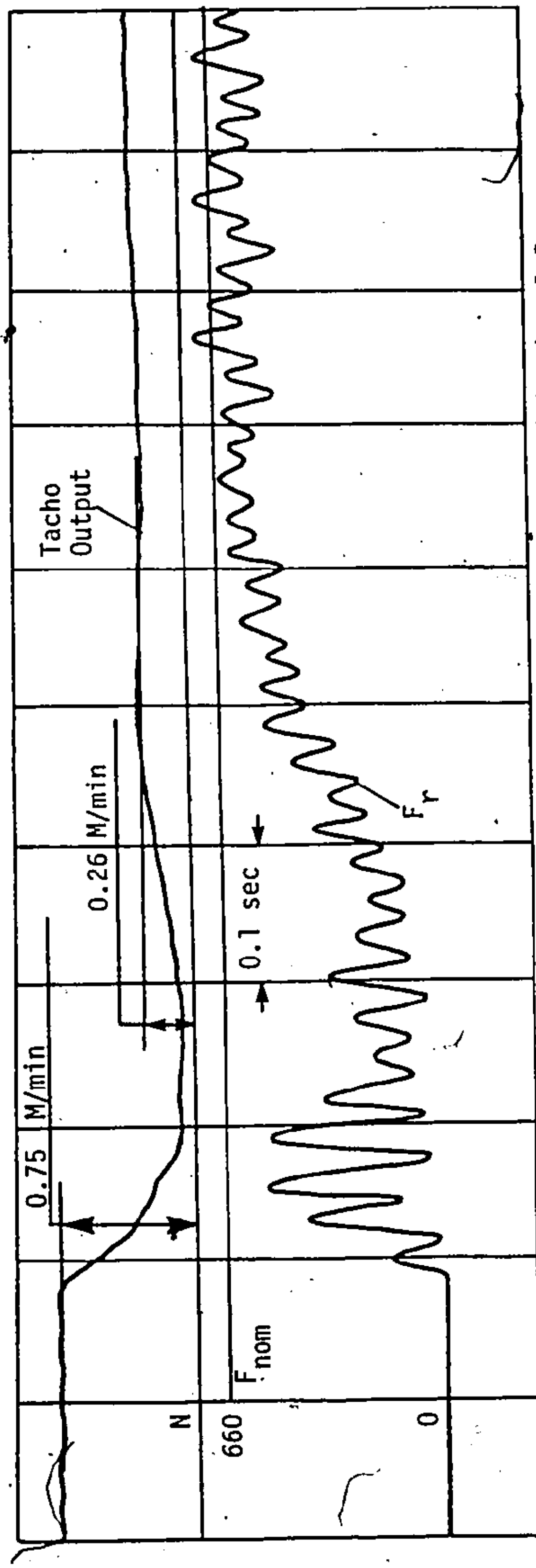

AISI 1020 Work Material, 19.05 mm Dia. - 4 Flute HSS End Mill, V = 35.34 M/min, b = 1.9 mm

Experimental Response of A/C System

FIGURE 5.25

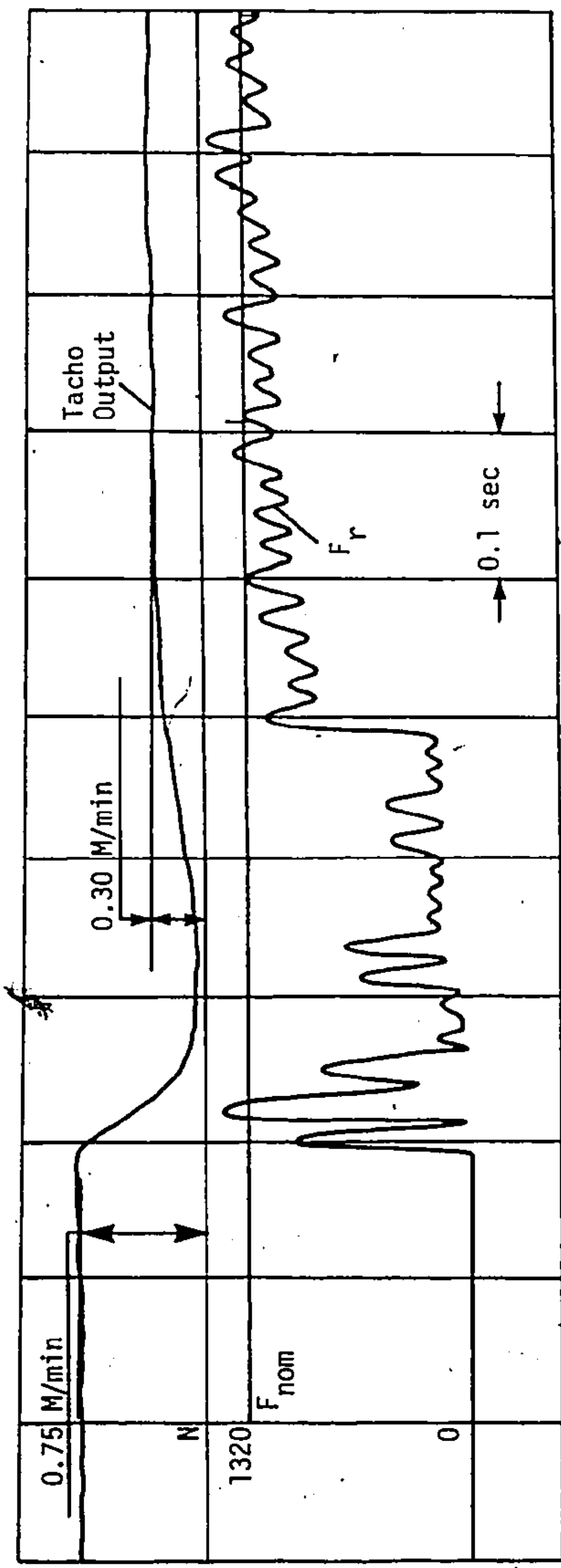

AISI 1020 Work Material, 19.05 mm Dia. - 4 Flute HSS End Mill, V = 35.34 M/min, b = 4.3 mm

Experimental Response of A/C System

FIGURE 5.26

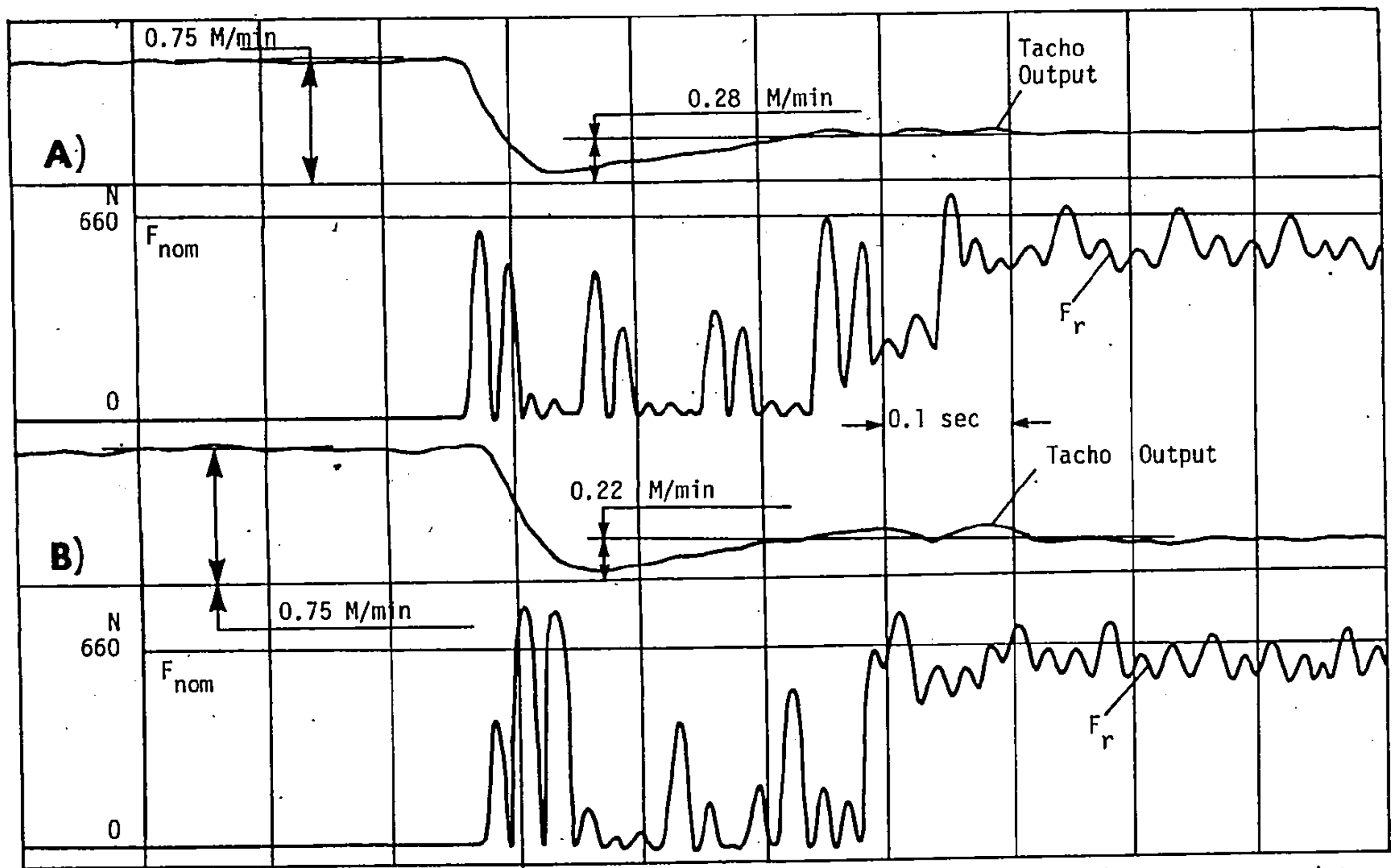

AISI 1020 Work Material, 19.05 mm Dia. - 4 Flute HSS End Mill, V = 35.34 M/min, A) b = 4.0 mm - B) b = 5.3 mm

Experimental Response of A/C System

FIGURE 5.27

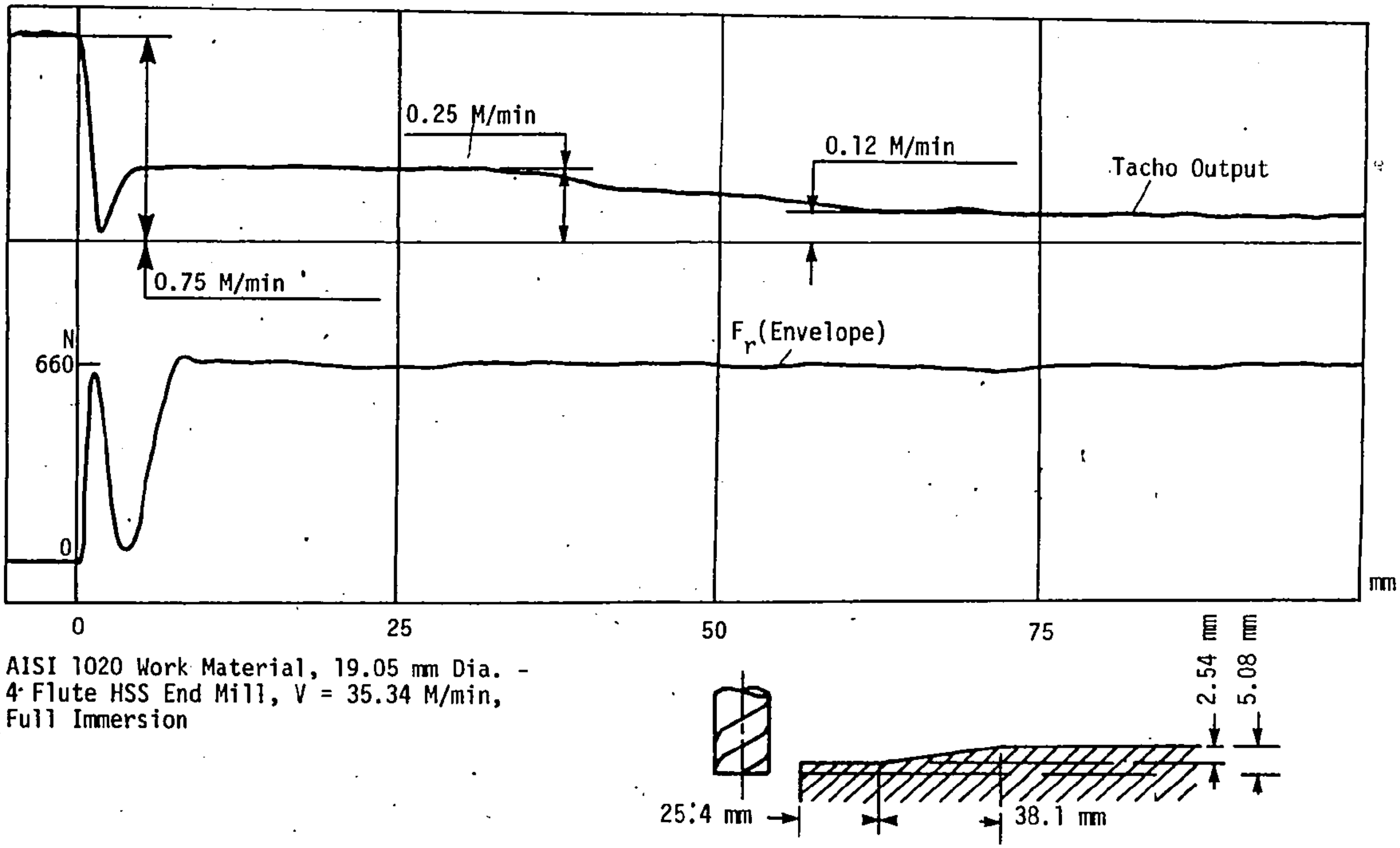

Experimental Response of A/C System

FIGURE 5.28

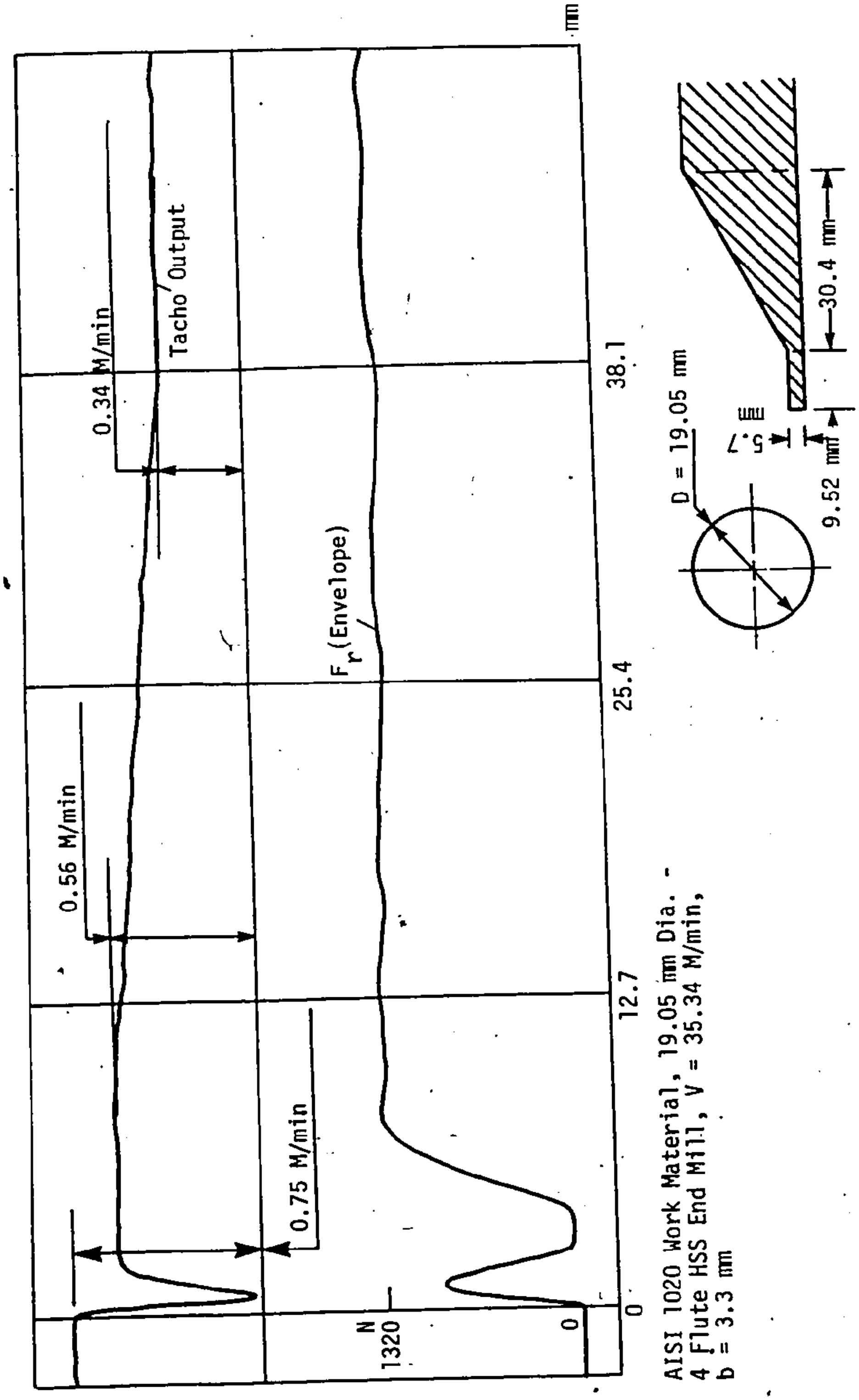

AISI 1020 Work Material, 19.05 mm Dia. -
4 Flute HSS End Mill, V = 35.34 M/min,
b = 3.3 mm

Experimental Response of A/C System

FIGURE 5.29

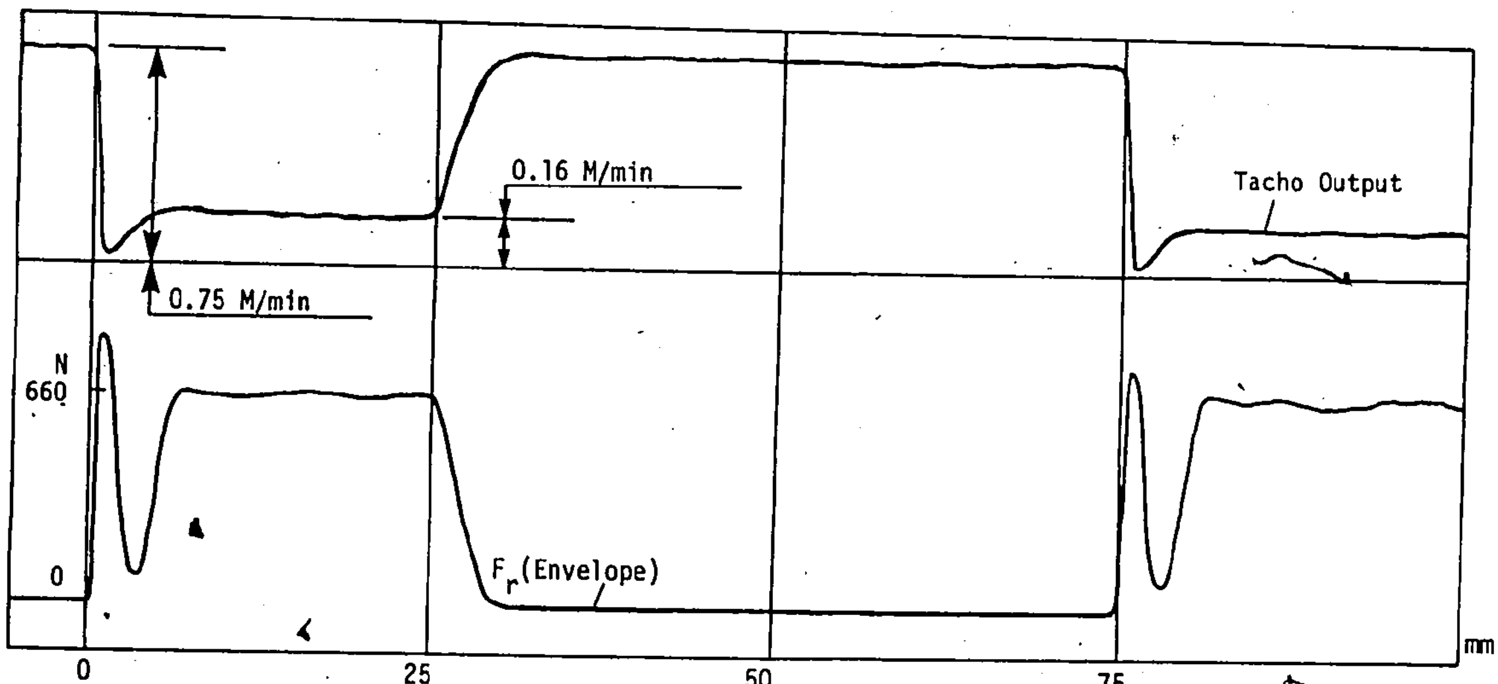

AISI 1020 Work Material, 19.05 mm Dia. -
4 Flute HSS End Mill, V = 35.34 M/min,
Full Immersion

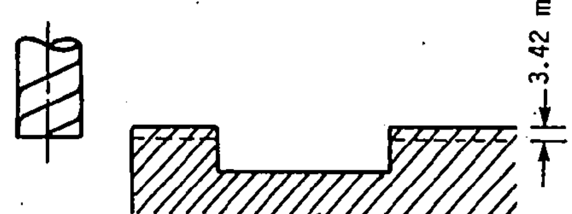

Experimental Response of A/C System

FIGURE 5.30

cutter flexibility. The finite flexibility between tool and workpiece reduces the chip thickness and therefore, the resulting force.

In order to experimentally verify the effect of the flexibility between tool and workpiece on the transient force peak during adaptive control, a table dynomometer (described in appendix II) was next used. The dynamometer has a natural frequency of 1100Hz and therefore, has excellent dynamic characteristics. The shift from the rotary to the table dynamometer results in a different value of static stiffness "K_S". In fact using the arrangement shown in figure 5.10 (without the rotary dynamometer) results in value of K_S = 32515N/mm (185000 lb/in) for a 38.1 mm (1.5 inch) overhang. This of course, means a faster force build up in transients. The table dynamometer is also simpler in its design and required less frequent calibration than the rotary one. Sample results obtained using the table dynamometer are shown in figures 5.31 and 5.32.

Figure 5.31 shows the experimental response of the A/C system, using the table dynamometer, when slotting AISI 1020 at two different levels of F_{nom} with a 19.05 mm (0.75 inch) dia. - 2 flute HSS end mill. Trace a) shows the results obtained for F_{nom} = 660N (150 lbs). The system stabilizes at 75 mm/min (3 in/min) feedrate. It is also seen that while the first tooth attains only 615N (140 lbs) due to the flexibility of the cutter and the effect of the helix angle, the

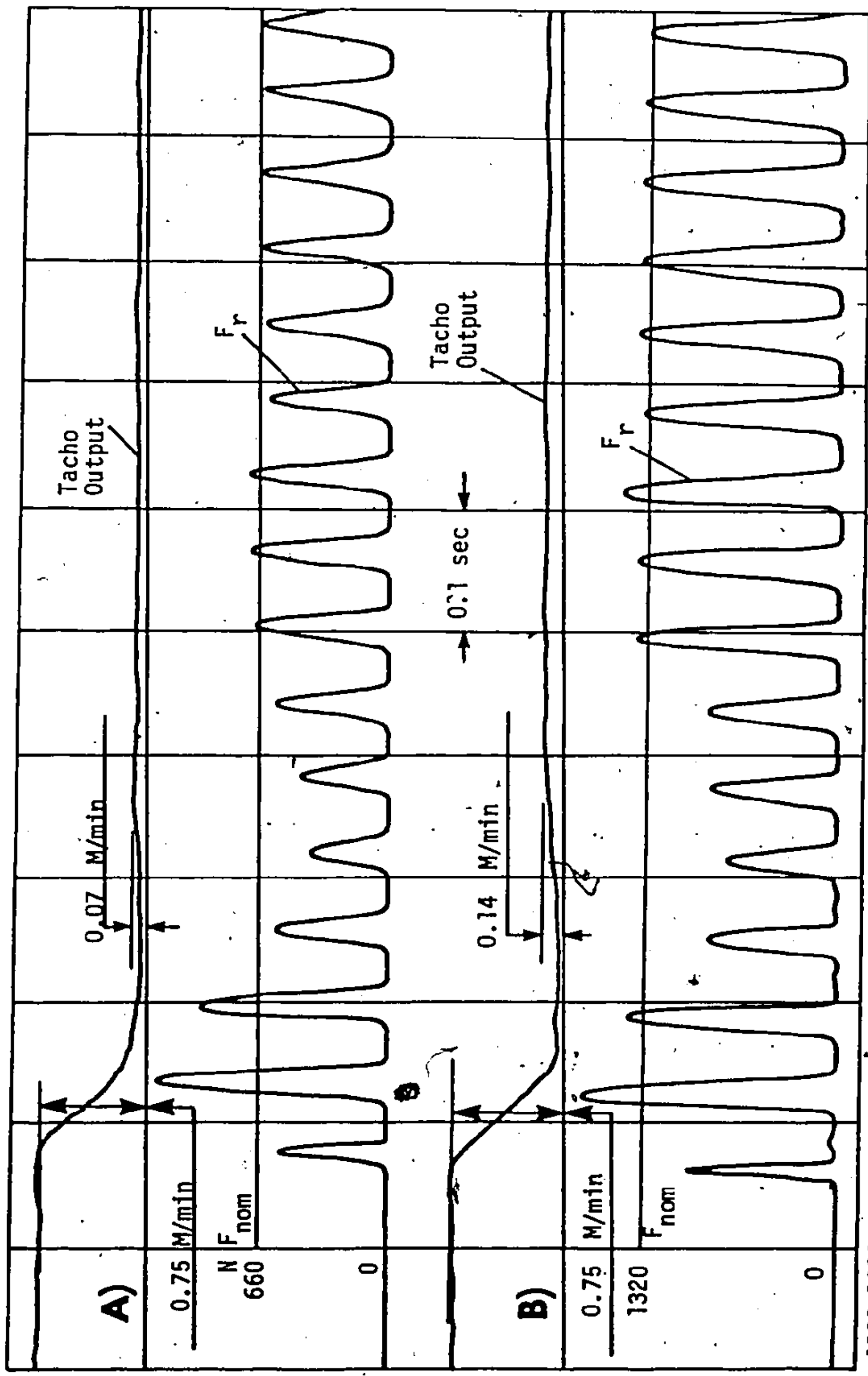

AISI 1020 Work Material, 19.05 mm Dia. - 2 Flute HSS End Mill, V = 35.34 M/min, b = 2.5 mm

Experimental Response of A/C System

FIGURE 5.31

second tooth attains approximately 320 lbs. For F_{nom} = 1320N (300 lbs), the corresponding result is shown in figure 5.31 b). The steady state feedrate in this case is 152.5 mm/min (6.1 in/min).

This experiment was next repeated using a 19.05 mm dia. - 4 flute HSS end mill and the results are shown in figure 5.32. In trace a) the system stabilizes at 105 mm/min (4.2 in/min), while in Trace b) it stabilizes at 245.25 mm/min (9.81 in/min).

5.7 Effect of Spindle Stiffness "K_S", Cutting Stiffness "K_C", and F_{nom} on the Dynamic Behaviour of the A/C System

5.7.1 Effect of "K_S"

In order to study the effect of the tool spindle flexibility on the A/C system behaviour, the state-space technique was first used. The conditions used are: -

F_{nom} = 1320N

K_{ac} = 25.4 mm/sec^2

B = 1.0 mm/sec^2

K_C = 1380 b N/mm^2

b = 6.5 mm

N = 600 rev/min

r = 9.52 mm

Considering first the case of a two teeth end mill, the simulated A/C response to the conditions described in section 5.4, for two different values of K_S is shown in figures 5.33 and 5.34. Assuming first K_S = 7030 N/mm (40000 lb/in), the force response is shown in figure 5.33. It is seen that the response

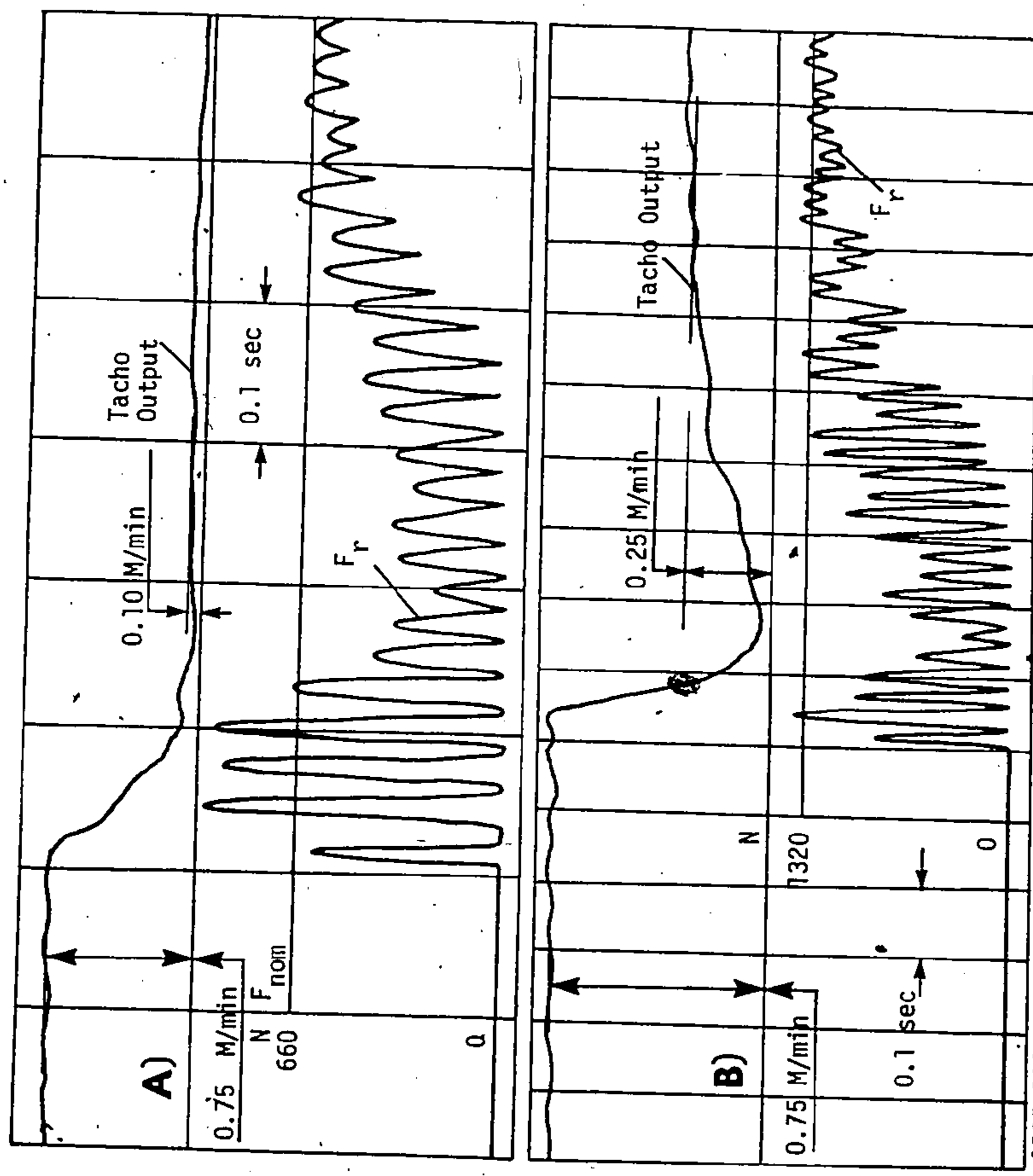

AISI 1020 Work Material, 19.05 mm Dia. - 4 Flute HSS End Mill, V = 35.34 M/min
b = 2.5 mm

Experimental Response of A/C System

FIGURE 5.32

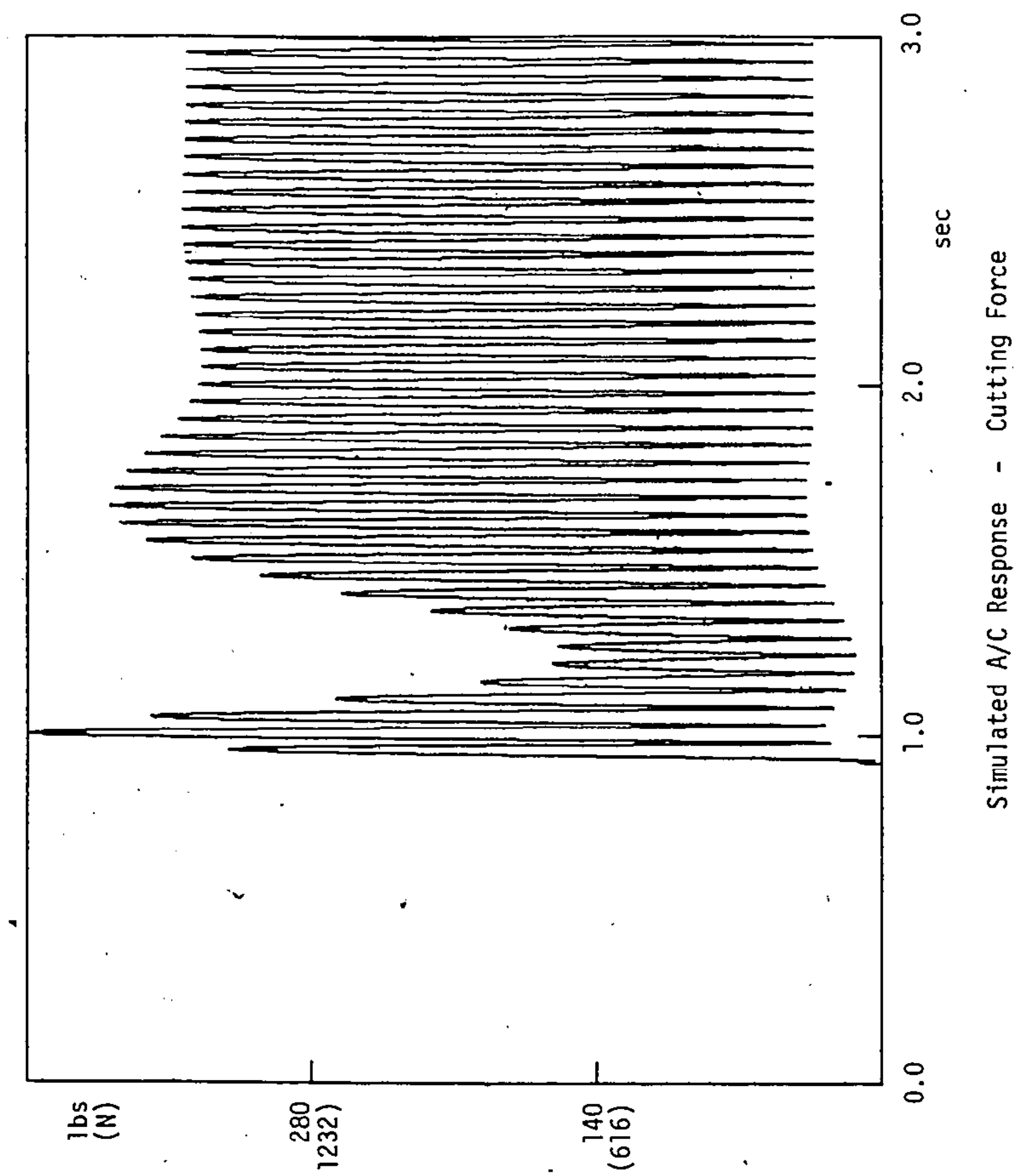
Simulated A/C Response - Cutting Force
sec
0.0
1.0
2.0
3.0
lbs
(N)
280
(1232)
140
(616)

FIGURE 5.33

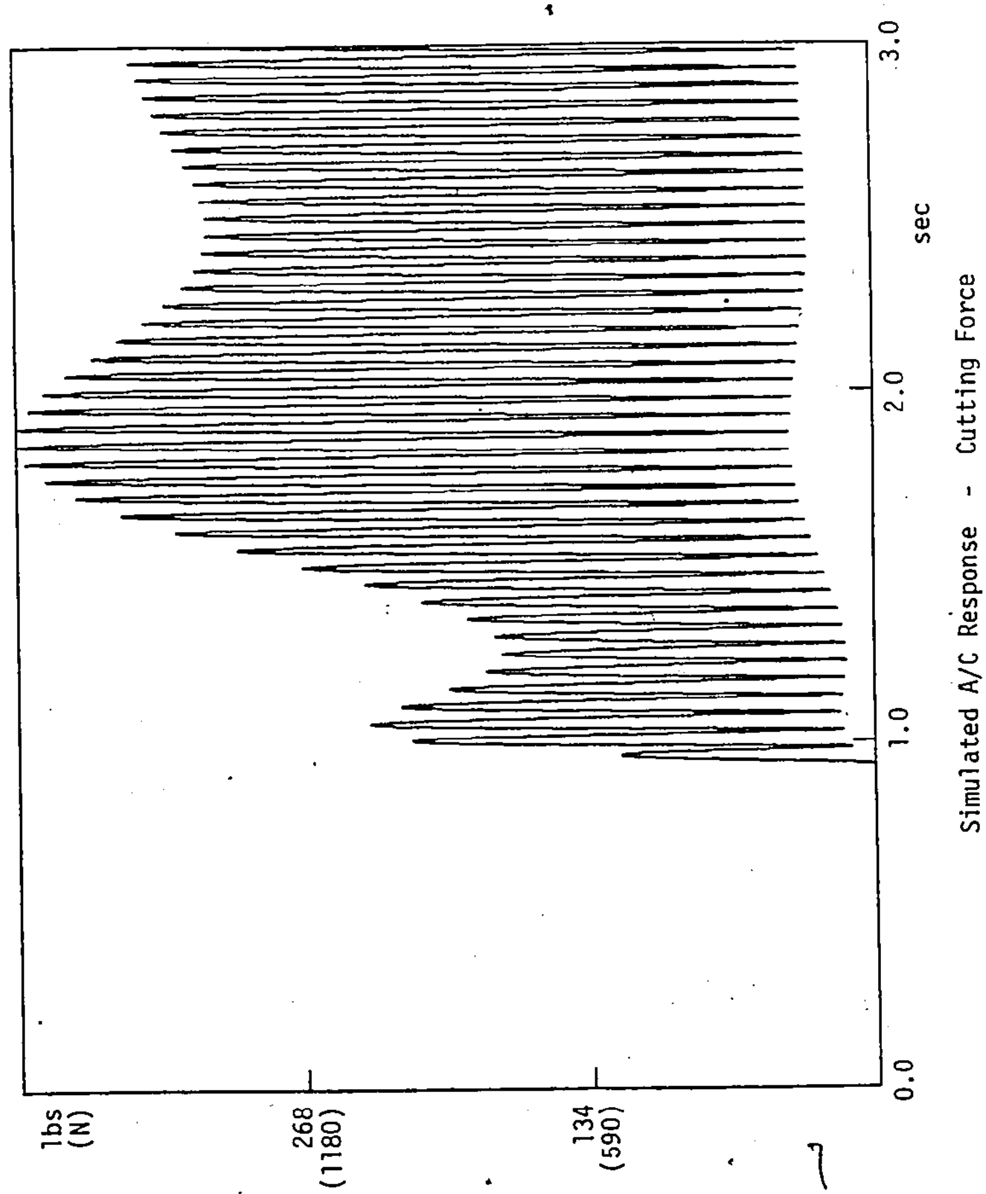
lbs
(N)
268
(1180)
134
(590)
0.0
1.0
2.0
3.0
sec
Simulated A/C Response - Cutting Force

FIGURE 5.34

becomes more oscillatory when decreasing the value of K_S to 2285N/mm (1300 lb/in) as shown in fig. 5.34. The results of the case of a 4-flute end mill (with otherwise the same conditions as in figures 5.33 and 5.34) are shown in figures 5.35 and 5.36. The same phenomena can be observed however, to a lesser degree.

The classical linear control theory (root locus analysis) is next used to better understand the effect of "K_S" on the dynamic behaviour of the A/C system.

Referring to figure 4.3, the closed loop transfer function of the NC servomechanism could be written as:

$$\frac{V(s)}{X(s)} = \frac{6398.424\ s}{(s + 427.414)\ (s + 14.970)}\ \text{Sec}^{-1} \qquad (5.20)$$

Including the effect of "K_S", and the cutting stiffness "K_C", the A/C Loop is added around the NC servo and it is shown in figure 5.37, where:

d is the cutter deflection in mm.

K'_C will have the units N/mm/sec.

The open loop transfer function of the A/C system is:

$$\frac{F_{act}(s)}{F_{nom}(s)} = \frac{6398.424 \times B \times K_S}{F_{nom}} \cdot \frac{(s + Kac/B)}{s(s + \frac{K_S}{K'_C})\ (s + 14.970)\ (s + 427.414)} \qquad (5.21)$$

Expression (5.21) shows that for a constant gain in the NC loop, the overall gain in the system is directly proportional to "K_S", the damping factor "B", and inversely proportional to the nominal force "F_{nom}". The transient behaviour of the system will

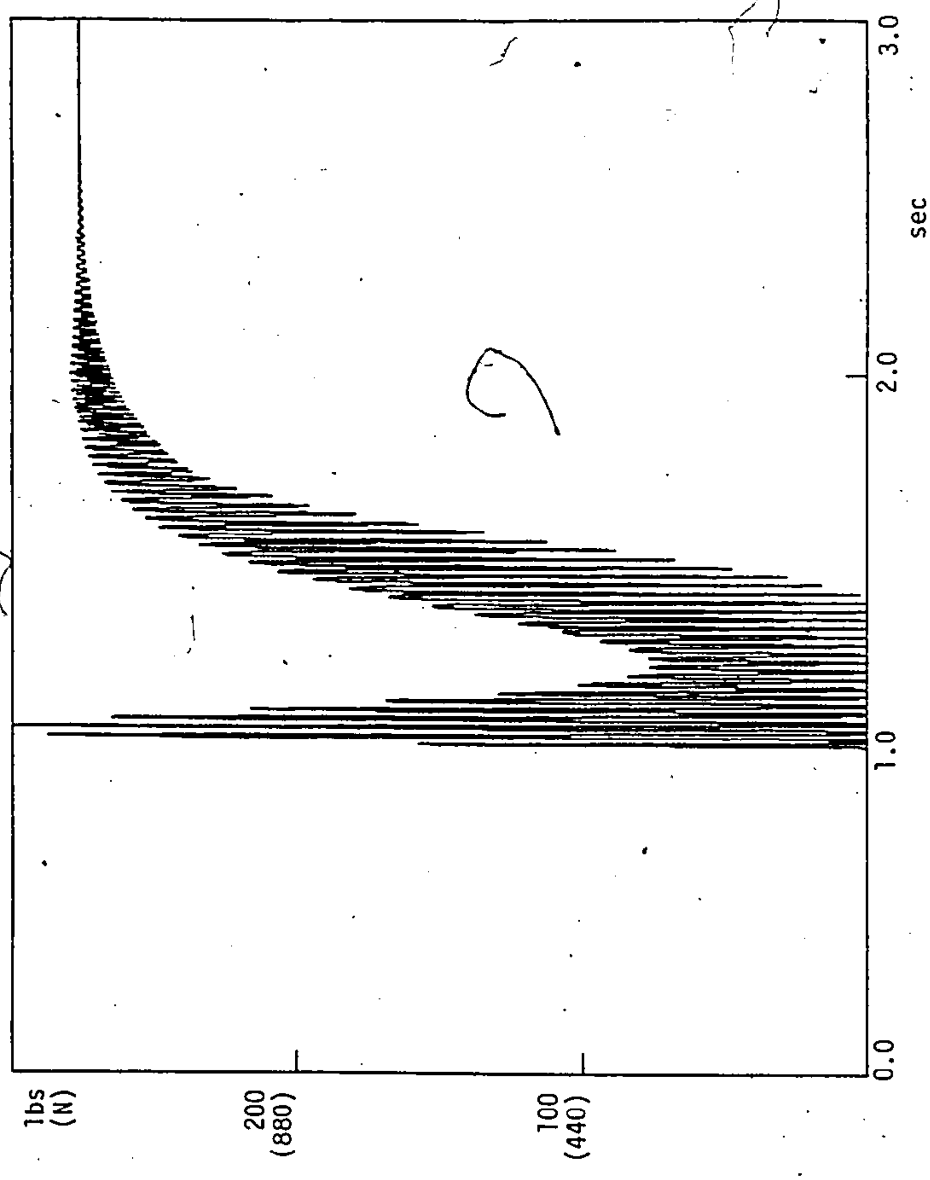

Simulated A/C Response - Cutting Force

FIGURE 5.35

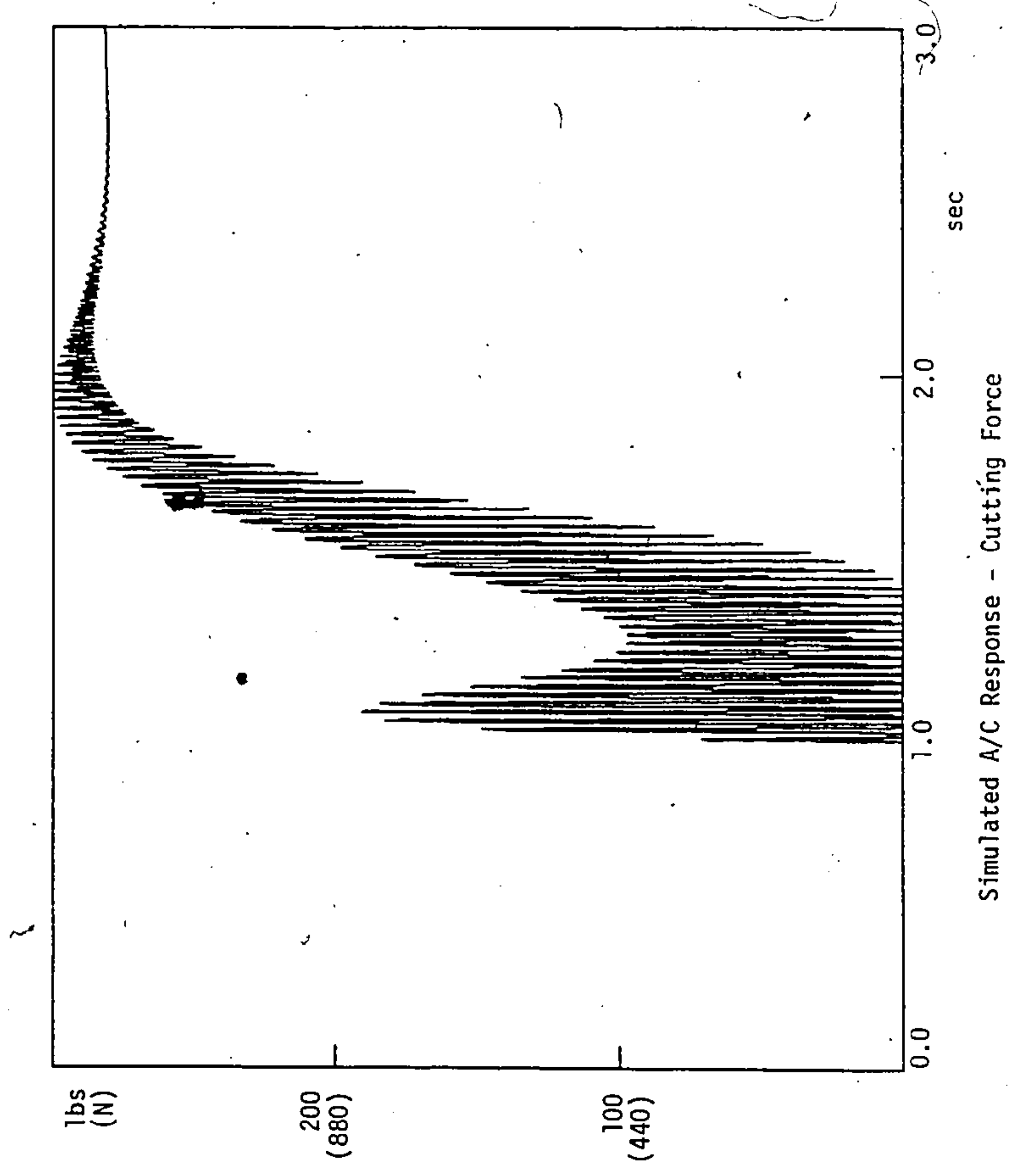
lbs
(N)
200
(880)
100
(440)
0.0
1.0
2.0
3.0
sec
Simulated A/C Response - Cutting Force

FIGURE 5.36

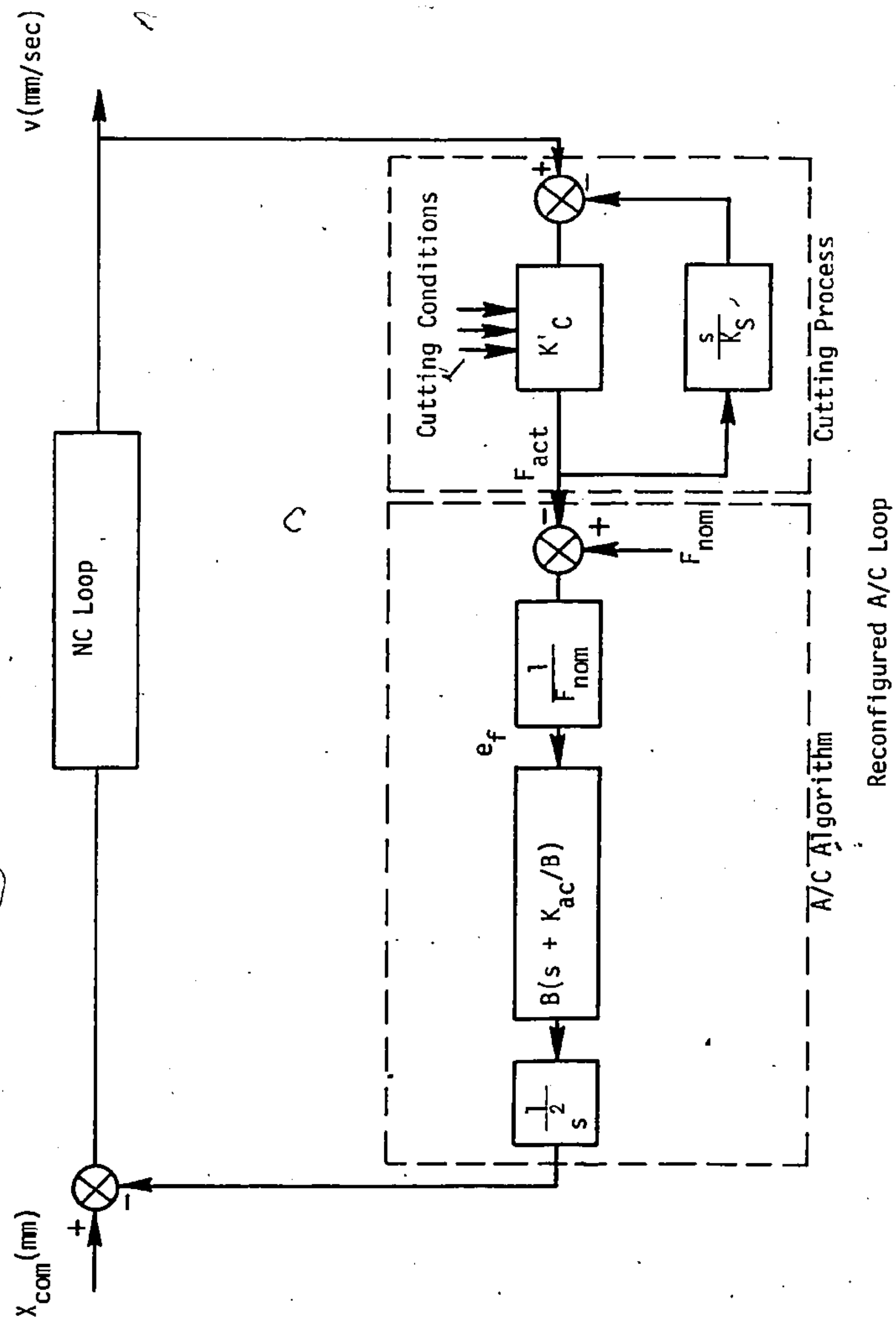
v(mm/sec)
NC Loop
X_com(mm)
Cutting Conditions
K'C
s/K_S'
Cutting Process
F_act
F_nom
1/F_nom
e_f
B(s + K_ac/B)
1/s^2
A/C Algorithm
Reconfigured A/C Loop

FIGURE 5.37

depends on the ration $\frac{K_S}{K'_C}$.

Let $K_{ac} = 25.4$ mm/sec^2

$B = 1.0$ mm/sec^2

$F_{nom} = 1320$N

$K_C = 1380$ b N/mm^2

b = 6.5 mm

Also, assuming a 4 teeth end mill rotating at 600 rev/min, then $K'_C = \frac{8970}{4 \times 10} = 224.25$ N/mm/sec.

Substituting first with $K_S = 7030$ N/mm in equation (5.21) yields:

$$\frac{F_{act}(s)}{F_{nom}(s)} = 34305 \frac{s + 25.0}{s(s + 14.970)(s + 30.936)(s + 427.414)} \qquad (5.22)$$

The root locus of the above system is shown in figure 5.38. The transient behaviour is mainly governed by two complex and conjugate roots ($-7.864 \pm j\,2.2481$). This results in a damping factor $\zeta = 0.96$ i.e. the system will exhibit no significant oscillations in the time domain.

Substituting with $K_S = 2285$ N/mm in equation (5.21) results in:

$$\frac{F_{act}(s)}{F_{nom}(s)} = 10816 \frac{(s + 25.0)}{s(s + 9.753)(s + 14.970)(s + 427.414)} \qquad (5.23)$$

The root locus plot of this particular case is shown in figure 5.39. The damping factor for this case is $\zeta = 0.64$. Accordingly, the following conclusions can be reached after examining the effect of varying "K_S" on the dynamic behaviour of the

$$GH(s) = \frac{K\,(s + 25.0)}{s(s + 14.970)\,(s + 30.936)\,(s + 427.414)}$$

$K = 34305$

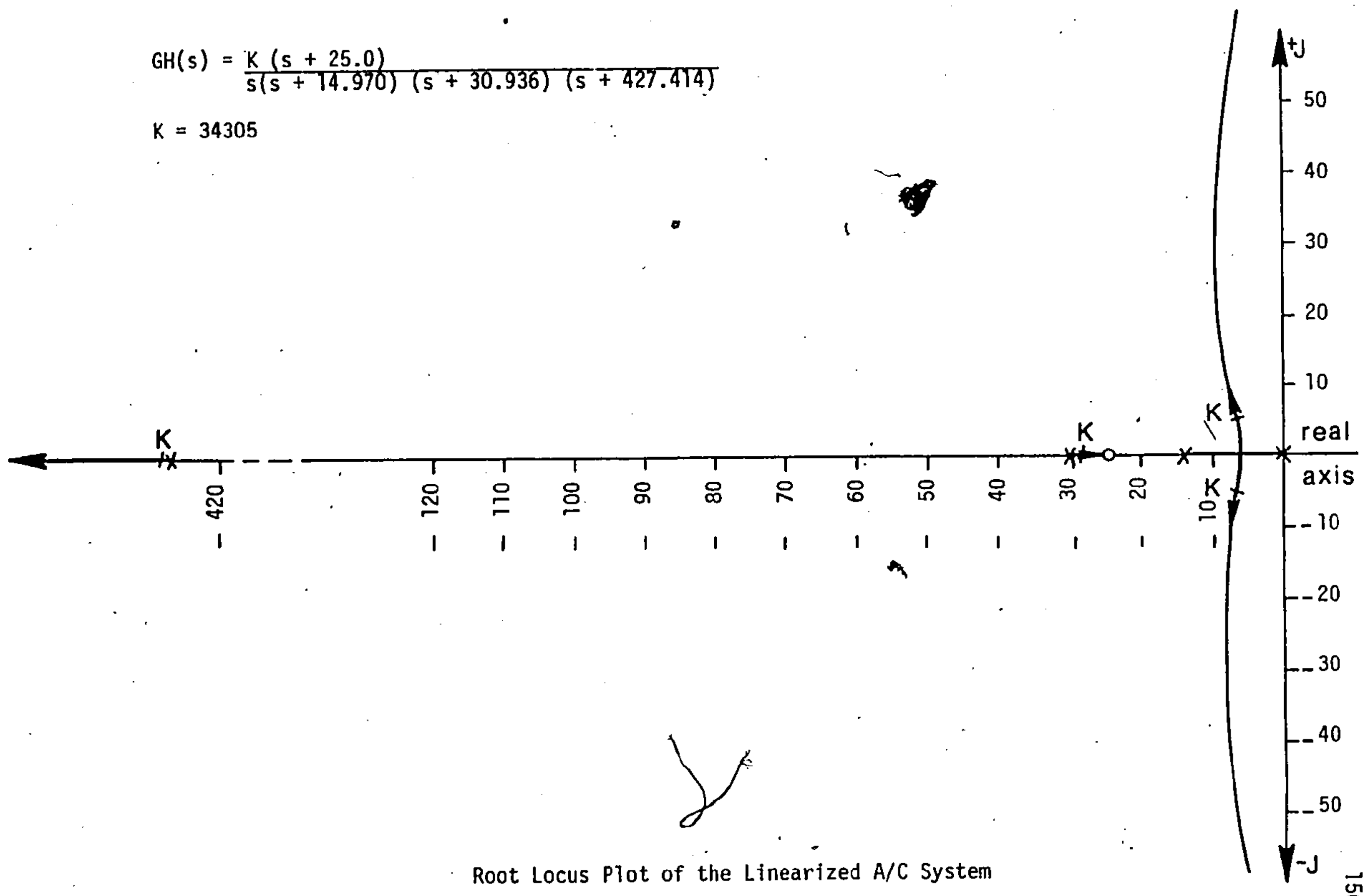

Root Locus Plot of the Linearized A/C System

FIGURE 5.38

$$GH(s) = \frac{K\,(s + 25.0)}{s(s + 9.753)\,(s + 14.970)\,(s + 427.414}$$

K = 30000

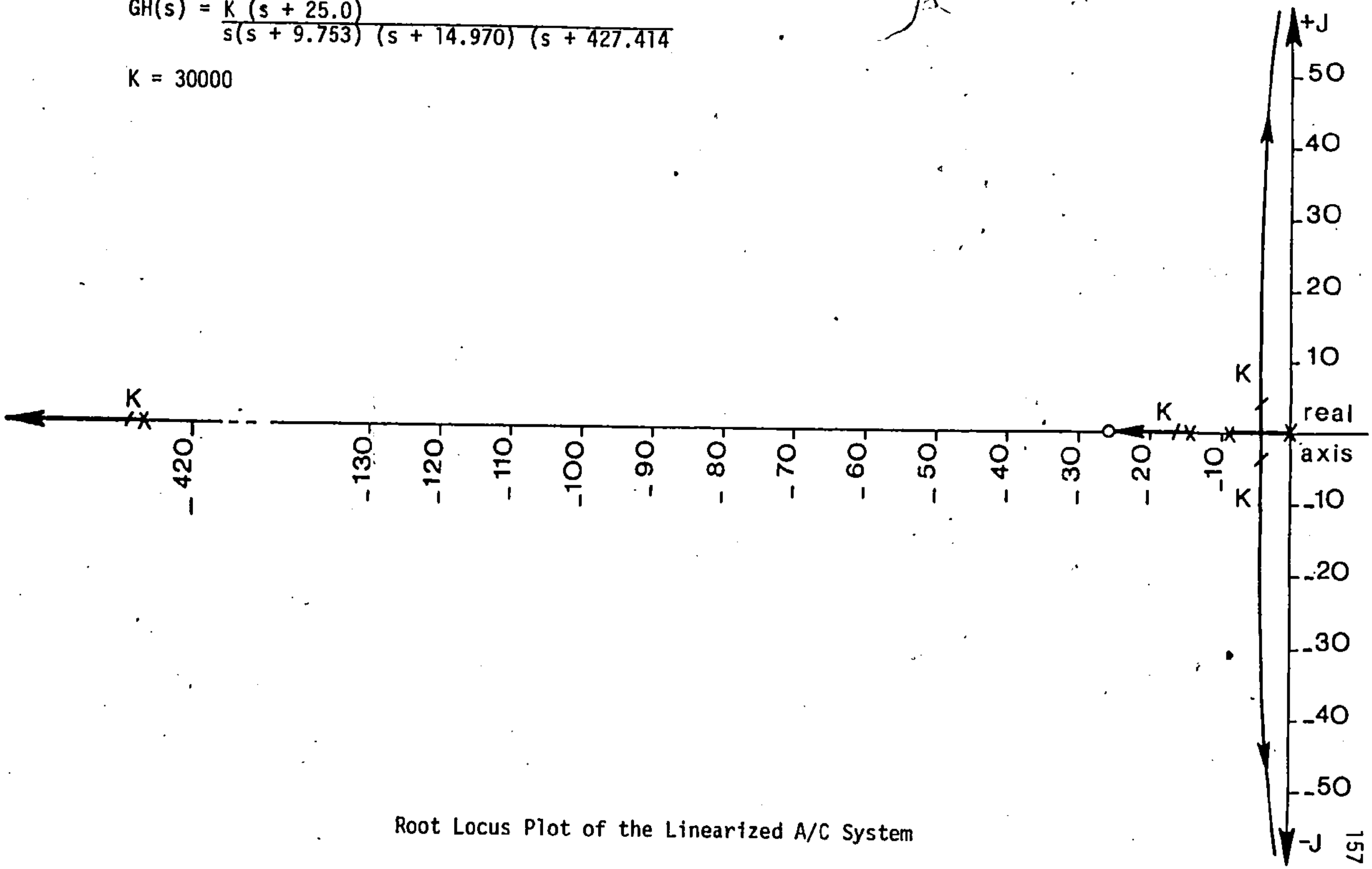

Root Locus Plot of the Linearized A/C System

FIGURE 5.39

system:

1. Decreasing the spindle stiffness "K_S" results in decreasing the overall gain in the system, however, the amount of damping decreases too mainly by shifting the pole $-\frac{K_S}{K'_C}$ (see expression 5.21) closer to the imaginary axis which results in increasing the amount of oscillations in the system transient behaviour.

2. This decrease in the amount of damping will be even more pronounced in the case of a two teeth end mill, since in this case $\frac{K_S}{K'_C}$ will be smaller i.e. closer to the imaginary axis.

5.7.2 Effect of the Cutting Stiffness "K'_C"

Consider two different cases:

i) $K_C = 3465$ N/mm

ii) $K_C = 13860$ N/mm

and assuming 4-teeth end mill rotating at 600 rev/min, then:

i) $K'_C = 86.625$ N/mm/sec

ii) $K'_C = 346.5$ N/mm/sec

Considering that $K_S = 7030$ N/mm

$F_{nom} = 1320$ N

$K_{ac} = 25.4$ mm/sec^2 & $B = 1.0$ mm/sec^2

Then, the corresponding open loop transfer functions are:

i) $$\frac{F_{act}(s)}{F_{nom}(s)} = 34.305 \frac{(s + 25.0)}{s(s + 14.970)(s + 80.434)(s + 427.414)} \quad \text{------------(5.24)}$$

ii) $$\frac{F_{act}(s)}{F_{nom}(s)} = 34\ 305\ \frac{(s + 25.0)}{s(s + 14.970)(s + 20.108)(s + 427.414)}$$ -------------(5.25)

The corresponding root locus plots for equations (5.24) and (5.25) are shown in figures (5.40) and (5.41) respectively. For the first case shown in figure (5.40), the system is clearly overdamped since all the roots lie on the real axis. However, we should expect a slow response due to the proximity of the first root (- 1.806) to the imaginary axis. Increasing K'_C to 346.5 N/mm/sec results in the root locus plot shown in figure (5.41). Two complex and conjugate roots (- 6.509 $\pm$ j 7.026) will mainly govern the transient behaviour of the system resulting in a damping factor ζ = 0.67.

Accordingly, the following conclusions can be reached:

1. Small values of K'_C results in slow system response and overdamping.

2. At high values of K'_C, the amount of damping decreases and the system behaviour becomes oscillatory.

5.7.3 Effect of the Nominal Force "F_{nom}"

Consider the case where:

K_S = 7030 N/mm; K'_C = 224.25 N/mm/sec

K_{ac} = 25.4 mm/sec^2; B = 1.0 mm/sec^2

and F_{nom} takes two different values:

i) F_{nom} = 3960 N

ii) F_{nom} = 660 N

The corresponding open loop transfer functions are:

$$GH(s) = \frac{K\,(s + 25.0)}{s(s + 14.970)^2\,(s + 80.434)\,(s + 427.414)}$$

K = 34305

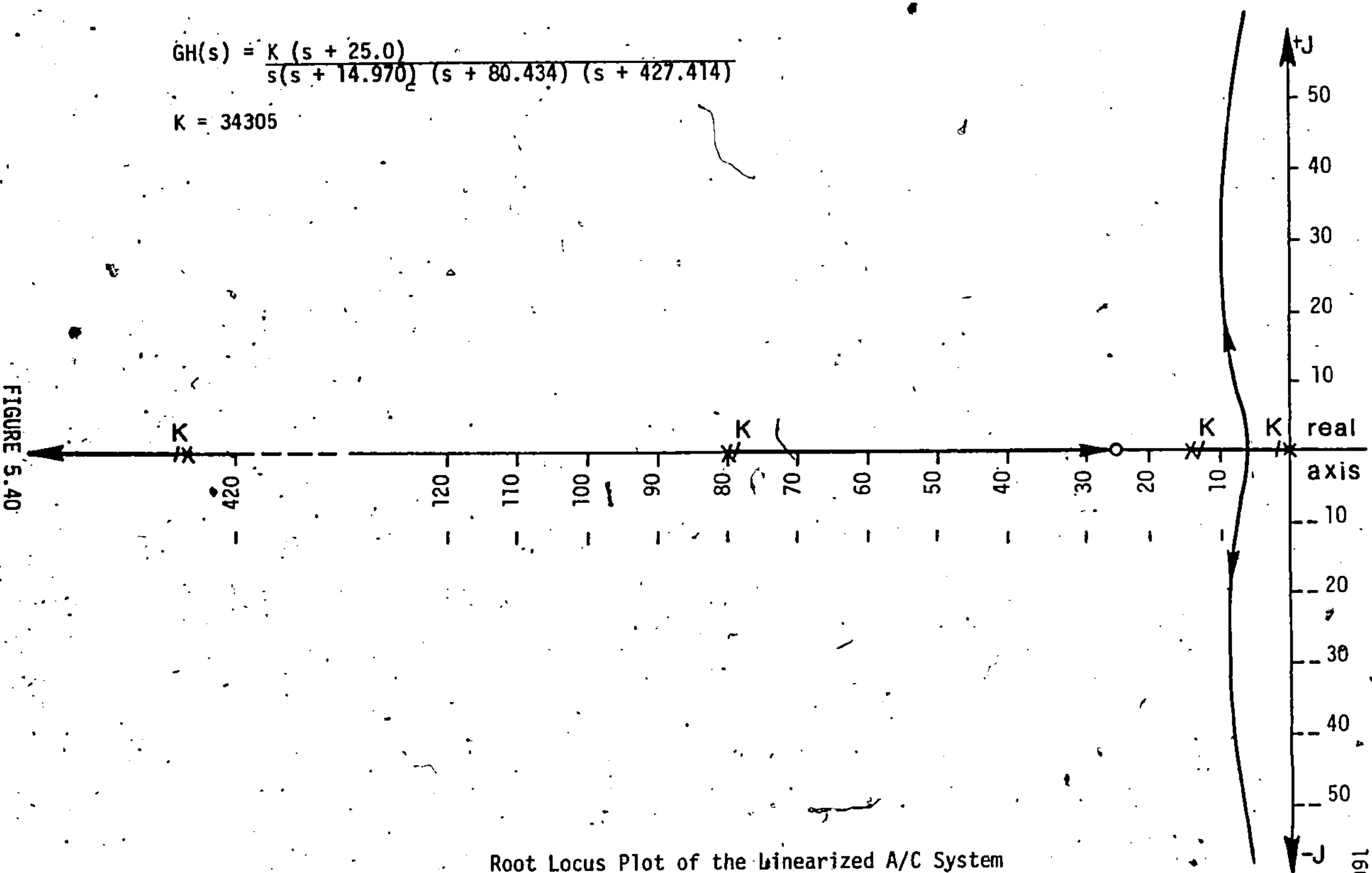

Root Locus Plot of the Linearized A/C System

FIGURE 5.40

$$GH(s) = \frac{K = (s + 25.0)}{s(s + 19.970)\,(s + 20.108)\,(s + 427.414)}$$

$K = 34305$

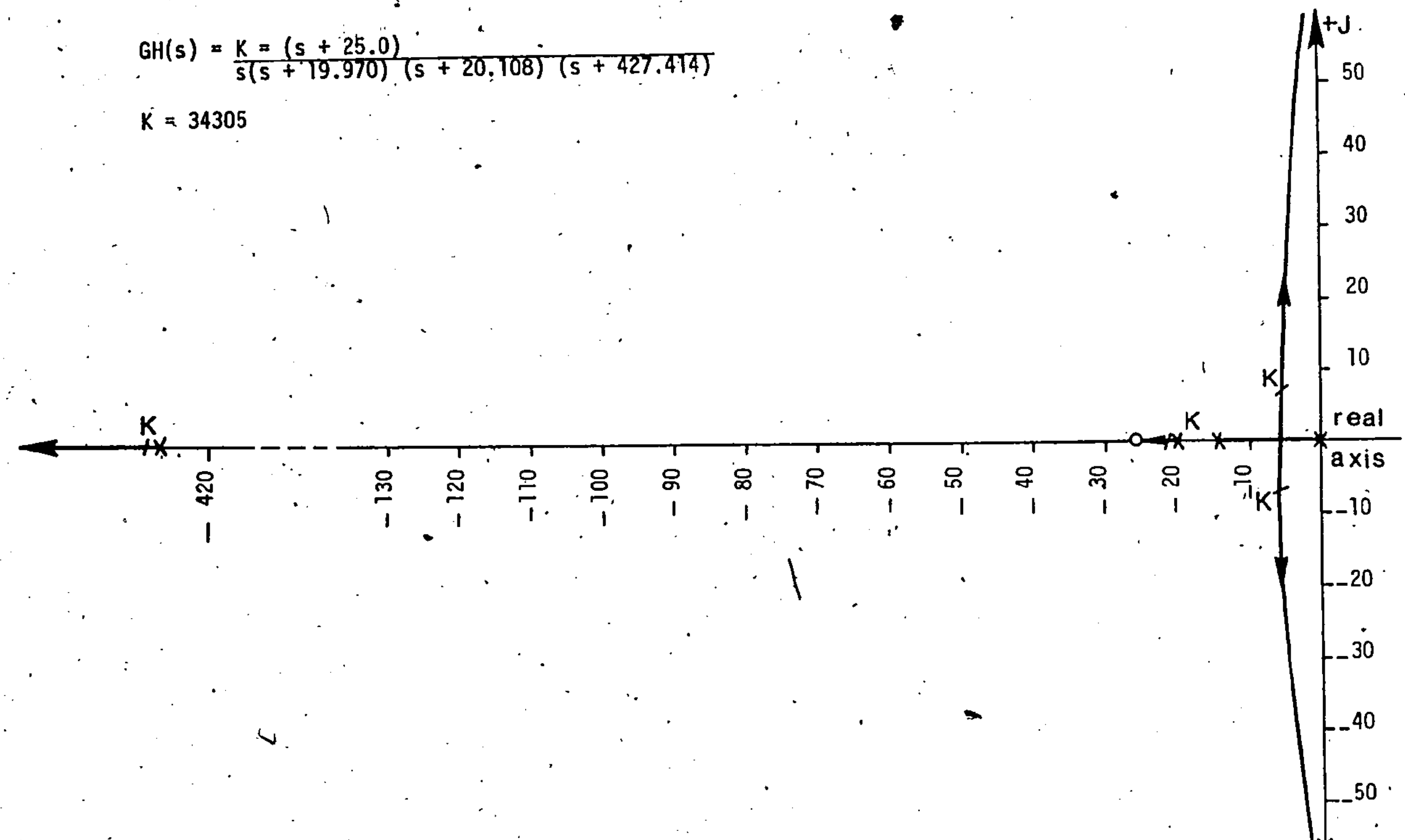

Root Locus Plot of the Linearized A/C System

FIGURE 5.41

i) $$\frac{F_{act}(s)}{F_{nom}(s)} = 11436.642 \frac{(s + 25.0)}{s(s + 14.970)(s + 30.936)(s + 427.414)}$$ -------------(5.26)

ii) $$\frac{F_{act}(s)}{F_{nom}(s)} = 68619.854 \frac{(s + 25.0)}{s(s + 14.970)(s + 30.936)(s + 427.414)}$$ -------------(5.27)

It is seen that decreasing F_{nom} increases the gain in the system and accordingly decreases the damping as shown in the corresponding root locus plot in figure 5.38.

5.8 Adaptive Control Algorithm "B"

A second strategy is presented in this section to cope with the collision situation discussed previously. The A/C strategy is as follows:

a) For F_{act} < 10 lbs (45N) equation (5.17) applies.

b) For F_{act} > 10 lbs (an event which occurs at time t = Tsec, say)

$$V_{com} = 0.0$$
$$X_{com} = 0.0$$ --(5.28)

for $T \leq t \leq T + 0.040$ sec.

c) Condition (b) held for 40 milliseconds after which V_{com} is controlled by equation (5.19).

d) for (T + 0.040)Sec $\leq t \leq$ (T + 0.140)Sec.

The gain "G_{NC}" in the NC loop is reduced to $G_{NC}/3$.

3) At $t \geq T + 0.140$ sec, the gain in the NC loop is G_{NC}.

The condition $V_{com} = 0.0$ is achieved by a special electronic circuit interfaced with the NC controller. This circuit is described in Appendix V. This circuit is also used to reduce the gain in the NC loop to 1/3 its original value for a period of 100 milliseconds.

The condition $X_{com} = 0.0$ is achieved by modifying the NC program in such a way that at time t = T, the flow of pulses from the computer to the NC controller is interrupted for a period of 40 milliseconds (see figure 3.6).

5.9 Experimental Results Using A/C Algorithm "B"

With the special action algorithm presented in section 5.8, it was possible to stop the rapid feed rather fast. In figure 5.42, records are reproduced showing the force and table velocity in such a transient and using the table dynamometer. Figure 5.42 a) shows the results obtained when slotting AISI 1020 with a 19.05 mm dia. - 4 flute HSS end mill. The axial depth of cut in this experiment was 2 mm. It is seen that a complete stop is achieved in about 20 msec, then the table accelerates slowly again to a feedrate which corresponds to the nominal force F_{nom}. In this case even the first tooth did not produce a force higher than F_{nom} and, after the initial stop it took about 0.5 sec to stabilize cutting at the nominal force. The fluctuations of the force correspond to the individual teeth of the cutter.

In figure 5.42 b) the experimental A/C response is shown for the case of slotting AISI 1020 at an axial depth of cut of 2.54 mm. The system stabilizes at 250 mm/min steady state feedrate. In both cases presented in figure 5.42 a)

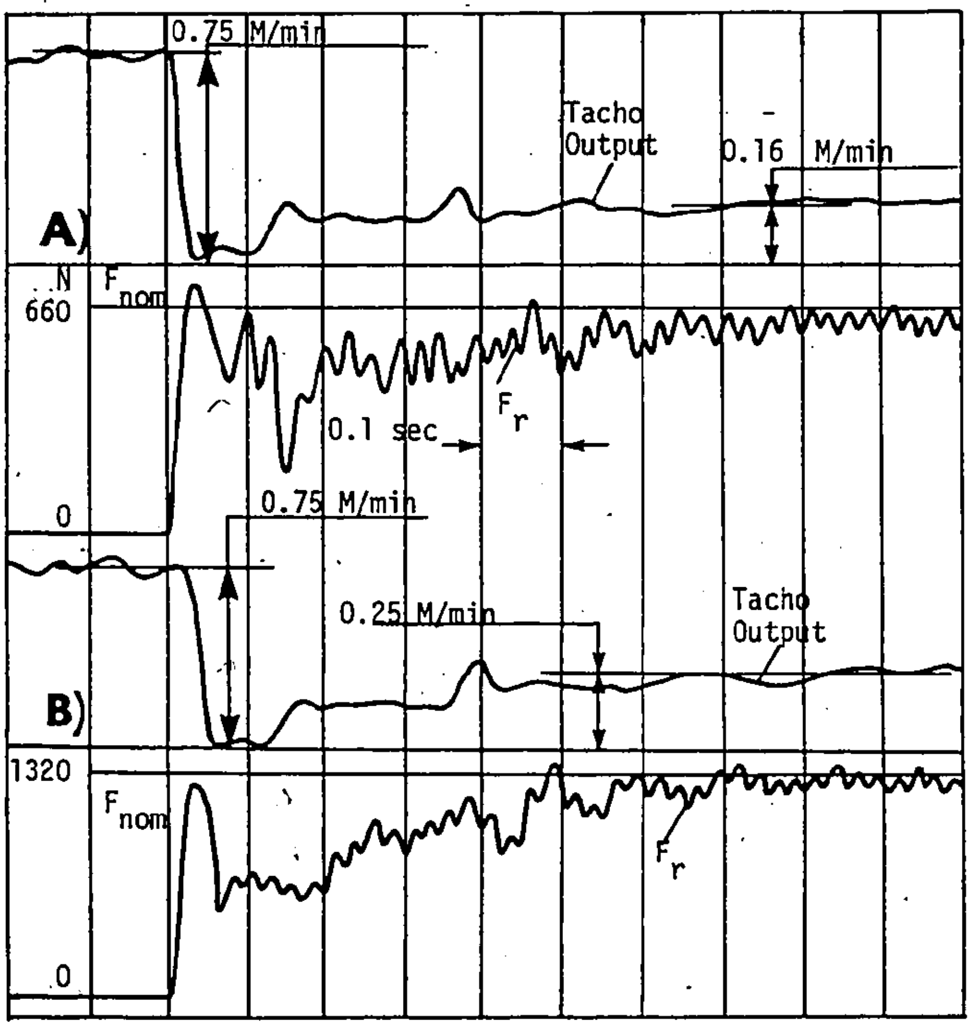

AISI 1020 Work Material, 19.05 mm Dia. - 4 Flute HSS End Mill, V = 35.34 M/min, A) b = 1.9 mm - B) b = 2.5 mm

Experimental Response of A/C System

FIGURE 5.42

and b) the interval between the individual teeth was 25 milliseconds.

Thus, it is obvious that the table can be stopped between the first and second tooth engagement. It may be concluded that the flexibility of the cutter makes it possible to approach the workpiece wall with rapid traverse. This will be illustrated in more detail in the following section.

5.10 Analysis of the Effect of Cutter Flexibility on the Force Peak in Adaptive Control Tests

It was shown so far that in an adaptive control system for end milling where the control criterion is to hold the force acting on the cutter at a value safely below the force which would break the cutter, the critical situation is that of a transient and it is typified by the case of the cutter moving fast, with a "rapid feed" f_r and entering the wall of the workpiece.

If as shown in figure 5.43 a) the cutter arrives at the wall in such an angular position that the tooth just slightly contacts the wall, this force signal can be used to slow down so as to prevent the next tooth to be overloaded by the very large chip thickness equal to the feed per tooth f_{tr} derived from rapid feed $f_{tr} = \frac{f_r}{N \times z}$, where N is the spindle speed and z is the number of teeth of the cutter. If, on the contrary, the first tooth just misses the cut as shown in b) then by the time the next tooth arrives to cut, the cutter has

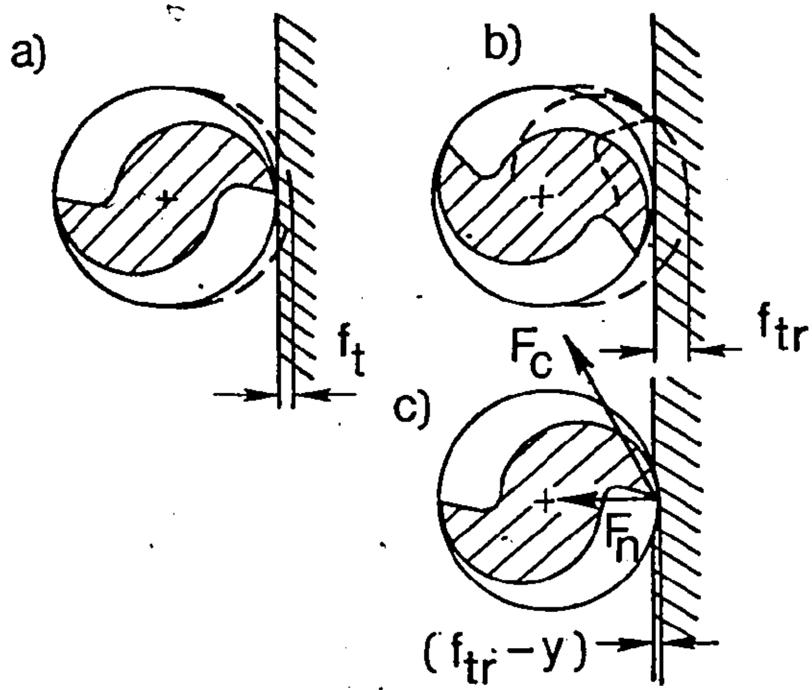

The Transient of Cutter Entering a Wall

FIGURE 5.43

already progressed too far and even if the feed was stopped immediately the tooth would be overloaded. Thanks to the flexibility of the spindle and of the cutter the situation b) actually does not arise as shown. The cutter deflects by the amount y and the actual chip thickness is smaller by this amount. While it is the cutting force F_C which may break the cutter, it is its normal component F_n which causes the deflection y.

Tlusty [74] investigated the essential features of the effect. In his analysis, the author assumed that there is only one tooth cutting and that the forces are proportional to chip thickness h_c and to the axial depth of cut b.

The worse case corresponds to the largest value of b. Such value b_{max} may be correlated to the dimensions of the cutter mainly from the point of view of chatter and this will be discussed in the next chapter. Thus,

$$F_C = K_C \, h_c b \;,\; F_n = 0.3 \, F_C \qquad (5.29)$$

Where for milling steel a value of $K_C = 2000\ \text{N/mm}^2$ and the ratio 0.3 may be taken as typical. It is:

$$h_c = f_t - y \;,\; y = F_n/K_t$$

where K_t is the stiffness on the tool. If we denote the ratio of the cutting stiffness to tool stiffness

$$\mu = \frac{K_C}{K_t}$$

we may write

$$h_c = f_t - 0.3\, F_t/K_t = f_t - 0.3\, K_C \, h_c b/K_t,$$

$$h_c = f_t/(1 + 0.3b\mu) \quad \text{------(5.30)}$$

In the denominator of equation (5.30) the second term will usually be much larger than 1.0. Therefore, (5.30) can be simplified as

$$h_c = f_t\ K_t/0.3\ b\ K_C \quad \text{------(5.31)}$$

and, using equation (5.29), it is:

$$F_C = f_t\ K_{t/0.3} \quad \text{------(5.32)}$$

We will now set this F_C equal to the maximum force F_C max which would cause a stress σ_S safe below the strength of the cutter

$$F_C\ \max = \frac{\pi\ d^3\ \sigma_S}{32\ L} \quad \text{------(5.33)}$$

where σ_S = 1500 N/mm^2.

Assuming further that the spindle is absolutely rigid and considering the flexibility of the cutter alone (which leaves us on the safe side), and adding a factor of 1.5 for the flexibility in the collet the stiffness on the tool is:

$$K_t = \frac{\pi\ d^4\ E}{1.5 \times 64\ L^3} \quad \text{------(5.34)}$$

Combining equations 5.32, 5.33, 5.34, an expression is obtained for the maximum rapid feed per tooth f_{tr} at which the first force peak will just only reach the maximum permissible force F_C max.

$$f_{tr} = 0.9\ \frac{\sigma_S}{E}\ \frac{L^2}{d}$$, where L is the cutter length

and for $E = 30 \times 10^6$ lb/in^2,

$$f_{tr} = 0.0064 \frac{L^2}{d} \quad \text{------------------------------------} (5.35)$$

This rapid feed may be very large. For illustration the values of f_{tr} and also of the rapid table velocity f_r (mm/min), assuming cutting speed V = 40 m/min and 2 teeth for d = 6.25 and 12.5 mm and 4 teeth for d = 18.75 and 25 mm, are given in table 5.1 for selected sizes of tools.

	f_{tr}(mm)				f_r(mm/min)			
l/d	6.25	12.5	18.75	25	6.25	12.5	18.75	25
50	2.6	1.3	0.9	0.6	10400	2600	2320	1300
75	5.8	2.9	1.9	1.4	23400	5860	5200	2920
100	10.2	5.1	3.4	2.6	41700	10400	9200	5200

Table 5.1[74]

CHAPTER 6

CONSTRAINTS IN ADAPTIVE CONTROL WITH FLEXIBLE END MILLS

6.1 Introduction

Finish end milling with rather flexible cutters may substantially be speeded up by using an adaptive control system controlling the cutting force, while the setting parameter is the feed rate. The control criterion is to hold the force acting on the cutter at a value safely below the force which would break the cutter. The flexibility of the cutter is beneficial in attenuating the overload in a sudden transient solution. The force signal is used to recognize the entry into and the exit from the workpiece by the milling cutter.

In addition to the force constraint discussed previously, two other constraints, to be taken into account, will be discussed in this chapter, namely: chatter and overload of the cutting edge.

During machining of metals, different kinds of vibrations will occur in the machine tool structure. These vibrations will lead to more or less periodical deviations in the cutting geometry. Among other things, such as the noise and the increasing tool wear, the vibrations result in a wavy surface of the workpiece and in this way the quality of the product is impaired.

From their nature, two major kinds of vibrations are distinguished, viz., forced vibrations and vibrations induced by the cutting process itself [73].

Forced vibrations can be caused by external excitation, e.g. external disturbing forces in the machine foundation; by machine components, e.g. inbalances and tooth impacts in the drive or in the gear train of the machine. Forced vibration is rather easy to control, since it can be prevented by eliminating the disturbance [75].

Vibrations caused by the cutting process can be distinguished into free vibrations and those which are self-induced [76]. "free-type" vibrations generally are of minor importance, because they will be damped in a very short period of time. This type of vibration can be caused by the shearing process, the instability of the built-up edge and the inhomogeneous nature of the workpiece material.

As distinct from the vibrations mentioned before, self-induced vibrations are caused by a dynamic force, generated by the vibration itself, which becomes extremely violent. Characteristic for this type of vibration is that the frequencies are always approximately equal to the natural frequencies of the machine tool structure. Commonly known as "self-excited chatter", particularly this type of vibration, which is of a very complex nature, should be avoided.

Chatter in end milling has a rather special character. In this chapter an attempt is made to investigate some of its basic features with particular emphasis on end milling cutters with high flexibility.

There are two basic forms of edge overload. One is purely mechanical and most often it occurs as the breakage of the tip of a tooth under heavy feed. The other is more of a thermal nature and it results from a high product of speed and feed and it occurs as rapid wear of a softened edge material. Very little data has been published about either of these phenomena. In this chapter, however, a review of the basic features of these phenomena will be presented.

6.2 The Chatter Constraint

According to Tlusty {77}, in dealing with chatter problems from the practical point of view, three main aspects are distinguished as it is diagrammatically indicated in Figure 6.1.

The machine tool structure S represents a three dimentional multi-degree-of-freedom system carrying the tools at one point and the workpiece at the opposite point. The tools T may be a single one (turning, boring, etc.) or multiple (milling, broaching, etc.). Vibration Y of the system S influences the cutting process C producing forces F acting on the structure and exciting vibrations Y, thus closing the loop.

The most powerful sources of self-excitation, those of "regeneration" and of "mode coupling" are associated with the structural dynamics of the machine tool and the feedback between subsequent cuts {78}. The existence of negative damping in the cutting process is another aspect of chatter {79}, and is considered by some researchers as a necessary con-

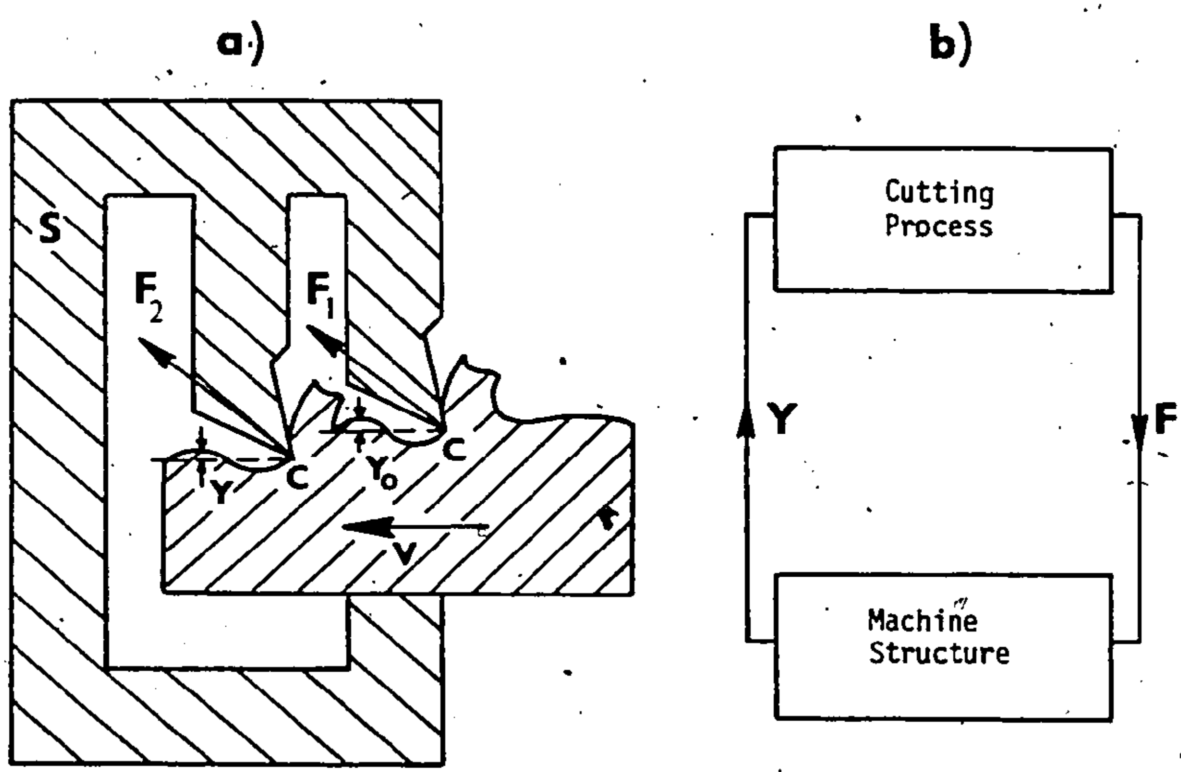

Structure, Tool, Cutting Process in the Closed Loop of Chatter

FIGURE 6.1

dition for chatter to occur [80].

The regeneration mechanism is based on the fact that the vibrating tool T_1 leaves an undulated surface with amplitude Yo (see figure 6.1). This surface is being cut by the following tooth T_2 of the milling cutter, which again leaves an undulated surface behind, with amplitude Y. The limit of stability is therefore, $|Y| = |Yo|$.

The three aspects of structure, cutting process and tool act differently and have different practical significance:

a) Assuming a single tool case and a single formula for the cutting force:

$$F = br\,(Y - Yo) \qquad (6.1)$$

Where (Y - Yo) is the variation in the undeformed chip thickness, b is the chip width and r is the cutting stiffness (co-efficient of proportionality) and is assumed to be a real number. The force varies in phase with chip thickness variation and no damping (either positive or negative) arises in the chip formation process.

In such a case the limit width of chip is [72]:

$$b_{lim} = -\frac{1}{2r\,R_e(G)_{min}} \qquad (6.2)$$

Where $R_e\,(G)_{min}$ is the magnitude of the minimum of the real part of the transfer function of the structure, oriented with respect to the direction of the cutting force and to the direction of the normal to the cut surface.

b) Regeneration of vibration can be disturbed and stability of machining increased by various kinds of special designs of multi-point cutting tools {81, 82} specifically, milling cutters.

c) It is generally accepted that damping is generated in the cutting process which can rather strongly affect chatter {77}. The knowledge of this damping force is most significant for a proper choice of cutting data. This is particularly valid for NC machining where the knowledge of the limits imposed by chatter on the choice of speeds and feeds for a given machine tool and a given tool is very important in order to obtain stable machining with maximum output.

There is another reason for studying the effects of cutting data on chatter and that is to make it possible to interpret results of exciter tests of machine tools expressed in transfer functions, so as to translate them into the corresponding metal removal rates.

6.2.1 Measurement of Dynamic Data by Excitation Tests

Exciter tests were carried out in order to measure the transfer function at the end of a mandrel representing the tool. Other measurements were carried out on the chuck, the quill, and the head of the milling machine. Most of these tests were done with a relative vibration pick-up (capacitance type) between the dummy tool end and the table of the machine. Some of these tests were done using a velocity pick-up. Excitation was by hammer blows. For each test, an average of 10 measurements was obtained and the resulting real and imaginary parts of the receptance were plotted using the Fourier Analyzer. In order to improve the results obtained from these tests, the mandrel was preloaded with approximately 30 kg in all of the measurements.

In the first set of these tests, a 63.5 mm(2.5 inch) diameter steel bar was placed in the collet with an overhang of 38.1 mm(1.5 inch) to simulate a shell end mill. Figure 6.2 shows plots of the real and imaginary parts of the receptance (in the frequency domain) generated by hitting the end of the simulated tool in the longitudinal, X-directions with a force transducer and measuring the vibration at that point with a capacitive probe. The frequency range covered was 0 to 2500 Hz. Main modes are 70, 225, 490, 740, and 790 Hz. In figure 6.3 the transfer function is reproduced, measured similarly as in figure 6.3, but in traverse Y-direction. Main modes appear to be at 160, 450, and 485 Hz.

A second set of shock excitation tests were performed using a 19 mm (0.75 inch) diameter steel bar placed in the collet with an overhang of 38.1 mm (1.5 inch) to simulate an end mill. The measurements shown in figures 6.4, 6.5 and 6.6 were taken in X-direction.

Figure 6.4 shows plots of the real and imaginary parts of the receptance generated by hitting on the chuck with a force transducer and measuring the vibration at that point with a capacitive probe. Main modes are 275 and 650 Hz.

Figure 6.5 shows the results obtained when the ex-

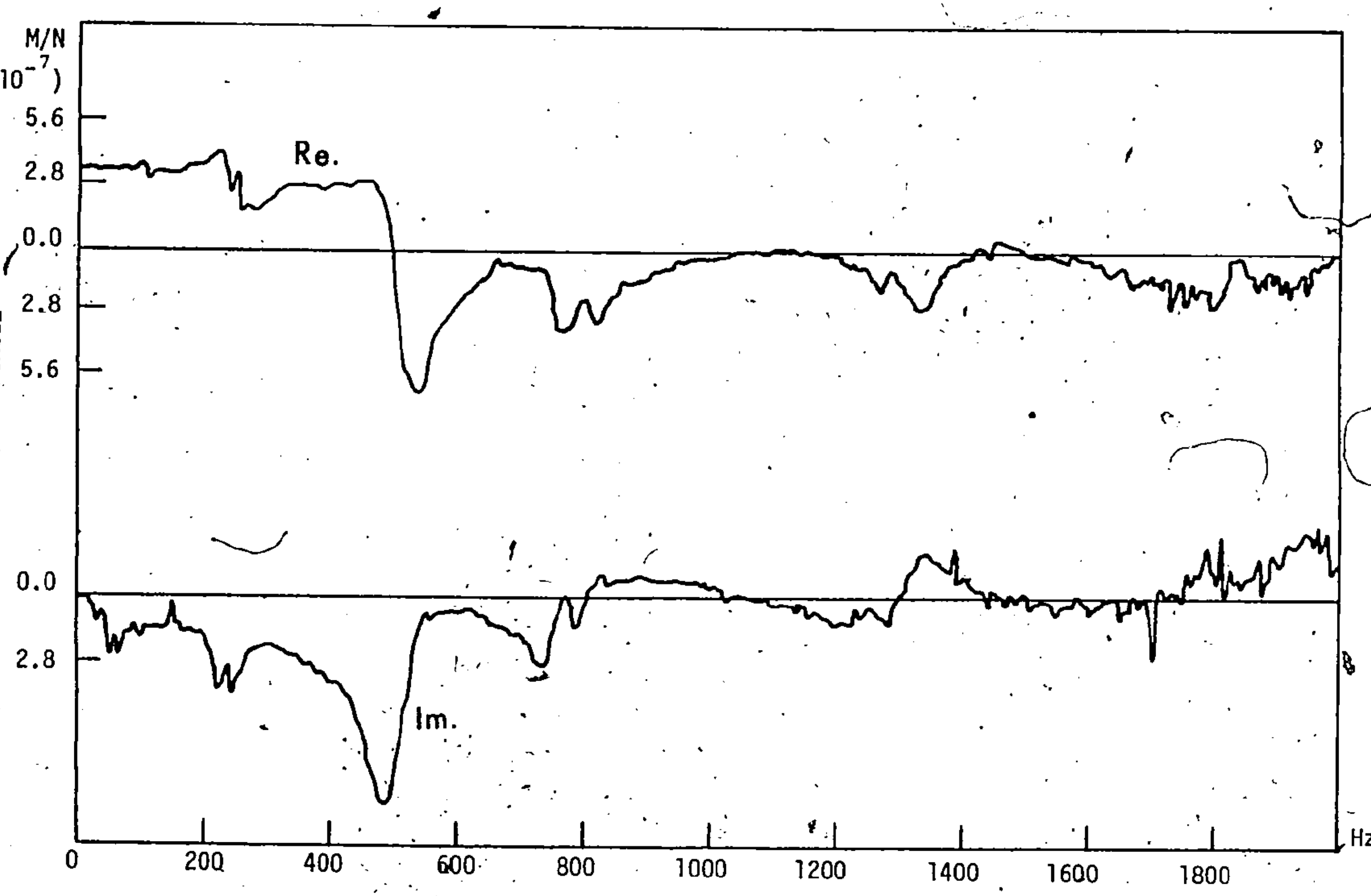

Measured Transfer Function

FIGURE 6.2

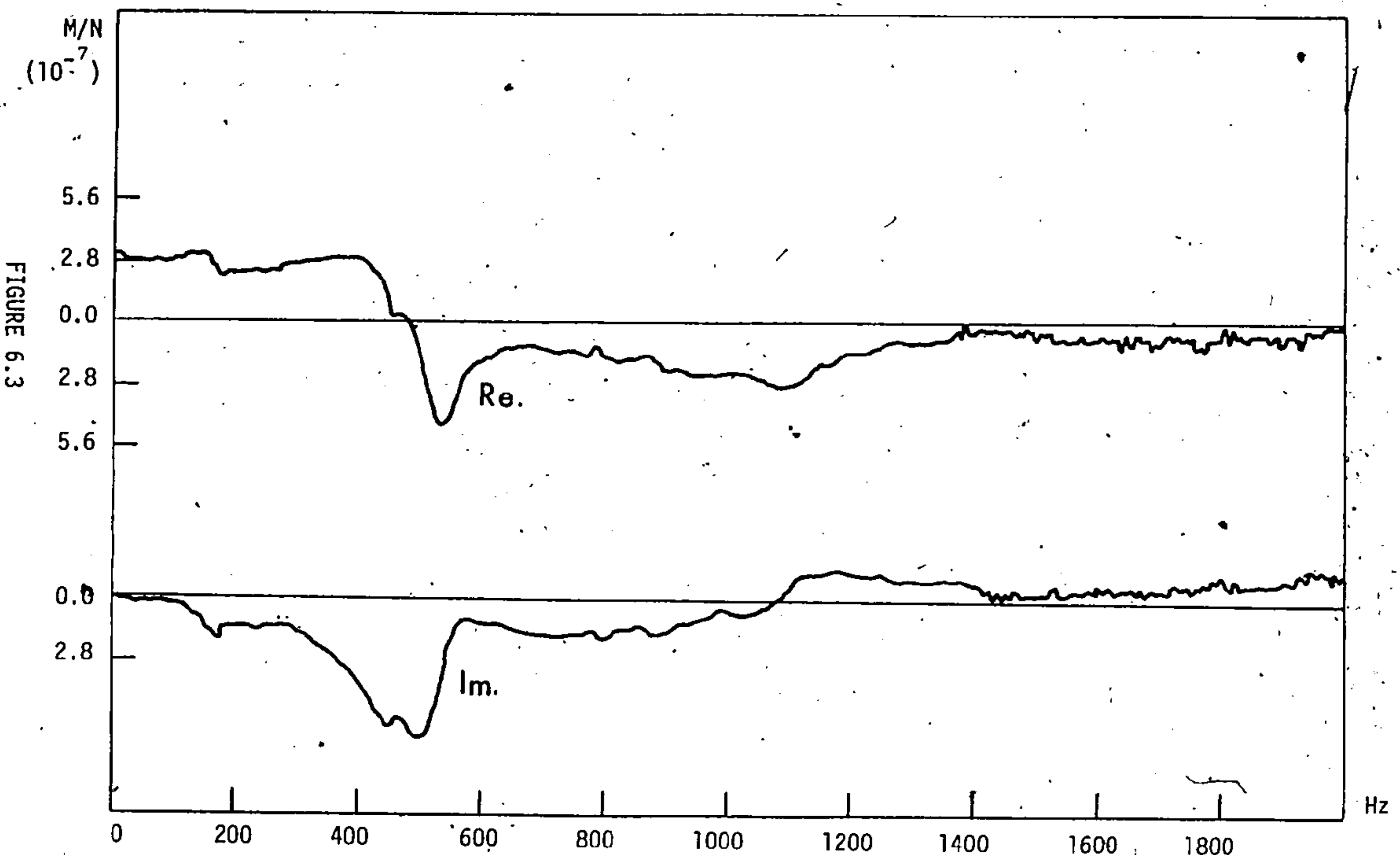

Measured Transfer Function

FIGURE 6.3

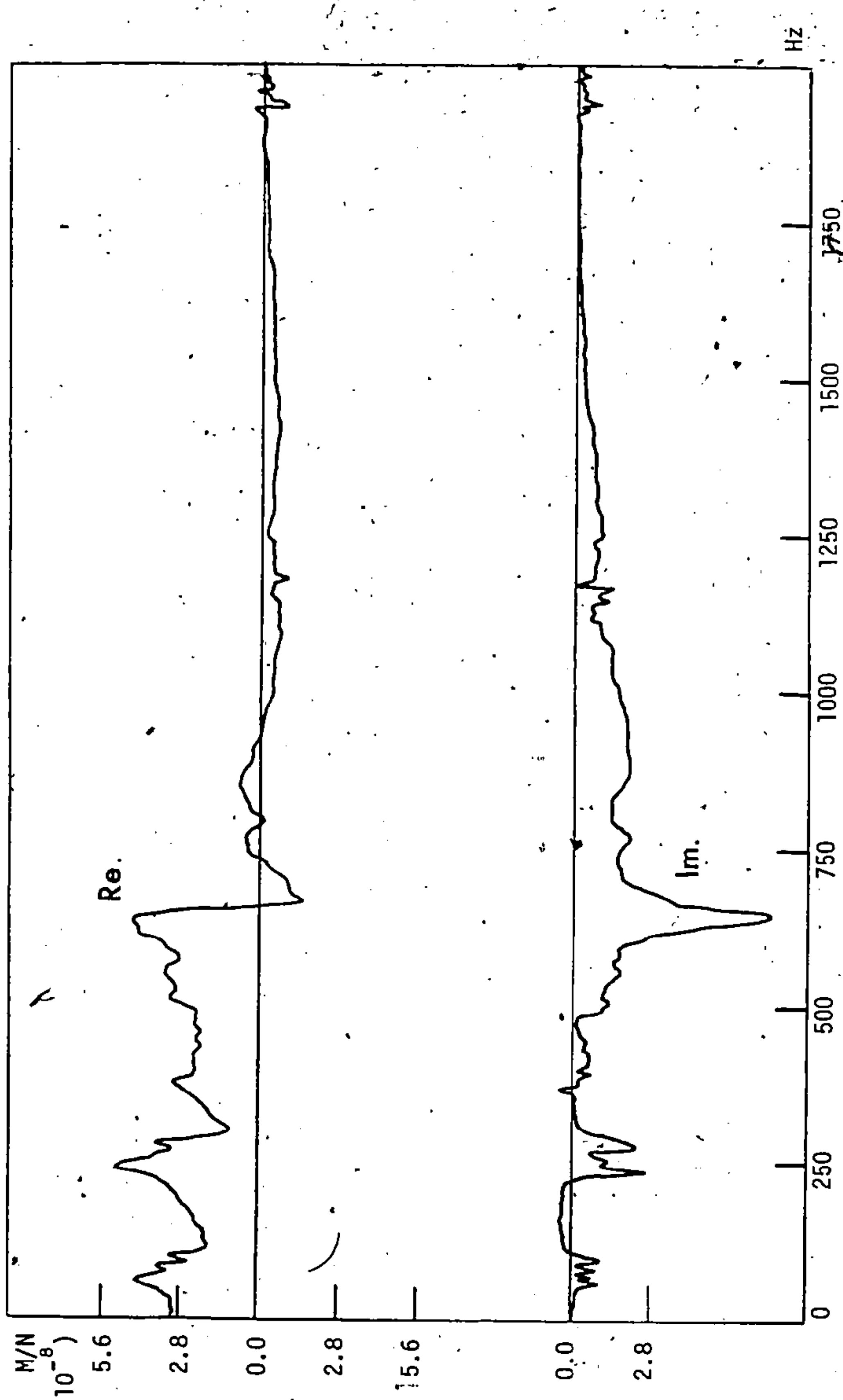

Measured Transfer Function

FIGURE 6.4

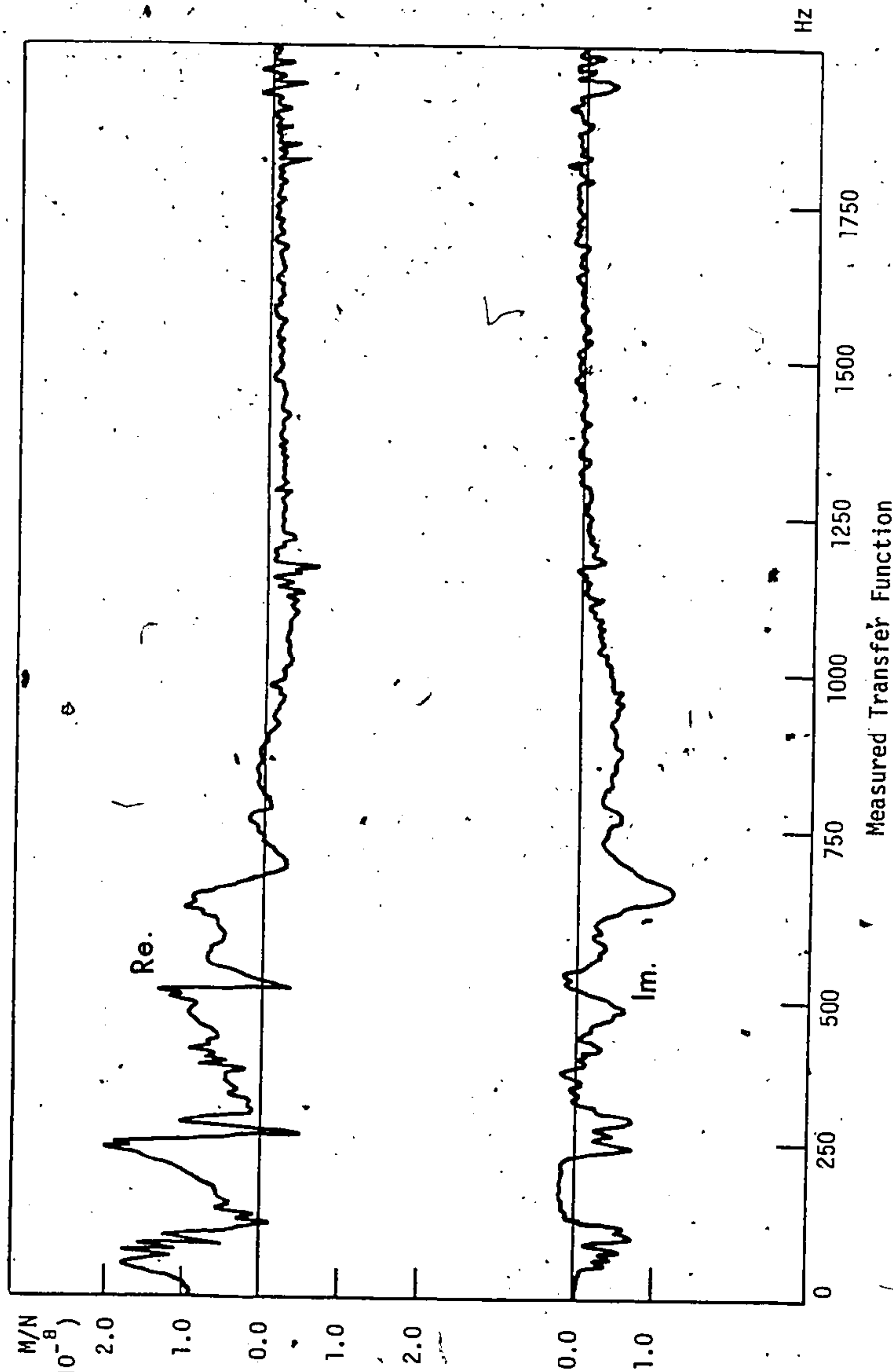
M/N
(10^{-8})
2.0
1.0
0.0
1.0
2.0
0.0
1.0
Re.
Im.
0
250
500
750
1000
1250
1500
1750
Hz
Measured Transfer Function

FIGURE 6.5

citation and the vibration are measured at the quill of the milling machine. Again, main modes are 275 and 650 Hz.

Similar measurements were performed in Y-direction. In figure 6.6, the resulting transfer function is obtained by hitting on the chuck and measuring the vibration at that point using a velocity pickup.

Finally, figure 6.7 shows the transfer function obtained by hitting on the chuck and measuring the resulting vibration at the end of the mandrel using a velocity pickup.

6.2.2 Cutting Tests

Cutting tests were carried out by end milling 1020 steel and Al. Alloy with several types of end milling cutters. In these tests, it was decided to use the cutting force signal produced during machining to detect chatter vibrations. For this reason, a special dynamometric table was designed and constructed in order to withstand the very high cutting forces produced during chatter tests. Using this dynamometer, the cutting force was monitored during cutting by means of four piezo-electric transducers (type: PCB 218A); two in each of X and Y directions. These transducers are very rigid and consequently have a high natural frequency, (68 KHz.). For each of the four force components, a proportional charge signal is produced in the measuring element. The charge signals produced by the two piezo-electric transducers in X direction were summed and fed to a charge amplifier where the resulting charge signal is converted into voltage

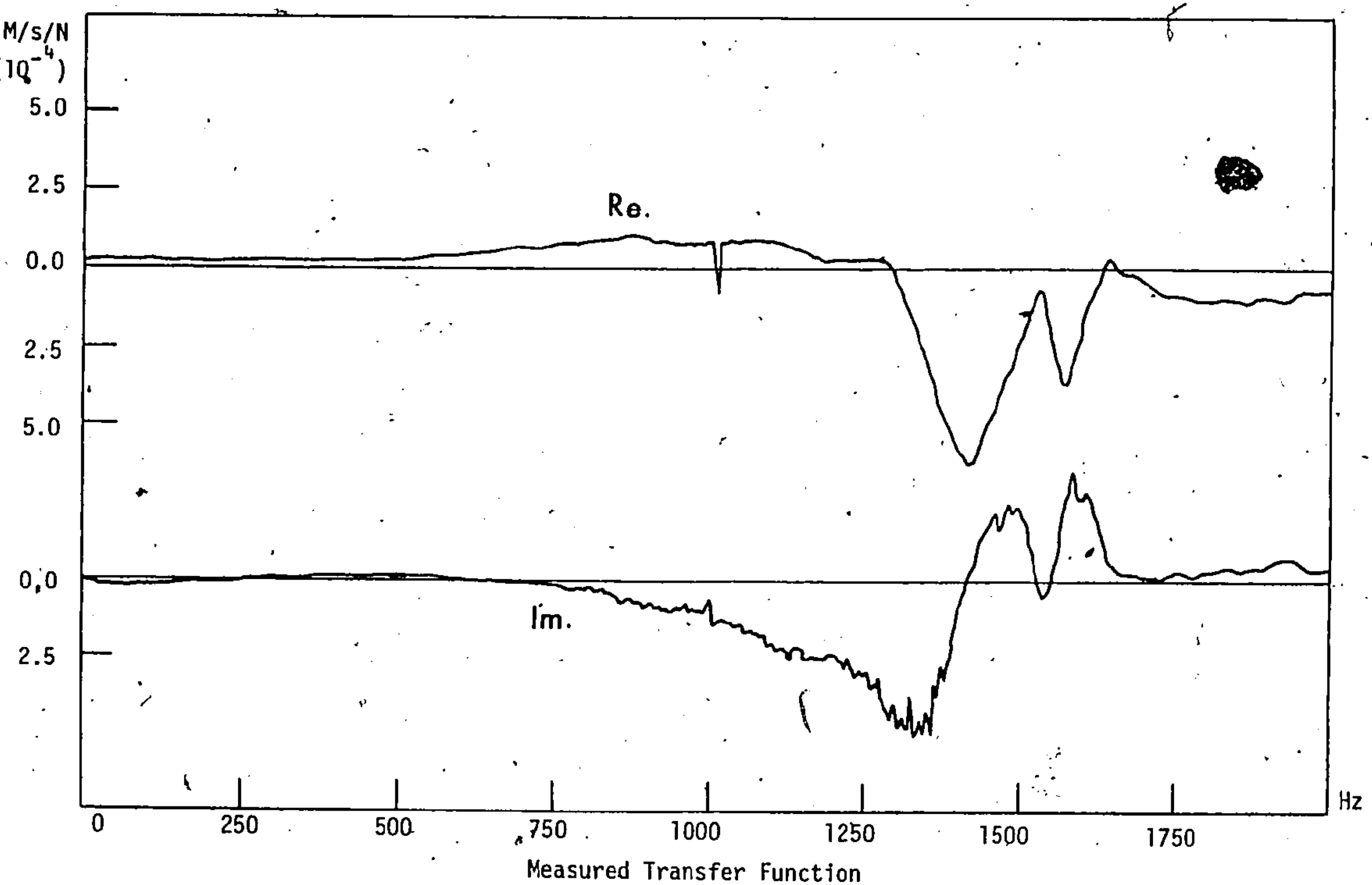
M/s/N
(10^-4)
5.0
2.5
0.0
2.5
5.0
0.0
2.5
Re.
Im.
0
250
500
750
1000
1250
1500
1750
Hz
Measured Transfer Function

FIGURE 6.6

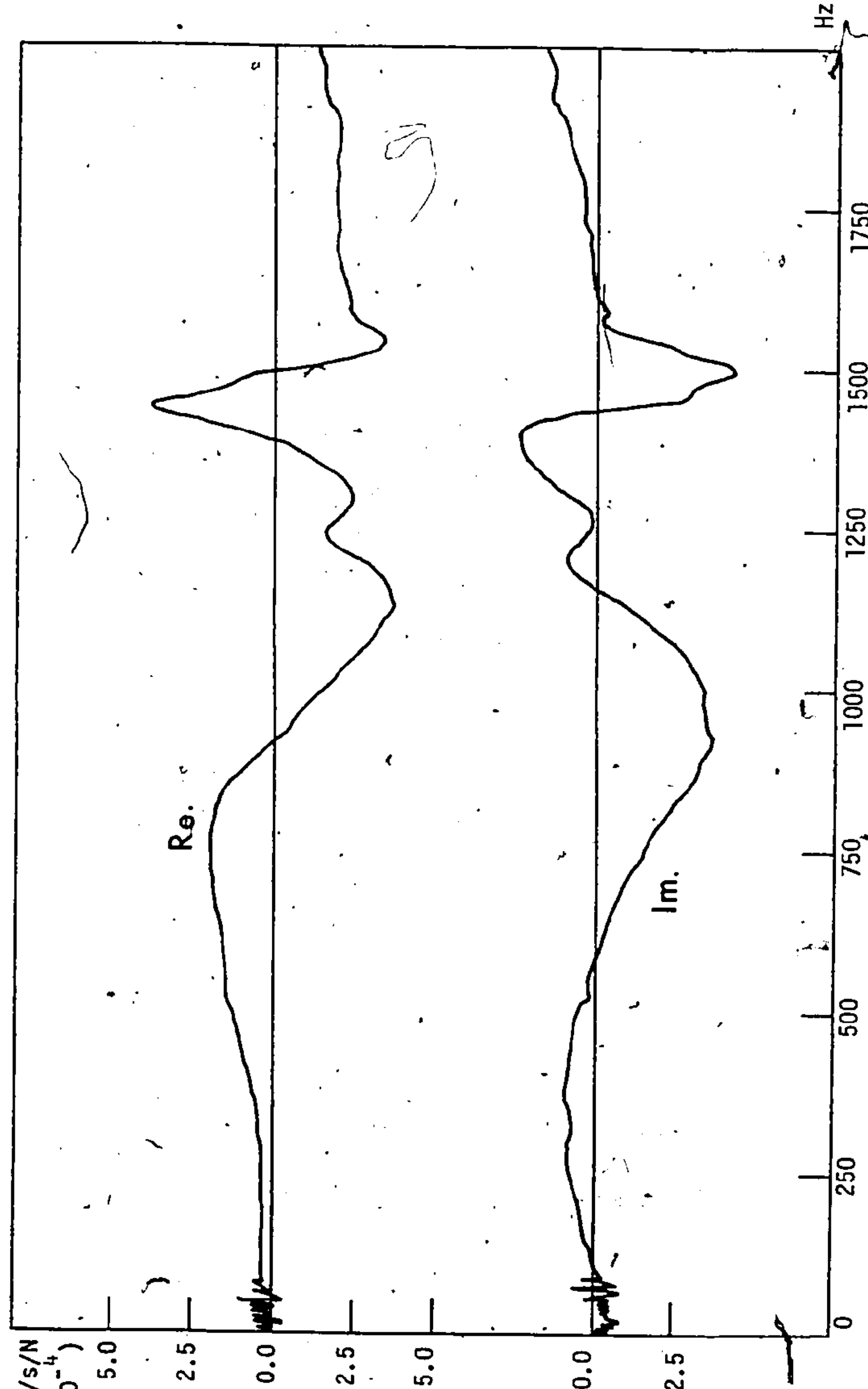

Measured Transfer Function

FIGURE 6.7

which was recorded by means of an ultra violet (U.V.) recorder. A similar arrangement was provided for the transducers in Y axis. During cutting, vibration was also simultaneously measured at the lower end of the head stock using a vibration pickup. The workpiece to be machined was clamped on top of the dynamometer. The dynamic characteristics of the dynamometer are shown in figures 6.9 and 6.10, measured in X and Y directions respectively.

In figure 6.9, the transfer function of the dynamometer is measured in X direction using the shock excitation technique. Trace a) shows a constant magnitude up to 750 Hz. while traces b) and c) show the corresponding real and imaginary parts of the transfer function. Figure 6.10 shows the results of the measurement performed in Y direction. Trace a) in this figure shows a constant magnitude up to 850 Hz.

In the cutting tests presented in this section, the cutting conditions (feed, cutting speed, tool geometry, material of the workpiece and radial width of cut) were kept constant during each experiment while the axial depth of cut was increased in increments until chatter occurred. Records reproduced in figure 6.11 represent chatter vibration measured when down milling with feed in X direction, and using a 63.5 mm (2.5 inch) diameter high speed steel shell end mill. In this case, the cutting force F and the normal to the cut surface have directions as indicated in the left down corner of the figure. These directions will engage modes with direction Y

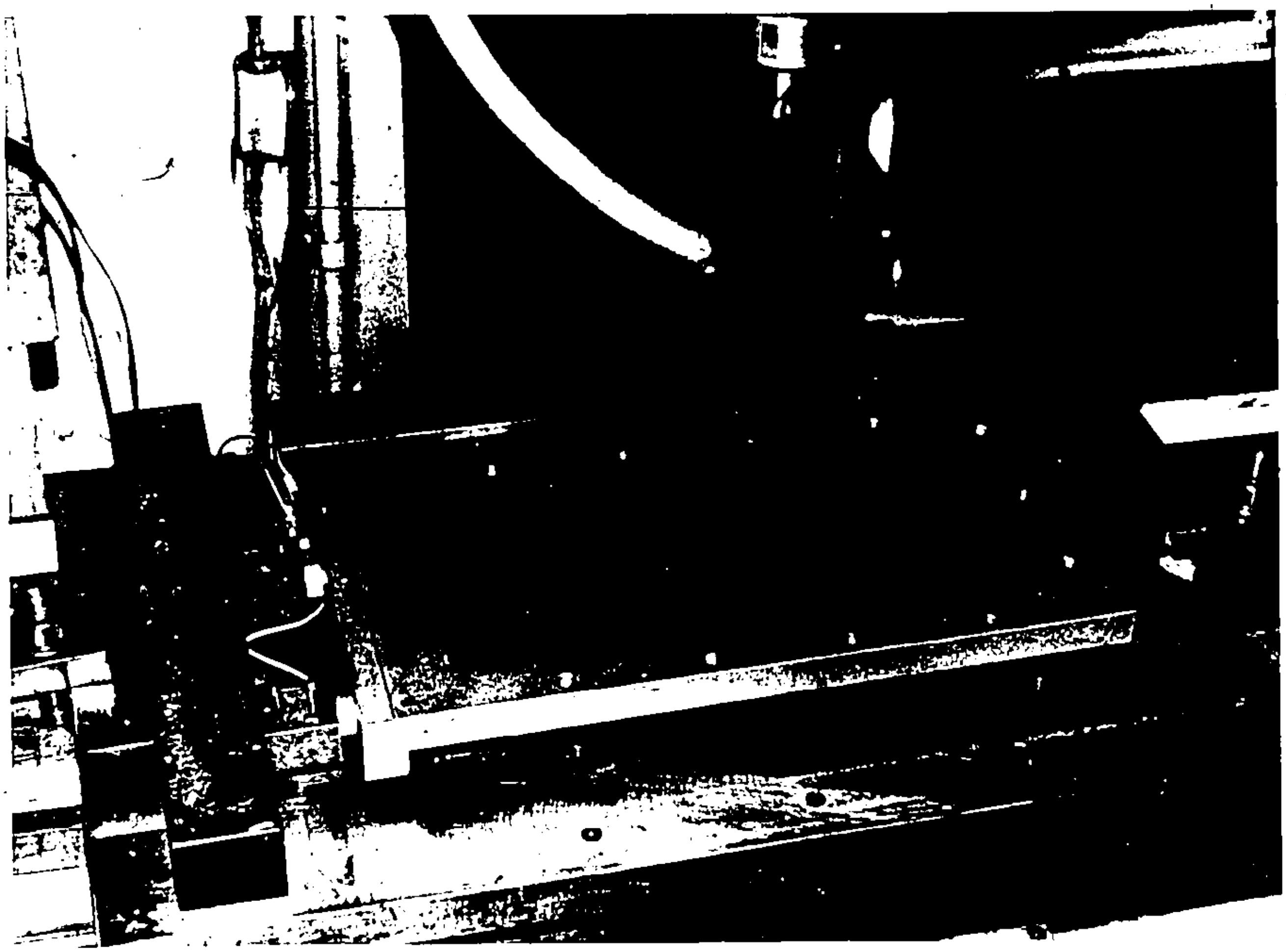

Picture of the Dynamometer Used in Chatter Tests

FIGURE 6.8

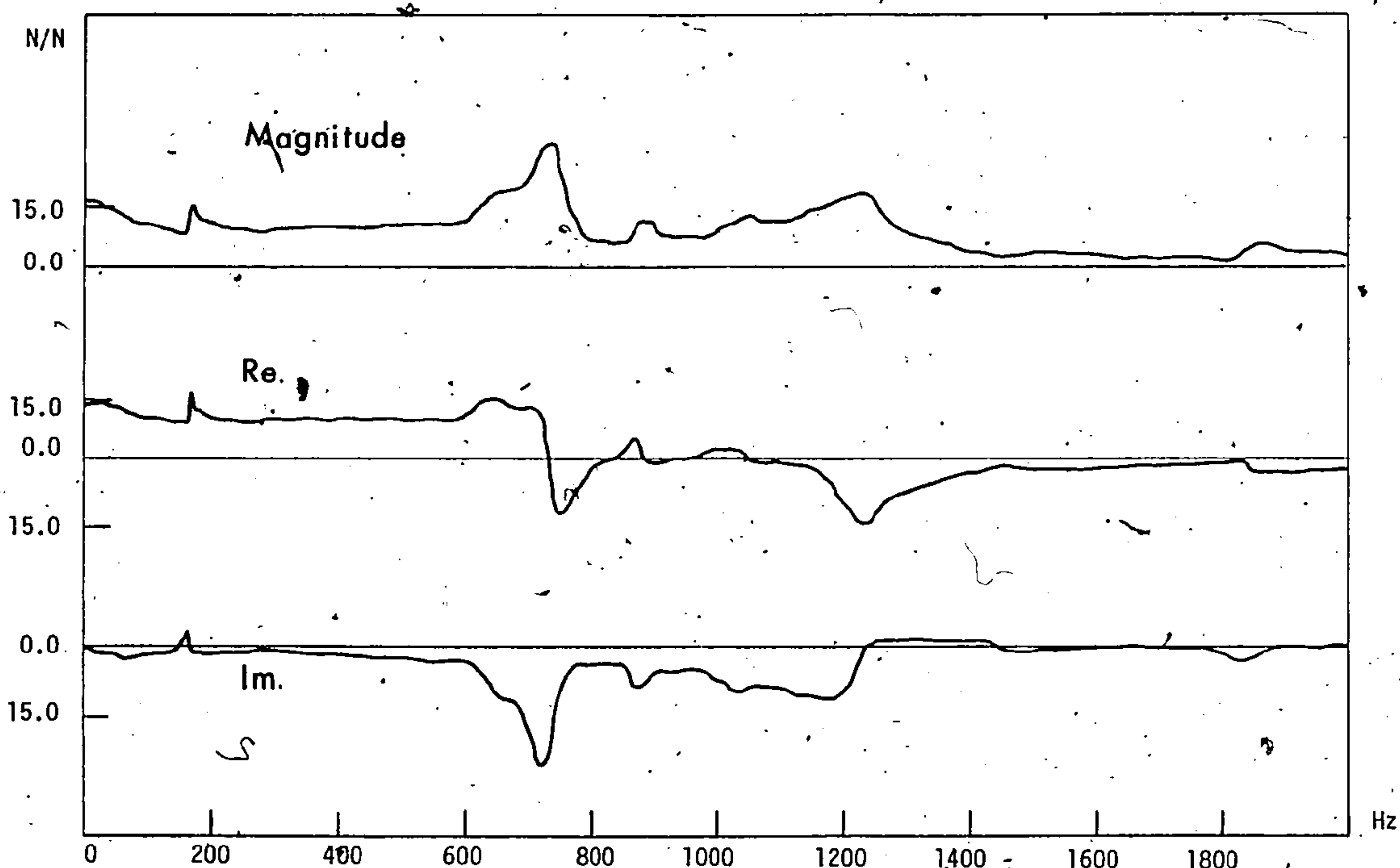

Measured Transfer Function

FIGURE 6.9

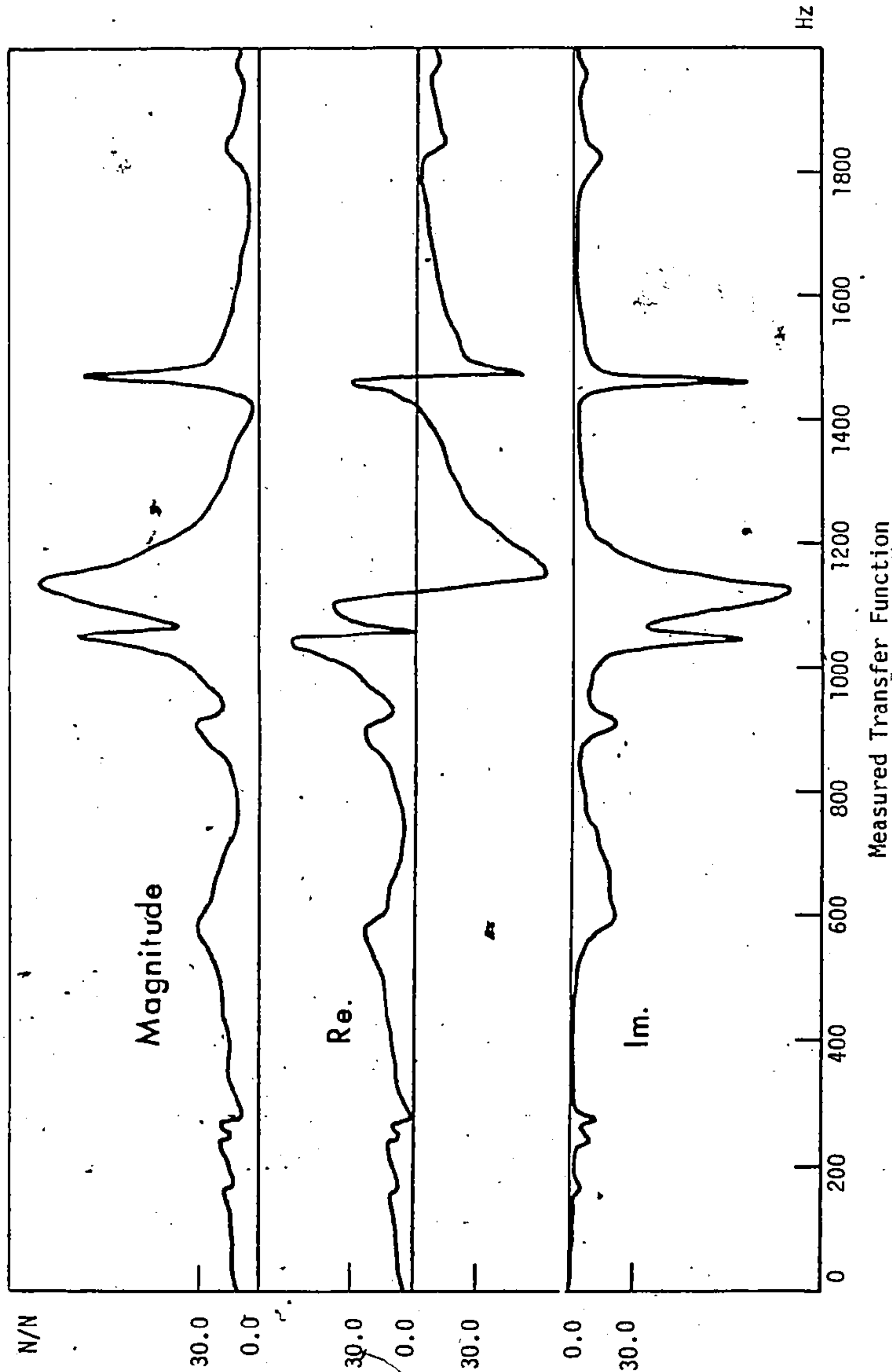
Magnitude
Re.
Im.
N/N
30.0
0.0
30.0
0.0
30.0
0.0
30.0
0
200
400
600
800
1000
1200
1400
1600
1800
Hz
Measured Transfer Function

FIGURE 6.10

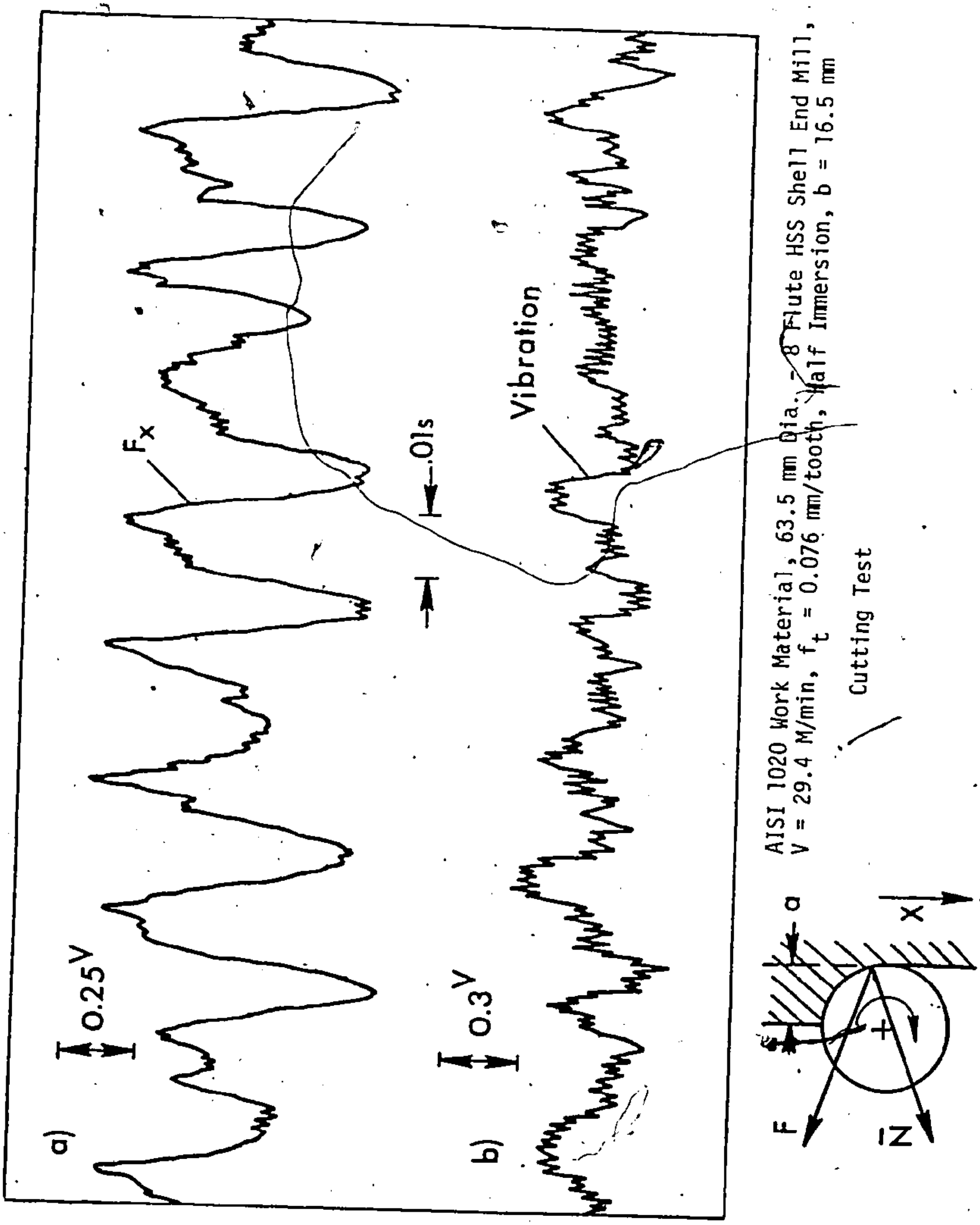

AISI 1020 Work Material, 63.5 mm Dia. - 8 Flute HSS Shell End Mill,
V = 29.4 M/min, f_t = 0.076 mm/tooth, Half Immersion, b = 16.5 mm

Cutting Test

FIGURE 6.11

(with a directional factor of about 0.75), i.e. those modes measured in the exciter tests. In figure 6.12, trace a) represents the force signal in X direction while trace b) is the vibration signal recorded using a velocity pickup and measured at the lower end of the head stock. The prevailing frequency as shown in trace a) is 85 Hz. The conditions of the cut were as given in figure 6.11. Infigure 6.12, the results obtained correspond to down milling in X direction using a 63.5 mm (2.5 inch) diameter carbide shell end mill. The cutting speed used in this experiment is higher than the one used in the previous cutting test (because of the use of a carbide cutter) and the chatter frequency as seen in trace b) of figure 6.12 was 650 Hz.

Cutting tests were next carried out using a 25.4mm (1 inch) diameter high speed steel end mill. Figure 6.13 shows the results obtained when slotting Al..Alloy. The figure corresponds to a case of stable machining. Trace a) is the vibration signal while traces b) and c) are the force signals in Y and X directions respectively. Figure 6.14 shows the chatter vibrations obtained when increasing the axial depth of cut to 21.6 mm (0.850 inch). Trace a) represents the measured vibrations, while trace b) is the force signal in X direction. The prevailed frequency as shown in trace b) is 650 Hz. This experiment was repeated with the same cutting conditions, but using a tool with 101.6 mm (4 inch) overhang, and the results obtained are shown in figure 6.15. It is seen

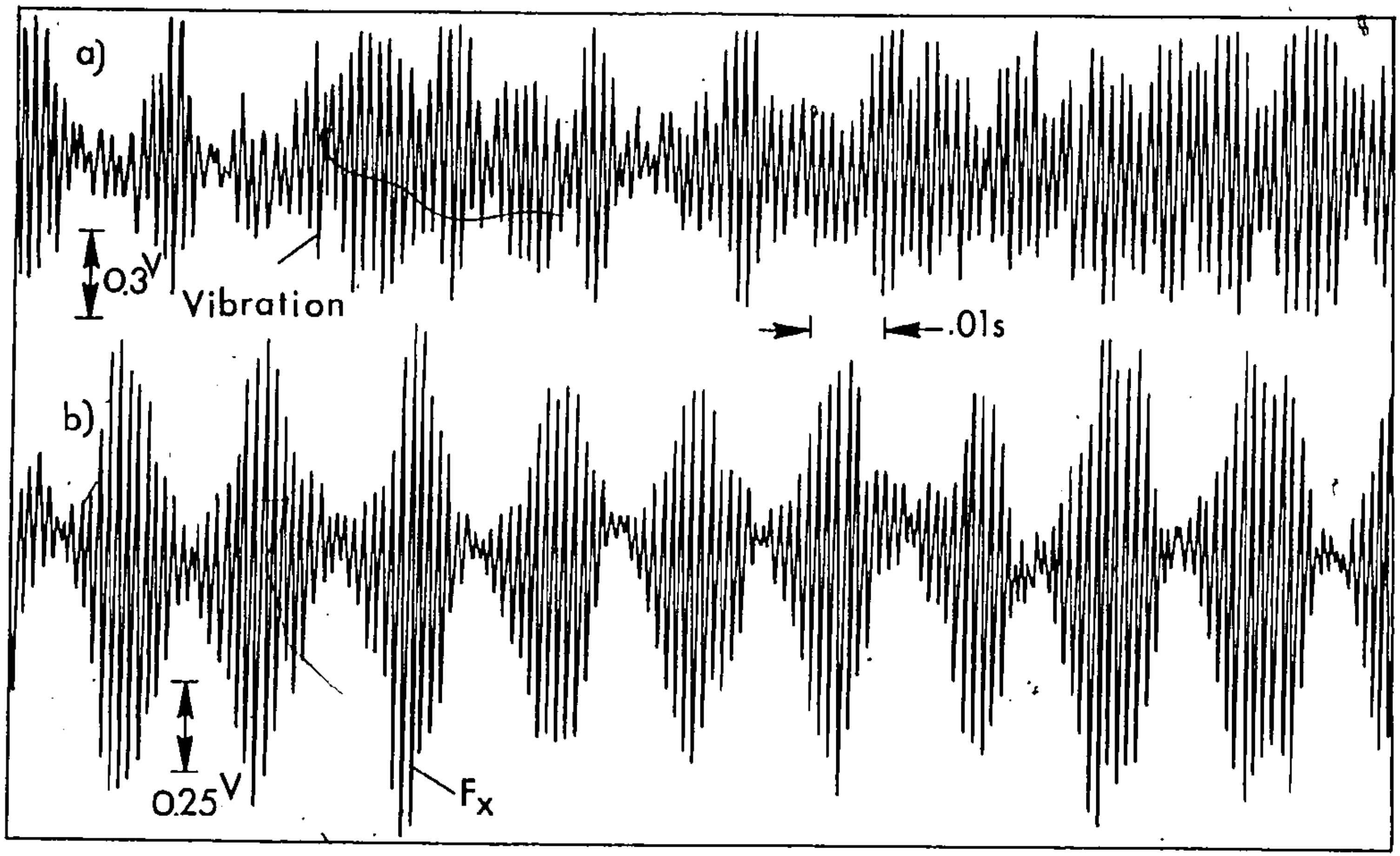

AISI 1020 Work Material, 63.5 mm Dia. - 6 Flute Carbide End Mill, V = 117.6 M/min, f_t = 0.076 mm/Tooth, Half Immersion, b = 10 mm, Down Milling in X - Direction

Cutting Test

FIGURE 6.12

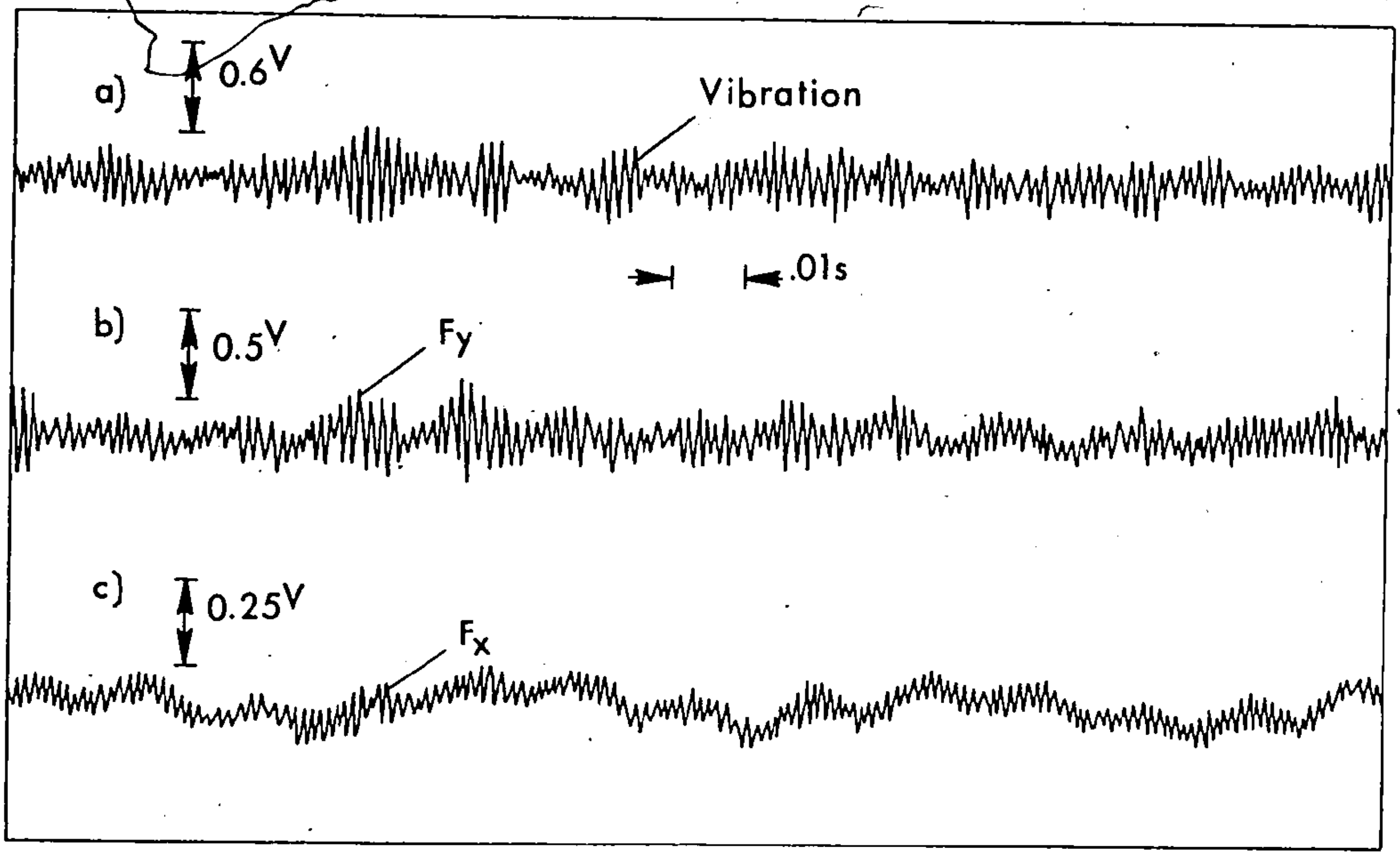

AL. Alloy Work Material, 25.4 mm Dia. - 4 Flute HSS End Mill, V = 94.2 M/min, f_t = 0.076 mm/tooth, Full Immersion, b = 17.8 mm, Down Milling in X - Direction

Cutting Test

FIGURE 6.13

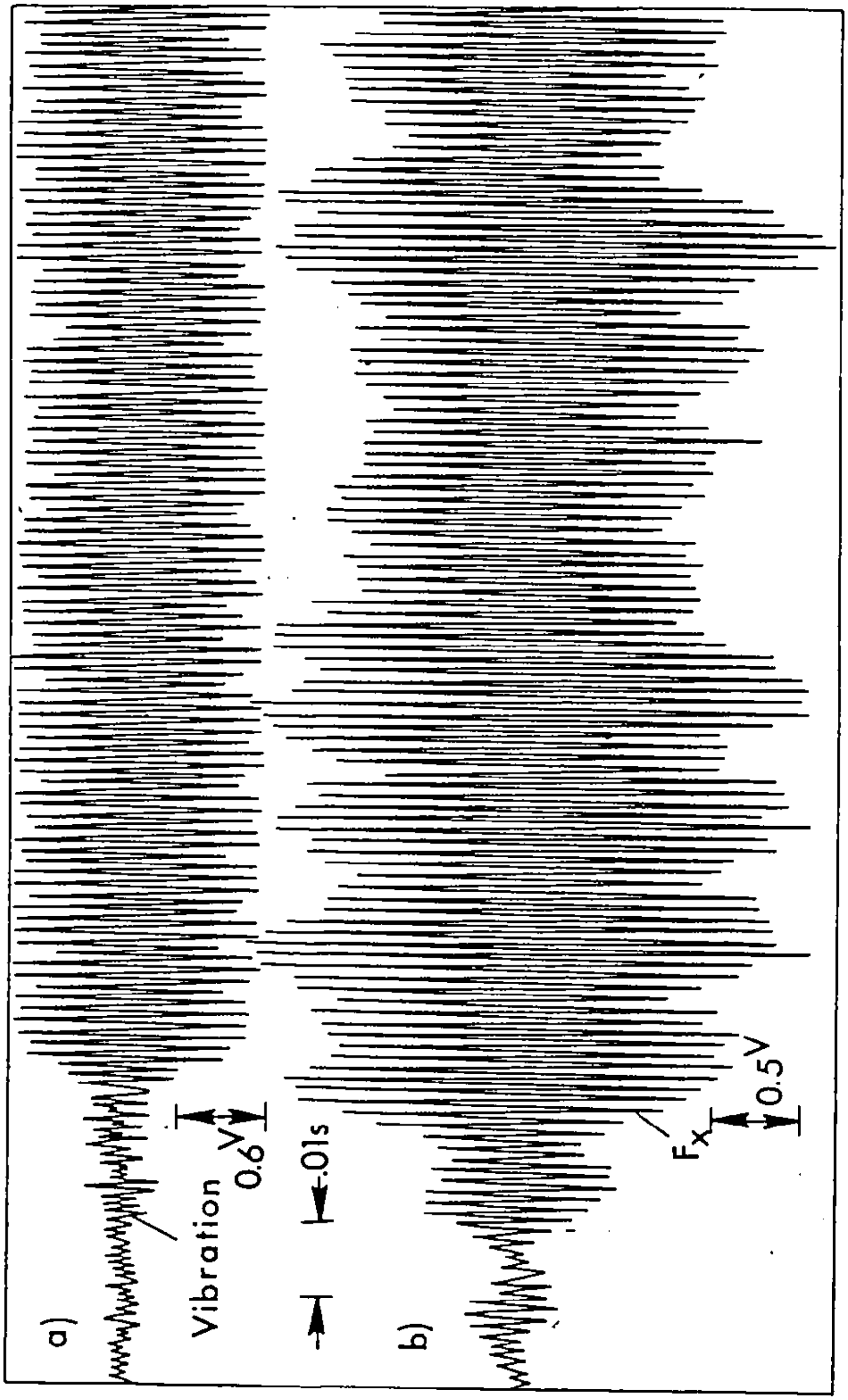

Al. Alloy Work Material, 25.4 mm Dia. - 4 Flute HSS End Mill, V = 94.2 M/min, f_t = 0.076 mm/tooth, Full Immersion, b = 21.6 mm, Down Milling in X - Direction, Tool Length = 38 mm

Cutting Test

FIGURE 6.14

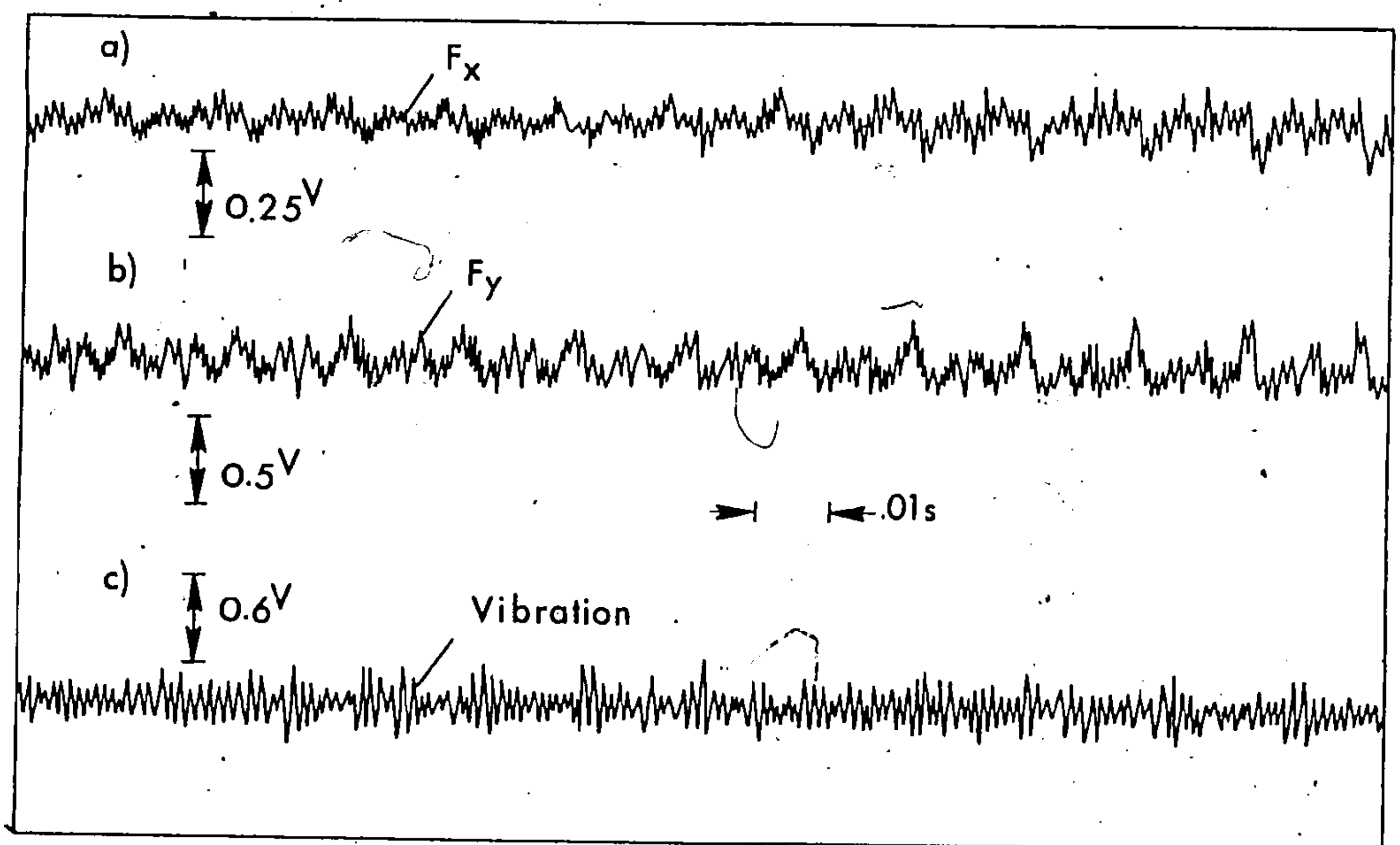

Al. Alloy Work Material, 25.4 mm Dia. - 4 Flute HSS End Mill, V = 94.2 M/min, f_t = 0.076 mm/tooth, Full Immersion, b = 21.6 mm, Down Milling in X - Direction, Tool Length = 101.6 mm

Cutting Test

FIGURE 6.15

that the use of the more flexible tool results in stable machining when compared with the case presented in figure 6.14.

Figure 6.16 shows the case of unstable machining when slotting steel 1020 in X direction at 20.3 mm (0.800 inch) axial depth of cut. The cutting speed used was 47.1 m/min (157 ft/min) and the chatter frequency obtained, as shown in trace a), was 100 Hz. Figure 6.17 shows the case of slotting in Y direction with otherwise the same cutting conditions as in the case presented in figure 6.16. Trace b) in figure 6.17 shows again a prevailing frequency of approximately 100 Hz.

6.2.3 Discussion of the Results of the Cutting Tests

The results of the cutting tests showed that chatter does not occur at the natural frequencies of the flexible tools (e.g. 25.4 mm dia., 38.1 mm long) which are rather high, i.e. above 1000 or even 2000 Hz. It occurs at frequencies around 600 Hz, these belonging to a spindle mode which is usually much stiffer than that of the tool. This is explained by the fact, at the cutting speed corresponding to high speed steel cutters, V = 35 m/min, the chatter mark wave length at 1800 Hz. (Say) would be W = (35 x 1000)/(60 x 1800) = 0.32 mm. With such a short length, the regeneration of waviness is attenuated because the flank of the tool rubs on the slopes of the waves and this gives rise to damping in the cutting process.

The situation is depicted, in a simplified way, in

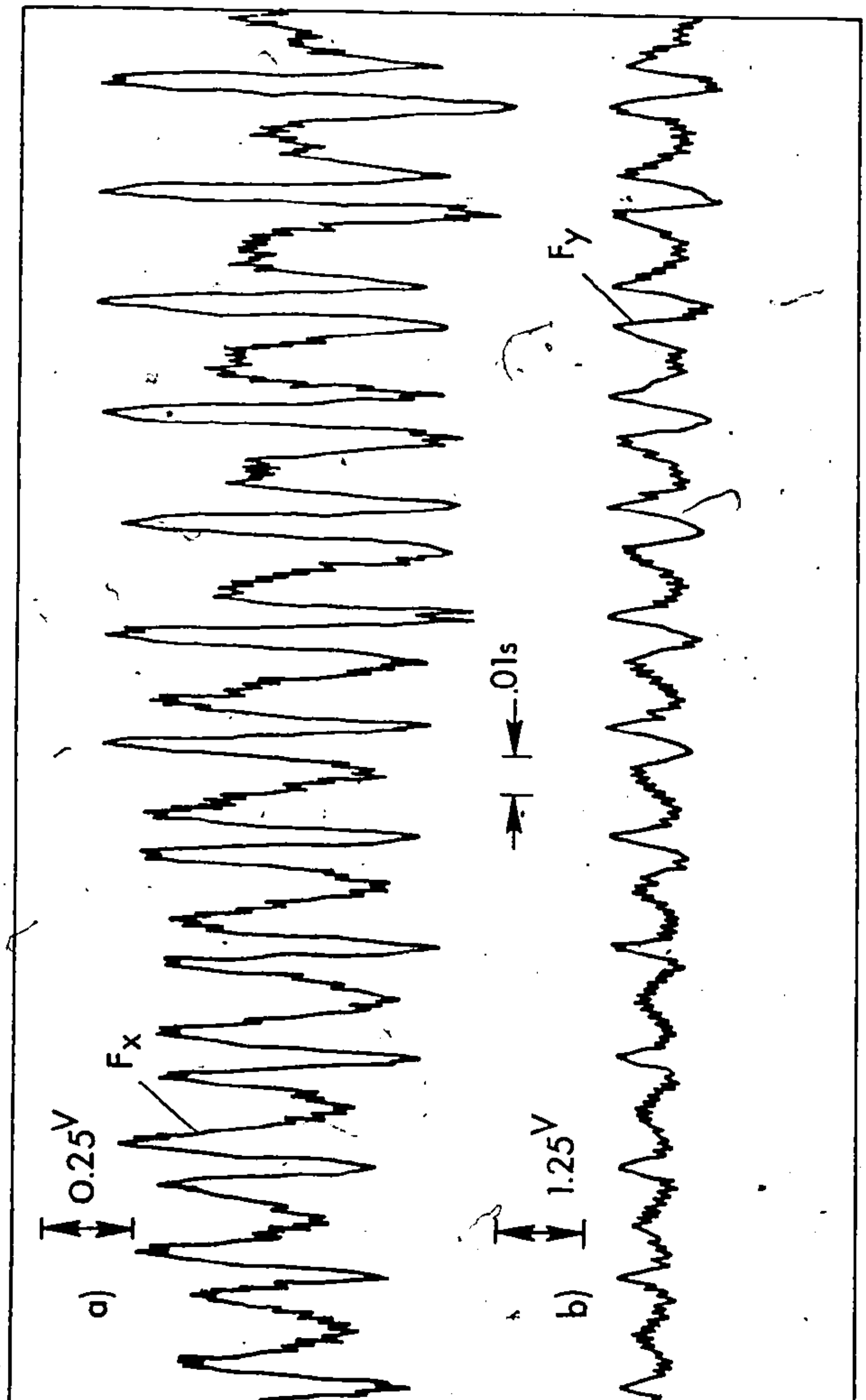

AISI 1020 Work Material, 25.4 mm Dia. - 4 Flute HSS End Mill, V = 47.1 M/min, f_t = 0.076 mm/tooth, Full Immersion, b = 20.3 mm, Milling in X - Direction

Cutting Test

FIGURE 6.16

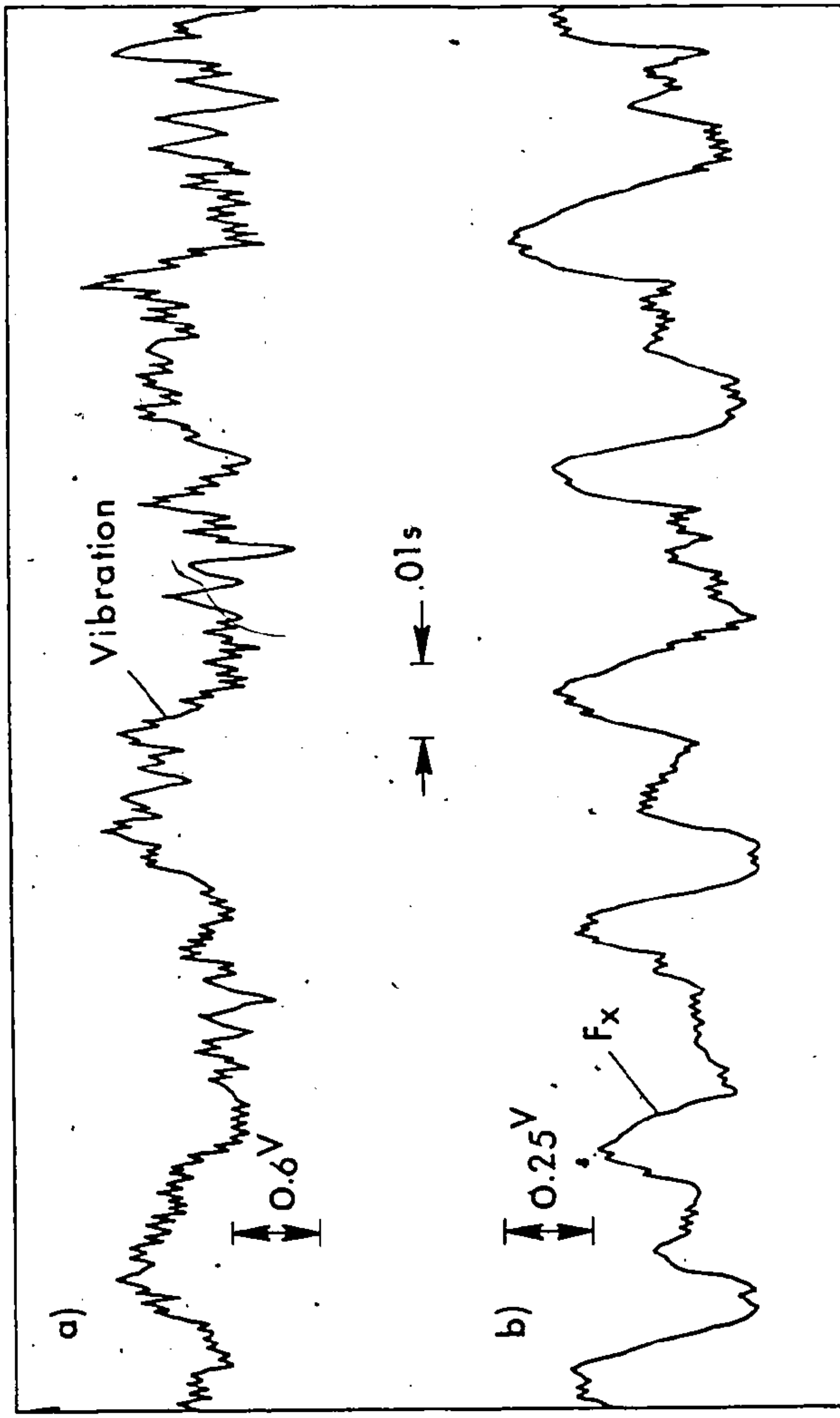

AISI 1020 Work Material, 25.4 mm Dia. - 4 Flute HSS End Mill, V = 47.1 M/min, f_t = 0.076 mm/tooth, Full Immersion, b = 20.3 mm, Milling in Y - Direction

Cutting Test

FIGURE 6.17

figure 6.18. The spindle-tool system exhibits two modes, A and B, as shown in figure 6.18 a). The lower mode, with a natural frequency of 650 Hz. is characterized by the bending of the spindle and displacements in the bearings. The higher mode at, say, 1800 Hz. is mainly due to the vibration of the tool. The real parts of the corresponding transfer functions are given in figure 6.18 b), where the mode A is stiffer than mode B. The resulting transfer function (as indicated by the broken line is in the lower frequency range strongly shifted upwards due to the high static flexibility of mode B. Consequently the minimum M_A, close to 650 Hz. is very "stiff". Even so, and with the minimum M_B, close to 1800 Hz. being much more "flexible", chatter occurs at 650 Hz., however, it is not very energetic.

Referring to figures 6.14 and 6.15, it is seen that chatter is attenuated by the effect of the more flexible tool (101.6 mm overhang). Then, there are phenomena outside of the range of these typical ones. On one side there are more rigid tools: shorter, with larger diameters. With these there is little attenuation of the spindle mode and energetic chatter occurs at "reasonable" depths of cut. On the other side, there are very long and flexible tools which have low natural frequencies. For instance, a tool d = 6.25 mm, l = 75 mm would have f = 550 Hz. and a tool d = 12.5 mm, l = 100 mm would have f = 630 Hz. At these frequencies the damping in the cutting process is low and these tools chatter at very low depths of cut.

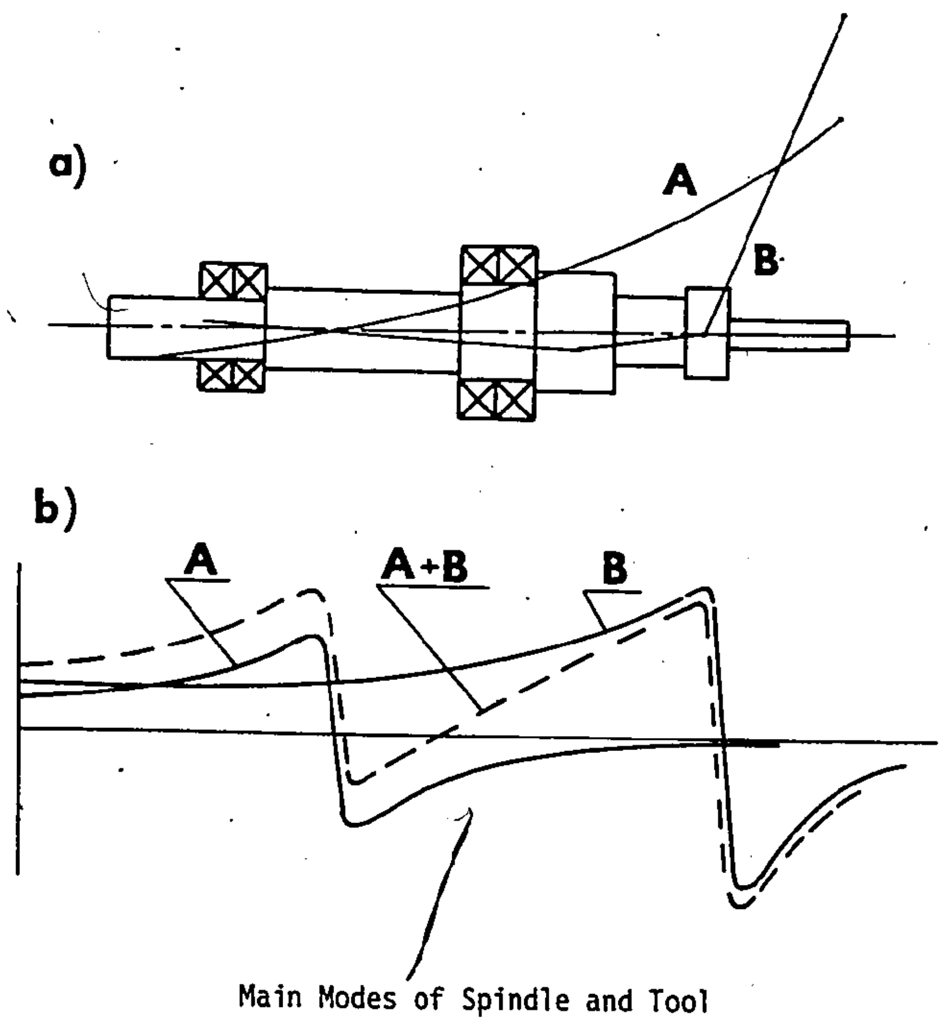

FIGURE 6.18

Also, in the cases where very high cutting speeds are used (e.g. for milling Al.), the wave length increases and chatter occurs due to the regeneration of waviness.

Accordingly, in the middle range of High Speed Steel cutters being considered here for milling steel, such that they are rather flexible but still have natural frequencies over 1000 Hz, that is from d = 6.25 mm, l = 50 mm to d = 18.75 mm, l = 75 mm, to d = 25 mm, l = 75 mm, chatter is not a serious phenomenon, and the flexibility of the cutter actually helps. Outside of this range, chatter becomes a constraint to be included in the A/C strategy. However, more research is needed to develop the data necessary for the definition of this constraint for the various applications.

6.3 Overload of the Cutting Edge

There are two basic forms of edge overload. One is purely mechanical and most often it occurs as the breakage of the tip of a tooth under heavy feed. The other is more of a thermal nature and it results from a high product of speed and feed and it occurs as rapid wear of a softened edge material.

Chipping of the edge and breakage are both phenomena of brittle fracture and differ mainly by their magnitude and they are related to the phenomenon of cracks. Breakage and chipping as brittle fractures develop from macrocracks which result from interlinking of microcracks originating in points where the tensile stress exceeds the tensile strength.

According to Tlusty [83], brittle fracture is associated with tensile stresses. These, in a tool, may be due to two basically different causes:

a) The load by the cutting force

b) The thermal load.

Very little data has been published about the phenomenon of cutter breakage. A paper in this area {66} has been recently published, however, it is not certain whether sufficient data has been generated. The graph given in {66} and reproduced in figure 2.10, gives cutter breakage forces versus axial depth of cut for a certain size of cutter, while it does not distinguish between tooth and shank breakage. In this paper, the authors explained that for HSS end mills, and at low axial depths of cut, because the load is not shared by multiple teeth, tooth breakage occurs. At high axial depths because of the increased bending moment, shank breakage occurs. It would be more practical, however, to separate tooth breakage and relate it to a maximum feed per tooth {84}.

It is therefore, necessary to limit feed rates once the tool is cutting even with a very small depth of cut. While at larger depths of cut, the feed rate is limited by the A/C control reacting to a large force signal, it is necessary to impose a feed rate constraint irrespectively of force (for low depths of cut).

As mentioned previously, the second form of edge overload is more of a thermal nature and it occurs as rapid wear of a softened edge material.

Yellowley [85,86] investigated the effect of thermal cycling on tool life in peripheral milling. He concluded that the range of thermal strain and the number of cycles of plastic strain have considerable influence on the tooth life obtained. Figure 6.19, reproduced from reference [86], shows the relationship between tooth life and range of thermal strain.

Tlusty [87] and Vashishta [88] produced experimental results showing the effect of speed and feed on tool wear in peripheral milling of low carbon steel. Some of these results are shown in figures 6.20 and 6.21, for the case of HSS cutter in interrupted cutting. Figure 6.20 shows the relationship between the maximum width of flank wear VB_{max} versus time and figure 6.21 shows the plot of the average width of flank wear land $VB_{av.}$ versus time. The effect of decreasing the feed on tool wear can easily be seen in these figures.

Accordingly, a feed constraint related to the cutting speed used and to the workpiece material has to be imposed so as to prevent overheating of the edge.

The author feels that considerable experimental and theoretical work is still needed to develop the data necessary for the definition of these constraints for the various applications.

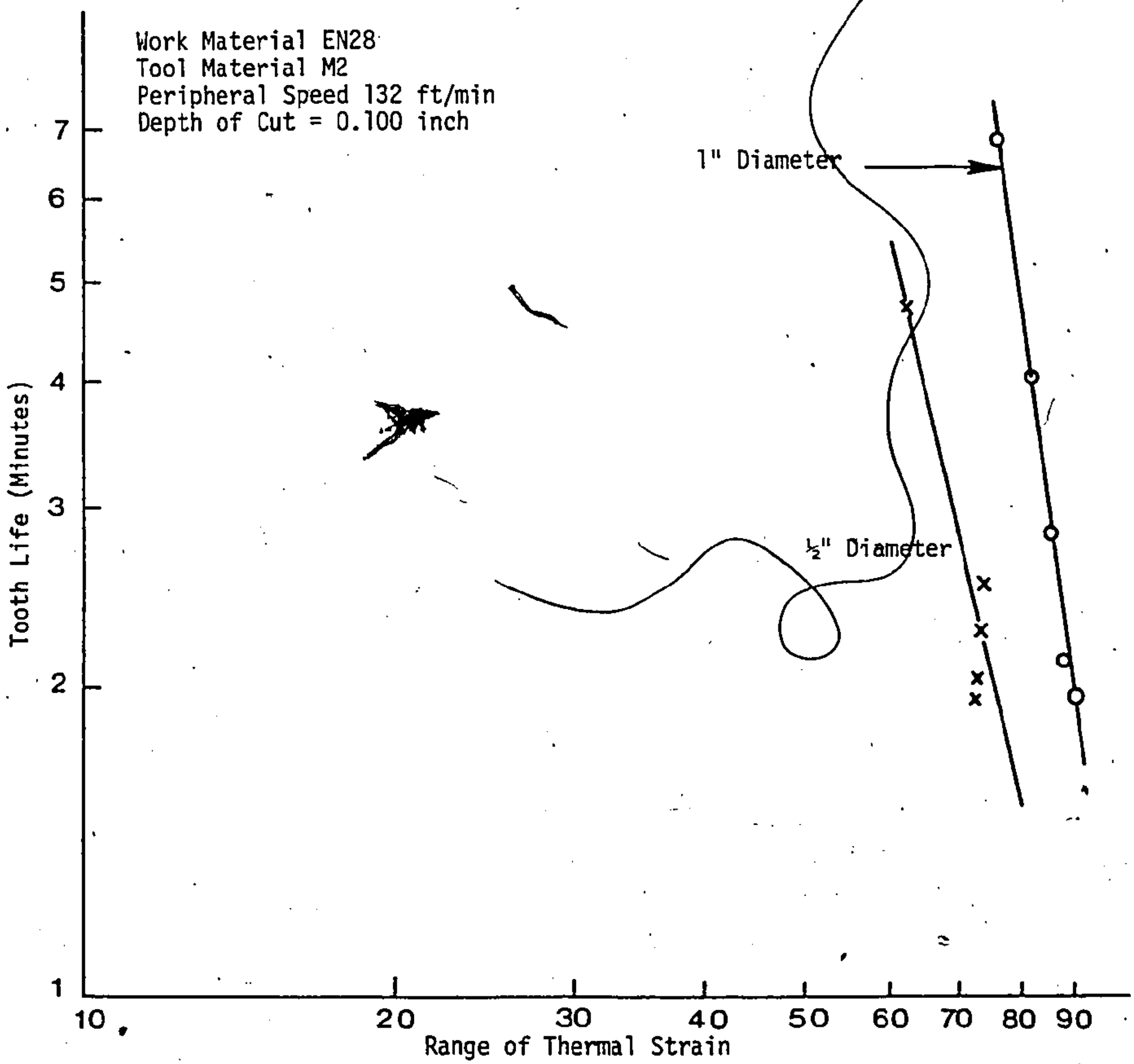

Relationship Between Tooth Life and Range of Thermal Strain[86]

FIGURE 6.19

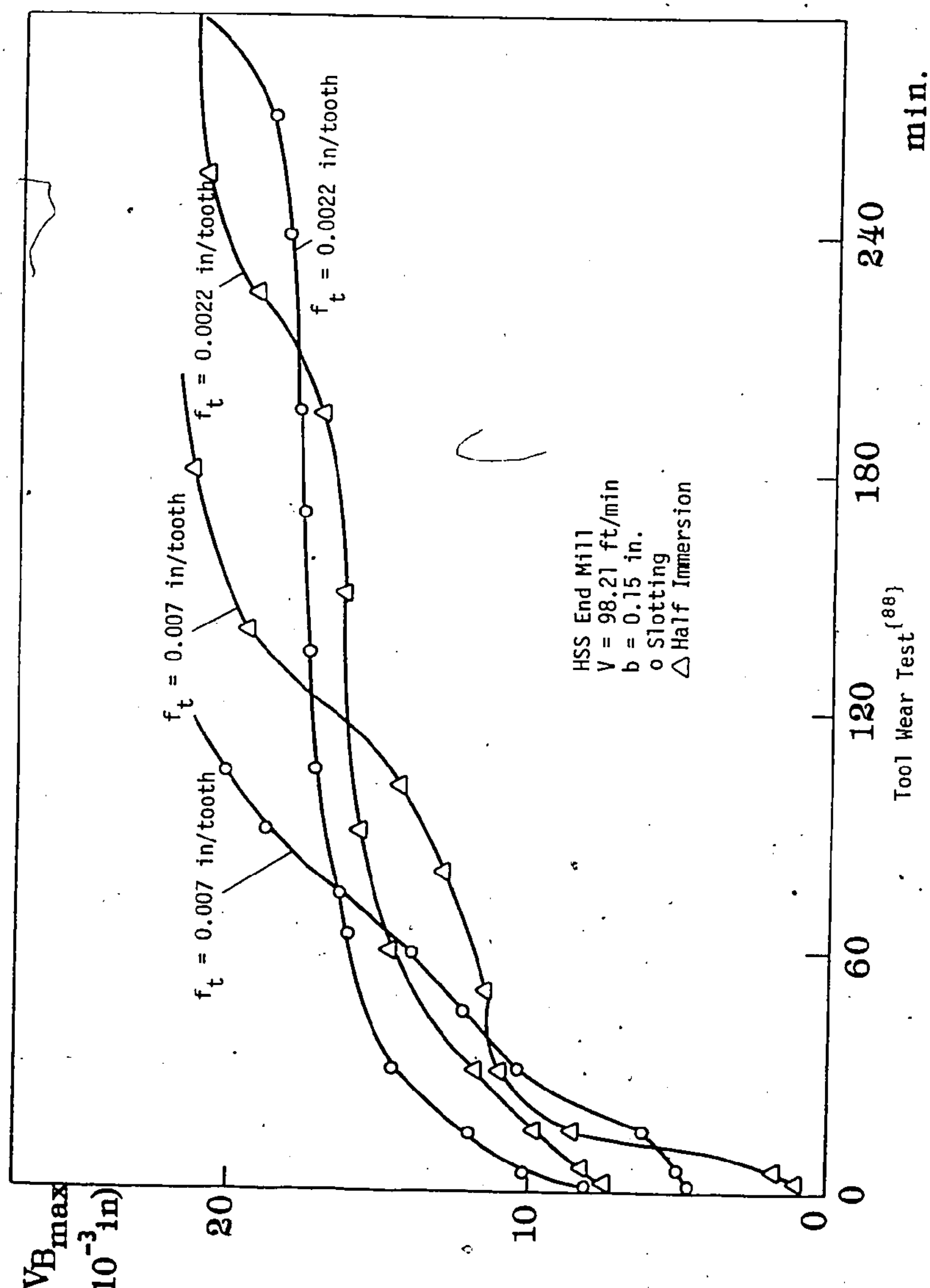

VBmax
(10-3in)
20
10
0
0
60
120
180
240
min.
Tool Wear Test(88)
HSS End Mill
V = 98.21 ft/min
b = 0.15 in.
o Slotting
△ Half Immersion
ft = 0.007 in/tooth
ft = 0.007 in/tooth
ft = 0.0022 in/tooth
ft = 0.0022 in/tooth

FIGURE 6.20

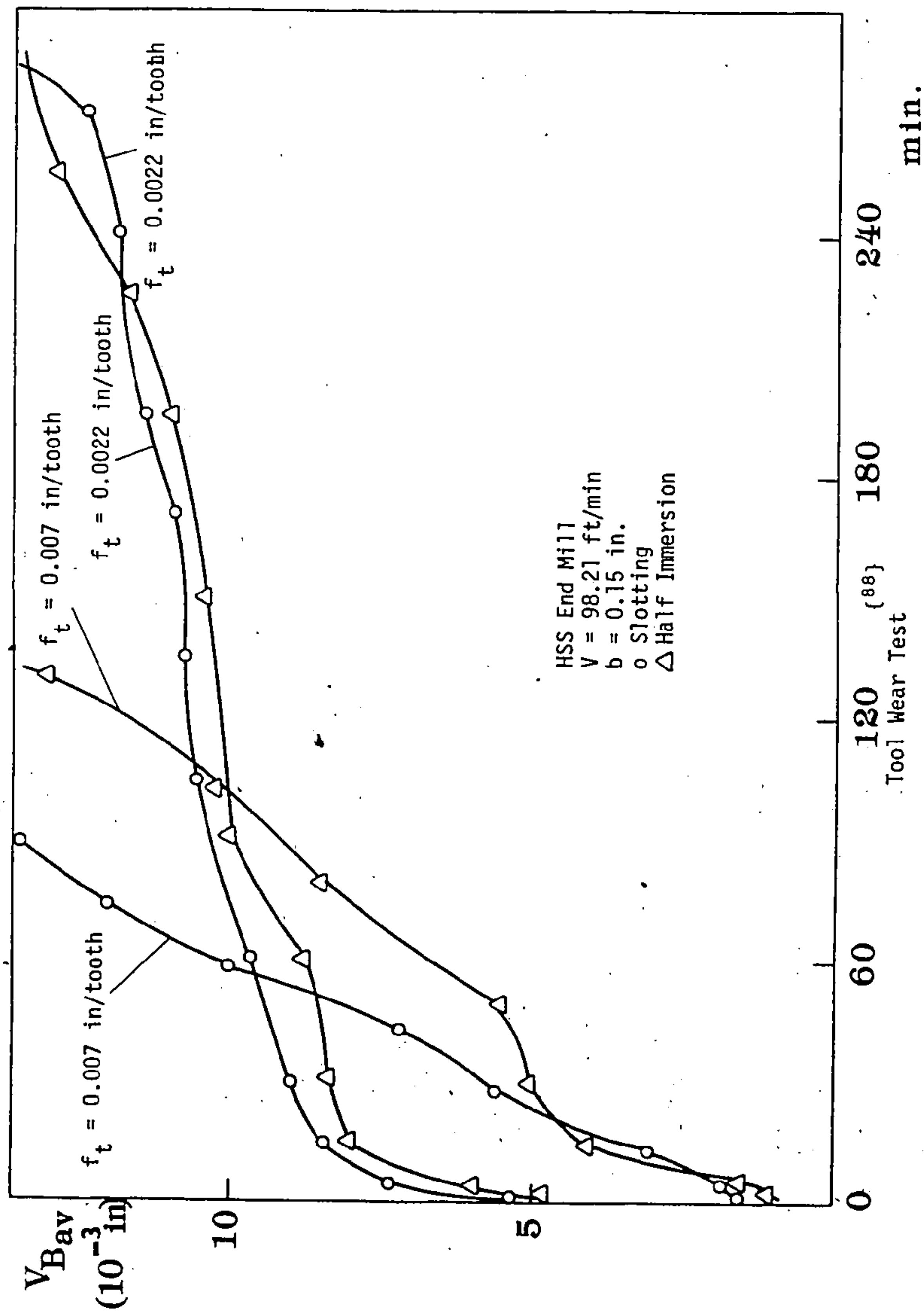
f t = 0.0022 in/tooth
f t = 0.0022 in/tooth
f t = 0.007 in/tooth
f t = 0.007 in/tooth
HSS End Mill
V = 98.21 ft/min
b = 0.15 in.
o Slotting
△ Half Immersion
Tool Wear Test (88)
0
60
120
180
240
min.
V Bav (10 -3 in)
10
5

FIGURE 6.21

CHAPTER 7

SUMMARY AND CONCLUSIONS

In this thesis the operating characteristics of an adaptive control constraint system for end milling with constant force are examined both experimentally and by digital computer simulation. The controlled variable is command feed rate. Special attention is devoted to the behaviour of the system during tool-work impact under rapid traverse conditions.

Two other constraints were considered for the adaptive control system, namely: chatter and overload of the cutting edge.

Accordingly, an experimental investigation of the phenomenon of chatter in end milling was carried out, as well as a review of the basic features of the phenomenon of cutting edge overload.

In this chapter, the main conclusions of this research are presented:

1. Finish end milling with rather flexible cutters may substantially be speeded up by using an adaptive control system where the control criterion is to hold the force acting on the cutter at a value safely below the force which would break the cutter. This criterion is applicable to finish milling of complex shapes, typically of die cavities.

Since adaptive control leads to high feed rates when cutting air, the high impact loads can damage the tool if a controlled impact system is not used.

2. The flexibility of the cutters is beneficial in attenuating the overload in a sudden transient situation and it is also beneficial in attenuating chatter. These benefits are obtained for a certain range of diameters and lengths of cutters. Within this range constraints on feed rate for edge overload must be considered and outside of this range the chatter constraint has to be included.

3. The tool-work deflection which occurs subsequent to collision, limits the rate of increase of the transient cutting forces and thereby allows the A/C system to respond before the forces reach a dangerous level.

4. The high-gain control required to react to tool-work collision can lead to operational instabilities. To take advantage of the maximum response of the NC system without causing instability in the A/C loop calls for a two level A/C strategy. During transient cutting demands such as a step in depth of cut the A/C feedback will therefore, trigger a special action A/C algorithm resulting in a very rapid deceleration, which will be allowed to persist only for a limited time before the A/C system automatically switches to the slow acting or limited acceleration condition. In this work, two A/C strategies were implemented: A/C algorithms "A" and "B".

5. The results of adaptive control experiments conducted using algorithm "B", (see for example figures 42(a) and 42(b),

showed that it is possible to stop the rapid feed rather fast (in about 20 msec) in transient conditions. In these experiments even the first tooth did not produce a force higher than the desired force F_{nom}.

6. The analytical analysis of the behaviour of the A/C system as a servomechanism using both the classical linear control theory and the numerical simulation (state-space technique) indicated that the system can become unstable with high gains in the A/C loop. This gain itself is variable since it is proportional to the radial and axial depth of cut a and b and inversely proportional to the desired force F_{nom}.

The time delay due to the fact that velocity changes are not felt in the interval between cutter teeth (equations 4. and 4.), has a strong effect on stability. With longer τ lower gains in the A/C algorithm have to be used. The use of a rate feedback, equation 4.18, has the effect of damping and it stabilizes the loop.

7. In the A/C experiments reported in this thesis, it was found that the variable gain in the system was not a very serious aspect because, in fact, it means that when running into heavier loads and using smaller cutters (lower F_{nom}) the response is faster than when relieving into lesser cuts.

However, further work need not be limited to the particular A/C algorithms discussed in Chapter Five. An arrangement is possible in which by using both the force signal and the tachogenerator signal, the gain may be kept almost constant. Accordingly, rather than commanding an acceleration or deceleration for instance, the commanded feed rate may be based directly upon the actual feed rate by using the output of the tacho-generator as an input to the computer.

8. Chatter in end milling has a rather special character. Based on the results of an experimental investigation limited to cutters with high flexibility and made from high speed steel (this means that cutting speed is about 40 m/min), the main features may be summarized as follows:

a) Typically, the more flexible mode of the tool does not generate chatter because it has a high natural frequency for which the damping in the cutting process is very high.

b) Chatter arises at the lower frequency of the spindle mode, however it is attenuated by the effect of the flexible tool.

c) The middle range of High Speed Steel cutters being considered here for milling steel, such that they are rather flexible, but have natural frequencies over 1000 Hz, that is from d = 6.25 mm, l = 50 mm to d = 18.75 mm, l = 75 mm to d = 25 mm, l = 75 mm, chatter is not a serious phenomenon, and the flexibility of the cutter actually helps. Outside of this range chatter becomes a constraint to be included in the A/C strategy.

9. It is necessary to limit feed rate once the tool is cutting even with a very small depth of cut. While at larger depths of cut the feed rate is limited by the A/C control

reacting to a large force signal, it is necessary to impose a feed rate constraint irrespectively of force (for low depths of cut) in order to prevent tooth breakage.

Similarly a feed constraint related to the cutting speed used and to the workpiece material has to be imposed so as to prevent overheating of the edge.

REFERENCES

1. American Standard Terminology for Automatic Control - A.S.A., C85.1 - 1963.
2. Zakaria, A. A., and Y. I. Elgomayel, "Tool Condition Monitoring for Adaptive Control", paper SME MR 74-143, 1974.
3. Weck, M., Verhaag, E., and M. Gather, "Adaptive Control for Face-Milling Operations with Strategies for Avoiding Chatter Vibrations and for Automatic Cut Distribution", Annals of the CIRP, Vol. 24/1, 1975, pp. 405 - 409.
4. Weck, M., and W. Mueller, "Chatter Vibration Sensors for Adaptive Control Systems for Turning and Milling Operations", Proceedings Fourth NAMRC, 1976, pp. 398 - 407.
5. Micheletti, G. F., Koenig, W., and H. R. Victor, "In Process Tool Wear Sensors for Cutting Operations", Key-Note paper C, Annals of the CIRP, 1976.
6. Frost-Smith, E. H., et al., "Optimization of the Machining Process and Overall System Concepts", Proc. MTIRA Conference on Adaptive Control of Machine Tools, April, 1970.
7. Wilkinson, A.J., "Constriction - Resistance Concept Applied to Wear Measurement of Metal Cutting Tools", Proc. I.E.E., Vol. 118, No. 2, 1971.
8. Opitz, H., Hake, O., "Wear Analysis of Hand Metal Cutting Turning Tool by Means of Radioisotopes", Microtecnic, Vol. 10, No. 1, 1956.

9. Merchant, M. E., et al., "Radioactive Cutting Tools for Rapid Tool Life Testing", Trans. ASME 75, 549, 1953.

10. Sata, T., "Rapid Tool Life Tests by Means of Irradiated Carbide Cutting Tools", J. of the Japan Soc. of Prec. Eng., 24, 453, 1958.

11. Autorenkollektiv, "Adaptive Control Systeme bei Spanenden und Abtragenden Bearbeitungsverfahren", Industrie - Anzeiger 96, 74, 1696 - 1710, 1974.

12. Micheletti, G. F., "Relationship Between Cutting Forces and Tool Wear in Steel Turning", 7th Int. MTDR Conf., Birmingham, Sept. 1966.

13. Micheletti, G. F., DeFillippi, A., and R. Ippolito, "Tool Wear and Cutting Forces in Steel Turning", CIRP Int. Conf. Manuf. Tech., Ann Arbor, 1967.

14. Hansel, W., "Technologische Aspekte Zum Einsatz von Adaptive Control - Einrichtungen beim Drchen", VDI-Z 117, 10, 462 - 67, 1975.

15. Yamazaki, K., et al., "A Study on Adaptive Control in AC Milling Machine", Annals of CIRP, Vol. 23/1, 1974.

16. Pilafidis, E. J., "Adaptive Control Systems and the Manufacturing Process", Cincinnati Milacron Report, May 1970.

17. Zlatin, N., Garrison, R. C., and Tipnis, V. A. - "An Instrumented Milling Machine for Developing Machining Data Required for Adaptive Control", Proc. of 3rd NAMRC, pp. 322 - 333, 1975.

18. Fraudin, C., and J. Lombard, "Magnetic Transducers for Measurement of Forces and Torques", Annals of CIRP, Vol. 23/1, 1974.

19. Weller, E. J., et al., "What Sound Can Be Expected from A Worn Tool?", Trans. ASME, Vol. 91, No. 3, pp. 525 - 534, 1969.

20. Kronenberg, M., "Machining Science and Applications", Pergamon Press, pp. 306 - 314, 1966.

21. Martin, P., et al., "Influence of Lathe Tool Wear on the Vibrations Sustained in Cutting", Proc. of the 15th MTDR Conference, pp. 251 - 257, 1974.

22. Thomson, R., "Surface Grinding Vibrations and Their Use in Grinder Performance Evaluation", SME paper No. MR 71 - 274, 1971.

23. Weller, E. J., Welchbrodt, B., "Listen To Your Tools - They Are Talking To You", ASTME Tech. Paper No. MR 67 - 444, 1967.

24. Olsen, K. V., "Surface Roughness of Turned Steel Components and the Relevant Mathematical Analysis", the Prod. Eng. 47, No. 12, 593, 1968.

25. Spurgeon, D., and R. Slater, "In Process Indication of Surface Roughness Using a Fibre Optics Transducer", Proc. of the 15th MTDR Conf., pp. 339, 1974.

26. Murray, H., "Exploratory Investigation of Laser Methods for Grinding Research", Annals of CIRP, Vol. 22/1, 1973.

27. Sade, T., et al., "In Process Measurements for AC of

Machines", JSPE Vol. 38, No. 10, pp. 788 - 795, 1972.

28. Veno, S., "In Process Measurement in Europe and U.S.", JSPE, No. 10, pp. 803 - 807, 1972.

29. Takeyama, H., et al., "Sensors of Tool Life for Optimization of Machining", Journal of Mech. Lab. of Japan, Vol. 14, No. 2, 1968.

30. Spur, G., Leonards, F., "Sensoren zur Erfassung von Prozesskenngrössen bei der Drehbearbeitung", Annals of CIRP, Vol. 24/1, 1975.

31. Shillman, N. F., "The On-Line Control of Cutting Conditions Using Direct Feedback", Proc. 12th Int. MTDR Conf., 1971.

32. Solaja, V., Vukelja, D., "Identification of Tool Wear Rate by Temperature Variation of a Carbine Tip", Annals of the CIRP, Vol. 22/1, 1973.

33. Boothroyd, G., Eagle, J. M., Chisholm, A. W. J., "Effect of Flank Wear On the Temperature Generated During Metal Cutting", Proc. of the 8th MTDR Conf., 1967.

34. Beadle, B. R., Bollinger, J. C., "Computer Adaptive Control of Machine Tool", Annals of the CIRP, Vol. 19, pp. 61 - 65, 1971.

35. Centner, R. M., and J. M. Idelsohn, "Adaptive Controller for a Metal Cutting Process", Proc. Joint Autom. Control Conf., Minneapolis, Minn., June 1963.

36. Centner, R. M., and J. M. Idelsohn, "Application of Adaptive Control to Manufacturing Processes", IFAC Proceedings, Paper No. 27.C, 1966.

37. Mathias, R. A., "Adaptive Control of the Milling Process", IEEE National Machine Tool Industry Conference, Paper No. 34CP67 - 716, Cleveland, 1967.

38. Marley, T. C., "Adaptive Control of Machine Tools", ASTME Paper No. MS68 - 812, 1968.

39. Porter, B., and Summers, R. D., "The Performance of Self-Optimalizing Strategies in the Adaptive Control of the Metal Cutting Process", International Journal of Machine Tool Design and Research, Vol. 8, 1968, pp. 217 - 237.

40. Takeyama, H., et al., "One Approach for Optimizing Control in Metal Cutting", Annals of the CIRP, Vol. 18, pp. 345 - 351, 1970.

41. Frost-Smith, E. H., "Optimization of the Machining Process and Overall System Concepts", Annals of the CIRP, Vol. 19, pp. 385 - 394, 1971.

42. Bedini, R., Lisini, G. G., and P. C. Pinott, "Adaptive Control in Milling", CIRP Third International Seminar on Optimization of Manufacturing Systems", Pisa, Italy, June 1971.

43. Bedini, R., and P. C. Pinotti, "A Hardwired Logic for the Adaptive Control of a Milling Machine", Int. J. Mach. Tool Des. Res., Vol. 16, pp. 193 - 207, 1976.

44. Bedini, R., Lisini, G. G., and P. C. Pinotti, "Experiments on Adaptive Control of a Milling Machine", Trans. of the ASME, Journal of Engineering for Industry, Paper No. 75 - WA/Prod. 18, 1975.

45. Selim, I. H., and A. Moisan, "Identification, Strategy and Simulation for the Adaptive Control of Machine-Tools", Annals of the CIRP, Vol. 23/1, 1974.

46. Fujita, A. N., et al., "Adaptive Control of Machine Tools Using Minicomputer", Annals of the CIRP, Vol. 23/18, 1974.

47. Peklenik, J., "Geometrical Adaptive Control of Manufacturing Systems", Annals of the CIRP, Vol. 18, pp. 265 - 272, 1970.

48. Jona, M. G., "Contribution to the Development of Geometrical Adaptive Control in Turning", Paper presented at the 11th International M.T.D.R. Conference, University of Manchester, 14th - 18th September, 1970.

49. Spur, G., and Pritschow, G., "Adaptive Control System for NC - Turning Machines, "III CIRP Seminar on Manufacturing Systems, Paper No. CPA-08, Pisa, 1971.

50. Kline, E. R., "Understanding Adaptive Control Systems for the Metal Working Industry", Paper presented at the ASTME ON CAMPUS ENGINEERING CONFERENCE, SP-114, Los Angeles Pierce College, Woodland Hills, California, 1968.

51. Kline, E. R., "End Milling Experience with Adaptive Control", ASTME Paper No. MR69-208, 1969.

52. Mathias, R. A., "Adaptive Controlled Profile Milling", SME paper No. MS 70-563, 1970.

53. Ledergerber, A., "Adaptive Control for Turning Operations", paper presented at the 12th International MTDR Conference,

University of Manchester, 1971.

54. Lankford, L. G., "Experimental Adaptive Machine Tool Control System", Proceedings of the 9th Annual Meeting & Technical Conference - Numerical Control Society, April 1972, Chicago, Illinois.

55. Milner, D. A., "Adaptive Control of Feedrate in the Milling Process", Int. J. Mach. Tool Des. Res., Vol. 14, pp. 187 - 197, 1974.

56. Milner, A. A., "Controller System Design for Feedrate Control by Deflection Sensing of a Machining Process", Int. J. Mach. Tool Des. Res., Vol. 15, pp. 19 - 30, 1975.

57. Tlusty, J., Koren, Y., and P. MacNeil, "Numerical and Adaptive Control for Die Sinking", Proceedings of the International Conference of Production Engineering, Tokyo, Japan Society of Precision Engineering, 1974.

58. Stute, G., and F. R. Goetz, "Adaptive Control System for Variable Gain in ACC Systems", 16th International MTDR Conference, 1976.

59. Tlusty, J., and P. MacNeil, "Dynamics of Cutting Forces in End Milling", Annals of the CIRP, Vol. 24/1, 1975.

60. Gieseke, E., "Adaptive Control Constraint and Automatic Cut Distribution System for Turning Operations", 14th International MTDR Conference, University of Manchester, 1974.

61. Weck, M., K. Shäfer, "Direct Digital Control for Turning Operations", 16th International MTDR Conference, 1976.

62. Brecker, J. N., Shum, L. Y., "Tool Collision and Machine Considerations in Adaptive Control Systems" Annals of the CIRP, Vol. 25/1, 1976.

63. Mathias, R., "An Adaptive Controlled Milling Machine", SME paper no. MS 76-260, 1976.

64. Donahue, E. J., "Applications of Adaptive Control in the Aerospace Industry", SME paper no. MS 76-274, 1976.

65. Mathias, R., "A Micro-Processor Approach to Adaptive Control Eliminates Most Tape Preparation Costs", SME Paper No. MS 75 - 724, 1975.

66. Tipnis, V. A., et al., "Mathematically Modelled Machining Data for Adaptive Control of End Milling Operations", Proceedings NAMRC - IV, pp. 279 - 286, 1976.

67. MacNeil, P. R., "Computer Adaptive Control in Milling", M.Eng. thesis, McMaster University, Hamilton, Canada, April 1975.

68. Koren, Y., Tlusty, J., "CNC/AC System for a Milling Machine - Part I", Metal Working Research Group Report No. 43, Mechanical Engineering Department, McMaster University, Hamilton, Canada, March 1974.

69. MacNeil, P., Koren, Y., and J. Tlusty, "CNC/AC System for a Milling Machine - Part II", Metal Working Research Group Report No. 45, Mechanical Engineering Department, McMaster University, Hamilton, Canada, June 1974.

70. Elbestawi, M. A., "Analysis of a Numerical and Adaptive Control Servomechanism", M.Eng. thesis, Department of

Mechanical Engineering, McMaster University, Hamilton, Canada, April 1976.

71. Tlusty, J., Elbestawi, M. A., "Analysis of Transients in an Adaptive Control Servomechanism for Milling with Constant Force", Journal of Engineering for Industry, Trans. ASME, Vol. 99, No. 3, August 1977.

72. Koenisberger, F., and Tlusty, J., "Machine Tool Structures", Pergamon Press, 1970.

73. Tlusty, J., Cowley, A., Elbestawi, M., "A Study of an Adaptive Control System for Milling with Force Constraint", Proceedings of the Sixth NAMRC, April, 1978.

74. Tlusty, J., Elbestawi, M., "Constraints in Adaptive Control with Flexible End Mills", CIRP Annals Vol. 28/1, 1979.

75. Kals, H., "Dynamic Stability in Cutting", Ph.D thesis, Technische Hogeschool te Eindhoven, The Netherlands, 1972.

76. Moriwaki, T., "Fundamental Study of Cutting Process Dynamics and Machining Chatter Control", Ph.D thesis, Kyoto University, Japan, 1973.

77. Tlusty, J., "Analysis of the State of Research in Cutting Dynamics", CIRP Annals 1978, Vol. 2, pp. 583 - 590.

78. Tlusty, J., Polacek, M., "The Stability of the Machine Tool Against Self-Excited Vibration in Machining", ASME Prod. Eng. Res. Conf., Pittsburgh, 1963.

79. Rao, S. B., "Analysis of the Dynamic Cutting Force

Coefficient", M.Eng. thesis, McMaster University, Hamilton, Canada, May 1977.

80. Boothroyd, G., "Fundamentals of Metal Machining and Machine Tools", McGraw-Hill, 1975.

81. Slavicek, J., "The Effect of Irregular Cutter Tooth Pitch on Stability of Milling", 6th MTDR Conf., Manchester, 1965, Pergamon Press.

82. Vanherck, P., "Increasing Milling Machine Productivity by the Use of Cutters with Non-Constant Cutting Edge Pitch", 8th MTDR Conf., Manchester, 1967, Pergamon Press.

83. Tlusty, J., "Breakage of Cutting Tools", The Society of Carbide Engineers, 7th Carbide Cutting and Forming Seminar, June 1975, McMaster University, Hamilton, Ontario, Canada.

84. Yellowley, I., et al., "The Economics of Peripheral Milling", Proc. Sixth NAMRC, April 1978, pp. 388 - 394.

85. Yellowley, I., "The Development of Machinability Testing Methods, With Specific Reference to High Strength Thermal Resistant Work Materials", Ph.D. thesis, Victoria Univ. of Manchester, 1974, Manchester, U.K.

86. Yellowley, I., and G. Barrow, "The Influence of Thermal Cycling on Tool Life in Peripheral Milling", Int. J. Mach. Tool Des. Res., Vol. 16, pp. 1 - 12, 1976.

87. Tlusty, J., Yellowley, I., and G. Konrad, "Tool Wear in the Peripheral Milling of a Low Carbon Steel", ASME Paper No. 76 - WA/Prod - 35.

88. Vashishta, S. K., "Tool Wear in End Milling Slots", M.Eng. thesis, McMaster Univ., Feb. 1974, Hamilton, Ontario, Canada.

89. Raven, Francis H., "Automatic Control Engineering", McGraw-Hill Book Company 1968.

90. Shinners, Stanley M., "Modern Control Theory and Application", Addison Wesley 1972.

91. Davies, W. D. T., "System Identification for Self Adaptive Control", Wiley-Interscience 1970.

APPENDIX I

THE A/C ROTARY DYNAMOMETER

APPENDIX I

THE A/C ROTARY DYNAMOMETER

The Adaptive Control Rotary Dynamometer is basically an instrumented tool holder which is bolted directly to the spindle of the milling machine. The milling cutter is place in a collet which is then drawn into the dynamometer, thereby securing the cutter. The structure of the A/C dynamometer is shown in figure I-1.

The design of this dynamometer was discussed in details in reference {67}. Structurally, the dynamometer consists of two planes; the upper plane A contains a flexure plate which is radially rigid so as to withstand radial cutting forces, yet flexible in torsion about the cutter axis and in angular tilt in a plane perpendicular to this axis. The radial stiffness is obtained by four relatively thick spokes which are the only connection between the inner bolt circle (connected to the tool holder) and the outer bolt circle (attached to the spindle). While the spokes are thick in a direction parallel to the cutter axis, they are quite thin at their extremities in the plane of the flexure plate; this is responsible for the torsional flexibility of the flexure plate. The angular flexibility is achieved by two slots parallel to plane A which are visible in figure I-1. They create a simple universal joint between plane A and the cutter axis. The flexure plate was machined from A-2 tool steel and subsequently hardened.

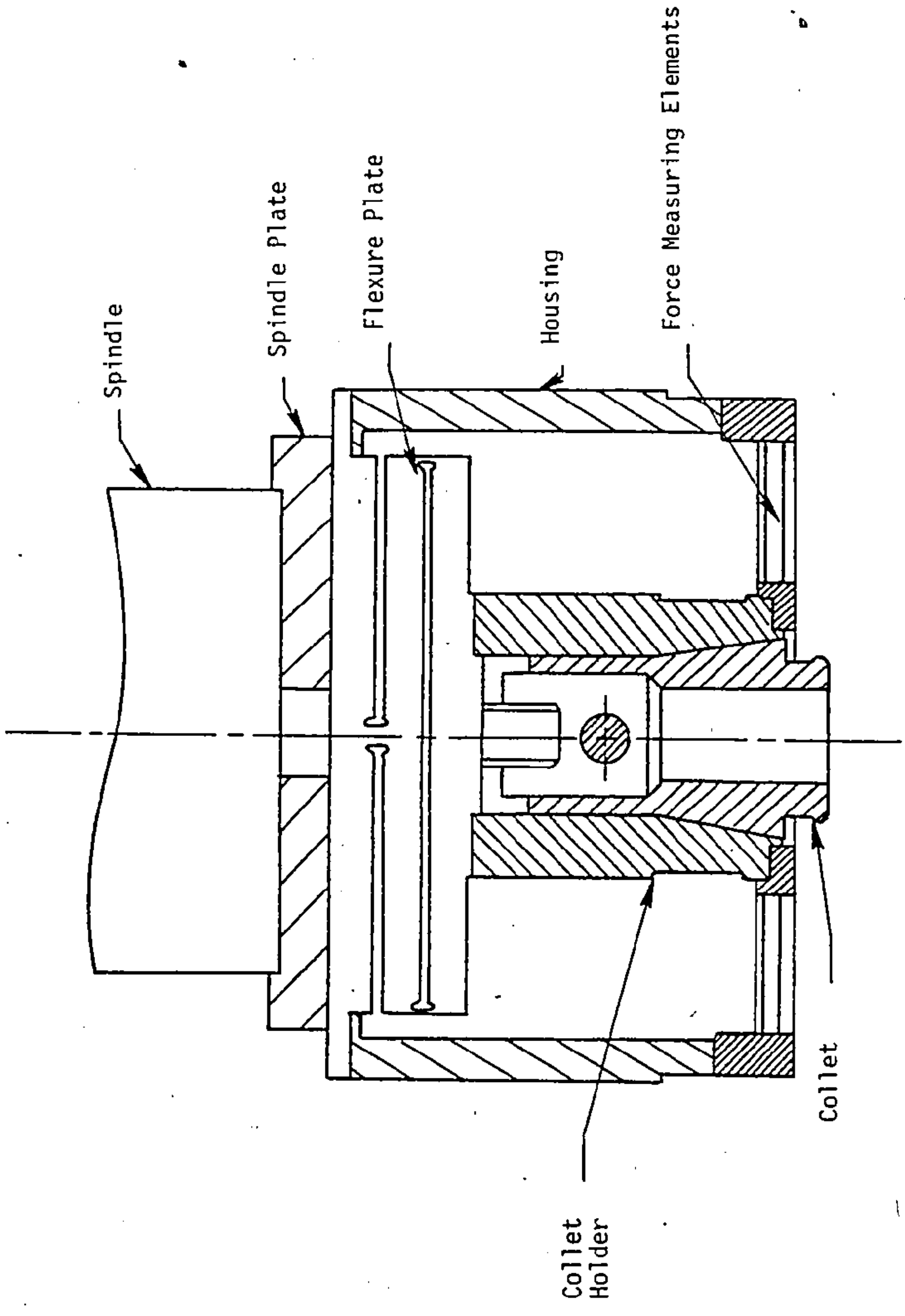

Cut-Away View of A/C Dynamometer

FIGURE I-1

The tool holder was also manufactured from hardened A-2 tool steel. The housing, made of aluminum, connects the outer rim of the flexure plate with outer rim of the baseplate in plane B. It also serves as a protective cover over the strain gauges within.

The measurement of force occurs in plane B. The tool holder is bolted to the inner ring of the base plate. The tool is therefore, connected to the spindle only through the spokes of the flexure plate and the spokes of the baseplate which have been instrumented with sixteen strain gauges. The strain gauges used were MICRO-MEASUREMENTS Ltd. type EA-13-250BG-120. The bond used was M-Bond AE-10. The base phase was milled from 7075-T6 aluminum. The base plate, consisting of four spokes joining the inner and outer bolt circles, has been designed to withstand radial cutting forces of 5000 lb. and torques of 400 in-lb.

The base plate houses two separate strain gauge bridges for force measurement containing eight gauges each. The two force bridges measure forces F_X and F_Y in two perpendicular directions in plane B. Gauges on opposite sides of a spoke were placed in opposite ends of the force bridge so as to minimize the effect of torque in the bridge.

Voltage is supplied to the bridges by a 10 volt D.C. power supply located in the Analog to Digital Processor. The strain gauges in the dynamometer were connected to a series of eight slip rings mounted on a nylon shaft supported by two ball bearings, at the top of the spindle. To minimize contact resistance and improve the signal to noise ratio, silver slip rings were chosen to mate with silver-graphite brushes (two brushes per ring). Connection between the slip ring shaft and the spindle was affected by a below S coupling so as to tolerate some shaft misalignment.

Figure I-2 shows the circuit diagram of the potentiometers located in the ADP for balancing the two bridges and for adjusting the gain used in amplifying the force signal.

The dynamic characteristics of the dynamometer were analyzed using the method of shock excitation with a Fourier Analyzer.

Figure I-3 shows a plot of the real part of the receptance (in the frequency domain) generated by hitting the end of a simulated tool (a 16 mm diameter steel bar was placed in the collet with an overhang of 76 mm to simulate an end mill) with a force transducer and measuring the vibration at that point with a capacitive probe. The figure indicates resonant frequencies of 480 Hz. (without dynamometer) and 340 Hz. (with dynamometer).

The sensitivity of the dynamometer is indicated by the calibration curves included in figures I-4 and I-5. The figures show the relation between the applied force and the digitized computer input for each channel. The slope of the curves may be increased by increasing the amplifier gain. The 10-bit A/D converters operate on $\pm$ 10 volts, and thus, their output range

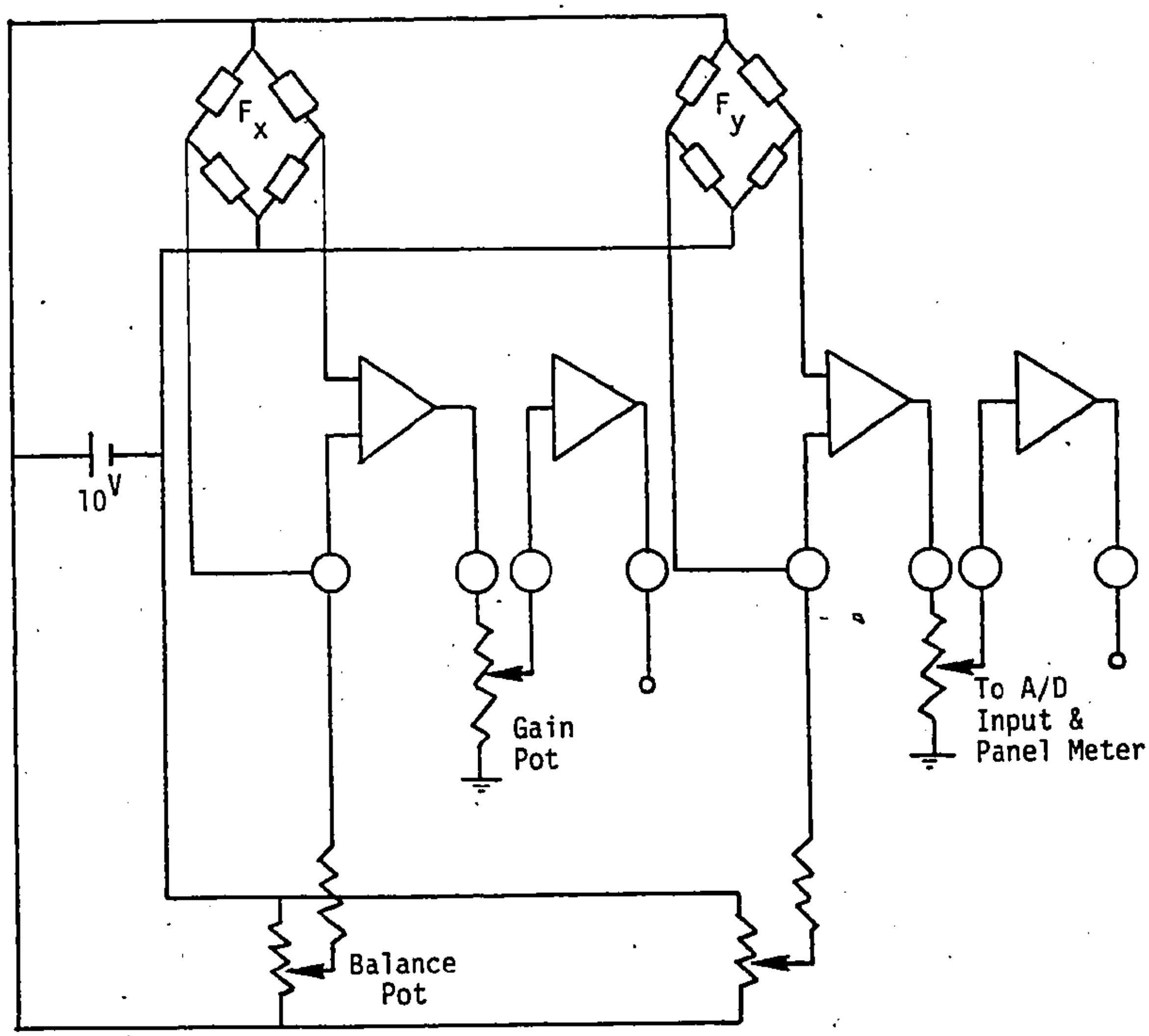

Bridges and Amplification in ADP

FIGURE I-2

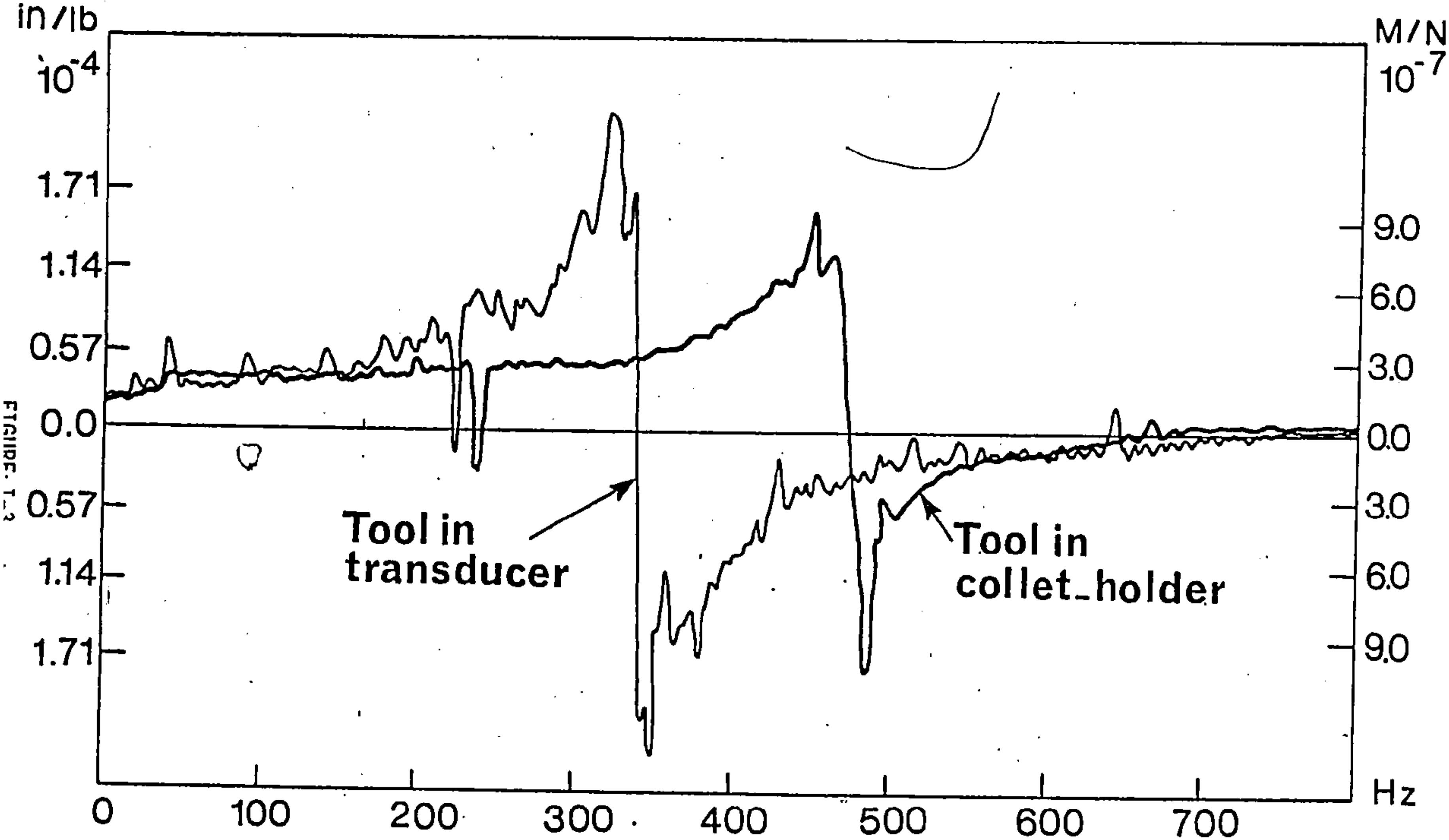

Real Receptance

FIGURE I-3

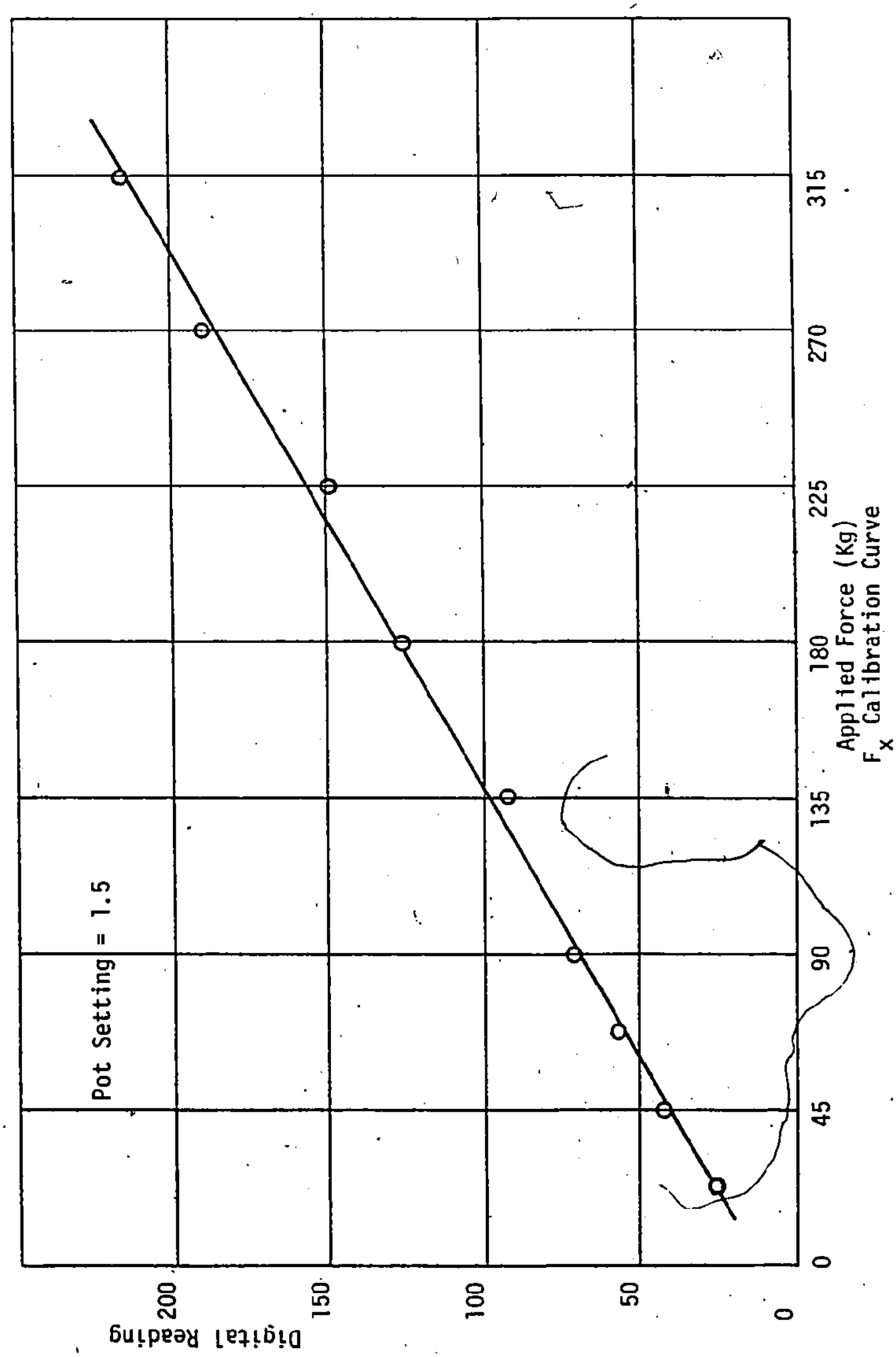

Pot Setting = 1.5
0
45
90
135
180
225
270
315
Applied Force (Kg)
F_x Calibration Curve
0
50
100
150
200
Digital Reading

FIGURE I-4

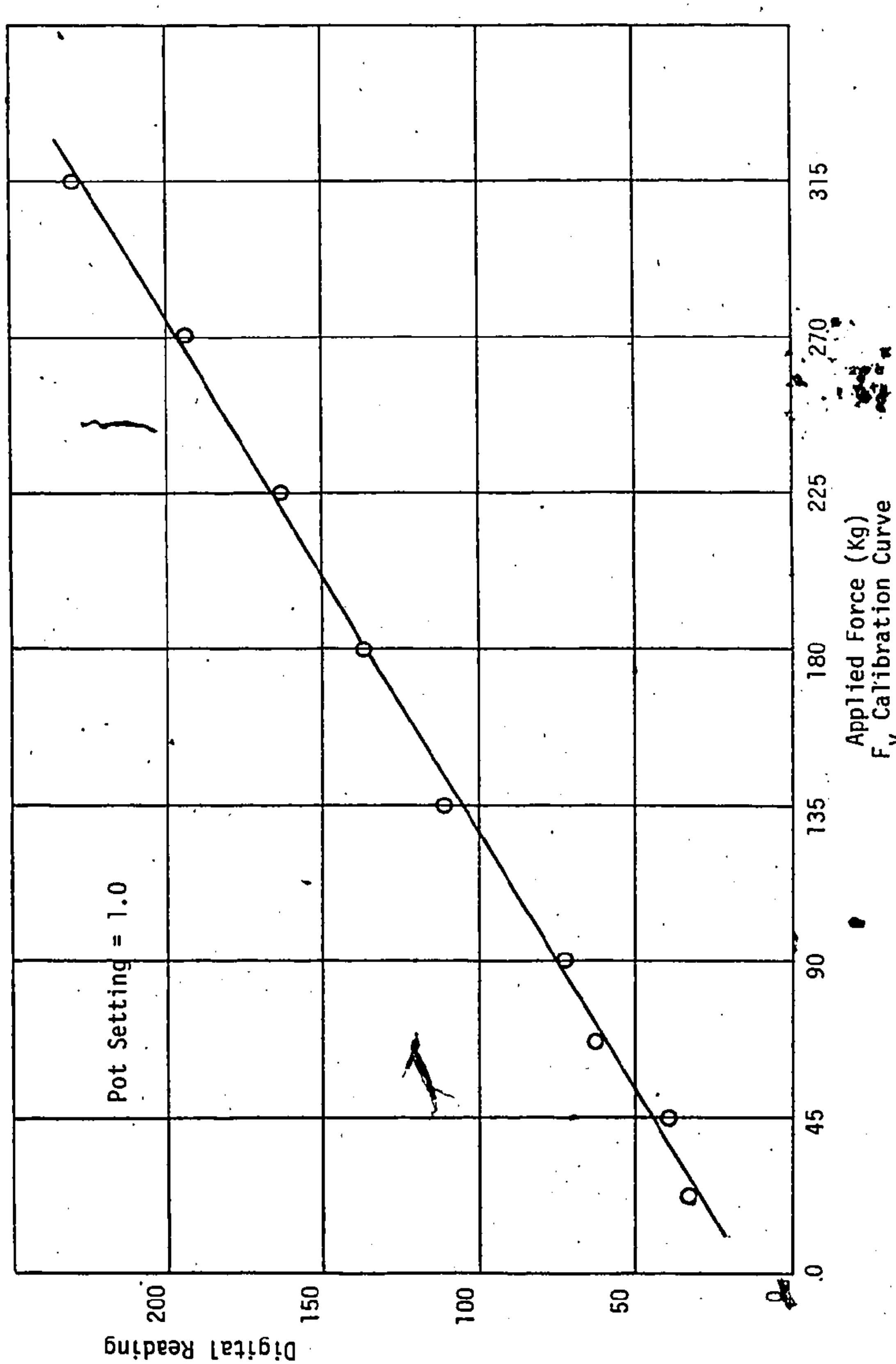
Pot Setting = 1.0
0
45
90
135
180
225
270
315
Applied Force (Kg)
F_y Calibration Curve
0
50
100
150
200
Digital Reading

FIGURE I-5

is $\pm$ 511 units. The amplifier gain was set so as to saturate the A/D converters only at a force of 1500 lb. on each of F_x and F_y. This corresponds to the noted potentiometer settings of 1.5 for F_x and 1.0 for F_y.

APPENDIX II

THE A/C TABLE DYNAMOMETER

APPENDIX II

THE A/C TABLE DYNAMOMETER

The A/C table dynamometer is a high quality 3 component dynamometer designed to decompose a force acting in any direction into three components perpendicular to one another. In A/C applications, however, only the two perpendicular components in the plane of the milling machine table are used. The table dynamometer itself is fixed to the table of the milling machine while the workpiece is fixed on top of the dynamometer.

The basic circuit of the measuring installation is illustrated in figure II-1. The load-sensitive elements are piezo-electric force transducers, in the form of thick washers. The three load cells were connected in parallel. The transducers signals (F_x and F_y) were fed to two charge amplifiers, whereby the electrostatic charge generated by the quartz was converted into a proportional voltage. A D.C. off-set was used to adjust the input voltage to the Analog-to-Digital Converters located in the ADP unit.

The dynamometer can withstand cutting forces of 680 kg for each component F_x and F_y. The sensitivity of the dynamometer is indicated by the calibration curves included in figures II-2 and II-3. The figures show the relation between the applied force and the digitized computer input for each channel (F_x and F_y).

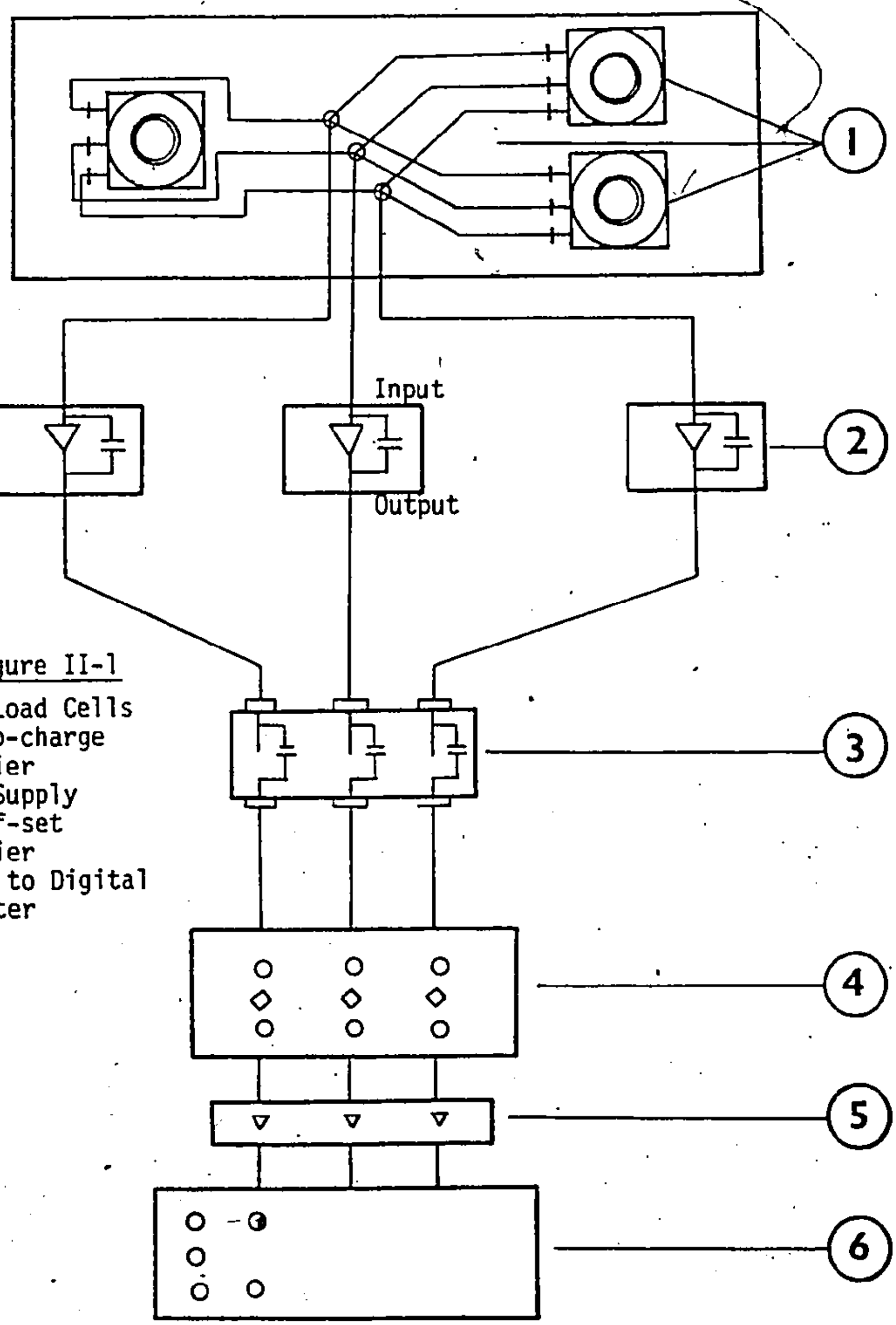

Key to Figure II-1

1. Three Load Cells
2. Electro-charge Amplifier
3. Power Supply
4. D-C Off-set
5. Amplifier
6. Analog to Digital Converter

Basic Circuit of the Measuring Installation

FIGURE II-1

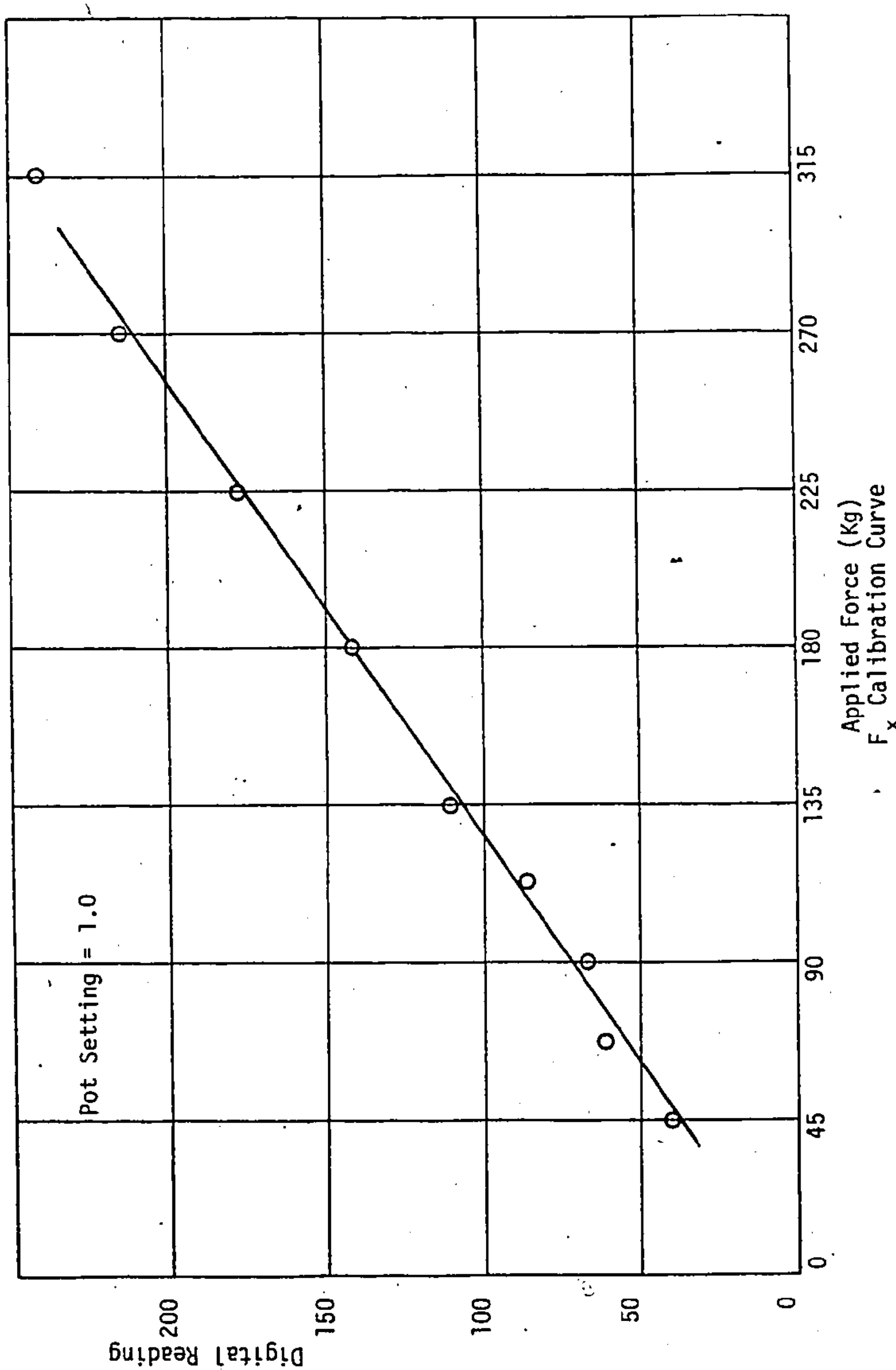
Pot Setting = 1.0
Digital Reading
0
50
100
150
200
0
45
90
135
180
225
270
315
Applied Force (Kg)
F_x Calibration Curve

FIGURE II-2

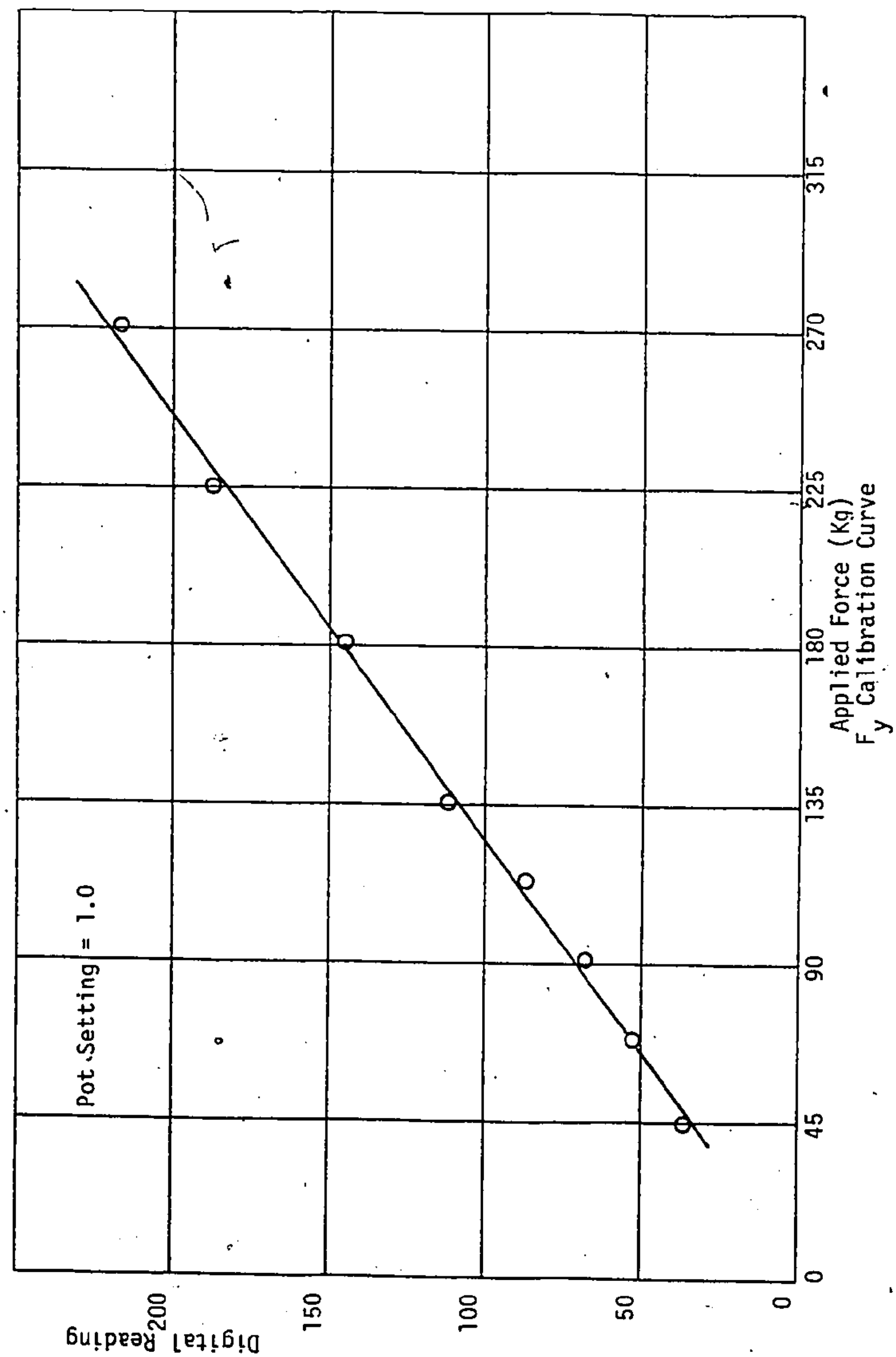
Pot Setting = 1.0
Digital Reading
0
50
100
150
200
Applied Force (Kg)
0
45
90
135
180
225
270
315
F_y Calibration Curve

FIGURE II-3

APPENDIX III

THE NUMERICAL CONTROL PROGRAM

```
                          ASMB,A,B,L
     00002                     ORG 2B
     00011               TTY   EQU 11B
     00014               TBG   EQU 14B
     00002 124003              JMP 3,I
     00003 000100              OCT 100
*    ESTABLISH INTERRUPT LINKAGE
*    N/C CONTROLDER ONLY.
     00010                     ORG 10B
     00010 106710              CLC 10B
     00011 106711              CLC 11B
     00012 106712              CLC 12B
     00013 106713              CLC 13B
     00014 014632              JSB CONTN
     00015 106715              CLC 15B
     00016 106716              CLC 16B
     00017 106717              CLC 17B
     00020 106720              CLC 20B
     00021 106721              CLC 21B
     00022 106722              CLC 22B
     00023 106723              CLC 23B
     00024 106724              CLC 24B
     00025 106725              CLC 25B
     00100                     ORG 100B
     00100 102100              STF 0
     00101 014105              JSB INIT
     00102 103714              STC TBG,C
     00103 124104              JMP ACP,I
     00104 002024        ACP   OCT 2024
*
*    INITIATOR ROUTINE.
*
     00105 000000        INIT  NOP
     00106 002400              CLA
     00107 071244              STA SIGN
     00110 061257              LDA M70
     00111 071243              STA CONT
     00112 061327              LDA SI
     00113 071314              STA H1
     00114 071315              STA H2
     00115 061321              LDA LA
     00116 071312              STA V1
     00117 071313              STA V2
*    SEND M-CODE OUT TO MILLING MACHINE.
     00120 061245              LDA M
     00121 003000              CMA
     00122 001727              ALF,ALF
     00123 102613              OTA 13B
     00124 103713              STC 13B,C
     00125 061245              LDA M
     00126 051324              CPA M6
     00127 102006              HLT 6B
     00130 051323              CPA M30
     00131 014572              JSB BEGIN
     00132 000000        GO    NOP
     00133 161267              LDA AN,I
     00134 102601              OTA 1B
```

PAGE 0003 #01 NUM. CONTROL ROUTINE- CNC/F

```
00135 161270        LDA AG,I
00136 071255        STA G
00137 051335        CPA FOUR
00140 024156        JMP G4
00141 051304        CPA G17
00142 071311        STA PLAN
00143 051305        CPA G18
00144 071311        STA PLAN
00145 051306        CPA G19
00146 071311        STA PLAN
00147 061311        LDA PLAN
00150 051304        CPA G17
00151 024172        JMP S17
00152 051305        CPA G18
00153 024301        JMP S18
00154 051306        CPA G19
00155 024411        JMP S19
00156 161277  G4    LDA AF,I
00157 003004        CMA,INA
00160 071341        STA AFF
00161 161265        LDA F,I
00162 051340        CPA ZERO
00163 024167        JMP YES
00164 161265        LDA F,I
00165 171265        STA F,I
00166 024171        JMP *+3
00167 061341  YES   LDA AFF
00170 171265        STA F,I
00171 024531        JMP M789
00172 061332  S17   LDA ONE
00173 071307        STA OP1
00174 061333        LDA TWO
00175 071310        STA OP2
00176 161271  A0    LDA AX,I
00177 002020        SSA
00200 003004        CMA,INA
00201 003004        CMA,INA
00202 071253        STA C1
00203 161271        LDA AX,I
00204 003004        CMA,INA
00205 002020        SSA
00206 024227        JMP A2
00207 061243        LDA CONT
00210 011260        AND SX
00211 071243        STA CONT
00212 161272  A1    LDA AY,I
00213 002020        SSA
00214 003004        CMA,INA
00215 003004        CMA,INA
00216 071254        STA C2
00217 161272        LDA AY,I
00220 003004        CMA,INA
00221 002020        SSA
00222 024235        JMP A4
00223 061243        LDA CONT
00224 011261        AND SY
00225 071243        STA CONT
```

```
00226 024232          JMP A3
00227 061332  A2      LDA ONE
00230 071244          STA SIGN
00231 024212          JMP AI
00232 061302  A3      LDA INCR
00233 041244          ADA SIGN
00234 071244          STA SIGN
00235 061255  A4      LDA G
00236 051303          CPA Z
00237 024531          JMP M789
00240 051333          CPA TWO
00241 024253          JMP S172
00242 051334          CPA THREE
00243 024257          JMP S173
00244 061253  S171    LDA C1
00245 003004          CMA,INA
00246 071247          STA Y
00247 061254          LDA C2
00250 003004          CMA,INA
00251 071251          STA Y2
00252 024517          JMP F789
00253 002400  S172    CLA
00254 051244          CPA SIGN
00255 024272          JMP S273
00256 024263          JMP S272
00257 002400  S173    CLA
00260 051244          CPA SIGN
00261 024263          JMP S272
00262 024272          JMP S273
00263 061333  S272    LDA TWO
00264 071255          STA G
00265 161274          LDA AI,I
00266 071247          STA Y
00267 161275          LDA AJ,I
00270 071251          STA Y2
00271 024517          JMP F789
00272 061334  S273    LDA THREE
00273 071255          STA G
00274 161274          LDA AI,I
00275 071251          STA Y2
00276 161275          LDA AJ,I
00277 071247          STA Y
00300 024517          JMP F789
00301 061332  S18     LDA ONE
00302 071307          STA OP1
00303 061335          LDA FOUR
00304 071310          STA OP2
00305 161271  B0      LDA AX,I
00306 002020          SSA
00307 003004          CMA,INA
00310 003004          CMA,INA
00311 071253          STA C1
00312 161271          LDA AX,I
00313 003004          CMA,INA
00314 002020          SSA
00315 024337          JMP B2
00316 061243          LDA CONT
```

PAGE 0005 #01 NUM. CONTROL ROUTINE- CNC/F

```
00317 011260        AND SX
00320 071243        STA CONT
00321 161273 B1     LDA AZ,I
00322 002020        SSA
00323 003004        CMA,INA
00324 003004        CMA,INA
00325 071254        STA C2
00326 161273        LDA AZ,I
00327 003004        CMA,INA
00330 002020        SSA
00331 024345        JMP B4
00332 041243        ADA CONT
00333 061243        LDA CONT
00334 011262        AND SZ
00335 071243        STA CONT
00336 024342        JMP B3
00337 061332 B2     LDA ONE
00340 071244        STA SIGN
00341 024321        JMP B1
00342 061302 B3     LDA INCR
00343 041244        ADA SIGN
00344 071244        STA SIGN
00345 061255 B4     LDA G
00346 051303        CPA Z
00347 024531        JMP M789
00350 051333        CPA TWO
00351 024363        JMP S182
00352 051334        CPA THREE
00353 024367        JMP S183
00354 061253 S181   LDA C1
00355 003004        CMA,INA
00356 071247        STA Y
00357 061254        LDA C2
00360 003004        CMA,INA
00361 071251        STA Y2
00362 024517        JMP F789
00363 002400 S182   CLA
00364 051244        CPA SIGN
00365 024402        JMP S283
00366 024373        JMP S282
00367 002400 S183   CLA
00370 051244        CPA SIGN
00371 024373        JMP S282
00372 024402        JMP S283
00373 061333 S282   LDA TWO
00374 071255        STA G
00375 161274        LDA AI,I
00376 071247        STA Y
00377 161276        LDA AK,I
00400 071251        STA Y2
00401 024517        JMP F789
00402 061334 S283   LDA THREE
00403 071255        STA G
00404 161274        LDA AI,I
00405 071251        STA Y2
00406 161276        LDA AK,I
00407 071247        STA Y
```

```
PAGE 0006 #01  NUM. CONTROL ROUTINE- CNC/F

00410 024517          JMP F789
00411 061333  S19     LDA TWO
00412 071307          STA OP1
00413 061335          LDA FOUR
00414 071310          STA OP2
00415 161272  C0      LDA AY,I
00416 002020          SSA
00417 003004          CMA,INA
00420 003004          CMA,INA
00421 071253          STA C1
00422 161272          LDA AY,I
00423 003004          CMA,INA
00424 002020          SSA
00425 024446          JMP C21
00426 061243          LDA CONT
00427 011261          AND SY
00430 071243          STA CONT
00431 161273  C11     LDA AZ,I
00432 002020          SSA
00433 003004          CMA,INA
00434 003004          CMA,INA
00435 071254          STA C2
00436 161273          LDA AZ,I
00437 003004          CMA,INA
00440 002020          SSA
00441 024454          JMP C4
00442 061243          LDA CONT
00443 011262          AND SZ
00444 071243          STA CONT
00445 024451          JMP C3
00446 061332  C21     LDA ONE
00447 071244          STA SIGN
00450 024431          JMP C11
00451 061302  C3      LDA INCR
00452 041244          ADA SIGN
00453 071244          STA SIGN
00454 061255  C4      LDA G
00455 051303          CPA Z
00456 024531          JMP M789
00457 051333          CPA TWO
00460 024472          JMP S192
00461 051334          CPA THREE
00462 024476          JMP S193
00463 061253  S191    LDA C1
00464 003004          CMA,INA
00465 071247          STA Y
00466 061254          LDA C2
00467 003004          CMA,INA
00470 071251          STA Y2
00471 024517          JMP F789
00472 002400  S192    CLA
00473 051244          CPA SIGN
00474 024511          JMP S293
00475 024502          JMP S292
00476 002400  S193    CLA
00477 051244          CPA SIGN
00500 024502          JMP S292
```

```
00501 024511         JMP S293
00502 061333  S292   LDA TWO
00503 071255         STA G
00504 161275         LDA AJ,I
00505 071247         STA Y
00506 161276         LDA AK,I
00507 071251         STA Y2
00510 024517         JMP F789
00511 061334  S293   LDA THREE
00512 071255         STA G
00513 161275         LDA AJ,I
00514 071251         STA Y2
00515 161276         LDA AK,I
00516 071247         STA Y
00517 161277  F789   LDA AF,I
00520 071342         STA AFFF
00521 161265         LDA F,I
00522 051340         CPA ZERO
00523 024527         JMP YESS
00524 161265         LDA F,I
00525 171265         STA F,I
00526 024531         JMP *+3
00527 061342  YESS   LDA AFFF
00530 171265         STA F,I
00531 161300  M789   LDA AM,I
*   INTERPRETM= 5 AS M=4.
00532 051336         CPA FIVE
00533 041302         ADA INCR
00534 071245         STA M
00535 161301         LDA PATH,I
00536 003004         CMA,INA
00537 071331         STA LIM
00540 161265         LDA F,I
00541 001100         ARS
00542 071256         STA TEMP
00543 001100         ARS
00544 041256         ADA TEMP
00545 006400         CLB
00546 100400         DIV LIM
00547 001331
00550 071326         STA DN
00551 035267         ISZ AN
00552 035270         ISZ AG
00553 035271         ISZ AX
00554 035272         ISZ AY
00555 035273         ISZ AZ
00556 035274         ISZ AI
00557 035275         ISZ AJ
00560 035276         ISZ AK
00561 035277         ISZ AF
00562 035300         ISZ AM
00563 035301         ISZ PATH
00564 002400         CLA
00565 171264         STA K,I
00566 071246         STA R-
00567 071250         STA R2
00570 071252         STA R3
```

```
00571 124105           JMP INIT,I
*  RE-INITIALIZE ALL VARIABLES.
00572 000000    BEGIN  NOP
00573 061266           LDA BAG
00574 071267           STA AN
00575 041263           ADA MEA
00576 071270           STA AG
00577 041263           ADA MEA
00600 071271           STA AX
00601 041263           ADA MEA
00602 071272           STA AY
00603 041263           ADA MEA
00604 071273           STA AZ
00605 041263           ADA MEA
00606 071274           STA AI
00607 041263           ADA MEA
00610 071275           STA AJ
00611 041263           ADA MEA
00612 071276           STA AK
00613 041263           ADA MEA
00614 071277           STA AF
00615 041263           ADA MEA
00616 071300           STA AM
00617 041263           ADA MEA
00620 071301           STA PATH
00621 002400           CLA
00622 071245           STA M
00623 060572           LDA BEGIN
00624 041312           ADA V1
00625 002021           SSA,RSS
00626 024631           JMP ED
00627 102030           HLT 30B
00630 024132           JMP GO
00631 124572    ED     JMP BEGIN,I
*
*  CONTINUATOR ROUTINE.
*
00632 000000    CONTN  NOP
00633 071241           STA SAVA
00634 075242           STB SAVB
00635 002400           CLA
00636 102201           SOC
00637 061237           LDA .2
00640 001500           ERA
00641 071240           STA SAVEO
00642 106714           CLC 14B
00643 061243           LDA CONT
00644 011257           AND M70
00645 071243           STA CONT
00646 061255           LDA G
00647 051303           CPA Z
00650 024654           JMP PTP
00651 051335           CPA FOUR
00652 024766           JMP DWEL
00653 025001           JMP FEED
00654 061253    PTP    LDA C1
00655 051303           CPA Z
```

PAGE 0009 #01 NUM. CONTROL ROUTINE- CNC/F

```
00656 024706        JMP COMP
00657 041321        ADA LA
00660 002021        SSA,RSS
00661 024711        JMP XA
00662 035253        ISZ C1
00663 061307        LDA OP1
00664 041243        ADA CONT
00665 071243        STA CONT
00666 061254 YPTP   LDA C2
00667 051303        CPA Z
00670 024676        JMP OP
00671 041321        ADA LA
00672 002021        SSA,RSS
00673 024745        JMP YA
00674 035254        ISZ C2
00675 061310        LDA OP2
00676 041243 OP     ADA CONT
00677 003000        CMA
00700 102613        OTA 13B
00701 103713        STC 13B,C
00702 061243        LDA CONT
00703 011257        AND M70
00704 071243        STA CONT
00705 024654        JMP PTP
00706 051254 COMP   CPA C2
00707 0252[illegible]        JMP IN
00710 02466[illegible]        JMP YPTP
00711 03531[illegible] XA     ISZ H1
00712 024732        JMP SLW
00713 061327        LDA SI
00714 071314        STA H1
00715 061312        LDA V1
00716 051322        CPA LB
00717 024727        JMP XB
00720 035312        ISZ V1
00721 035253 LX     ISZ C1
00722 000000        NOP
00723 061307        LDA OP1
00724 041243        ADA CONT
00725 071243        STA CONT
00726 024732        JMP SLW
00727 061325 XB     LDA DM
00730 071314        STA H1
00731 024721        JMP LX
00732 061254 SLW    LDA C2
00733 051303        CPA Z
00734 025205        JMP OT
00735 041321        ADA LA
00736 002021        SSA,RSS
00737 024745        JMP YA
00740 035254        ISZ C2
00741 061310        LDA OP2
00742 041243        ADA CONT
00743 071243        STA CONT
00744 025205        JMP OT
00745 035315 YA     ISZ H2
00746 025205        JMP OT
```

```
00747 061327        LDA SI
00750 071315        STA H2
00751 061313        LDA V2
00752 051322        CPA LB
00753 024763        JMP YB
00754 035313        ISZ V2
00755 035254  LY    ISZ C2
00756 000000        NOP
00757 061310        LDA OP2
00760 041243        ADA CONT
00761 071243        STA CONT
00762 025205        JMP OT
00763 061325  YB    LDA DM
00764 071315        STA H2
00765 024755        JMP LY
00766 035252  DWEL  ISZ R3
00767 061252        LDA R3
00770 051336        CPA FIVE
00771 024773        JMP *+2
00772 025221        JMP OUT
00773 002400        CLA
00774 171264        STA K,I
00775 071252        STA R3
00776 135265        ISZ F,I
00777 025221        JMP OUT
01000 025220        JMP IN
01001 061252  FEED  LDA R3
01002 141265        ADA F,I
01003 071252        STA R3
01004 041320        ADA MAX
01005 002020        SSA
01006 025221        JMP OUT
01007 071252        STA R3
01010 061255        LDA G
01011 051337        CPA NINE
01012 025014        JMP DCEL
01013 025025        JMP SLCT
01014 002400  DCEL  CLA
01015 171264        STA K,I
01016 161265        LDA F,I
01017 041330        ADA FM
01020 002020        SSA
01021 025025        JMP SLCT
01022 161265        LDA F,I
01023 041326        ADA DN
01024 171265        STA F,I
01025 061255  SLCT  LDA G
01026 051332        CPA ONE
01027 025034        JMP LINE
01030 051333        CPA TWO
01031 025073        JMP CIRC2
01032 051334        CPA THREE
01033 025137        JMP CIRC3
01034 002400  LINE  CLA
01035 051253        CPA C1
01036 025053        JMP DDA2
01037 061246        LDA R
```

```
01040 041247         ADA Y
01041 071246         STA R
01042 041331         ADA LIM
01043 002020         SSA
01044 025053         JMP DDA2
01045 071246         STA R
01046 061307         LDA OP1
01047 041243         ADA CONT
01050 071243         STA CONT
01051 035253         ISZ C1
01052 000000         NOP
01053 002400   DDA2  CLA
01054 051254         CPA C2
01055 025202         JMP CHECK
01056 061250         LDA R2
01057 041251         ADA Y2
01060 071250         STA R2
01061 041331         ADA LIM
01062 002020         SSA
01063 025202         JMP CHECK
01064 071250         STA R2
01065 061243         LDA CONT
01066 041310         ADA OP2
01067 071243         STA CONT
01070 035254         ISZ C2
01071 000000         NOP
01072 025202         JMP CHECK
01073 002400   CIRC2 CLA
01074 051254         CPA C2
01075 025114         JMP BDDA2
01076 061246         LDA R
01077 041247         ADA Y
01100 071246         STA R
01101 041331         ADA LIM
01102 002020         SSA
01103 025114         JMP BDDA2
01104 071246         STA R
01105 061310         LDA OP2
01106 041243         ADA CONT
01107 071243         STA CONT
01110 035254         ISZ C2
01111 000000         NOP
01112 035251         ISZ Y2
01113 000000         NOP
01114 002400   BDDA2 CLA
01115 051253         CPA C1
01116 025202         JMP CHECK
01117 061250         LDA R2
01120 041251         ADA Y2
01121 071250         STA R2
01122 041331         ADA LIM
01123 002020         SSA
01124 025202         JMP CHECK
01125 071250         STA R2
01126 061243         LDA CONT
01127 041307         ADA OP1
01130 071243         STA CONT
```

```
01131 035253         ISZ C1
01132 000000         NOP
01133 061247         LDA Y
01134 041302         ADA INCR
01135 071247         STA Y
01136 025202         JMP CHECK
01137 002400  CIRC3  CLA
01140 051253         CPA C1
01141 025160         JMP CDDA2
01142 061246         LDA R
01143 041247         ADA Y
01144 071246         STA R
01145 041331         ADA LIM
01146 002020         SSA
01147 025160         JMP CDDA2
01150 071246         STA R
01151 061307         LDA OP1
01152 041243         ADA CONT
01153 071243         STA CONT
01154 035253         ISZ C1
01155 000000         NOP
01156 035251         ISZ Y2
01157 000000         NOP
01160 002400  CDDA2  CLA
01161 051254         CPA C2
01162 025202         JMP CHECK
01163 061250         LDA R2
01164 041251         ADA Y2
01165 071250         STA R2
01166 041331         ADA LIM
01167 002020         SSA
01170 025202         JMP CHECK
01171 071250         STA R2
01172 061243         LDA CONT
01173 041310         ADA OP2
01174 071243         STA CONT
01175 035254         ISZ C2
01176 000000         NOP
01177 061247         LDA Y
01200 041302         ADA INCR
01201 071247         STA Y
01202 161264  CHECK  LDA K,I
01203 041316         ADA KN1
01204 171264         STA K,I
01205 161343  OT     LDA FLAG,I
01206 051344         CPA TEN
01207 025214         JMP *+5
01210 061243         LDA CONT
01211 003000         CMA
01212 102613         OTA 13B
01213 103713         STC 13B,C
01214 000000         NOP
01215 061253         LDA C1
01216 041254         ADA C2
01217 051303         CPA Z
01220 014105  IN     JSB INIT
*   RETURN TO MAIN OR A/C ROUTINE.
```

```
01221 161264  OUT    LDA K,I
01222 041317         ADA KN2
01223 171264         STA K,I
01224 061240         LDA SAVEO
01225 000040         CLE
01226 103101         CLO
01227 002020         SSA
01230 002200         CME
01231 000010         SLA
01232 102101         STO
01233 061241         LDA SAVA
01234 065242         LDB SAVB
01235 103714         STC TBG,C
01236 124632         JMP CONTN,I
*
*
*
01237 000002  .2     DEC 2
01240 000000  SAVEO  NOP
01241 000000  SAVA   NOP
01242 000000  SAVB   NOP
01243 000070  CONT   OCT 70
01244 000000  SIGN   NOP
01245 000000  M      NOP
01246 000000  R      NOP
01247 000000  Y      NOP
01250 000000  R2     NOP
01251 000000  Y2     NOP
01252 000000  R3     NOP
01253 000000  C1     NOP
01254 000000  C2     NOP
01255 000000  G      NOP
01256 000000  TEMP   NOP
01257 000070  M70    OCT 70
01260 000060  SX     OCT 60
01261 000050  SY     OCT 50
01262 000030  SZ     OCT 30
01263 000400  MEA    OCT 400
01264 020000  K      OCT 20000
01265 020004  F      OCT 20004
01266 030000  BAG    OCT 30000
01267 030000  AN     OCT 30000
01270 030400  AG     OCT 30400
01271 031000  AX     OCT 31000
01272 031400  AY     OCT 31400
01273 032000  AZ     OCT 32000
01274 032400  AI     OCT 32400
01275 033000  AJ     OCT 33000
01276 033400  AK     OCT 33400
01277 034000  AF     OCT 34000
01300 034400  AM     OCT 34400
01301 035000  PATH   OCT 35000
01302 177777  INCR   DEC -1
01303 000000  Z      NOP
01304 000021  G17    DEC 17
01305 000022  G18    DEC 18
01306 000023  G19    DEC 19
```

PAGE 0014 #01 NUM. CONTROL ROUTINE- CNC/F

```
01307 000001  OP1   DEC 1
01310 000002  OP2   DEC 2
01311 000021  PLAN  DEC 17
01312 176030  V1    DEC -1000
01313 176030  V2    DEC -1000
01314 177776  H1    DEC -2
01315 177776  H2    DEC -2
01316 000041  KN1   DEC 33
01317 000045  KN2   DEC 37
01320 172110  MAX   DEC -3000
01321 001750  LA    DEC +1000
01322 177634  LB    DEC -100
01323 000036  M30   DEC 30
01324 000006  M6    DEC 6
01325 177766  DM    DEC -10
01326 177742  DN    DEC -30
01327 177776  SI    DEC -2
01330 177730  FM    DEC -40
01331 154360  LIM   DEC -10000
01332 000001  ONE   DEC 1
01333 000002  TWO   DEC 2
01334 000003  THREE DEC 3
01335 000004  FOUR  DEC 4
01336 000005  FIVE  DEC 5
01337 000011  NINE  DEC 9
01340 000000  ZERO  DEC 0
01341 000000  AFF   NOP
01342 000000  AFFF  NOP
01343 014040  FLAG  OCT 14040
01344 000012  TEN   DEC 10
                    END
** NO ERRORS*
```

APPENDIX IV

THE ADAPTIVE CONTROL PROGRAM

PAGE 0002 #01 ADAPTIVE CONTROL PROGRAM #A/C-19/VERSION1

```
                        ASMB,A,B,L
02024                          ORG 2024B
00012                   ADC    EQU 12B
02024 002400                   CLA
02025 172464                   STA TIME,I
02026 102112                   STF ADC
02027 026042                   JMP INPUT
*      LOOPING FOR THE PERIOD OF DELAY
02030 002400            WAIT   CLA
02031 072520                   STA COUNT
02032 162464                   LDA TIME,I
02033 042504                   ADA DELAY
02034 002021                   SSA,RSS
02035 026042                   JMP INPUT
02036 162464                   LDA TIME,I
02037 042473                   ADA TIME1
02040 172464                   STA TIME,I
02041 026030                   JMP WAIT
* BEGIN READING A TO D CONVERTER
02042 002400            INPUT  CLA
02043 003000                   CMA
02044 102612                   OTA ADC
02045 102712                   STC ADC
02046 102312                   SFS ADC
02047 026046                   JMP *-1
02050 102512                   LIA ADC
02051 106712                   CLC ADC
02052 072523                   STA TEMP1
02053 012472                   AND CODE
02054 072524                   STA TEMP2
02055 066524                   LDB TEMP2
02056 062523                   LDA TEMP1
02057 012471                   AND SORCE
02060 052467                   CPA CHAN1
02061 076521                   STB F1
02062 052470                   CPA CHAN2
02063 076522                   STB F2
02064 002400                   CLA
02065 102612                   OTA ADC
02066 103712                   STC ADC,C
02067 106712                   CLC ADC
02070 062520                   LDA COUNT
02071 052477                   CPA THREE
02072 026101                   JMP ABSOL
02073 036520                   ISZ COUNT
02074 062514                   LDA NEGTN
02075 072517                   STA SLOW
02076 036517                   ISZ SLOW
02077 026076                   JMP *-1
02100 026042                   JMP INPUT
* TAKE THE ABSOLUTE VALUE OF INPUTS
02101 062521            ABSOL  LDA F1
02102 016423                   JSB ABS
02103 072521                   STA F1
02104 062522                   LDA F2
02105 016423                   JSB ABS
02106 072522                   STA F2
```

```
*  SORT F1 AND F2 IN PREPARADION FOR SQUARE ROOT
   02107 062521  SORT  LDA F1
   02110 003004        CMA,INA
   02111 042522        ADA F2
   02112 002021        SSA,RSS
   02113 026121        JMP SORT2
   02114 062521  SORT1 LDA F1   HERE F1>F2
   02115 072526        STA P
   02116 062522        LDA F2
   02117 072527        STA Q
   02120 026125        JMP ROOT
   02121 062521  SORT2 LDA F1 HERE F1<F2
   02122 072527        STA Q
   02123 062522        LDA F2
   02124 072526        STA P
*  CALCULATE SQUARE ROOT OF F1**2 + F2**2
   02125 062527  ROOT  LDA Q
   02126 100200        MPY Q
   02127 002527
   02130 100400        DIV P
   02131 002526
   02132 001100        ARS
   02133 072530        STA Y
   02134 100200        MPY Y
   02135 002530
   02136 100400        DIV P
   02137 002526
   02140 001100        ARS
   02141 072531        STA Z
   02142 100200        MPY Y
   02143 002530
   02144 100400        DIV P
   02145 002526
   02146 042526        ADA P
   02147 042530        ADA Y
   02150 072525        STA RR
   02151 062531        LDA Z
   02152 003004        CMA,INA
   02153 042525        ADA RR
   02154 072534        STA FORCE
*
*  FORCE=P+Q**2/2*P-Q**4/8*P**3+Q**6/16*P**5
*
*  DATA COLLECTIOM ROUTINE
*
   02155 000000        NOP
   02156 062534        LDA FORCE
   02157 172552        STA ARRAY,I
   02160 036552        ISZ ARRAY
*
*  PEAK STORAGE ROUTINE
*
*
*
   02161 062572        LDA X6
   02162 072573        STA X7
   02163 062571        LDA X5
```

```
02164 072572        STA X6
02165 062570        LDA X4
02166 072571        STA X5
02167 062567        LDA X3
02170 072570        STA X4
02171 062566        LDA X2
02172 072567        STA X3
02173 062565        LDA X1
02174 072566        STA X2
02175 062534        LDA FORCE
02176 072565        STA X1
*
*
*
02177 062565        LDA X1
02200 003004        CMA,INA
02201 042566        ADA X2
02202 002021        SSA,RSS
02203 026207        JMP R1
02204 062565        LDA X1
02205 072574        STA S
02206 026211        JMP R2
02207 062566   R1   LDA X2
02210 072574        STA S
02211 062574   R2   LDA S
02212 003004        CMA,INA
02213 042567        ADA X3
02214 002021        SSA,RSS
02215 026221        JMP R3
02216 062574        LDA S
02217 072574        STA S
02220 026223        JMP R4
02221 062567   R3   LDA X3
02222 072574        STA S
02223 062574   R4   LDA S
02224 003004        CMA,INA
02225 042570        ADA X4
02226 002021        SSA,RSS
02227 026233        JMP R5
02230 062574        LDA S
02231 072574        STA S
02232 026235        JMP R6
02233 062570   R5   LDA X4
02234 072574        STA S
02235 062574   R6   LDA S
02236 003004        CMA,INA
02237 042571        ADA X5
02240 002021        SSA,RSS
02241 026245        JMP R7
02242 062574        LDA S
02243 072574        STA S
02244 026247        JMP R8
02245 062571   R7   LDA X5
02246 072574        STA S
02247 062574   R8   LDA S
02250 003004        CMA,INA
02251 042572        ADA X6
```

```
02252 002021          SSA,RSS
02253 026257          JMP R9
02254 062574          LDA S
02255 072574          STA S
02256 026261          JMP R10
02257 062572  R9      LDA X6
02260 072574          STA S
02261 062574  R10     LDA S
02262 003004          CMA,INA
02263 042573          ADA X7
02264 002021          SSA,RSS
02265 026271          JMP R11
02266 062574          LDA S
02267 072574          STA S
02270 026273          JMP R12
02271 062573  R11     LDA X7
02272 072574          STA S
02273 062574  R12     LDA S
02274 072534          STA FORCE
*
*
02275 062555          LDA TTT
02276 052475          CPA ONE
02277 026304          JMP *+5
02300 062543          LDA ZERO
02301 172564          STA FLAG,I
02302 062475          LDA ONE
02303 072555          STA TTT
02304 000000          NOP
*
*
* AIR-GAP DETECTOR
*
*
*
02305 062534          LDA FORCE
02306 042545          ADA FSET
02307 002020          SSA
02310 026317          JMP CHEK1
02311 062543          LDA ZERO
02312 072512          STA DEX
02313 062550          LDA CRN
02314 052543          CPA ZERO
02315 026336          JMP CHEK3
02316 126463          JMP POLCY,I
02317 062551  CHEK1   LDA STEP
02320 052543          CPA ZERO
02321 026323          JMP CHEK2
02322 026336          JMP CHEK3
02323 062512  CHEK2   LDA DEX
02324 042475          ADA ONE
02325 072512          STA DEX
02326 062512          LDA DEX
02327 042547          ADA NETFV
02330 002020          SSA
02331 126463          JMP POLCY,I
```

```
     02333 072512       STA DEX
     02334 062543       LDA ZERO
     02335 072550       STA CRN
*
* TRANSIENT SCHEME
*
*
     02336 062542 CHEK3 LDA KOUNT
     02337 052543       CPA ZERO
     02340 026342       JMP CHEK4
     02341 026353       JMP CHEK5
     02342 062544 CHEK4 LDA FE
     02343 003004       CMA,INA
     02344 142466       ADA FEED,I
     02345 002020       SSA
     02346 126463       JMP POLCY,I
     02347 062534       LDA FORCE
     02350 042545       ADA FSET
     02351 002020       SSA
     02352 126463       JMP POLCY,I
     02353 062506 CHEK5 LDA FDMIN
     02354 172466       STA FEED,I
* SWITCH OFF
*
*
     02355 062475       LDA ONE
     02356 072560       STA LLO
     02357 016433       JSB OFF
     02360 000000       NOP
     02361 062542       LDA KOUNT
     02362 042475       ADA ONE
     02363 072542       STA KOUNT
     02364 062542       LDA KOUNT
     02365 042553       ADA NTW5
     02366 002020       SSA
     02367 026377       JMP CHEK6
     02370 062543       LDA ZERO
     02371 072542       STA KOUNT
     02372 062543       LDA ZERO
     02373 072551       STA STEP
     02374 062475       LDA ONE
     02375 072550       STA CRN
     02376 126463       JMP POLCY,I
     02377 062475 CHEK6 LDA ONE
     02400 072551       STA STEP
     02401 026420       JMP RETRN
*
*
*
*       THIS ROUTINE ENSURES THAT 30<FEED<3000
     02402 062532 NEWFD LDA DELFD
     02403 142466       ADA FEED,I
     02404 172466       STA FEED,I
     02405 042507       ADA FMIN
     02406 002020       SSA
     02407 026416       JMP MIN
     02410 042510       ADA FMAX
```

```
02411 002020         SSA
02412 026420         JMP RETRN
02413 062505  MAX    LDA FDMAX
02414 172466         STA FEED,I
02415 026420         JMP RETRN
02416 062506  MIN    LDA FDMIN
02417 172466         STA FEED,I
02420 002400  RETRN  CLA
02421 172464         STA TIME,I CLEAR THE COUNTER
02422 026030         JMP WAIT
*
* THIS ROUTINE PLACES THE SIGN BIT OF THE 10-BIT INPUT
* WORD IN THE M.S.B. AND TAKES THE ABS. VALUE
02423 000000  ABS    NOP
02424 100040         LSL 16
02425 100046         LSL 6
02426 101020         ASR 16
02427 101026         ASR 6
02430 002020         SSA
02431 003004         CMA,INA
02432 126423         JMP ABS,I
*
*
*
* SUBROUTINE OFF SWITCHES OFF THE ANALOG SWITCH
* SUBROUTINE ON SWITCHES ON THE ANALOG SWITCH
*
* SUBROUTINE SLOW DECREASES THE GAIN IN THE
* CORREC. NETWORK BY A FACTOR OF FOUR
*
*
02433 000000  OFF    NOP
02434 002400         CLA
02435 006400         CLB
02436 066562         LDB CWSEN
02437 106616         OTB ASYNC
02440 062556         LDA TEN
02441 172564         STA FLAG,I
02442 126433         JMP OFF,I
*
02443 000000  ON     NOP
02444 002400         CLA
02445 006400         CLB
02446 066563         LDB CWREC
02447 106616         OTB ASYNC
02450 062543         LDA ZERO
02451 172564         STA FLAG,I
02452 126443         JMP ON,I
*
*
*
*
*
*
02453 000000  SLW    NOP
02454 002400         CLA
02455 006400         CLB
```

```
02456 066557        LDB CWSLW
02457 106616        OTB ASYNC
02460 062543        LDA ZERO
02461 172564        STA FLAG,I
02462 126453        JMP SLW,I
*
02463 002600 POLCY  OCT 2600
02464 020000 TIME   OCT 20000
02465 020001 FOPT   OCT 20001
02466 020004 FEED   OCT 20004
02467 010000 CHAN1  OCT 10000
02470 020000 CHAN2  OCT 20000
02471 070000 SORCE  OCT 70000
02472 001777 CODE   OCT 01777
02473 000012 TIME1  DEC 10
02474 000372 TIME2  DEC 250
02475 000001 ONE    DEC 1
02476 000002 TWO    DEC 2
02477 000003 THREE  DEC 3
02500 000144 HUN    DEC 100
02501 000040 THIRT  DEC 32
02502 000017 FIFTN  DEC 15
02503 000034 TWEN8  DEC 28
02504 176030 DELAY  DEC -1000
02505 005670 FDMAX  DEC 3000
02506 000036 FDMIN  DEC 30
02507 177742 FMIN   DEC -30
02510 172146 FMAX   DEC -2970
02511 176600 NLIM   DEC -640
02512 000000 DEX    NOP
02513 001200 PLIM   DEC 640
02514 177766 NEGTN  DEC -10
02515 000146 HUNTO  DEC 102
02516 072460 BIG    DEC 30000
02517 000000 SLOW   NOP
02520 000000 COUNT  NOP
02521 000000 F1     NOP
02522 000000 F2     NOP
02523 000000 TEMP1  NOP
02524 000000 TEMP2  NOP
02525 000000 RR     NOP
02526 000000 P      NOP
02527 000000 Q      NOP
02530 000000 Y      NOP
02531 000000 Z      NOP
02532 000000 DELFD  NOP
02533 000000 ERROR  NOP
02534 000000 FORCE  NOP
02535 000000 FACTR  NOP
02536 000000 ACC    NOP
02537 000000 EPREV  NOP
02540 000004 B      DEC 4
02541 000000 DAMP   NOP
02542 000000 KOUNT  NOP
02543 000000 ZERO   NOP
02544 005656 FE     DEC 2990
02545 177766 FSET   DEC -10
```

```
02546 000031  TWT5  DEC 25
02547 177735  NETFV DEC -35
02550 000000  CRN   NOP
02551 000000  STEP  NOP
*
02552 040000  ARRAY OCT 40000
02553 177747  NTW5  DEC -25
02554 000055  FORT5 DEC 45
*
02555 000000  TTT   NOP
02556 000012  TEN   DEC 10
00016         ASYNC EQU 16B
02557 100010  CWSLW OCT 100010
02560 000000  LLO   NOP
02561 000000  DLY   NOP
02562 160010  CWSEN OCT 160010
02563 140010  CWREC OCT 140010
02564 014040  FLAG  OCT 14040
02565 000000  X1    NOP
02566 000000  X2    NOP
02567 000000  X3    NOP
02570 000000  X4    NOP
02571 000000  X5    NOP
02572 000000  X6    NOP
02573 000000  X7    NOP
02574 000000  S     NOP
02600               ORG 2600B
* SWITCH ON
*
02600 062560        LDA LLO
02601 052475        CPA ONE
02602 026604        JMP *+2
02603 026613        JMP ST2
02604 000000        NOP
02605 062561        LDA DLY
02606 042475        ADA ONE
02607 072561        STA DLY
02610 052554        CPA FORT5
02611 026613        JMP ST2
02612 026620        JMP ST1
02613 016443  ST2   JSB ON
02614 062543        LDA ZERO
02615 072561        STA DLY
02616 072560        STA LLO
02617 026621        JMP *+2
02620 016453  ST1   JSB SLW
02621 000000        NOP
*
*
*
* CALCULATE FORCE ERROR
02622 062534        LDA FORCE
02623 003004        CMA,INA
02624 142465        ADA FOPT,I
02625 100200        MPY THIRT
02626 002501
```

```
02630 102465
02631 072533              STA ERROR
02632 042511              ADA NLIM
02633 002021              SSA,RSS
02634 026677              JMP EBIG
02635 062533       ESMAL  LDA ERROR
02636 100200              MPY ONE
02637 002475
02640 072535              STA FACTR
02641 162464              LDA TIME,I
02642 103101              CLO
02643 042474              ADA TIME2
02644 006400              CLB
02645 100400              DIV HUN
02646 002500
02647 100200              MPY FACTR
02650 002535
02651 100400              DIV TWEN8
02652 002503
02653 102201              SOC
02654 026702              JMP DLMAX
02655 072536              STA ACC
02656 062537              LDA EPREV
02657 003004              CMA,INA
02660 042533              ADA ERROR
02661 100200              MPY B
02662 002540
02663 100400              DIV HUN
02664 002500
02665 072541              STA DAMP
02666 062533              LDA ERROR
02667 002020              SSA
02670 016712              JSB NEG
02671 062541              LDA DAMP
02672 042536              ADA ACC
02673 072532       E1     STA DELFD
02674 062533              LDA ERROR
02675 072537              STA EPREV
02676 026402              JMP NEWFD
02677 062513       EBIG   LDA PLIM ERROR>640
02700 072533              STA ERROR ERROR=640
02701 026635              JMP ESMAL
02702 062533       DLMAX  LDA ERROR
02703 002020              SSA
02704 026707              JMP NMAX
02705 062516       PMAX   LDA BIG
02706 026673              JMP E1
02707 062516       NMAX   LDA BIG
02710 003004              CMA,INA
02711 026673              JMP E1
02712 000000       NEG    NOP
02713 062536              LDA ACC
02714 072536              STA ACC
02715 126712              JMP NEG,I
                          END
** NO ERRORS*
```

APPENDIX V

HARDWARE LOGIC FOR A/C ALGORITHM "B"

APPENDIX V

HARDWARE LOGIC FOR A/C ALGORITHM "B"

This appendix describes the hardware logic used to implement the A/C algorithm "B". Referring to figure 3.2 in Chapter 3 of this thesis, it was shown that in the position control loop, the phase difference between the command and feedback signals is converted into a DC voltage and passed through a single pole low pass filter before being amplified and used to drive the motor. Figure V-1 shows the circuit diagram of the low pass filter. Two analog switches "S_1" and "S_2" were added to the filter circuit. The first switch "S_1" is used to interrupt the velocity command to the velocity loop during transient conditions for a period of 40 milliseconds. "S_2" is used to reduce the gain in the NC loop to 1/3 its original value for a period of 100 milliseconds.

This reduction in the NC gain is necessary to prevent a serious overshoot in the system response (table velocity) when nullifying the condition $V_{com} = 0.0$. The operation of both switches is controlled by the A/C algorithm resident in the minicomputer. The circuit diagram of the analog switches is shown in figure V-2.

During steady state milling, the switch "S_2" is in the "ON" condition and the gain in the low pass filter is approximately unity. As discussed in Chapter 3, the A/C program switches control to a transient routine in the case of tool-work collision under rapid traverse or milling across a step in the axial depth of cut. This transient condition is recognized from the sampled values of the cutting force. The transient routine sends a pulse through I/O channel 16 to the flip flop "F-F" shown in figure V-2, which in turn "switches off" S_1. This routine simultaneously, and through a common memory location with the NC program causes the latter to stop the flow of command pulses to the NC controller (see figure 3.6). The transient routine in the A/C program also, as mentioned, controls the duration of the condition V_{com} = 0.0. This is done by counting the number of computer instruction executed (each instruction takes about 2 msec).

After a period of 40 milliseconds, the transient routine sends a second pulse, which through the flip flop "switches on" S_1 and in the same time "switches off" S_2, thereby reducing the gain in the filter (and accordingly the NC Loop) to 1/3 its original value.

A third pulse is sent to revert the gain to its original value. The circuit shown in figure V-2 was added to the control boards in the NC controller.

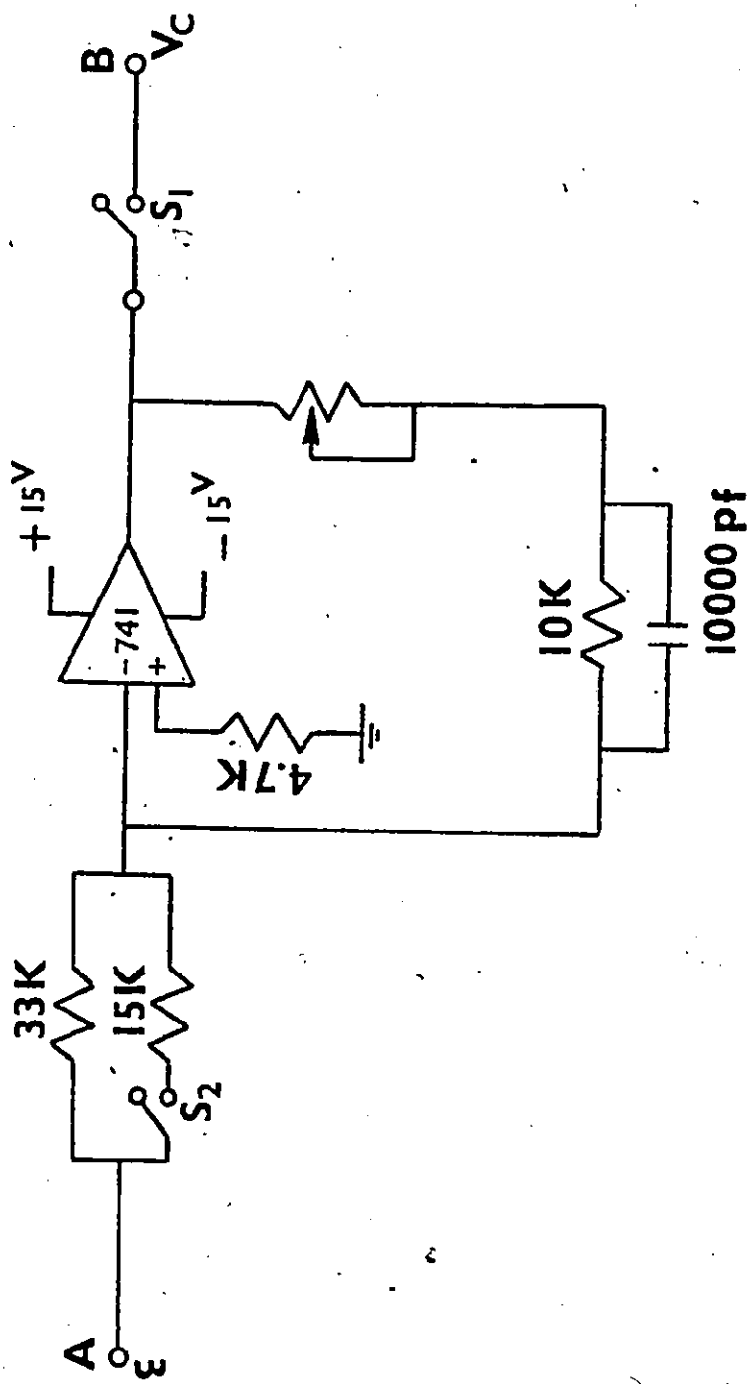

Circuit Diagram of Low Pass Filter in the NC Loop

FIGURE V-1

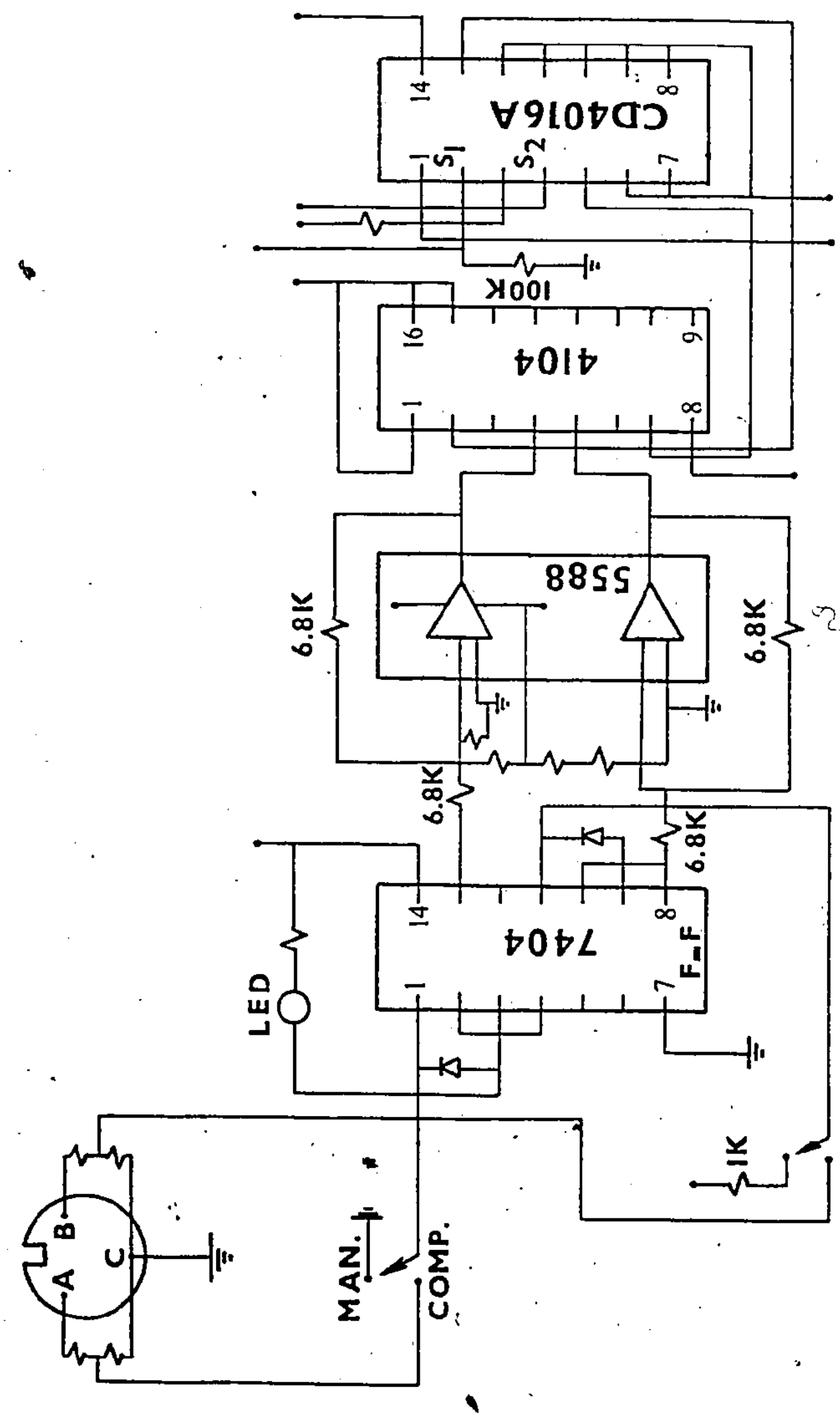

4104 = Low Voltage to High Voltage Translator

Circuit Diagram of the Analog Switches

FIGURE V-2